Australian Geomechanics Society

ENGINEERS AUSTRALIA

ISSN 0818-9140

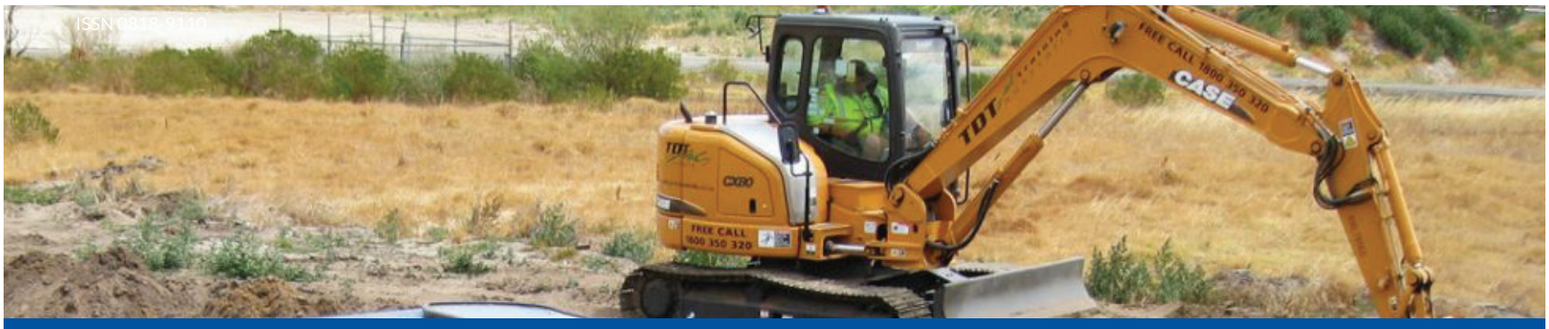

INNOVATIONS IN GEOTECHNICAL CONSTRUCTION & DESIGN

PROCEEDINGS OF THE 2019 AGS SYMPOSIUM
HELD IN
AUSTRALIAN NATIONAL MARITIME MUSEUM, DARLING HARBOUR, NSW
ON
NOVEMBER 15TH 2019

ORGANISING COMMITTEE:
A. Parsa, C. Rujikiatkamjorn, S. Mirlatifi, H. Khabbaz,
A. Hulskamp, AHMK Zaman, P. Rajarathnam, M. Baringa and T. Gourlay

EDITORS:
H. Khabbaz, A. Parsa, AHMK. Zaman and C. Rujikiatkamjorn

ENGINEERS AUSTRALIA

Published by The Australian Geomechanics Society,
National Secretariat,
P.O. Box 955, ST IVES, NSW 2075

AusIMM THE MINERALS INSTITUTE

The Australian Geomechanics Society (AGS) is jointly sponsored by: Engineers, Australia and The Australasian Institute of Mining and Metallurgy

Australian Geomechanics Society

Geomechanics is the application of engineering principles to the earth sciences to improve continually the accuracy, efficiency, cost-effectiveness and safety of construction projects both above and below ground, including the recovery of the earth's mineral resources. It remains an imprecise discipline due to the infinite variety of conditions in the earth's crust but correspondingly offers a fascinating and rewarding field of research and practice.

The Australian Geomechanics Society was founded in 1970. Its origins lie in the National Committee of Soil Mechanics of the Institution of Engineers, Australia, established in 1953 and the call for a corresponding society in rock mechanics. In 1973 the society was expanded to include the third discipline of engineering geology and has remained substantially unchanged since that date.

The society is affiliated to the International society of Soil Mechanics and Geotechnical Engineering (ISSMGE), the International Society for Rock mechanics (ISRM) and the International Association for Engineering Geology and the Environment (IAEG).

CORPORATE MEMBERSHIP OF THE AGS

$770.00 and look at what your organisation gets -
Membership for two nominees who each receive:

- Membership fee ($209)
- Membership of the three International Societies ($176)
- IAEG Bulletin ($44)

An extra copy of *Australian Geomechanics* for company library ($154)

Acknowledgement in front section of every issue of *Australian Geomechanics*

Total benefit is $836 All prices include GST.

Contact Peter Robinson on secretary@australiangeomechanics.org or go to www.australiangeomechanics.org **for application forms and more information**.

Programme

08:00 - 08:45	*Registration*
08:45 - 09:00	Opening Address

SESSION 1 – GEOTECHNICAL LESSONS LEARNT FROM DESIGN AND CONSTRUCTION OF DEEP FOUNDATIONS

09:00 - 09:35	*Keynote Lecture:* *Harry Poulos* - Some Inadequacies of Common Design Procedures for Deep Foundations
09:35 - 09:55	*Brad Azari & Sam Mirlatifi* - Geotechnical challenges for construction of diaphragm walls and foundation of Sydney's tallest building, crown Sydney hotel resort
09:55 - 10:15	*Antonio Ramirez Martinez* - Optimising precast cantilever walls founded in Sydney sandstone
10:15 - 10:30	*Questions*
10:30 - 11:00	*Morning tea & coffee*

SESSION 2 – ADVANCES IN GEOTECHNICAL SITE CHARACTERISATION AND GROUND MODELLING

11:00 - 11:20	*Robert Bertuzzi* - Geotechnical innovations in the tunnelling industry
11:20 - 11:40	*Demeke Jembere* - An empirical model to correlate rock mass classification and hydraulic conductivity of Hawkesbury sandstone in Sydney
11:40 - 12:00	*Firman Siahaan* - In-situ waste characterisation for primary settlement assessment for high embankment of infrastructure projects built over municipal solid waste
12:00 - 12:10	*Questions*
12:10 - 13:00	*Lunch*

SESSION 3 – GEOTECHNICAL ADVANCES AND CHALLENGES IN DEEP EXCAVATION AND GROUND IMPROVEMENT

13:00 - 13:35	*Keynote Lecture:* *David Puller* - The design and construction of very deep excavations – recent advances
13:35 - 13:55	*Jim Yang & Ken Chen* - Ground improvement and verification for stage 1 IMEX earthworks
13:55 - 14:15	*Kim Chan* - The approach of preload and surcharge release for embankments constructed over PVD improved soft soils
14:15 - 14:35	*Babak Hamidi* - Ground improvement of Granville harbour wind farm foundations using CMC
14:35 - 14:50	*Questions*
14:50 - 15:20	*Afternoon Tea and Coffee*

SESSION 4 – DIGITAL TECHNOLOGIES, NEW MATERIALS AND SMART DESIGN IN GEOTECHNICAL ENGINEERING

15:20 - 15:40	*Patrick Wong* - Design and construction of plastic geocellular rain water harvesting/stormwater detention tanks
15:40 - 16:00	*Aasha Pancha* - Listening to the earth: an unconventional scientific approach to understanding sub-surface ground conditions
16:00 - 16:20	*Henry Zhang* - Green Square - enabling urban renewal through trenchless construction and smart retaining wall design
16:20 - 16:40	*Bowei Yu* - A novel multiple-liner design for preventing desiccation of geosynthetic clay liners: an experimental investigation
16:40 - 17:00	*Questions*
17:00 - 17:20	*Closing remarks and thanks*
17:20 – 17:40	*Drinks and canapés*
17:40	*Close*

J STEEL/GIKEN HAS A LONG AND SUCCESSFUL HISTORY PROVIDING ENGINEERING AND PROCUREMENT STRATEGIES TO THE CONSTRUCTION INDUSTRY IN AUSTRALIA, NEW ZEALAND AND ACROSS THE SOUTH PACIFIC.

We recognise that successful outcomes are only possible when a project's core elements of Engineering, Procurement, Construction and Construction Management are aligned in their purpose. Our reputation for quality and cost-efficiency is built from our fully integrated capabilities across these elements.

In collaboration with our global partners, we consistently challenge traditional methods, delivering safe, efficient and environmentally acceptable outcomes for a wide range of civil, marine and general engineering and construction applications.

Our focus is engineering these outcomes while catering to every project requirement with a holistic and calculated approach.

SERVICES

ENGINEERING DESIGN

CONSTRUCTION MANAGEMENT

PROCUREMENT & PRODUCT SUPPLY

QUALITY CONTROL & INSPECTION

LOGISTICS AND DELIVERY

www.jsteel.com.au
www.giken.com

Innovations in Geotechnical Construction and Design

PREFACE

This document contains the accepted papers submitted and peer reviewed for the 23rdannual symposium organised by the Sydney Chapter of the Australian Geomechanics Society (AGS). It is hoped that the symposium will keep practicing geotechnical engineers, engineering geologists, and other engineering professionals informed of recent developments in this field. It also recognises the need to gather the experience of those practicing throughout Australia and to allow transfer of knowledge and sharing of their experiences.

These symposia continue to be one of the best forms for bringing together the key stakeholders of the Australian geological and geotechnical community. The main objective of the symposium, held on 15 November 2019, is to present overviews of geotechnical aspects of transport infrastructure construction, site characterisation, numerical simulation, collapsed structures, reliability analysis and new insights into experiences, technologies and strategies.

This symposium is the cooperative effort of many authors and qualified reviewers. The editors and organising committee wish to thank the authors, who have generously contributed their time to prepare the various papers and the colleagues of the authors, who have assisted with time, secretarial, drafting and other facilities. Appreciation is also extended to our sponsors for their support. Without them, the Symposium would not be possibly the best ongoing forum for the Australian Geomechanics and groundwater community.

Ali Parsa, Cholachat Rujikiatkamjorn, Sam Mirlatifi, Hadi Khabbaz, Adrian Hulskamp, AHMK Zaman, Puvaneswary Rajarathnam, Miren Baring and Tony Gourlay

On behalf of the AGS Symposium Organising Committee,
The Australian Geomechanics Society, Sydney Chapter

Annual Seminars of AGS Sydney Chapter

No.	Date	Topic	Chairman & Organising Team
1	1997	Pavement Design Beyond 2000	A Leventhal
2	1998	Recent Developments in Piling Practice in Sydney	P Andrews
3	1999	Flexible Retaining Walls: Design to Prevent Failure	P Andrews and P Hewitt
4	2000	Computer Methods	P Hewitt and J Carter
5	2001	Excavation Retention	T Walker and P Hewitt
6	2002	Landslide Risk Management	B Walker and T Walker
7	2003	Geotechnical Instrumentation and Construction Works Compliance Testing	G Scholey and T Walker
8	2004	The Engineering Geology of the Sydney Region – Revisited	G Scholey, M Parmar, G Young and G McNally
9	2005	Geotechnical Aspects of Tunnelling	H Buys and T Gourlay
10	2006	Soft Ground Engineering	H Buys, R Moyle and P Hewitt
11	2007	Engineering Advances in Earthworks	R Moyle, R Lindbeck and H Liu
12	2008	Foundation Design and Construction	R Moyle, R Lamont and B Ewers
13	2009	Geosynthetics – New Materials for Modern Infrastructure	B Ewers, H Buys and H Liu
14	2010	Seismic Engineering- Design for Management of Geohazards	C Rujikiatkamjorn, J McIlveen, R Lamont and M Haysler
15	2011	Coastal and Marine Geotechnics- Foundations for Trade	C Rujikiatkamjorn, J McIlveen, G Blumberg, J Smith and C Y Tey
16	2012	Advances in Geotechnical Aspects of Roads and Railways	H Khabbaz, C Y Tey, O Stahlhut and C Rujikiatkamjorn
17	2013	Retaining Structures: Recent Advances and Past Experiences	H Khabbaz, C Rujikiatkamjorn, M van Uden, C McColgan and S Mirlatifi
18	2014	Resilient Geotechnics	H Khabbaz, C Rujikiatkamjorn, S Mirlatifi, C McColgan and M van Uden
19	2015	Recent Developments and Experiences with Groundwater and Excavation	C Rujikiatkamjorn, S Mirlatifi, Katarina David, A. Hulskamp, and M van Uden
20	2016	Ground Stabilisation Techniques for Problematic Soils and Unstable Rocks	C Rujikiatkamjorn, S Mirlatifi, A. Hulskamp, T Mcwilliam and H Khabbaz
21	2017	Geotechnical innovations and challenges for transport infrastructure	S Mirlatifi, , C Rujikiatkamjorn, G Vorobieff, D Airey, A Parsa, A Hulskamp, H Khabbaz, H Buys and K Oj,
22	2018	Advances in Site Investigations, Monitoring and Instrumentation	A. Parsa, H. Khabbaz, S. Mirlatifi, C. Rujikiatkamjorn, A. Hulskamp, AHMK Zaman, and P. Rajarathnam
23	2019	Innovations in Geotechnical Construction and Design	A. Parsa, C. Rujikiatkamjorn, S. Mirlatifi, H. Khabbaz, A. Hulskamp, AHMK Zaman, P. Rajarathnam, M. Baringa, and T. Gourlay

TABLE OF CONTENTS

[All papers have been refereed in accordance with the full DETYA (Department of Education, Training and Youth Affairs) review process, unless stated otherwise.]

SOME INADEQUACIES OF COMMON DESIGN PROCEDURES FOR DEEP FOUNDATIONS

Harry G. Poulos

Senior Consultant, Coffey Services Australia, and Emeritus Professor, University of Sydney

ABSTRACT

This paper examines some aspects of common deep foundation design that the author considers may be inadequate. The following aspects are considered:

- Ignoring foundation interactions;
- Ignoring the beneficial effect of the raft;
- Assuming a rigid cap or raft;
- Over-simplification of the geotechnical profile;
- Ignoring the beneficial effects of basement walls;
- Ignoring the effects of ground movements;
- Ignoring kinematic effects in seismic design.

Each inadequate aspect will be considered in turn, with examples given of the possible consequences. Some aspects lead to conservative designs, while others tend to be unconservative. Suggestions will be offered for addressing the perceived inadequacies, some of which are likely to involve the application of innovative techniques.

1 INTRODUCTION

In relation to design, "innovation" is a word that tends to be over-used and abused, as a descriptor of processes or ideas. A simple dictionary definition of "innovation" is as follows:

The process of translating an idea, invention or process into a good or service that creates value for which customers will pay.

One of the characteristics of innovation is that the innovative idea or process must satisfy a specific need, and thus such a need requires recognition and explanation. This paper will not address innovation overtly, but will focus on a number of perceived inadequacies in common design practice for deep foundations, which are as follows:

1. Ignoring foundation interactions;
2. Ignoring the beneficial effect of the raft;
3. Assuming a rigid cap or raft;
4. Over-simplification of the geotechnical profile;
5. Ignoring the beneficial effects of basement walls;
6. Ignoring the effects of ground movements;
7. Ignoring kinematic effects in seismic design.

Each inadequate aspect will be considered in turn, with examples given of the possible consequences. Some suggestions will be offered for addressing the perceived inadequacies.

2 IGNORING FOUNDATION INTERACTION EFFECTS

As an example of the effect of ignoring interaction within a piled raft system, the case is considered of a high-rise building in Doha, Qatar, an impression of which of shown in Figure 1.

The tower was designed to have a central high-rise tower 510 m tall, which was to be surrounded by a low-rise podium area. The foundation system was designed as a piled raft.

The foundation system is shown in Figure 2 and consisted of the following components:

1. 525 piles, with diameters of 1.0, 1.2 and 1.5 m.
2. Piles founded at four different levels: RL -26 m, -29 m, -54 m, and -60 m.
3. A raft thickness of 4.0 m for the majority of the foundation footprint.
4. Locally thickened areas of the raft beneath the lift over-run and core-wall areas of 6 m, 8.3 m and 12 m thickness.
5. A raft thickness of 0.8 m below the outer podium area.

Figure 1: Doha tower (artist's impression)

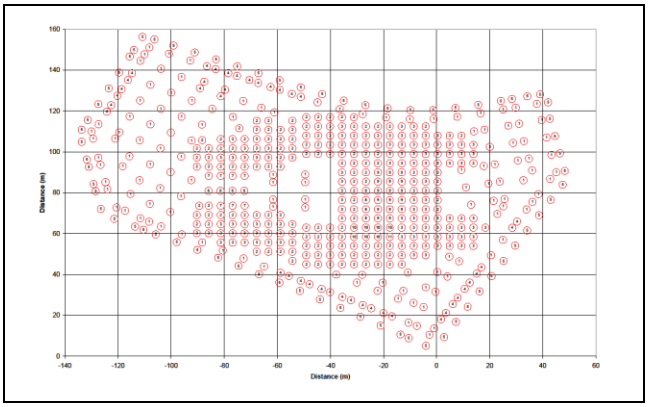

Figure 2: Foundation layout

The geotechnical model developed for the site was based on available in-situ and laboratory test data, and is shown in Table 1.

Table 1: Geotechnical model for Doha site

Stratum	*Top RL m*	*Thickness m*	*E'v MPa*	*E'h MPa*	*fs kPa*	*fb kPa*
Simsima L'stone	-18	3.5	2500	1750	600	-
Midra Shale	-21.5	3.0	700	490	525	-
Rus (1)	-24.5	75.5	500	350	425	5.9
Rus (2)	-100	Large	1000	-	-	-

The column loads were applied as uniformly distributed loads over the base area of the columns for the assessment of the pile loads and as one uniformly distributed load over the whole area of the tower footprint (0.95 MPa) for the assessment of the settlement and pile stiffness values. The serviceability assessment used the dead load plus the live load.

Analyses were undertaken to compute the settlement and pile load distribution within the foundation system, taking account of the flexibility of the raft foundation. The computer program GARP (Small and Poulos, 2007) was employed, using a finite element formulation to model the raft and idealizing the piles as non-linear interacting springs. A raft thickness of 4 m was used in the analyses, with the finite element mesh for the raft having a total of 945 elements and 3006 nodes.

The analyses carried out are listed in Table 2.

Table 2: Summary of analyses for Doha Tower

Run No.	*Details*
Q1	Normal analysis – all interactions included
Q2	Zero pile-pile interactions, but raft-raft, pile-raft and raft-pile interactions included
Q3	Zero pile-pile, pile-raft and raft-pile interactions; only raft-raft interaction accounted for

The computed maximum settlement for the three cases in Table 2 are shown in Figure 3. It can be seen that ignoring the pile-pile interactions reduces the maximum settlement from 81 mm to 41 mm, and ignoring the raft-pile and pile–raft interactions as well further reduces the maximum settlement to 20 mm. Thus, the settlement could be underestimated by a factor of 4 in this case if no consideration is given to the interactions among the piles and with the raft. Unfortunately such an approach is not uncommon among designers that are focused primarily on the structure itself.

The effect of ignoring interactions on the maximum rotation and the maximum raft bending moment in the x-direction are shown in Figures 4 and 5. The computed rotation becomes smaller if the interactions are ignored, with the maximum computed rotation decreasing by about 25% if all interactions are ignored. In contrast, the effect of ignoring interactions on the maximum bending moment is less marked.

Figure 6 compares the calculated maximum axial load in any of the piles. Ignoring all interactions (other than raft-raft) leads to a significant increase in the maximum pile load (almost 25%), and consequently, to more stringent requirements for reinforcement of the piles.

Clearly, it is vitally important not to ignore the interactions that exist within a pile raft foundation system. To do so gives an unconservative estimate of settlement and differential settlement, but a conservative estimate of axial pile loads.

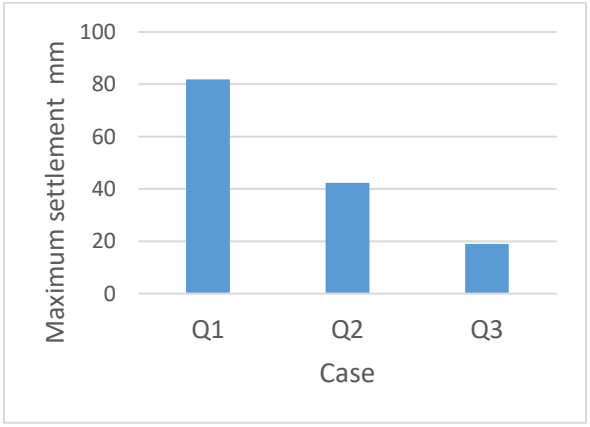

Figure 3: Effect of ignoring foundation component interactions on maximum settlement

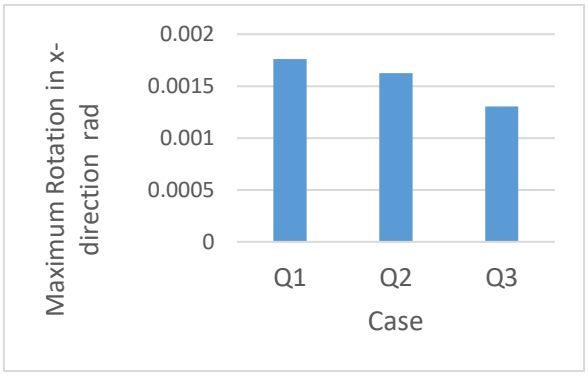

Figure 4: Effect of ignoring foundatiuon component interactions on maximum x-rotation

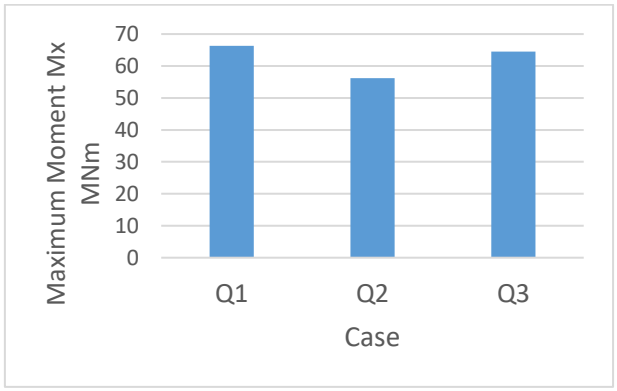

Figure 5: Effect of ignoring foundatiuon component interactions on maximum x-moment

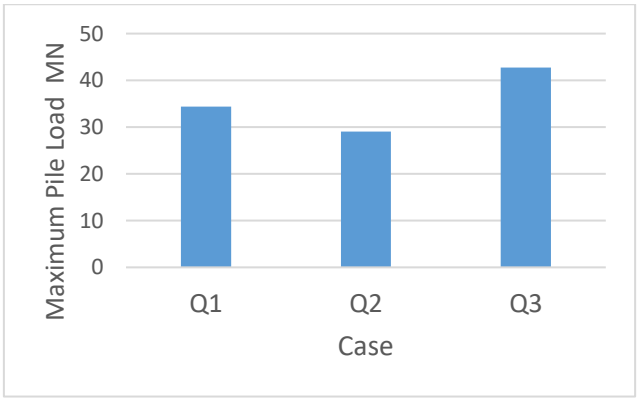

Figure 6: Effect of ignoring foundation component interactions on maximum axial pile load

2.1 IMPROVEMENTS IN PRACTICE

Improvements in design practice may be achieved in the following ways:

1. Emphasising that load test data on single piles should not be used directly to represent piles within a group, but that such data should be interpreted properly and adjusted to allow for group effects.
2. Using design methods and software that take proper consideration of the various foundation interactions.
3. Assisting the structural designer by providing values of pile stiffness values that take proper account of these interactions.

3 IGNORING THE PRESENCE OF THE RAFT

It is not uncommon for foundation designers to ignore the effect of raft-soil contact and to assume that the piles carry the entire structural load.

For the same case as considered above, ignoring the effect of the raft-soil contact can be simulated by setting the limiting pressure on the base of the raft to (almost) zero. All the load is then carried by the piles, which are now free-standing. Table 3 compares various aspects of the computed behaviour of the foundation system. The following characteristics are noted when the presence of the raft is ignored:

1. The computed maximum settlement is increased dramatically.
2. The maximum rotation is increased dramatically.
3. The maximum pile load is almost doubled.
4. The maximum bending moment in the raft is increased, but by a more modest amount than the other characteristics.

It seems clear that such a design, based on this over-conservative approach, would be inadequate and would almost certainly not satisfy the serviceability criteria, despite the presence of 525 piles in the system. However, by taking rational account of the presence of the raft, the settlements and rotations of the foundation are much more likely to be acceptable and to satisfy the serviceability design criteria.

Table 3: Effect of Ignoring the Raft Resistance

Value	*Allowing for raft*	*Ignoring the raft*
Max settlement mm	81.8	174.6
Min settlement mm	7.6	7.2
Max x-rotation rad	0.00176	0.01260
Max x-moment MNm	66.3	70.3
Min x-moment MNm	-46.2	-45.0
Max pile load MN	34.4	67.2
% load on raft	24.6	0

A. IMPROVEMENTS IN PRACTICE

Overcoming this perceived deficiency is relatively simple:

1. Recognition of the beneficial effects that the raft can provide;
2. Using a design approach that considers the effects of raft stiffness and capacity and that properly accounts for the various pile and raft interactions within the foundation system.

4 ASSUMING A RIGID PILE CAP OR RAFT

When designing or analyzing pile groups or piled rafts, it is common to make the simplifying assumption that the pile cap or raft is perfectly rigid. Because rafts in some modern high-rise buildings can be as thick as 5-6m, a rigid raft assumption may at first sight seem very reasonable. However, making this common assumption can lead to misleading outcomes, as it tends to over-estimate the loads in the outer piles within the system and under-estimate the loads in inner piles. As a consequence, the computed values of pile head stiffness may also be affected.

This leads on to the following important question: how thick does a raft have to be to be considered as rigid? To answer this question, recourse may be made to the work of Brown (1969), who considered the behaviour of a flexible circular raft on a finite elastic layer. Brown defined the relative flexibility of the raft via a factor K, given by:

$$K = E_r(1-\nu_s^2)(t/a)^3 /E_s \quad (1)$$

where E_r= Young's modulus of raft

ν_s = Poisson's ratio of soil

t = raft thickness

a = raft radius

E_s = Young's modulus of soil.

Brown's results indicated that a raft could be considered as perfectly flexible if $K \leq 0.01$, and virtually rigid if $K \geq 10$.

The criterion for rigidity can be facilitated by assuming that the factor K also applies to a rectangular raft having an area equal to that of the circular raft. If the average dimension of the raft is B, so that the area is B^2, then the requirement for rigidity can be approximated as follows:

$$(t/B)_{rigid} \approx \sqrt{\pi}.\ [K_{rigid}/(E_r/E_s).\ (1-\nu_s^2)]^{1/3} \quad (2)$$

where K_{rigid} = value of K for a rigid raft, i.e. 10.

A similar equation can be written for the relative thickness, $(t/B)_{flex}$, when a raft is perfectly flexible, by substituting, in Eq. 2, the value of K for a flexible raft (i.e. 0.01) instead of that for a rigid raft.

Figure 7 plots the relationship between the relative raft thickness, t/B, for both rigid and flexible rafts, for typical values of E_r (30000MPa) and ν_s (0.3). Rafts with a t/B value on or above the line for a rigid raft would be classed as rigid, those falling on or below the line for a flexible raft would be flexible, while those falling between the lines for rigid and flexible rafts would be classed as partially flexible.

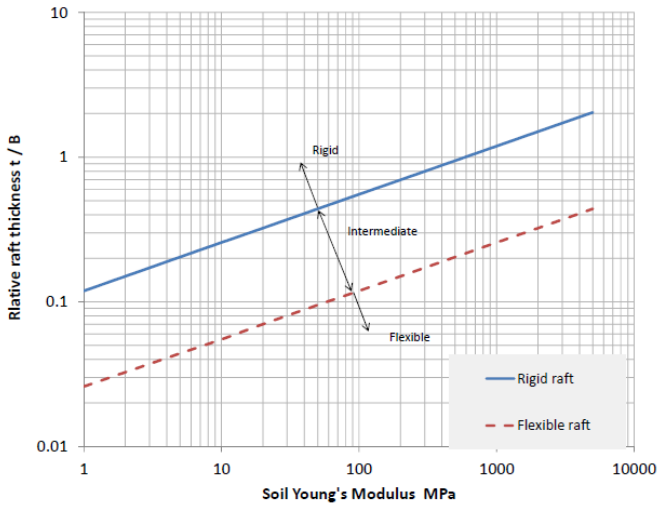

Figure 7: Thickness requirements for rigid and flexible rafts

The following points can be noted:

- The value of $(t/B)_{rigid}$ for a rigid raft increases as the soil modulus increases.

- Even for very soft soils, for example Es = 10 MPa, $(t/B)_{rigid}$ is about 0.25. Thus, for an average dimension of 50m, the raft would need to be about 12.5m thick to be truly rigid.
- For a very stiff soil layer, for example, Es = 500 MPa, $(t/B)_{rigid}$ is almost 1.0. Thus, for an average dimension of 50m, the raft would need to be about 50m thick!
- For a more common raft thickness of 3m, a raft with an average dimension of 50m would have t/B = 0.06, and this would be almost perfectly flexible even for a soft soil, and certainly perfectly flexible for the very stiff soil.

It therefore seems clear that pile caps and piled rafts supporting high-rise structures are likely to tend towards the perfectly flexible category.

As an example of the effects of assuming a rigid pile cap, the case of the 151 storey Incheon Tower, shown in Figure 8, has been considered. The foundation layout is shown in Figure 9.

Figure 8: Incheon Tower (artist's impression)

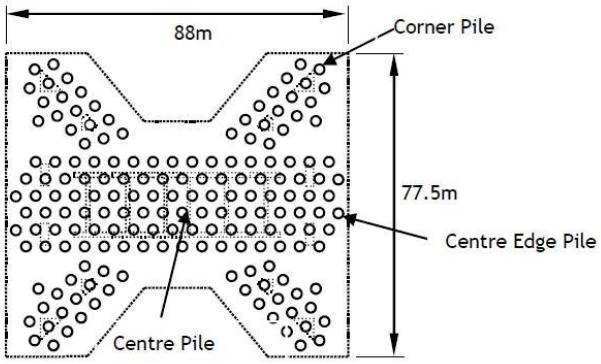

Figure 9: Pile Layout Plan Incheon Tower (*Abdelrazaq et al., 2011*)

The detailed design analyses were carried out using the program CLAP (Combined Load Analysis of Piles, Coffey, 2011) and a later version of the program GARP (Small and Poulos, 2007), CLAP is a development of the DEFPIG program (Poulos, 1990), and was used for the ultimate limit state load cases (ULS). GARP was used for analysing the serviceability (SLS) loadings. As part of the design process, estimates were required of the maximum axial loads in each pile within the foundation system, and initially, the program CLAP was used. CLAP implicitly assumes that the raft supporting the piles is rigid, and as a consequence, the computed axial loads on some piles were found to be very large.

To investigate the effect of the rigid raft assumption, the foundation performance was re-assessed using GARP, taking the flexibility of the raft into account. The serviceability load case (i.e dead and live loads) was considered and the loads were applied at column and core locations.

Table 4 presents a summary of foundation settlement, axial loads and stiffness on the corner, centre edge and centre piles of the foundation (see Figure 9). The maximum predicted settlement occurred within the heavily loaded core area, while the computed pile stiffness values were greatest for the outer piles. As the analysis considered non-linear pile behaviour, the outer piles had a higher initial stiffness, but this stiffness degraded more rapidly under increasing loading than the central piles.

Considering a rigid raft for the foundation, the total and differential settlements were predicted to be smaller, with higher pile head loads for corner and centre-edge piles, thus resulting in higher vertical pile stiffness values, especially on the outer piles, when compared with those for a flexible raft.

When the flexibility of the raft was incorporated, the pile load distribution was found to be more uniform, with slightly higher pile loads being predicted at the centre of the foundation where the heavily loaded core is located. The loads on piles for a rigid raft case were approximately two times the loads for a flexible raft, except for the centre piles.

Table 4: Summary of foundation performance

		Rigid Raft	Flexible Raft
Pile Load (MN)	Centre Pile	24	49
	Centre Edge Pile	65	33
	Corner Pile	85	43
Pile Stiffness (MN/m)	Centre Pile	511	726
	Centre Edge Pile	1418	932
	Corner Pile	1604	1292
Raft Settlement (mm)	Maximum	52	67
	Minimum	26	28

It is interesting to refer to Figure 7 to assess the relative flexibility of the 5.5m thick raft. The average dimension of the foundation was about 70m, so that the ratio t/B was about 0.08. The average Young's modulus within a depth equal to this dimension was about 275 MPa, and for this modulus, the value of t/B for a rigid raft would be about 0.75, i.e. the raft would need to be about 52.5m thick. In fact, even for a flexible raft, the value of t/B from Figure 13 would be about 0.17, so that the raft, with a t/B of less than half this value, could be classed as perfectly flexible. Based on the assessment, it is concluded that it is important to model the flexibility of the raft to avoid having to design for unrealistically large loads in the outer piles within the group, and also to obtain more realistic distributions of settlement within the foundation footprint.

A. IMPROVEMENTS IN PRACTICE

The potential inaccuracies of assuming a rigid raft can be overcome via the following procedures:

- Checking whether the ratio of raft thickness to raft size justifies a rigid raft assumption;
- If not, using an analysis that takes account of raft flexibility. This may be via a piled raft analysis, a structural analysis in which relevant values of the pile stiffness are used, or via a three-dimensional finite element, or finite difference, analysis, in which all components of the foundation system are appropriately modelled.

5 OVER-SIMPLIFICATION OF THE GEOTECHNICAL PROFILE

Over-simplification of the geotechnical profile can occur for several reasons, including:

1. Inadequate ground investigation to an appropriate depth which will be influenced by the foundation;
2. The use of simplified analysis and design tools that do not allow readily for variable ground conditions below the founding level of the foundation system;
3. Inadequate attention given to the potential variability of ground stiffness with depth, even in a relatively homogeneous geo-stratum.

Two examples will be given below to illustrate the consequences of ground profile over-simplification.

5.1 ASSUMED UNIFORM CONDITIONS BELOW FOUNDATION LEVEL

It is not uncommon for foundation analysts to assume that the ground conditions below the pile tips remain constant and extend to relatively large depths. The consequences of this assumption may be that pile-pile interactions are over-estimated. Such an over-estimation was experienced by the author in relation to the foundation design for the Emirates twin towers in Dubai (Poulos and Davids, 2005). These towers are shown in Figure 10.

Figure 10: The Emirates Towers soon after completion of construction

Predictions of the behavior of a single test pile were found to be in reasonable agreement with the measured behaviour of test piles. On this basis, the parameters developed for a single pile were used to predict the settlement of the piled rafts supporting the two separate towers.

Conventional pile capacity analyses were used to assess the ultimate geotechnical capacity of the piles and raft. In additional to the conventional analyses, more complete analyses of the foundation system were undertaken with an early version of the computer program GARP (Poulos, 1994). This program utilized a simplified boundary element analysis to compute the behaviour of a rectangular piled raft when subjected to applied vertical loading, moment loading, and free-field vertical soil movements. The raft was represented by an elastic plate, the soil was modelled as a layered elastic continuum, and the piles were represented by hyperbolic springs which can interact with each other and with the raft. Beneath the raft, limiting values of contact pressure in compression and tension were specified, so that some allowance could be made for non-linear raft behaviour. In addition to GARP, the program DEFPIG (Poulos and Davis, 1980) was used for the pile stiffness values and pile-pile interaction factors, and for computing the lateral response of the piles.

For the analysis of settlements under the design loads, the same values of Young's modulus were used as for the single piles. Measurements were available only for a limited period during the construction process and these are compared with the predicted time-settlement relationships in Figure 11 for typical points within the Hotel Tower. To the author's disappointment, it was found that, for both towers, the actual measured settlements were significantly smaller than those predicted, being only about 25% of the predicted values after 10-12 months.

The disappointing lack of agreement between measured and predicted settlement of the towers prompted a "post-mortem" investigation of possible reasons for the poor predictions. At least four such reasons were examined:

1. Some settlements may have occurred prior to the commencement of measurements;
2. The assumed time-load pattern may have differed from that assumed;
3. The rate of consolidation may have been much slower than predicted;
4. The interaction effects among the piles within the piled raft foundation may have been over-estimated.

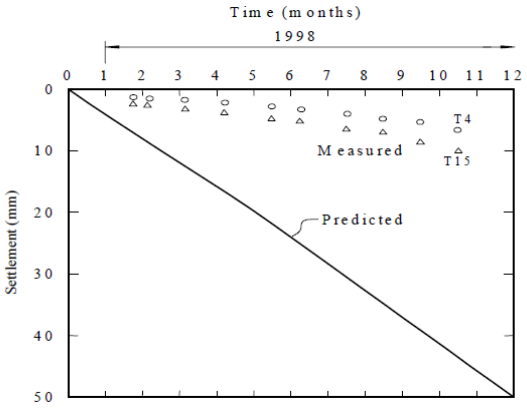

Figure 11: Predicted and measured time-settlement behaviour of Hotel tower

Of these, based on the information available during construction, the first three did not seem likely, and the last was considered to be the most likely cause. Calculations were therefore carried out to assess the sensitivity of the predicted settlements to the assumptions made in deriving interaction factors for the piled raft analysis with GARP. In deriving the interaction factors originally used, it had been assumed that the soil or rock between the piles had the same stiffness as that around the pile, and that the rock below the pile tips had a constant stiffness for a considerable depth. In reality, the ground between the piles is likely to be stiffer than near the piles, because of the lower levels of strain, and the rock stiffness below the pile tips is likely to increase significantly with depth, both because of the increasing level of overburden stress and the decreasing level of strain. The program DEFPIG was therefore used to compute the interaction factors for a series of alternative (but credible) assumptions regarding the distribution of stiffness both radially and with depth. The ratio of the soil modulus between the piles to that near the piles was increased to 5, while the modulus of the material below the pile tips was increased from the original 70 MPa to 600 MPa (the value assessed for the rock at depth). The various cases are summarized in Table 7.

Figure 12 shows the computed relationships between interaction factor and spacing for a variety of parameter assumptions. It can be seen that the original interaction curve used for the predictions lies considerably above those for what are considered (in retrospect) more realistic assumptions. Since the foundations analyzed contained many piles, the potential for over-prediction of settlements is considerable, since small inaccuracies in the interaction factors can translate to large errors in the predicted group settlement. In addition, Al-Douri and Poulos (1994) indicate that the interaction between piles in calcareous deposits may be much lower than those for a laterally and vertically homogeneous soil. Unfortunately, this experience was not incorporated in the Class A pile group settlement predictions for the towers.

Curve No.	Modulus of Layer below MPa	Modulus of Soil between Piles to Near-Pile Values
1	80	1.0
2	80	5.0
3	200	5.0
4	600	5.0
5	600	1.0

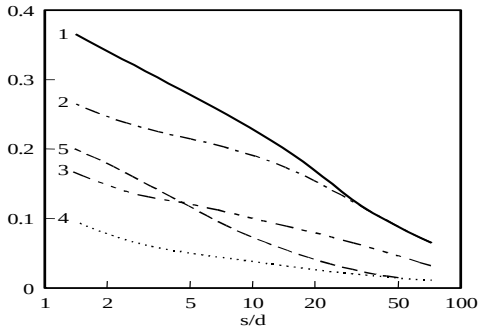

Figure12: Sensitivity of computed interaction factors to analysis assumptions

Table 5: Summary of Revised Calculations for Hotel Tower

Case	*Modulus below 53 m MPa*	*Ratio of max. to near-pile modulus*
Case 1: (Original calculations)	80	1
Case 2	80	5
Case 3	200	5
Case 4	600	5
Case 5	600	1

Revised settlement calculations, on the basis of these interaction factors, gave the results shown in Figure 13. The interaction factors used clearly have a great influence on the predicted foundation settlements, although they have almost no effect on the load sharing between the raft and the piles. For Case 4, the maximum settlement is reduced to 29% of the value originally predicted, while the minimum settlement was only 25% of the original value. If this case were used for the calculation of the settlements during construction, the settlement at Point T15 after 10.5 months would be about 12 mm, which is in reasonable agreement with the measured value of about 10 mm.

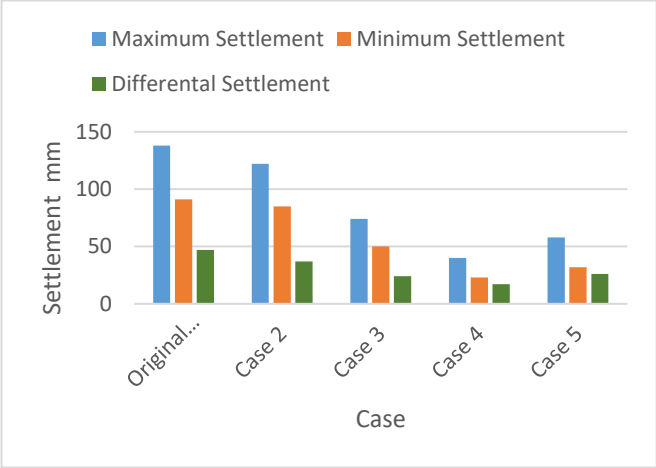

Figure 13: Effect of ground profile assumption on computed settlements

This project demonstrated the vital importance of proper characterization of the ground, not only along the piles, but also beneath the piles. Especially for foundation systems of considerable width (as is typical of tall buildings), the assumptions made about ground stiffness at depth can have a profound effect on the computed settlements.

5.1.1 Improvements in Practice

The inadequacies of over-simplifying the ground profile and assuming constant properties with depth can be countered by:

1. Carrying out a proper ground investigation to the depth that will be influenced by the foundation system;
2. If use is made of a method of analysis which involves interaction factors, they should be computed for the actual ground profile and not for idealised case where the properties remain constant with depth.
3. The interaction factors used should allow for a limit to the distance within which pile-pile interaction occurs, and account should also be taken of the fact that the ground stiffness increases with decreasing strain level.

4.2 EFFECT OF IGNORING COMPRESSIBLE UNDERLYING LAYERS

Golder and Osler (1968) have described an interesting case of a series of furnace foundations on piles, which were founded at a relatively high level, well above a deep layer of compressible Leda Clay. Figure 14 shows the stratigraphy of the site and some of the key engineering properties revealed by the investigations. The configuration of the pile group is also shown in this figure. A number of the original boreholes extended to depths up to 236 feet (72m) without encountering bedrock.

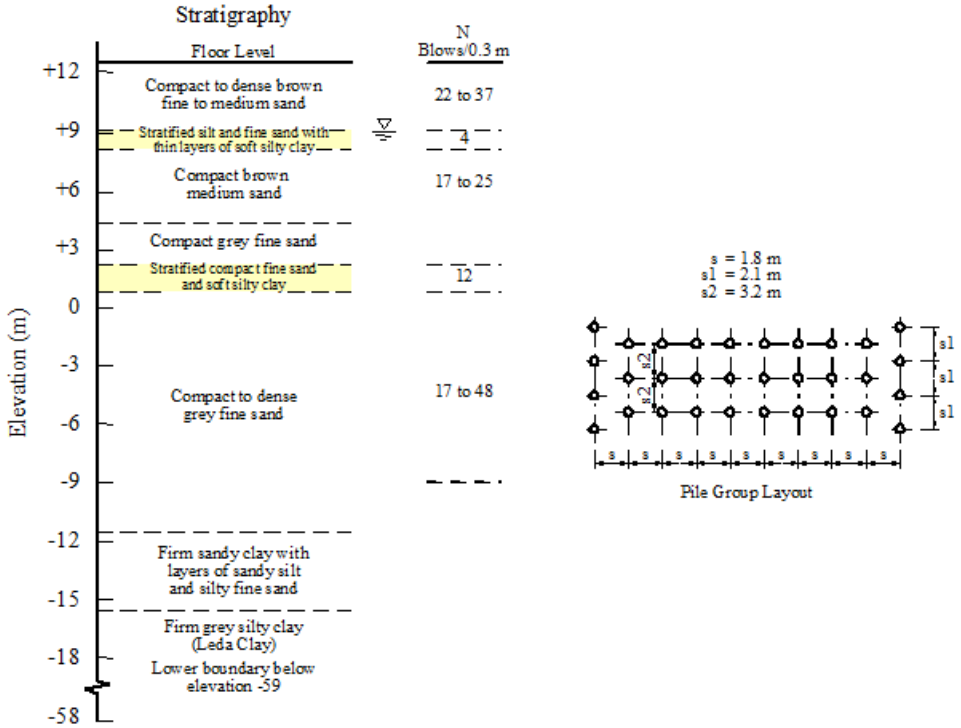

Figure 14: Stratigraphy and pile group layout for furnace foundation (Golder and Osler, 1968)

A load test was carried out on a pile similar to that used for the furnace foundations. At a typical working load of 75 US tons (668 kN), the measured settlement was about 0.04 inches (1.0 mm). Applying normal pile group settlement theory to this result, it might have been expected that the settlement of a 32-pile furnace group would have been of the order of 3 to 6 mm.

15 years of settlement records were available for a bank of five furnaces, and these measurements enable some interesting conclusions to be drawn regarding the sources of settlement of the foundations. Figure 15 reproduces the measured settlements over the bank of five furnaces, and reveals the following interesting characteristics:

- The maximum settlement nearly 15 years after construction was about 73 mm and was continuing to increase;
- The measured settlements were an order of magnitude greater than those which may have been expected simply on the basis of the pile load test;
- The settlement of the end furnaces (Furnace 1 and Furnace 5) was clearly affected by the other furnaces, and showed a significant tilt.

It was estimated by Golder and Osler that, taking into account the settlement of the compressible layers below the pile tips, the anticipated final settlement of the end furnace (No.1) could be of the order of 87 mm, consisting of 10 mm of pile group settlement, 13 mm consolidation of the silty clay layer below the pile tips, and 64 mm from the deep Leda clay. Clearly, the major source of settlement in this case was the underlying compressible clay layer. This had little or so effect on the settlement of the test pile, but had a critical influence on the settlement of the extensive pile group.

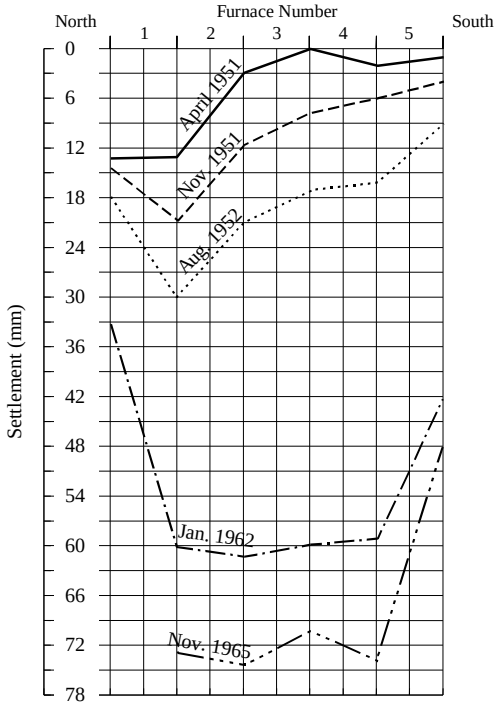

Figure 15: Settlement observations along north-south line through furnaces 1 to 5 (Golder and Osler, 1968).

5.2.1 Improvements in Practice

The inadequate design approach revealed in this case history can be improved via the following processes:

1. Carrying out a detailed ground investigation to a depth that the entire foundation system will influence. This case clearly demonstrates the importance of taking account of the compressibility of underlying compressible layers below the pile tips;
2. Considering the interaction among adjacent foundations.
3. Avoid relying solely on the results of a single pile load test to predict pile group behaviour, without a proper appreciation of the ground conditions.

6 IGNORING THE BENEFICIAL EFFECTS OF BASEMENT WALLS

Many structures, especially tall buildings, incorporate a basement into the substructure to provide parking and storage facilities. In the design of foundation systems, the effect of the basement is often ignored when assessing the foundation capacity and stiffness, even though the basement may extend to a considerable depth below the surface.

Chow and Poulos (2019) have explored the effects of a basement on the capacity and stiffness of a piled or piled raft system, using the three-dimensional finite element program PLAXIS 3D. A numerical example was presented to illustrate the effects of a basement wall on the capacity and stiffness of the foundation system The wall was assumed to be rectangular in shape, of plan dimensions B_r x L_r, and embedded to a depth of D_r below the ground surface, as shown in Figure 16. The direction of lateral loading was parallel to the dimension L_r.

A square raft of 16 m x 16 m in dimension was assumed to be supported by a 4 x 4 pile group with a centre-to-centre spacing of 4 m, embedded in a deep uniform stiff clay profile. The piles had a diameter of 1 m and a length of 24 m. The piled raft was assumed to be rigidly connected to the basement walls.

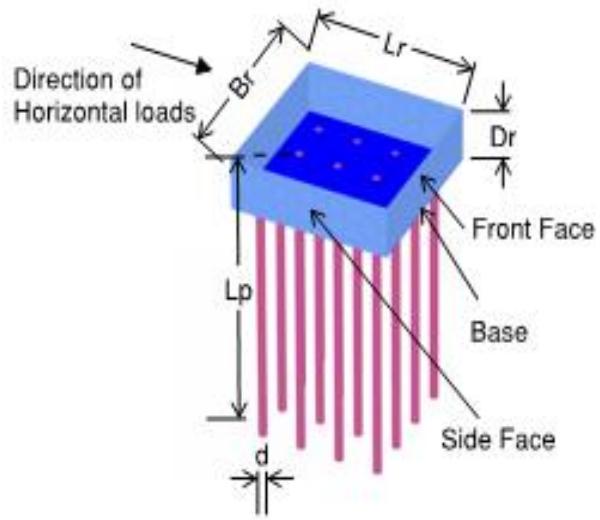

Figure 16: Geometry of basement wall and foundation system

The foundation system was subjected to rapidly applied loading, such that the soil would have an undrained behavior with an undrained shear strength of 80 kPa. A constant shear resistance of 50 kPa was assumed along basement walls and the beneath the underside of the raft. The ultimate skin friction (f_s) on the piles was assumed to be 56 kPa based on the α-method, $f_s = \alpha s_u$. The ultimate bearing capacity (f_b) and lateral yield pressure were assumed to be $9s_u$ = 720 kPa. The parameters used for the analysis are summarized in Table 6. Figure 17 illustrates the foundation layout in plan and section.

The finite element mesh used for the analysis employed a total of 19836 elements and 29568 nodes. The soil was modeled as a homogenous continuum obeying the Mohr Coulomb criterion. The piles were modeled by embedded beam elements with interface elements, while the raft and basement walls were modeled by plate elements. In order to simulate the slip along the raft base and basement walls, a thin layer of 0.1 m thick with the strength as specified (base shear of raft and shear resistance along basement wall) was introduced underneath the raft and adjacent to the basement walls.

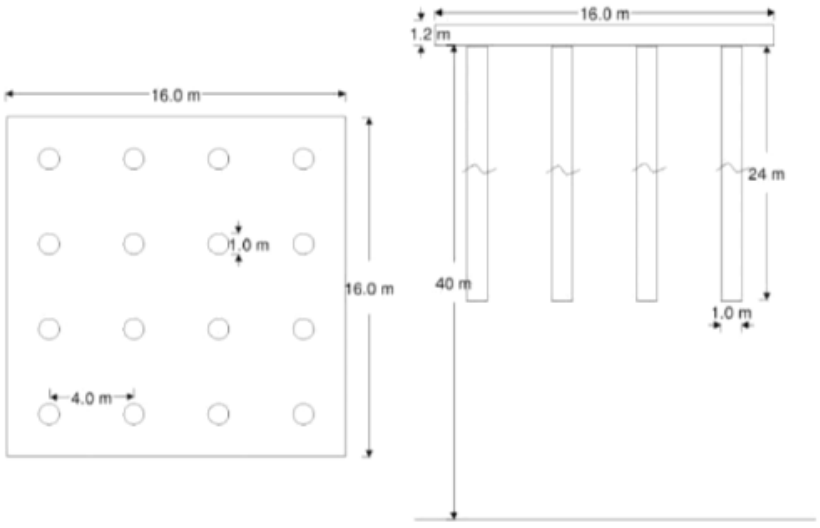

Figure 17: Details of foundation system analysed

The depth of the basement wall depth varied from 0 to 10 m and the foundation system was subjected to three load cases:

- uniform vertical loading,
- uniform horizontal loading, and
- bending moment applied at the centre of the foundation.

Table 6: Parameters for problem considered

Parameter		*Value*
Young's Modulus of Clay (MPa)	Ev (vertical)	50
	Eh (horizontal)	35
Undrained Shear Strength of Clay, cu (kPa)		80
Ultimate Skin Friction (kPa)		56
Ultimate End Bearing (kPa)		720
Young's Modulus of Pile (MPa)		30,000
Young's Modulus of Raft (MPa)		30,000
Thickness of Raft (m)		1.2
Base Shear along raft (kPa)		50
Young's Modulus of Basement Wall (kPa)		30,000
Thickness of basement wall (m)		0.5
Shear Resistance along Basement Wall		50

Figure 18 presents the computed percentage increase in vertical and lateral capacity as compared with those of the piled raft with no wall. The results indicate that with wall embedment, both the vertical and lateral capacity of the foundation system increase. The horizontal capacity increases dramatically, while the vertical capacity increases relatively modestly. It should be emphasised that, with a wider foundation system, the relative increase in capacity will be less than that shown in Figure 18 for a relatively limited width of pile group.

The author has also attempted to undertake simplified analyses by representing the basement walls as a series of equivalent piles having the same axial stiffness and bending stiffness as the wall. The piles had a diameter equal to the thickness of the wall and a length equal to that of the wall. The parameters of the equivalent piles were such that they provided an equal axial and lateral capacity as that of the walls.

For axial loading, a later version of the program GARP was employed (Small and Poulos, 2007), while for lateral and moment loading, the program CLAP was used. In the latter cases, the pile cap was assumed to be rigid.

Figure 19 shows, for typical working load levels, the percentage reduction in responses, i.e maximum settlement under vertical load, lateral deflection under lateral load, and rotation under moment loading. It can be seen that in all three cases, there is a reduction in response with increasing wall depth, with the lateral deflection and rotation experiencing the largest reductions. For the lateral loading, the rate of reduction of lateral deflection decreases once the wall depth exceeds about 6m. This tends to reflect the fact that the wall has an effective length which, when exceeded, results in little or no additional reduction in deflection

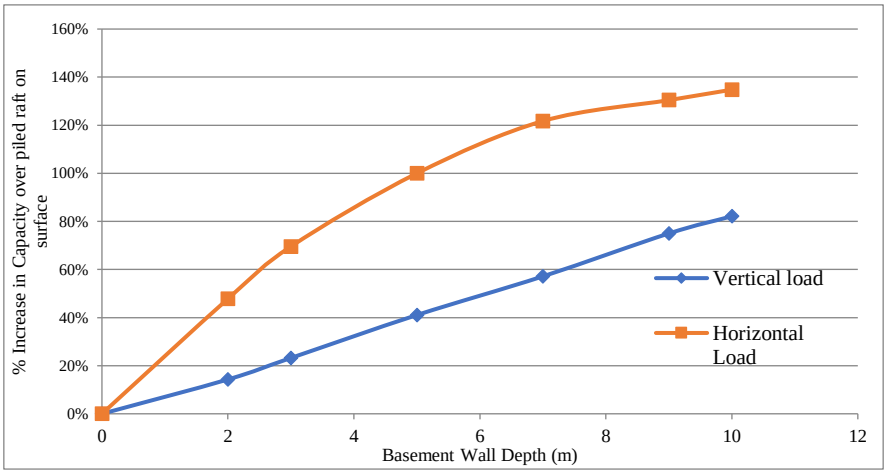

Figure 18: Percentage increase in capacity due to basement wall embedment (Chow and Poulos, 2019)

.

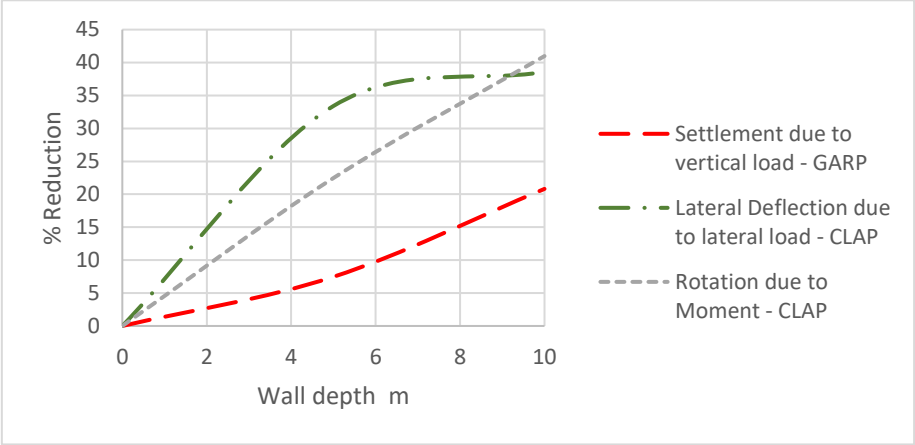

Figure 19: Reduction in responses due to basement wall

For axial loading, the reduction in maximum settlement is accompanied by an increase in the differential settlement, since the walls act to "hold up" the outer edges of the raft. However, for the case analyzed, the increase in differential settlement is relatively modest, being only about 12% for a 5 m deep wall, and about 20% for a 10 m deep wall.

At the same time, there is also a modest re-distribution of axial loads, as shown in Figure 20. The loads in the corner and mid-side piles tend to reduce, while the load on the centre piles increases. The piles nearest the corner of the raft are most affected, with a decrease in axial load of about 15% being experienced for the 10 m deep wall.

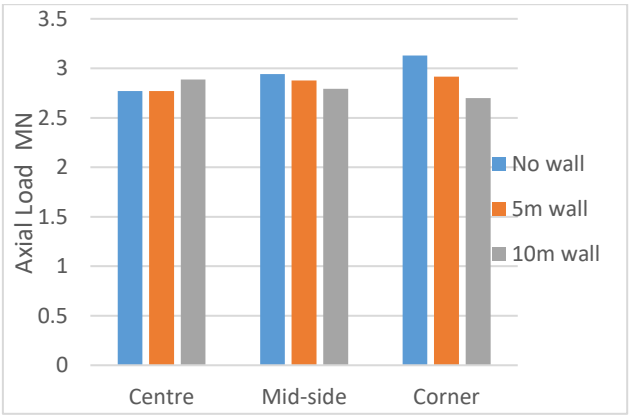

Figure 20: Effect of basement walls on axial load distribution

The presence of the walls has a "shielding" effect on the foundation piles and thus tends to reduce the bending moments developed within these piles. Table 7 shows the computed percentage reduction in pile head bending moments due to the wall, for both horizontal and moment loading. This reduction is most significant for walls up to about 5-6 m deep, and the effect diminishes thereafter. The reductions in pile head moment suggest that the requirements for structural design of the piles are reduced because of the presence of the walls.

Table 7: Percentage reduction in average pile head bending moment

Wall depth m	% reduction in head moment due to horizontal loading	% reduction in head moment due to moment loading
0	0	0
5	44	30
10	45	37

The implications of the above analysis results are as follows:

For both vertical and horizontal loads, the displacements decrease as the depth of basement walls increases.

The basement walls provide additional vertical and horizontal resistance to the foundation system, and thus can provide a larger margin of safety against failure (especially horizontal) than a piled raft without embedment.

The basement walls provide additional rotational stiffness to the foundation system thus contributing to the reduction of its angular rotation.

The induced bending moments within the foundation piles tend to be reduced significantly (in this example), with most of the benefit arising from relatively shallow walls. There is also a modest re-distribution of axial load within the foundation piles.

It should be recognized that the larger the area of the foundation footprint, the smaller will be the effect of the basement walls surrounding the foundation system. Nevertheless, it seems highly desirable to incorporate the basement walls into the foundation design to avoid undue conservatism in relation to the forces and bending moments in the piles, and on the other hand, to avoid under-estimating differential settlements in the vicinity of the walls.

6.1 IMPROVEMENTS IN PRACTICE

As a simple preliminary approach, the effects of basement walls may be allowed for as follows:

- By adding a proportion of the vertical and lateral resistances of the walls to the resistances of the foundation system, taking due account of the possible interactions between the walls and the deep foundations;
- By adding a proportion of the estimated vertical and lateral stiffnesses of the walls to those of the foundation system. Calibration of this proportion is ongoing, but as an initial estimate, a factor of 0.4 may be reasonable;
- By modelling the walls as a series of piles of equivalent vertical and lateral stiffness. The author is currently investigating the validity of this approach, and example of the outcomes are given above.

For detailed design purposes, a three-dimensional finite element, or finite difference, analysis can of course be undertaken, representing the basement walls as embedded structural elements with appropriate stiffness and interface strengths.

7 IGNORING EXTERNAL GROUND MOVEMENTS

In contemporary urban environments, it is not unusual for excavations of tunnelling works to be carried out in proximity to planned or existing deep foundations. If such works are known or anticipated, it is possible to make allowances in the design of the deep foundations. If they are carried out after construction of the deep foundations, then it is necessary to assess the impact of such works on the integrity and movement of the existing foundations.

Consideration is given here to the effects of tunnelling adjacent to a deep foundation, as shown in Figure 21. The ground movements due to the tunnel can be estimated via the equations developed by Loganathan and Poulos (1998) and the effect of these movements can be analysed as per the approach described by Chen et al (1999).

For the case shown in Figure 21, a volume loss of 1% is assumed for the 6m diameter tunnel, and the centreline of the tunnel is assumed to be 12m from the centreline of the pile, which is 36m long and 1.2m in diameter. The pile head is assumed to be fixed into a pile cap so that rotation is restrained. A horizontal load of 1 MN and a vertical load of 5 MN are applied at the pile head.

Pile-soil interaction analyses have been carried out to compute the induced horizontal displacement, bending moment, vertical settlement and axial load in the pile. These are shown in Figures 22 to 25 in turn.

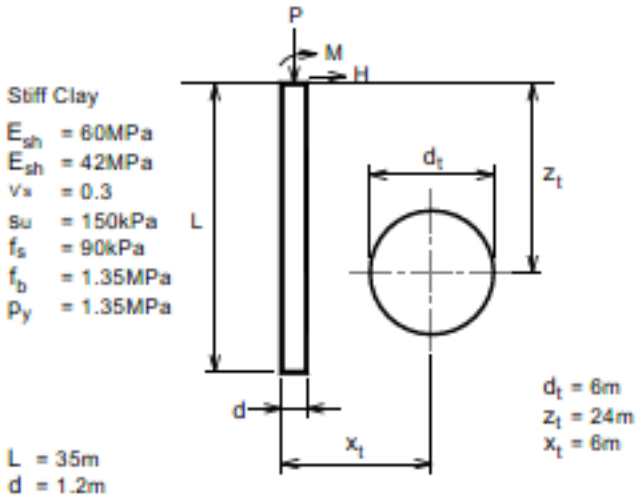

Figure 21: Example of a pile near a new tunnel

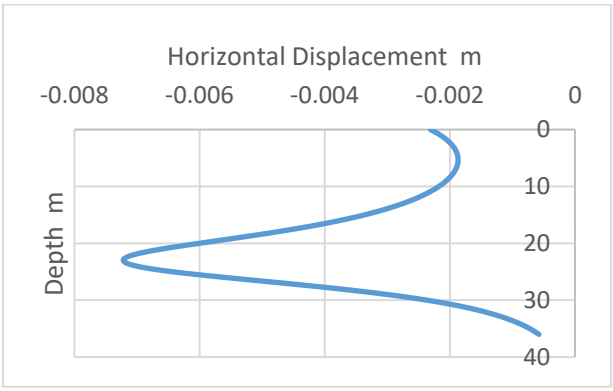

Figure 22: Horizontal displacements in pile due to applied load and tunnel

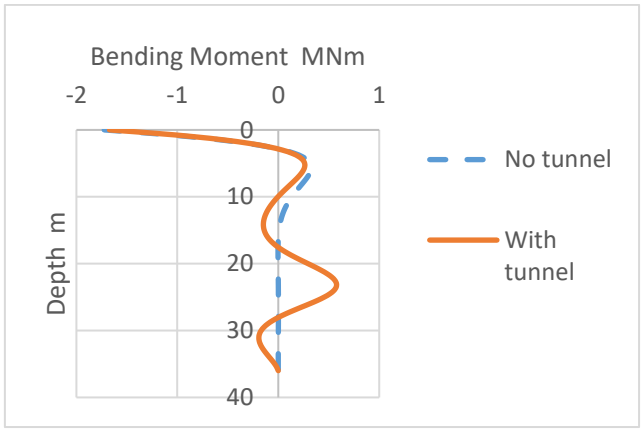

Figure 23: Bending moments in pile due to applied load and tunnel

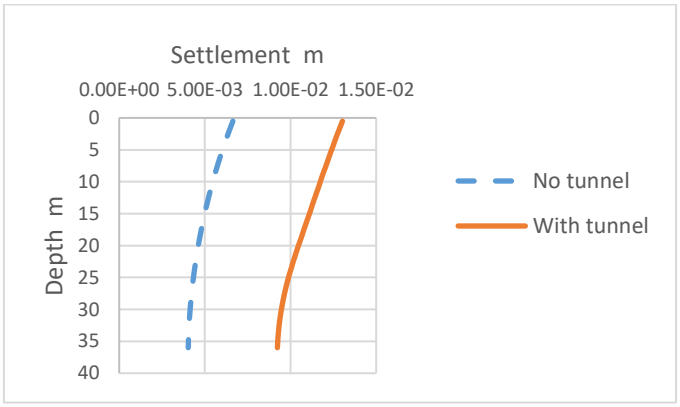

Figure 24: Vertical settlement of pile due to applied load and tunnel

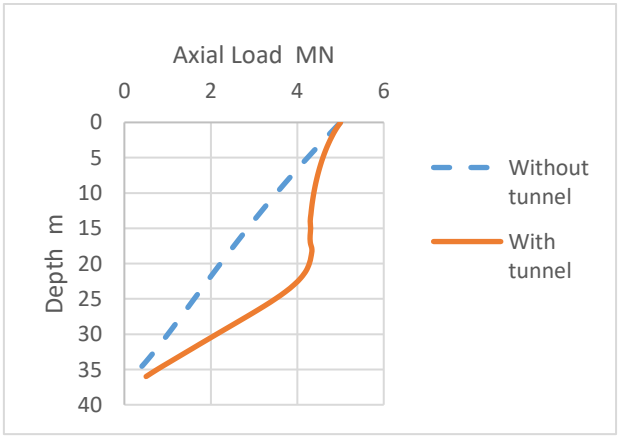

Figure 25: Axial forces in pile due to applied load and tunnel

From these figures, the following observations can be made:

1. The maximum horizontal displacement occurs near the level of the tunnel invert, and is significantly greater than the pile head displacement;
2. The maximum moment at the pile head is little affected by the tunnel, but there is a significant additional moment developed near the level of the tunnel invert. In many cases, this would be at a lower level than that at which the reinforcement is often terminated;

3. The tunnelling causes the pile head settlement to almost double in this case;
4. There is a "downdrag" component of axial force near the level of the tunnel invert, although in this case, the maximum axial force is still the applied force at the pile head.

This simple example illustrates that potentially harmful effects can arise from tunnel construction near existing piles. In particular, large bending moments can be developed in the pile near the level of the tunnel invert, which may be below the usual cut-off level for bored pile reinforcement. Consequently, if the possibility of future tunnelling operations is recognized, then consideration should be given to the use of full-length reinforcement.

Only a single pile is considered in this example, but group effects can be slightly beneficial and result in a modest reduction of the moments and axial forces induced in the pile.

A further example of the effects of ground movements often being overlooked is in the design of pile-supported embankments and bridge abutments. Many designers focus on the vertical response of the piles to the embankment loading, but significant lateral ground movements can be developed also, and these can cause significant bending moments and shears in the piles, especially those towards the edges of the embankment or abutment. Such cases have been considered by Stewart et al (1992, 1994) and Ellis and Springman (2001), while and some approximate design charts have been presented by Poulos (1994). It is clear that one-dimensional thinking (considering only vertical movements and effects) should be avoided when designing deep foundations for embankment-induced ground movements.

7.1 IMPROVEMENTS IN PRACTICE

Improvements in practice to cope with imposed ground movements may be made by:

- Recognizing or anticipating situations in which the ground surrounding the foundation may be liable to movements due to external influences; in many cases, lateral as well as vertical ground movements may occur.
- Taking account of such movements in making assessments of the foundation movements, and the forces and actions within the foundation system. Methods that can be used include simple hand methods (for example, the effects of vertical ground movements in imposing negative skin friction on piles), chart solutions for lateral ground movements, for example, Chen and Poulos (1997), or detailed finite element or finite difference analyses in which the source of ground movement is included within the modelling process.

It should be emphasized that group effects in such cases can be beneficial, and so estimating the response of a single pile is often both adequate and conservative.

8 IGNORING KINEMATIC SEISMIC EFFECTS

As a structure responds to seismic loading, inertial lateral loads are imposed on a foundation system. The influence of such inertial effects on the seismic response of pile foundations is well-recognized, and depends on the frequency content of the earthquake and the natural period of the pile-soil-cap-mass system. However, an earthquake also imposes kinematic actions on a deep foundation system because of the movement of the ground in response to the seismic excitation, and the consequent pile-soil interaction.

Mylonakis et al (1997) have identified the following characteristics:

1. Inertial bending can be significant, especially in the upper part of the piles, when the dominant period of the earthquake is similar to the fundamental period of the soil-pile-structure system.
2. Kinematic bending can be significant when the dominant period of the soil motions is similar to the natural period of the soil strata.

The three most likely areas of damage of a pile are the pile head, interfaces between layers of different stiffness, and the pile toe. Pile head damage is most likely in homogeneous strata while damage at strata interfaces is most likely when there is a marked stiffness contrast between the soil layers. The kinematic bending strains at the pile toe may be significant when the toe is restrained.

To facilitate an understanding of the relative importance of inertial and kinematic effects, analyses have been performed on the fixed head single pile shown in Figure 26. The analysis has been carried out via the pseudo-static approach described by Tabesh and Poulos (2001), so that the results provide an envelope of maximum bending moments and shears along the pile. It is assumed that the site is subjected to the 1994 Northridge earthquake with a maximum bedrock acceleration of 0.2g.Three cases have been considered:

- A pile with no vertical load/cap mass;
- A pile with a lateral inertial load of 0.2MN;

- A pile with the same lateral inertial load as in the second case, but where the kinematic ground movements are included in the analysis.

Figure 27 shows the computed distributions of bending moment along the pile. Two key points emerge from this figure:

1. If kinematic effects are ignored, and only inertial (lateral load) effects are considered, the maximum moment at the pile head can be seriously under-estimated.
2. If only inertial effects are considered, the moment at depths in excess of about 7m becomes insignificant, but with the kinematic effects incorporated, there is a significant moment between depths of about 7 to 10m, i.e. in the vicinity of the interface between the softer upper layer and the stronger lower layer.

The importance of considering both kinematic as well as inertial effects is clearly emphasized in this example. As with the example of ground movements due to tunnelling, it is possible that full-length reinforcement would be required for bored piles, especially if significant layering of the soil profile exists and there is a distinct stiffness contrast between adjacent layers.

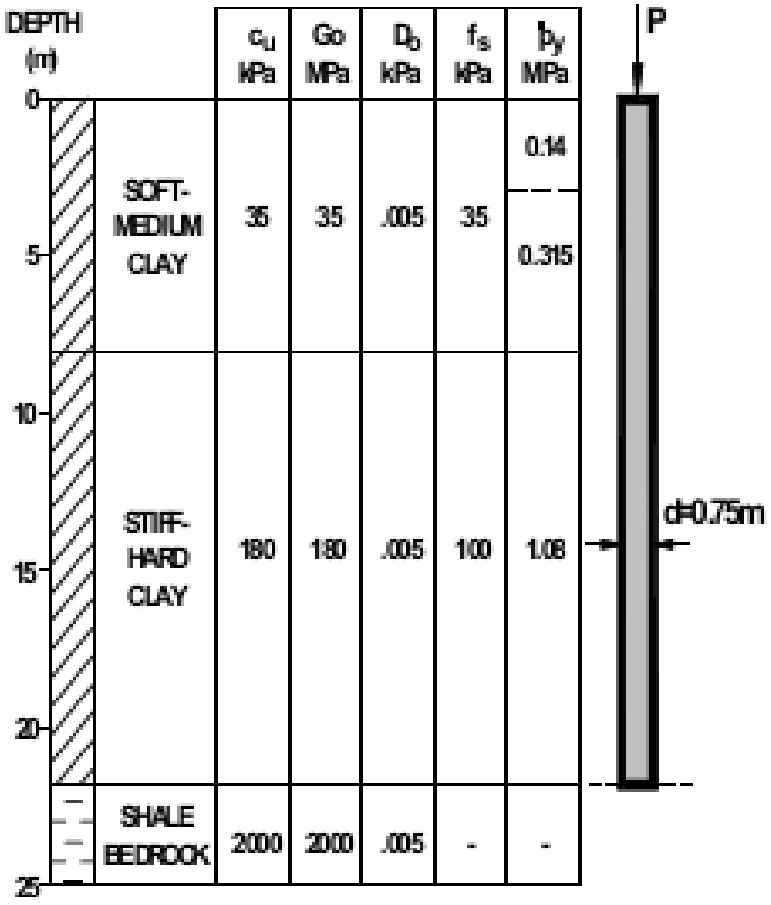

Figure 26: Example for effect of kinematic loading

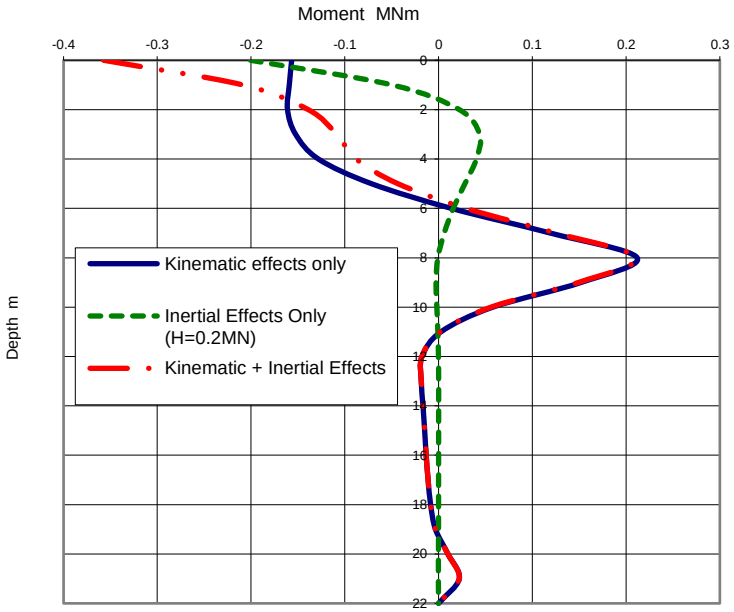

Figure 27: Computed bending moment distributions

A. IMPROVEMENTS IN PRACTICE

There are a number of relatively simple methods available for estimating the maximum moment in a pile due to kinematic soil movements. These include Nikolaou et al (2001), Di Laora et al (2012), and Dezi et al (2010) for single piles, and Dezi and Poulos (2016) for square pile groups. In all cases, the maximum moment tends to be at the interface between layers of differing stiffness. Such approaches are generally adequate to provide an indication of the potential for structural damage of the pile. If a more detailed investigation is warranted, then pseudo-static or full dynamic analyses are available.

9 ASSUMPTION OF ELASTIC BEHAVIOUR OF PILES

In designing piles for lateral loading, it is common to assume that a pile itself remains elastic during the entire loading process. While this may be a reasonable assumption for steel piles, it may be an over-simplification for concrete piles. A typical moment-curvature relationship for a bored pile is shown in Figure 28, and it can be seen that there is significant non-linearity in the relationship.

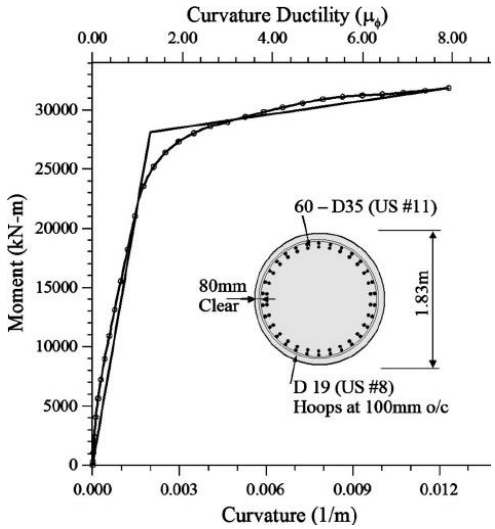

Figure 28: Typical moment – curvature relationship for bored pile

The effect of such pile non-linearity has been examined in a number of papewrs, for example, Ashour et al (2001), Kramer and Heavey (1988), Hsueh et al (2004). Kramer and Heavey have shown that even a simple elastic-plastic relationship for the pile can provide results that are in reasonable agreement with measurements of lateral pile behaviour. Figures 29 and 30 show an example of the improved agreement with observed behaviour when a simple non-linear elastic-plastic model is used for the pile.

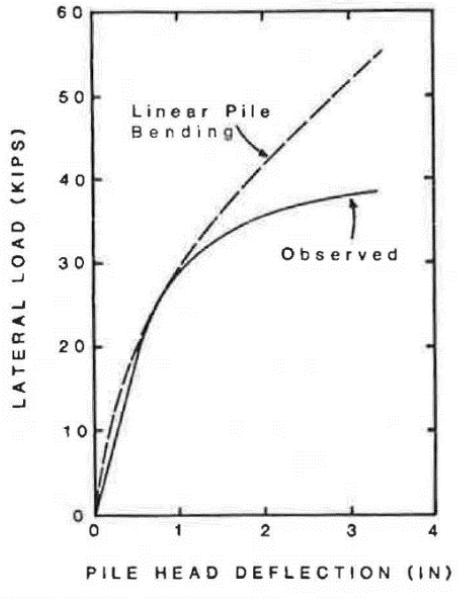

Figure 29: Comparison between linear model and observed behaviour (Kramer and Heavey, 1988)

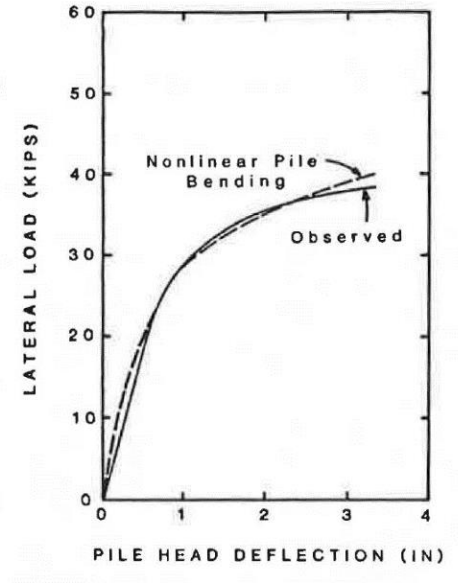

Figure 30: Comparison between non-linear model and observed behaviour (Kramer and Heavey, 1988)

A further example of the effects of using a non-linear pile model are shown in Figure 31 for a 0.76 m diameter bored pile in stiff clay (Ashour et al, 2001). Here, the load-deflection curve for a non-linear pile model is shown together with solutions for various values of the bending stiffness (EI) of an elastic pile. A would be expected, at low loads, the solution for the non-linear pile is the same as that for a linear pile with the same initial bending stiffness. However, as the load increases, there is a gradual transition from the initial curve for a linear pile across curves for decreasing values of EI.

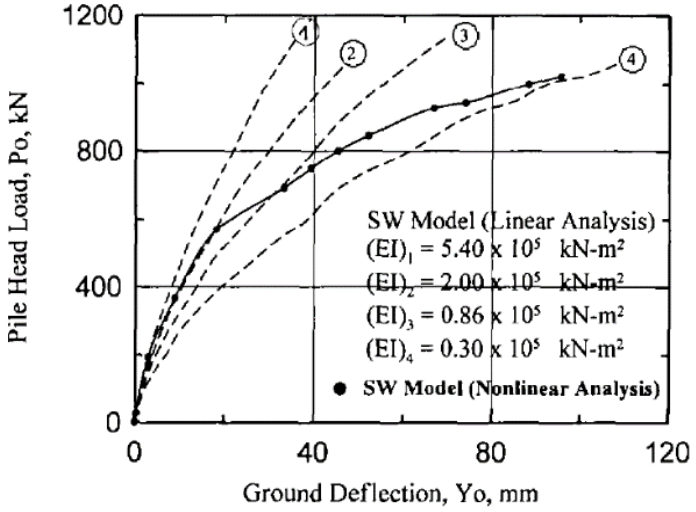

Figure 31: Load-deflection curves for non-linear pile model and for various EI values for a linear model (Ashour et al 2001)

9.1 IMPROVEMENTS IN PRACTICE

As a practical approximation, it may be feasible to use a series of computed load-deflection curves, for different pile stiffness values, to construct a non-linear curve, by starting the transition once the initial cracking moment of the pile section is reached, and then gradually moving across the curves for decreasing bending stiffness. From Figure 36, it may be expected that, for relatively low levels of lateral load, the use of a concrete modulus perhaps 1/3 to 1/2 of the small-strain value might provide an adequate result, but in any case, a measure of judgement is required to adopt an equivalent modulus to represent the non-linearity of the pile behaviour in bending.

For more detailed assessments of pile non-linear behaviour, commercial software packages are available, for example later versions of the programs LPILE and GROUP8 (Ensoft, 2015).

10 CONCLUSIONS

This paper has examined a number of aspects of design which are considered by the author to be inadequate, or else in need of improvement. These commonly-employed aspects have the potential to lead to inaccurate predictions of deep foundation behaviour.

The following factors are found to have the potential to lead to unconservative designs:

1. Ignoring foundation interactions;
2. Ignoring the effects of ground movements;
3. Ignoring the kinematic effects of ground movements in seismic design.

Conversely, the following factors may lead to conservative, and hence unnecessarily expensive, design outcomes:

1. Ignoring the beneficial effect of the raft;
2. Assuming a rigid cap or raft;
3. Over-simplification of the ground profile;
4. Ignoring the beneficial effects of basement walls;

With the design tools that are now available, all of the above perceived inadequacies can be addressed satisfactorily. There is however ample scope for innovation to be employed to develop effective and economical means of designing deep foundations and incorporating the key features of a particular project. The main challenges that remain in relation to foundation design are the recognition and modelling of the factors that can influence deep foundation behaviour, and the ever-present challenge of appropriate assessment of the relevant geotechnical parameters.

11 REFERENCES

Al-Douri, R. and Poulos, H.G. (1994). Behaviour of pile groups in calcareous sand. *Geotech. Eng.* Vol. 25, No. 2, pp 3-19.

Ashour, M., Norris, G.and Shamsabadi, A.(2001). Effect of the non-linear behaviour of pile material on the response of laterally loaded piles. *Int. Conf. on Recent Advances in Geot. Earthquake Eng. and Soil Dynamics*, 15.

Brown, P.T. (1969). Numerical Analyses of Uniformly Loaded Circular Rafts on Deep Elastic Foundations. *Geotechnique* 19(3): 399-404.

Chen, L.T. and Poulos, H.G. (1997). Piles subjected to lateral soil movements. *Jnl. Geot. and Geoenv. Eng.* ASCE, 123(9): 802-811.

Chen, L.T., Poulos, H.G**.** and Loganathan, N. (1999). Pile responses caused by tunnelling. *Jnl. Geotech. and Geoenvir. Eng.*, ASCE, 125(3): 207-215.

Chow, H.S.W. and Poulos, H.G. (2019). "Effects of basement resistance on tall building foundation behaviour". *Proc. 13th ANZ Conf. on Geomechanics*, Perth, Paper 27.

Coffey (2011). *CLAP users' manual*. Coffey Geotechnics, Sydney, Australia.

Dezi, F., Carbonari, S. and Leoni, G. (2010). Kinematic bending moments in pile foundations. *Soil Dynamics and Earthquake Engineering*, 30: 119-132.

Dezi, F. and Poulos, H.G. (2016). Kinematic bending moments in square pile groups. *International Journal of Geomechanics*, doi: 10.1061/(ASCE)GM.1943-5622.0000747,04016066.

Di Laora, R., Mandolini, A. and Mylonakis, G. (2012). Insight on kinematic bending of flexible piles in layered soil. *Soil Dynamics and Earthquake Engineering*, 43: 309-322.

Ellis, E.A. and Springman, S.M. (2001). Full-height piled bridge abutments constructed on soft clay. *Geotechnique*, 51(1): 3-14.

Ensoft (2015). GROUP8 and LPILE. Ensoft, Austin, TX, USA.

Fleming, W.G.K., Weltman, A.J., Randolph, M.F. & Elson, W.K. (2009). *Piling engineering.* 3rd Edition, Spon Press, London.

Geocentrix. (2013). REPUTE v2. Geocentrix, Banstead, Surrey, UK.

Golder, H.Q. & Osler, J.C. (1968). Settlement of a furnace foundation, Sorel, Quebec. *Can. Geot. Jnl.*, 5(1): 46-56.

Hsueh, C-K, Lin, S-S, and Chern, S-G. (2004). Lateral performance of drilled shaft considering nonlinear soil and structural material behaviour. *Jnl. Marine Science & Technology*, 12 (1): 62-70.

Juang, C., Schuster, M., Ou, C., and Phoon, K. (2011). Fully probabilistic framework for evaluating excavation-induced damage potential of adjacent buildings. J. Geotech. Geoenviron. Eng., 10.1061/(ASCE)GT.1943-5606.0000413, 130-139.

Kramer, S.L. and Heavey, E.J. (1988). Analysis of laterally loaded piles with nonlinear bending behaviour. *Trans. Res. Record* 1169, 70-74.

Loganathan, N. and Poulos, H. G. (1998), Analytical prediction for tunneling-induced ground movements in clays, *J. Geotech. Engrg ASCE, 124, No.9, 846-856*.

Mandolini, A. and Viggiani, C. (1997). Settlement of piled foundations. *Géotechnique*, 47(4): 791-816.

Mylonakis, G., Nikolaou, A. and Gazetas, G. (1997). Soil-pile-bridge seismic interaction: kinematic and inertial effects. Part 1: soft soil. *Earthquake Eng. and Struct. Dynamics*, 26(3): 337-369.

Nikolaou, S., Mylonakis, G., Gazetas, G. and Tazoh, T. (2001). Kinematic pile bending during earthquakes: analysis and field measurements. *Geotechnique*, 51(4): 425-440.

Pirello, S. and Poulos, H.G. (2013). Comparison of four pile group analysis programs". *Advances in Foundation Engineering*, Ed. K.K. Phoon, T.S. Chua, H.B. Yang and W.M. Cham, Singapore, 291-297.

Poulos, H.G. (1968) Analysis of the settlement of pile groups. *Geotechnique*, 18:449-471.

Poulos, H.G. (1988). Modified calculation of pile-group interaction". *Jnl. Geot. Eng.*, ASCE, Vol. 114, No. 6, pp. 697-706.

Poulos, H.G. (1990). DEFPIG user's manual. Centre for Geot. Research, Univ. of Sydney.

Poulos, H.G. (1994). Settlement prediction for driven piles and pile groups. *Spec. Tech. Pub. 40, ASCE*, 2: 1629-1649.

Poulos, H.G. (1994a). Analysis and design of piles through embankments. *Proc. Int. Conf. Design and Constrn. Deep Founds.*, US FHWA, 3: 1403-1421.

Poulos, H.G. (1999). The design of piles with particular reference to the Australian piling code. *Aust. Geomechanics*, 34(4): 25-39.

Poulos, H.G. (2017). *Tall building foundation design.* CRC Press, Boca Raton, USA.

Poulos, H.G. and Badelow, F. (2015). Geotechnical parameter assessment for tall building foundation design". *Int. Jnl. High-Rise Buildings*, 4(4): 227-239.

Poulos, H.G., Carter, J.C. and Small, J.C. (2001). Foundations and retaining structures – research and practice. *Theme Lecture, Proc. 15th Int. Conf. Soil Mechs. Geot. Eng*., Istanbul, Balkema, 4:2527-2606.

Poulos, H.G. and Davids, A.J. (2005). Foundation design for the Emirates Twin Towers, Dubai. *Can. Geotech. J.*, 42**:** 716-730.

Poulos, H.G. and Davis, E.H. (1980). *Pile foundation analysis and design*. John Wiley, New York.

Randolph, M.F. (1994). Design methods for pile groups and piled rafts. State of the Art Rep., *Proc., 13th ICSMFE*, New

Delhi, Vol. 5, 61–82.
Randolph, M.F. (2003). Science and empiricism in pile foundation design. 43rd Rankine Lecture, *Geotechnique*, 53(10): 847-875.
Randolph, M.F. (2004). PIGLET. Analysis and design of pile groups. Users' Manual, University of Western Australia, Perth, Australia.
Small, J.C. and Poulos, H.G. (2007). A method of analysis of piled rafts. *Proc. 10th ANZ Conf. Geomechanics*, Brisbane, Australian Geomechanics Society, Vol. 2, pp.602-607.
Stewart, D.P., Jewell, R.J. and Randolph, M.F. (1992). Bridge abutments on soft clay – experimental data and simple design methods. Proc. 6th Aust. – NZ Conf. Geomechanics, Christchurch, 199-204.
Stewart, D.P., Jewell, R.J. and Randolph, M.F. (1994). Design of piled dbridge abutments on soft clay for loading from lateral soil movements. Geotechnique, 44(2): 277-296.
Tomlinson, M.J. (2004). *Pile design and construction. 4th Ed.,* Spon, London.
Zhang, L. and Ng, A.M.Y. (2006). Limiting tolerable settlement and angular distortion for building foundations. *Geotech. Special Publication No. 170, Probabilistic Applications in Geotechnical Engineering*, ASCE (on CD Rom).

THE DESIGN AND CONSTRUCTION OF VERY DEEP EXCAVATIONS – RECENT DEVELOPMENTS

David John Puller (BSc MSc DIC CEng FICE)

Director

Geotechnical Experts Limited

ABSTRACT

Technical advancements in construction plant, materials and numerical analysis tools have made possible a step change in the achievable depth of excavations required for infrastructure, building and mining projects. This has been in response to an increased complexity in such projects particularly in connection with rail, water and power infrastructure sectors around the globe. Such advances do not come without some risks and a clear understanding of the limitations of the techniques, capabilities of construction monitoring and the benefits of practical design details are key to successful execution. In addition, a sound knowledge of the behaviour and testing of materials particularly fresh concrete and support fluids is essential in the minimisation of defects in deep earth retaining structures, which can be extremely costly to remediate.

This paper considers the state of the art in the construction of very deep and complicated excavations by making reference to a number of recent case histories, where records have been broken and new technologies have been deployed. The construction of diaphragm walls to depths well in excess of 100 m and with wall thickness of 1800 mm and using concrete with a 28-day cube strength in excess of 60 MPa are now possible, provided great care is taken. Improved verticality tolerances of better than 1 in 400, coupled with precise monitoring and advanced design techniques, means that the structural capacity of earth retaining walls in shaft construction have increased significantly which has led to the realisation of deeper excavations, together with deep openings which may be necessary for associated tunnels.

The author will also include the presentation of recent improvements in safety both in cage lifting, handling and splicing as well as around open diaphragm wall excavations. A better understanding of the causation of defects in concrete which has been placed under support fluid via a tremie, has been gained through painful experience and has greatly benefitted from the recent publication of useful guidance in Australia, UK and by the EFFC (European Federation of Foundation Contractors). This has led to a number of new site tests on fresh concrete for mix stability and bleed potential which are gaining increasing traction in the industry. In addition, the introduction of more stringent testing on support fluid such as bentonite during excavation means that instances of defects including leaks, inclusions and areas of poor concrete cover can be reduced. However, despite the availability of extensive guidance on good reinforcement cage detailing for diaphragm cages, examples of poor practice still remain, with great potential to lead to extensive defects such as mattressing which may compromise the durability of permanent works. The author will highlight examples of good and bad practice.

1 INTRODUCTION

The requirements of new transportation infrastructure in road and rail to be threaded beneath existing assets has led to the development of deeper excavations in increasingly challenging ground conditions for cut and cover approaches and shafts for ventilation as well as TBM launch and reception. For example, on the Tuen Mun – Chek Lap Kok Link Project in Hong, a 500 m long section of highway tunnel was constructed within a 43 m deep excavation within a cellular diaphragm wall also known as the “Caterpillar” comprising 15 interlocking cells (Schwob, 2019). Other new infrastructure projects for stormwater storage have also required exceptionally large shafts for pumping stations, for example the Lee Tunnel Project in the UK (Stanley, 2014) which included the construction of five very deep diaphragm wall shafts up to 98 m deep with the deepest for a pumping station 38 m in diameter and an excavation depth of 86.5 m. Meanwhile in countries such as Mexico twelve level basements have been constructed for car parking for commercial buildings. Finally, in a somewhat unusual application a diaphragm wall shaft of 120 m depth was fully excavated as part of a mining project in the UK.

.

2 CONSTRUCTION PROCESSES ASSOCIATED WITH VERY DEEP EXCAVATIONS

Earth and groundwater retention to facilitate such deep excavations is generally beyond the range of application of sheet and bored piling techniques and necessitates the installation of diaphragm walling. A key driver in the achievement of very deep diaphragm walls is due to the advancements made in the development of excavation plant by equipment manufacturers such as Bauer and Soletanche Bachy (see **Figure *1***). The Trench Cutters or Hydrofraises produced by both companies are able to excavate panels to well in excess of 100 m and equipped as they are with the latest on-board monitoring equipment which enables real time correction of the vertical alignment during excavation by the operator such that tolerances better than 1 in 400 are achievable.

Figure 1: Bauer Trench Cutter (left) and Soletanche Bachy Hydrofraise (right)

For the purpose of this paper, the author would like to focus on the design and construction of deep diaphragm wall shafts. A structural slurry wall or diaphragm wall consists of a series of reinforced concrete panels which are usually structurally discontinuous and abut each other at panel joints which are commonly defined by temporary steel or occasionally permanent precast concrete stopends. However, in the case of diaphragm walls greater than ca. 75m in depth the use of such stopends is impractical and the excavation usually necessitates the use of a trench cutter or hydrofraise with joints created by overcutting concrete previously formed in primary panels with secondary panels (see **Figure *2***).

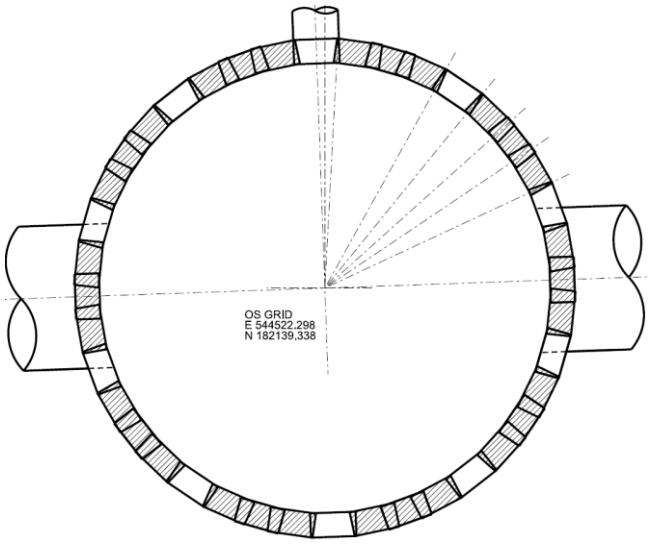

Figure 2: Example of shaft panel layout incorporating overcut panel joints (Lee Tunnel Project)

This form of panel joint is generally considered to be less watertight than in the case of a joint formed using a stopend system. However, in the case of a circular shaft where the nature of structural forces is in most cases overwhelmingly hoop compressive across panel joints it is generally found that groundwater leakage across overcut joints formed in this way is acceptably low.

Effective centralisation of primary panel cages to minimise the risk entanglement with reinforcement during overcutting secondary panels with potentially disastrous consequences for plant is essential. Two different temporary works solutions are shown in **Figure *3*** below. On the left at Lee Tunnel, corrugated plastic pipes were used as spacers together with triangular polystyrene wedges to minimise the volume of concrete in the panel overcut. At the Woodsmith Mine (on the right) sacrificial glass fibre reinforcement was used to centralise primary cages.

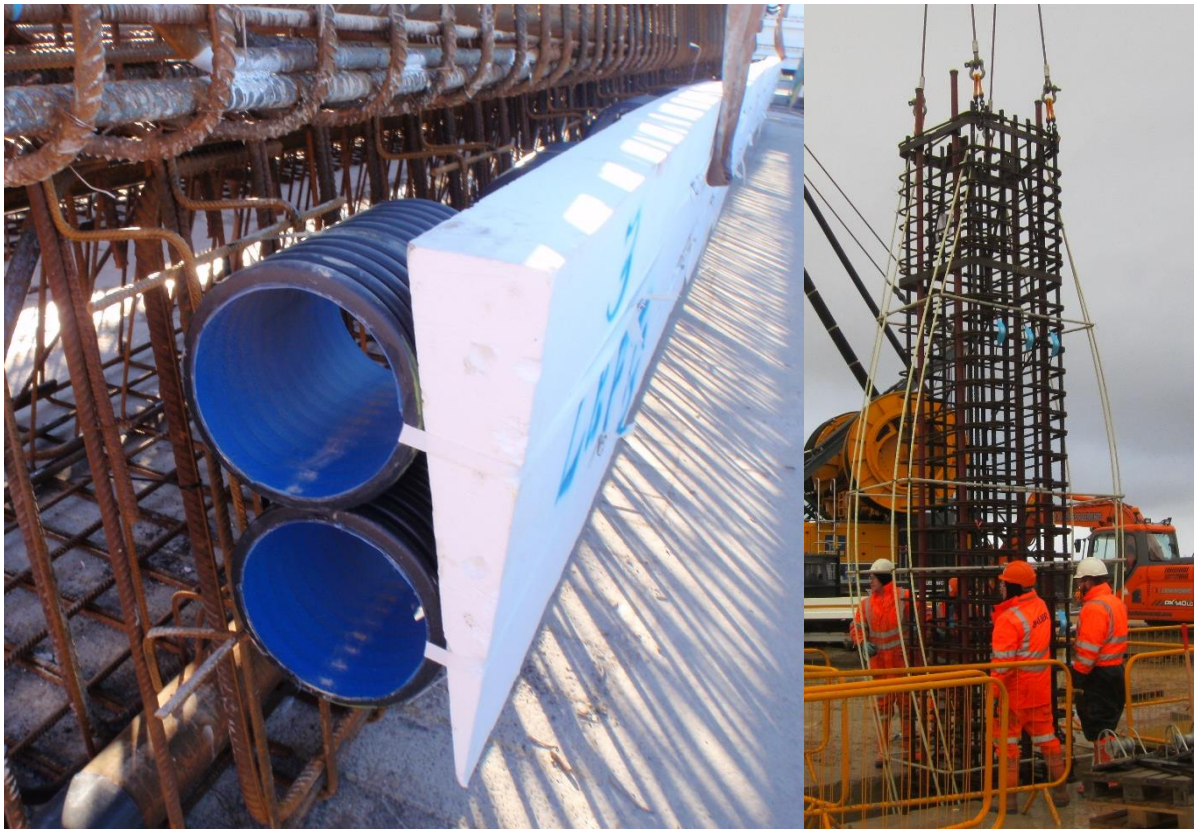

Figure 3: Measures taken to minimise risk of overcutting primary panel reinforcement

The design of diaphragm wall shafts is frequently governed by the magnitude of hoop stresses which are generated by earth and groundwater pressures and which can be concentrated locally around opening for tunnels. Since hoop stresses must be resisted across the net contact area between panel joints allowing for construction tolerances, advances in both wall thickness with 1800 mm now in use and improved accuracy during excavation, has permitted bigger and deeper shafts. Verticality monitoring using a combination of on-board real time systems together with confirmatory checks after excavation using Koden (Ultrasonic Drilling Monitor) provides reliability that tolerances specified in the design have been achieved.

Acknowledging the fact that the excavation tool whether hydrofraise or trench cutter can be effectively steered by the operator adjusting hydraulic pads as excavation proceeds, means that a simple verticality tolerance of 1 in xxx is not strictly appropriate for very deep diaphragm walls and in fact an absolute deviation of xx cm is more relevant. For example at the Woodsmith Mine, 120 m deep shaft panels were constructed to within a 20 cm absolute deviation which would correspond to a verticality of 1 in 600. This was achieved by Bauer using a combination of Cutter Inclination Survey (CIS) together with a Koden check on every panel (see **Figure *4***). The shaft design required only a 1200 mm thick wall with a concrete strength of a C45/55 for an 8 m diameter shaft which was excavated over its full depth to 120 m.

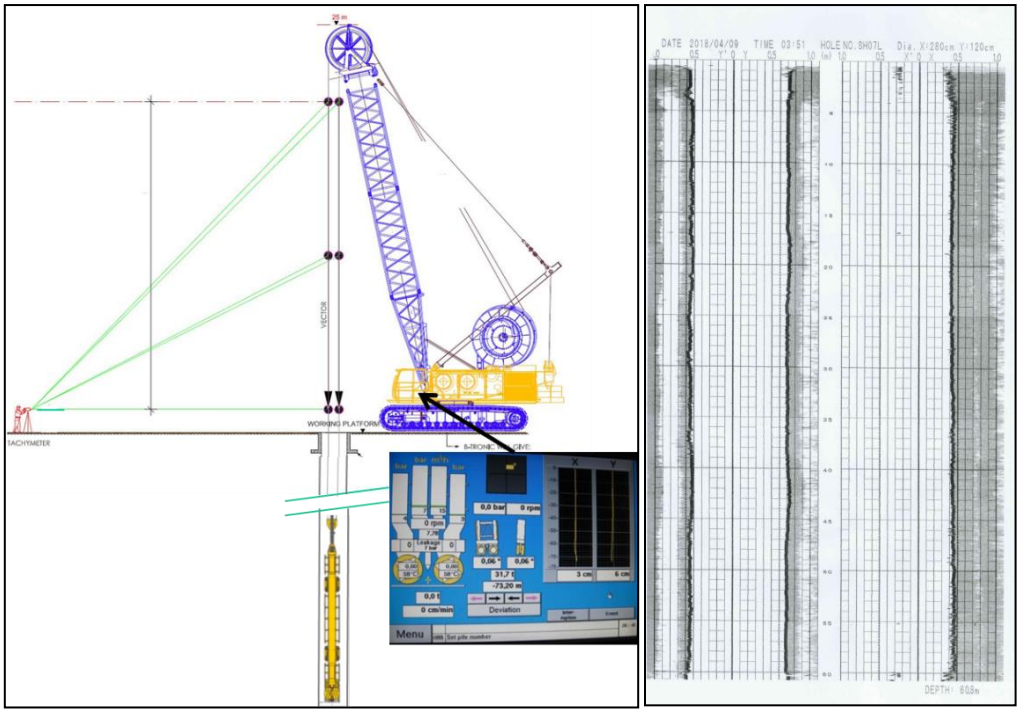

Figure 4: Verticality monitoring during excavation by CIS (left) and afterwards by Koden (right)

3 IMPROVED UNDERSTANDING OF THE BEHAVIOUR OF CONSTRUCTION MATERIALS

3.1 TREMIE CONCRETE

The construction of very deep diaphragm walls places additional requirements on the performance of concrete which must be placed via a tremie through a support fluid. Large pour volumes in excess of 1,000 m3 require high workability over an extended duration and with panel depths reaching 100 m this means that mix stability and the control of bleed under high pressures is particularly important. It is often the case that structures for infrastructure projects are designed for an intended life of greater than 100 years and this together with potential exposure to de-icing salts and/or marine conditions places high requirements on durability.

The combination of these requirements in the fresh and hardened state has led to increasingly complex concrete mix designs with various admixtures and cement combinations. As a consequence, a deeper understanding of the behaviour of tremie concrete has become essential and accompanying new methods of specifying and testing have become accepted practice.

The Concrete Institute of Australia Guide first published in 2012 showed much foresight paving the way for new forms of concrete testing to be introduced (Concrete Institute of Australia, 2012). Later on, The European Federation of Foundation Contractors (EFFC) Guide to Tremie Concrete for Deep Foundations (EFFC-DFI, 2018) and Institution of Civil Engineers Specification for Piling and Embedded Retaining Walls (ICE, 2017) were published with more developed requirements and guidance on concrete mix design, control and testing as well as tremie practice. The key driver in developing these new guidelines was the avoidance of defects primarily in the cover zone of completed panels. For example, excessive bleed rate can cause channelling or outwash of fines from the concrete in the cover zone and along reinforcement bars. Premature loss of workability coupled with poor reinforcement detailing can cause mattressing features whereby concrete is unable to flow around and coalesce fully around reinforcement bars leaving a patterning visible on the surface of panels on exposure.

As a result, gone are the days when simply testing workability by slump or flow table together with strength testing of cube or cylinder is sufficient. In order to minimise the risk of defects associated with excessive bleed, mix instability of loss of workability it is essential that any concrete mix design which has not been previously used successfully in comparable works is validated in pre-start trials and is subject to the following tests.

a) Visual Stability Index (VSI)

Visual Stability Index is a qualitive measure of segregation resistance and water retention. Unstable concrete with a VSI of 2 or 3 will exhibit a halo of water around concrete placed on a flow table and may indicate clear segregation of coarse aggregate. Only concrete with a VSI of 0 or 1 should be considered acceptable (see **Figure 5**).

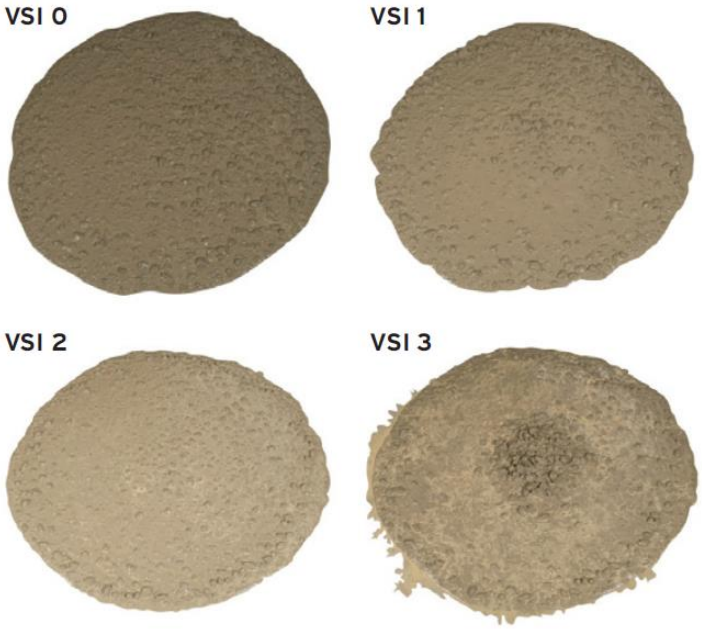

Figure 5: Assessment of visible stability index according to EFFC Guide

b) Bleeding and Bleeding Rate

Bleed rate can be assessed at atmospheric pressures in a steel vessel according to ASTM C1610. If the rate at which bleed water is expelled over the first two hours of bleeding exceeds 0.1 ml/min then there is an increased risk of channelling. Bleed rates below 0.1 ml/min are considered acceptable.

c) Bauer Filtration

The Bauer Filtration test is a rapid test lasting only 5 minutes where a cylinder of 1.5 litres of concrete is subjected to a pressure of 5 bars and the filtrate volume displaced is measured. Values greater than 22 ml are considered to be indicative of a risk of segregation and excessive bleed.

d) Consistence (Workability) Retention

Workability retention involves repeating flow or slump testing at intervals (usually 30 minutes) to assess whether there is a risk of sudden loss in workability which may lead to problems of adequate flow of concrete during tremie placement, taking into account the size of the panel and the likely duration of the pour.

3.2 SUPPORT FLUID

Support fluid, usually in the form of bentonite slurry is maintained in the trench to maintain stability from excavation through to completion of concreting. However, in the case of deep diaphragm walls excavated by trench cutter or hydrofraise the support fluid also provides the transport medium for the spoil during excavation and this means that in certain soils the support fluid can load up with fine material very rapidly. This can contribute to excessively thick bentonite cake which can be difficult to remove effectively. This can in turn adversely affect the end bearing and shaft friction resistance of walls subject to vertical loading. Also fragments of thick filter cake

can break off and become included in the concrete or within the reinforcement cage particularly at box outs and reservations. In order to reduce the risk of excessive cake build up, the ICE Specification indicates a recommended maximum density of 1.35 g/cm^3 for bentonite support fluid during excavation. The EFFC/DFI Guide to Support Fluids published in 2019 provides an excellent reference dealing with bentonite and polymer support fluids.

The author would like to make one further point with respect to best practice using support fluids in deep diaphragm walling and that is it is highly recommended to keep separate storage of excavation and concreting muds and to carry out a full exchange prior to concreting in order to afford the concrete, placed by tremie, the best opportunity to fully displace the slurry with minimum risk of entrapment within the body of the panel.

4 IMPROVEMENTS IN DESIGN AND MONITORING

Deep excavation design is routinely undertaken using three dimensional numerical models. Whereas once circular shaft analysis would be carried out assuming axisymmetric conditions, nowadays the ability to consider for example the effects of surface surcharges, openings in the wall for tunnels or multiple cellular shafts lends itself to three-dimensional modelling. In the case of the Woodsmith Mine the analysis required consideration of the main 120 m deep service shaft located within a 55 m deep headgear chamber (see *Figure 6*). Such deep and complex excavations should always be accompanied by an effective geotechnical monitoring scheme in order to compare actual performance with design predictions.

In designing geotechnical monitoring for diaphragm wall shafts it should be borne in mind that the structure will have high stiffness and that wall deformations are likely to very small and less than can be accurately monitored by inclinometers (Schwamb, 2016). Alternatives using strain gauges and/or fibre optics should be considered in order to obtain useful data.

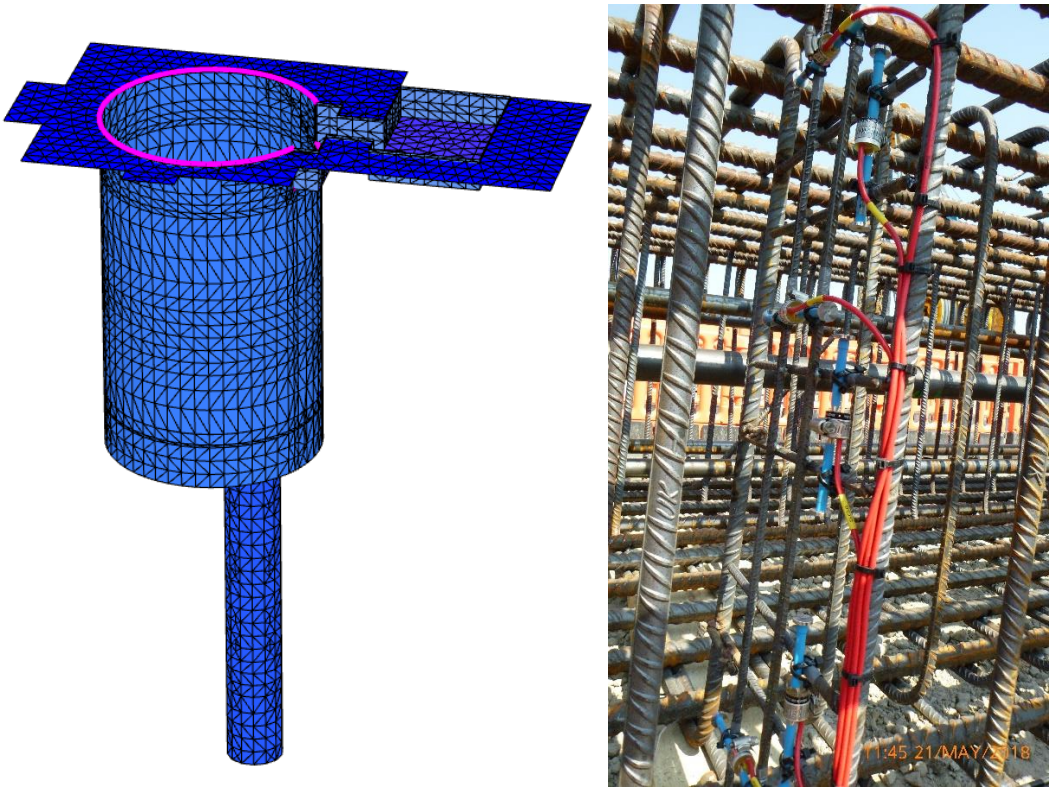

Figure 6: Sophisticated numerical modelling complemented by effective geotechnical monitoring

5 IMPROVEMENTS IN CONSTRUCTION SAFTY IN DIAPHRAGM WALLING

As constructors continue to strive to reduce the potential to cause harm to operatives during construction, processes evolve and practices considered unavoidable in the past can be replaced by improvements which lead to a step change in health safety risks. The author would like to highlight three areas of development in diaphragm wall construction.

5.1 EDGE PROTECTION AND PANEL COVERS

Previously, diaphragm wall excavations were carried out without edge protection leading to potentially hazardous conditions especially on poorly lit sites during night shift working. Recently though, simple systems have been developed employing railings which are temporarily fixed to guide walls to act as barriers to keep operatives out of harms way. Concreting covers are also placed on guide walls to provide a safe working platform for operatives involved in handling tremies during concreting (see Figure 7).

Figure 7: Edge protection barriers fixed to guide walls (left) and panel covers during concreting (right)

5.2 CAGE DESIGN

In the past, the incorporation of temporary works steel in reinforcement cages to facilitate fabrication, handling, transportation, loading and unloading, storage and then lifting to the vertical prior to lowering into the panel was based on previous experience, usually without any specific design. However, this has changed during the last few years in the UK supported by the Federation of Piling Specialists (FPS) and cage design is now required to be carried out by a competent designer (FPS, 2016). For example, taking into account cage weight and centre of gravity suitable lifting points must be established for safe lifting and the cage must be designed to be suitably rigid taking into account all bending moments and shear forces induced in the cage during lifting.

5.3 CAGE SPLICING

Hand injuries remain amongst the commonest form of injury in construction and yet operatives are still required to place their hands in harms way when splicing together reinforcement cages during lowering into the open trench. This unsafe practice is unavoidable if cages are spliced by welding or bull dogs but there are now a number of faster and safer cage splicing systems available which do not require fingers to be placed in dangerous locations. For example, the Superlatch system employs a spring-loaded latch which rides over and then engages with a lifting band at the splice location (see Figure 8). However, challenges still remain as reservation tubes installed in cages for grouting, sonic testing or inclinometers require pushing together at cage splices which still represents a risk to operatives.

Figure 8: Superlatch cage splicing system

6 RECOMMENDATIONS FOR SUCCESSFUL OUTCOMES

The significant advances in diaphragm wall equipment, concrete materials and numerical analysis means that diaphragm wall shafts in excess of 100 m depth are readily achievable. However, with these advances there are accompanying risks which need to be mitigated and the following recommendations are made by the author.

a) Employ at least two independent methods of monitoring actual deviation of excavation (on board real time and post-excavation using Koden).
b) Utilise effective measures to ensure that primary panel reinforcement cages remain in their intended plan position to minimise risk of overcutting reinforcement.
c) Carry out rigorous testing on full scale concrete batching trials unless the same concrete mix design has been used successfully on a comparable application. Tests to include Visual Stability Index, workability retention, bleed to ASTM and Bauer Filtration as a minimum.
d) Consider checks of support fluid density during excavation in order to minimise risk of excessive filter cake build up.
e) Ensure effective geotechnical monitoring is implemented using strain gauges and/or fibre optics to ensure reliable measurements.
f) And most importantly, deploy the latest in best safety practice by providing edge protection around open trenches and panel covers as safe working platforms during concreting. Ensure reinforcement cages are designed by a competent person to be handled and lifted safely. Utilise safe systems for splicing cages together during installation in the panel.

Figure 9: Diaphragm wall shaft

7 REFERENCES

Concrete Institute of Australia. (2012). Recommended Tremie Practice for Deep Foundations. First Edition.

EFFC-DFI. (2018). Guide to Tremie Concrete for Deep Foundations. Second Edition.

EFFC-DFI. (2019). Guide to Support Fluids for Deep Foundations. First Edition.

Federation of Piling Specialists. (2016). Guidance Note – The design for splicing and lifting prefabricated and site fabricated reinforcement cages for piling and walling works.

Institution of Civil Engineers. (2017). Specification for Piling and Embedded Retaining Walls. Third Edition. London.

Schwamb, T., Elshafie, M.Z.E.B., Soga, K. and Mair, R.J. (2016). Considerations for monitoring circular excavations. *Proc Institution of Civil Engineers*.

Schwob, A. and Combe, B. (2019). Tuen Mun - Chek Lap Kok Link in Hong Kong. Innovative technologies and methodologies for an outstanding project. *Proc. Rapid Excavation and Tunnelling Conf*. 986-998.

Stanley, S., Sayavong, S., Hard, D., Gatward, J. and Puller, D. (2014). Design and construction of the Thames Water Lee Tunnel Shafts. *Proc. 5th Deep Foundations Institute & European Federation of Foundation Contractors Joint Conference; Global Perspectives on Sustainable Execution of Deep Foundation Works*.

GEOTECHNICAL CHALLENGES FOR CONSTRUCTION OF DIAPHRAGM WALLS AND FOUNDATION OF SYDNEY'S TALLEST BUILDING, CROWN SYDNEY HOTEL RESORT

Brad Azari[1], Sam Mirlatifi[2], Henk Buys[3], Ian Cullen[4]
[1]Geotechnical Engineer, AECOM, Sydney, Australia. brad.azari@aecom.com
[2]Technical Director, John Holland, Sydney, Australia. sam.mirlatifi@jhg.com.au; Formerly Associated Director, AECOM, Sydney, Australia.
[3]Technical Director, AECOM, Sydney, Australia. henk.buys@aecom.com.au
[4]Director, Bauer Foundations Australia and PCBAJV Board Member, Australia. ian.cullen@baueraustralia.com.au

ABSTRACT

Crown Sydney Hotel Resort is the Stage 1C component of Barangaroo South and is being developed as a single high rise mixed use tower of 72 stories (271m high), rising over a multi-level podium and a 3 level basement car park (total 75 levels). The Crown Sydney Hotel Resort basement retaining wall comprised 33 diaphragm wall (D-wall) panels and 36 barrettes for the foundation of the main tower and more than 130 bored piles (including bored compression piles, bored tension piles, bored sleeved piles and permanent plunge column piles). AECOM were engaged as designers of the foundation works by Piling Contractors Bauer Australia Joint Venture (PCBAJV) who constructed the foundation works as the D&C foundation contractor. The depth of foundation elements varied from 25 m to 50 m below ground level.

AECOM provided an initial concept design followed by a detailed design services and then, during construction, full time on-site geotechnical inspection of the basement diaphragm walls and foundations. This paper will focus on the challenges of geotechnical verification of diaphragm wall panel, barrette and pile foundation construction and how these challenges were met. During fulltime site inspection, hydraulic trench cutter penetration rates various sandstone rock classes have been measured and compared with the borehole data. Rate of penetration of the piling rig into the various sandstone rock classes, rock quality and rock apparent temperature were closely monitored and recorded as part of verification of the socket requirements. Monitoring, data collection and comparing the data with available boreholes, allowed AECOM to develop a method to reliably check the rock socket compliance with requirements across the site. Other geotechnical observations and lessons learned during the inspection of the pile, diaphragm wall and barrette construction are also presented in this paper.

1 INTRODUCTION

The Barangaroo South Precinct is a 22 ha land parcel located on the north-western edge of the Sydney CBD. Crown Sydney Hotel Resort is located on Stage 1C of Barangaroo South. Crown Sydney Hotel Resort will be Sydney's tallest building with 75 floors (including basements) and a height of 271m. Furthermore, Crown Sydney Hotel Resort will be the first 6-star luxury hotel. The project is currently under construction and is expected to be completed in 2021. Crown Sydney Hotel Resort (the Crown development site) is surrounded on 3 sides by other areas of the Barangaroo development precinct and, on the western side, is adjacent to Darling Harbour (see Figure 1).

A full top down methodology for concurrent tower and basement construction was adopted in order to meet overall project deadlines for Stage 1C with all foundation elements constructed in-situ from ground level (see Figure 2). The perimeter retention walls and the tower and podium foundations were installed from ground level, after which the ground floor slab was fully constructed, with the subsequent, concurrent construction of the tower and podium occurring simultaneously with the excavation and construction of the basement works. In order to facilitate the top down methodology, plunge columns were selected to support the ground floor slab and the construction of the podium levels above, while basement excavations were taking place below. The plunge columns consist of a rolled steel I-Section inserted into a concrete bored pile. The plunge columns are embedded into and are supported by the concrete bored piles with cut-off levels below the lowest basement slab level (B3 Slab). The plunge columns have prefabricated collar plates that are connected to the basement level slabs as the basement is constructed.

Figure 1: Crown Sydney Hotel Resort location (Courtesy of Wilkinson Eyre Architect)

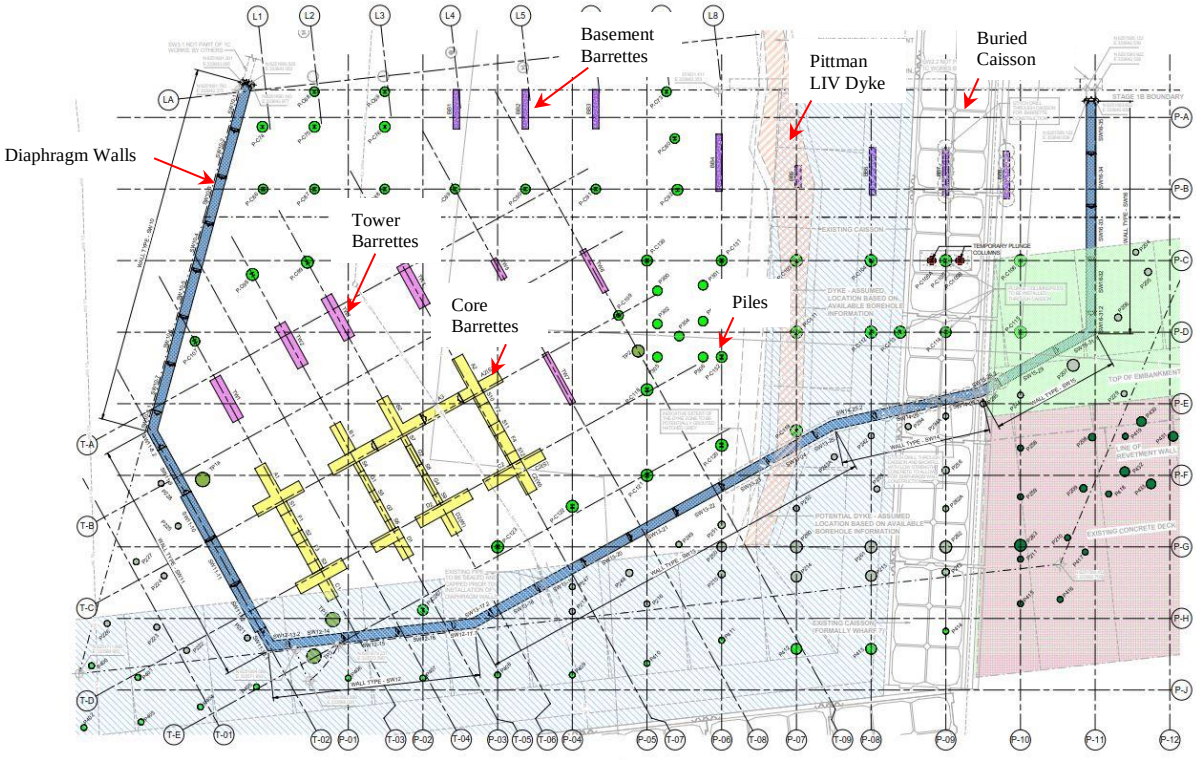

Figure 2: Crown Sydney Hotel Resort basement foundation plan

2 GROUND CONDITIONS

The development is located at a site that has undergone significant alteration in the past century. Prior to the early development of Sydney, the site was a part of Sydney Harbour and completely under water. Earliest development and use of the site had finger wharfs being constructed and, later, reclamation and conversion of the site to a container wharf has seen the site backfilled with highly variable, uncontrolled fill containing slag, concrete, bricks, wood and steel mixed in with sandy and clayey soils. The nature and type of fill and the methods of those times meant that the material was very porous with potentially large voids. The originally marine influenced erosional environment has led to buried sandstone cliffs across the site, resulting in rock levels that vary significantly over short distances across the site. Furthermore, the Pittman LIV Dyke, a caisson wall, buried rock revetments running across the site, and a suspended wharf deck all added further complexity to the site geology and challenges to the foundation design and construction methodology.

3 APPROACH TO ASSESSMENT OF GROUND CONDITIONS

In addition to the available borehole information, targeted ground investigations were conducted to better understand the ground conditions at the site, in particular along the alignment of the perimeter retaining walls and at the tower core foundations, and to also further assess the location and geotechnical properties of the Pitman LIV Dyke. In addition to previous site investigation works conducted by Lendlease and Crown for the tender, PCBAJV and AECOM carried out additional geotechnical investigations comprising more than 60 geotechnical boreholes up to 57.5m depth (Crown Sydney Hotel Resort; Geotechnical Investigation 2016). The site is underlain by fill and alluvium overlying Triassic age Hawkesbury Sandstone. The ground investigations confirmed that the fill and alluvium layers are highly variable in nature and in thickness. As a result, the rock level variation is considerable and in addition a few buried cliff lines with significant drops were identified at the site.

Figure 3 below shows the rock level variations and possible buried cliff lines along the diaphragm wall alignment. Even with the substantial amount of geotechnical information available (Figure 4), it was not possible to determine the subsurface conditions at the location of each foundation element or address all existing features, subsurface conditions or ground behaviour during the trench excavations.

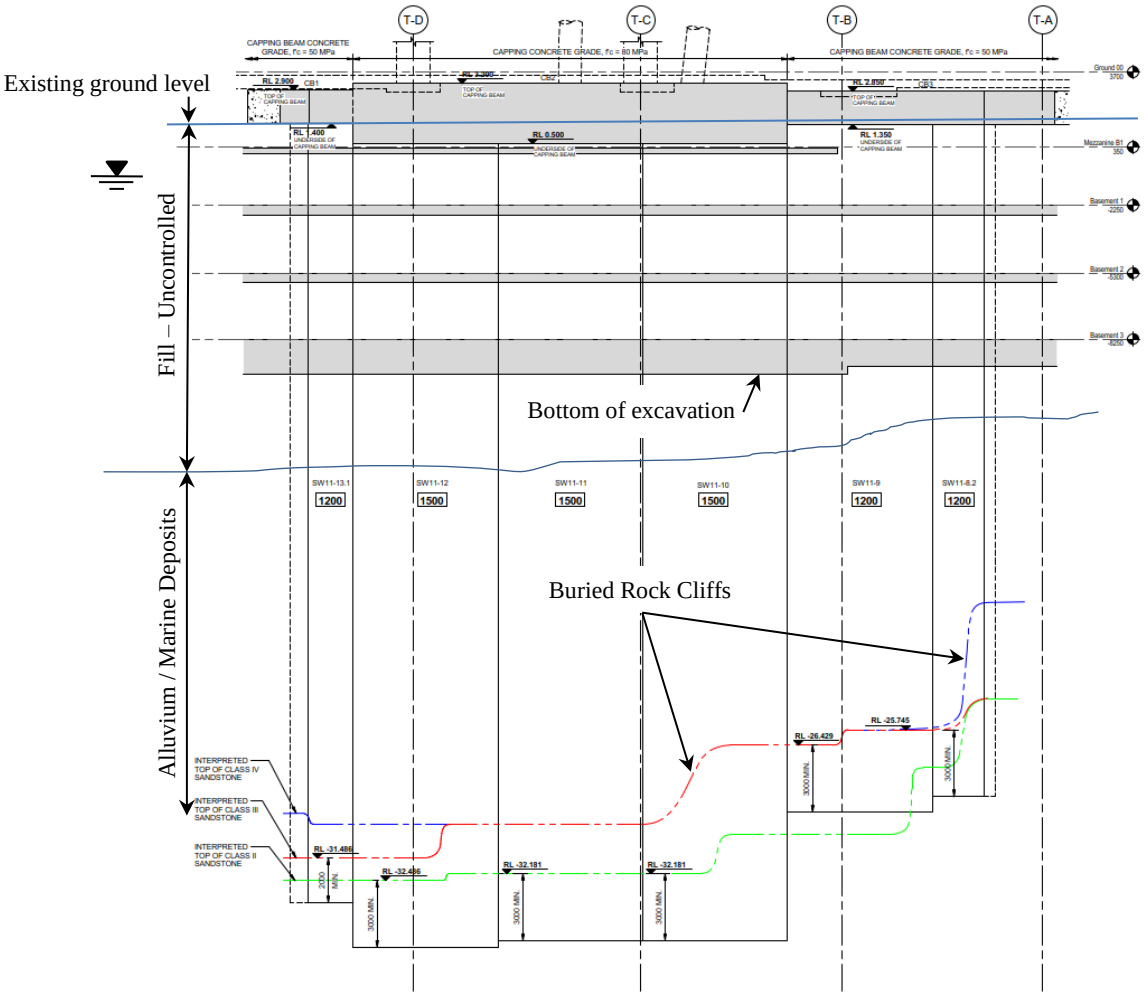

Figure 3: Typical diaphragm wall elevation showing ground conditions, rock level variation and buried cliff lines

Also, as the basement foundations were subject to large uplift pressures due to permanent hydrostatic loads, the rock socket verification was one of the key aspects of the design and construction of the diaphragm walls and piles. Therefore, PCBAJV and AECOM established an approach to reliably check the rock socket requirements where there was not enough borehole data at some of the pile and diaphragm wall locations. To achieve this for diaphragm walls and barrettes, geotechnical boreholes were drilled at nearly all panel locations prior to detailed design. Then, during construction, AECOM provided a full time on-site geotechnical engineer to observe, monitor, record and inspect excavation of diaphragm wall panels and barrettes to establish a correlation between grab and hydraulic cutter excavation and ground

conditions recorded in the borehole logs. A similar process was followed for piles, where a number of targeted geotechnical boreholes were drilled at the exact location of specific piles prior to the construction. These piles were then constructed first monitoring and recording installation to establish a correlation between the drilling performance and ground conditions in the borehole logs. Then during full-scale pile construction, the AECOM geotechnical engineer attended installation of all piles and was able to verify that ground conditions complied with the design assumptions using the correlations established earlier.

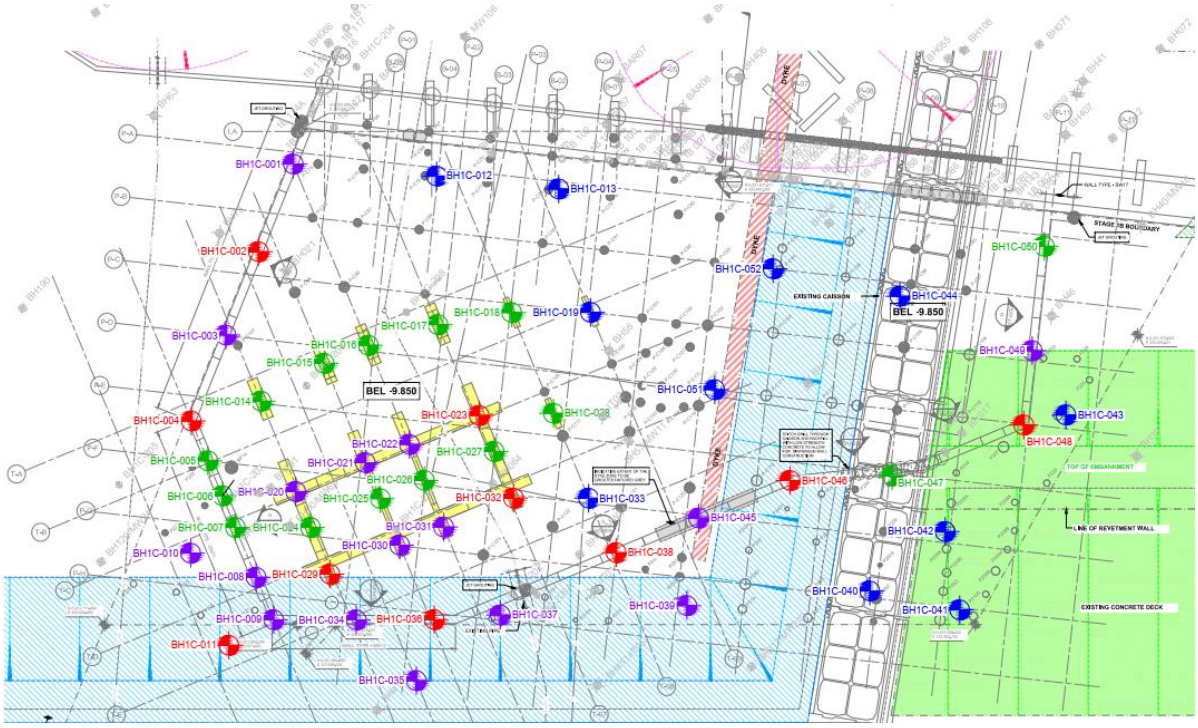

Figure 4: Locations of the targeted geotechnical boreholes (after Crown Sydney Hotel Resort 2016) in addition to the previously available boreholes

4 CONSTRUCTION METHODOLOGY

4.1 DIAPHRAGM WALLS AND BARRETTES

The diaphragm wall panels and barrettes were constructed by excavating the panels under bentonite to the required depth using clamshell grabs and hydraulic trench cutters (Figure 5). The diaphragm wall was constructed in a series of panels. Panels were constructed in a planned sequence, with every second panel constructed initially as primary panels. This is followed by construction of the secondary and closing panels between the previously constructed primary panels.

Due to the frequent variation of groundwater level (tidal effect) at the site, the variable depth of fill, and the high soil permeability, ground treatment was carried out along the diaphragm wall alignment and every barrette location to mitigate the risk of ground collapse and loss of bentonite during the diaphragm wall and barrette excavation and construction. Pre-treatment consisted of grouting at 2.5m centres with a flowable quick-setting grout to help bind the fill, fill any voids and reduce porosity

Due to the ground conditions, the excavation of diaphragm wall panels and barrettes was carried out in two stages. A clamshell grab is used to excavate fill, alluvium and weak or highly weathered rock in each panel. Upon reaching refusal of the clamshell grab, the grab is exchanged with the hydraulic trench cutter and the excavation process is continued into the rock using a hydraulic trench cutter to the designed level.

During excavation, the sides of the excavated trench are supported by bentonite slurry. Upon completion of the excavation, the working bentonite slurry is replaced by fresh bentonite slurry prior to installing the reinforcing cage and concreting. The panel is dipped with a weighted tape to verify that it has been excavated to the required depth. The steel reinforcement cage is lowered into the cleaned slurry and concrete is then tremied into the trench (Figure 6). As the concrete level rises, displaced bentonite is drawn off and pumped back to the bentonite plant for treatment and re-use.

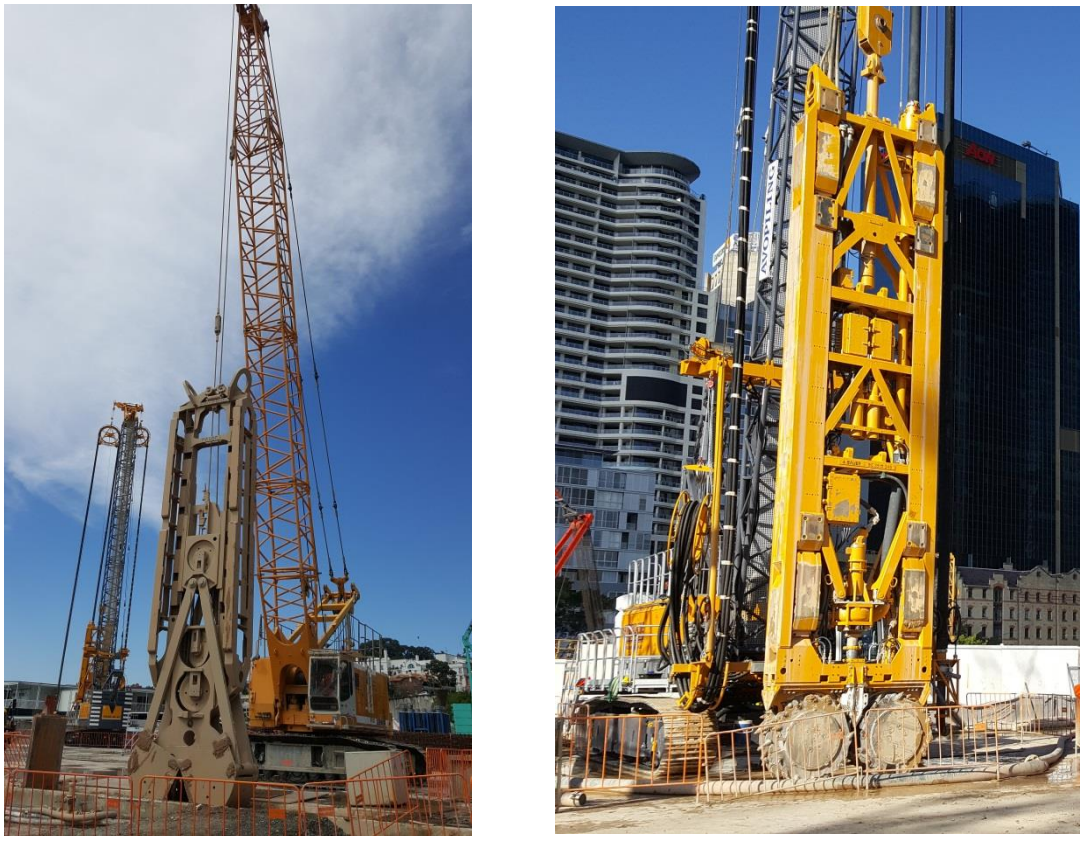

(a) (b)

Figure 5: (a) Clamshell grab; (b) hydraulic trench cutter

(a) (b)

Figure 6: (a) Lowering steel cage; (b) pouring concrete

4.2 PILES

Similar to what was done for the diaphragm walls, due the variation of groundwater level (tidal effect) at the site, the variable depth of fill, and the high soil permeability, ground treatment was carried out at every pile location to mitigate the risk of ground collapse and loss of bentonite during the piling. Pre-treatment consisted of grouting the zone of the pile with a flowable quick-setting grout to help bind the fill, fill any voids and reduce porosity. Thereafter, the following stabilizing techniques were used:

- Single wall temporary casing with bentonite slurry
- Single wall permanent casing with bentonite slurry
- Temporary double wall segmental casings

Pile construction commenced by stabilizing the top section of pile hole using appropriately sized temporary or permanent casing. The starter casing was then advanced into the ground applying a combination of rotary torque and crowd force directly from the drilling rig. The starter casings were fitted with either interchangeable or permanent teeth (depending on the casing type) in order to advance the casing through hard soils (Figure 7).

Figure 7: (left) Single wall casings with permanent teeth, and (right) double wall casing with interchangeable teeth

(a) (b) (c)

Figure 8: (a) Auger, (b) drilling bucket and (c) core barrel

To excavate to the design depth a combination of drilling tools (e.g. Auger, Drilling Bucket and Core Barrel) were used (Figure 8). Initially, the auger was used to establish the location of the pile and excavate through the fill above the groundwater level. The Drilling Bucket was used for most of the pile excavation in the fill below groundwater level and when the bentonite slurry was introduced into the pile shaft. The sandy to clayey fill had inclusions of slag, concrete and steel over significant lengths of the pile shafts (Figure 9). In addition, the piles had to be constructed through existing buried caissons. A combination of Core Barrel and Drilling Bucket was used to core through these zones and also into the high strength rock that formed the pile socket. The Core Barrel initially cuts the core and the Drilling Bucket is then used to collect and bring out the rock fragments.

Rock commencement and final founding levels were confirmed by the geotechnical representative on site to confirm the rock socket requirements. During excavation, bentonite slurry was used to stabilize the hole. After completion of excavation, the base of the shaft was cleaned with a cleaning bucket and then the working bentonite slurry was completely replaced by fresh bentonite slurry. To assure that pile base was clean, bentonite slurry was tested to meet sand content requirement of less than 2%. The piles were dipped with weighted tape. The steel reinforcement cage was then lowered into the bentonite slurry and concrete was tremied into the hole (Figure 10).

(a) (b) (c)

Figure 9: Examples of obstructions hit during construction

(a) (b)

Figure 10: (a) Lowering steel cage into bentonite slurry, (b) pouring concrete

Plunge columns were installed in selected basement piles as part of the top-down construction method to support the ground floor slab. To install the plunge columns, the I-Section column was inserted into the concrete of the completed pile no later than three hours after the concrete pour. The I -Section column was then suspended from a support platform positioned on top of the casing to precisely locate the plunge column. The support platform was left in place until the concrete reached the required strength to support the column. The shaft above pile cut-off level was then backfilled with stabilized sand and the support frame and casing were then removed. Figure 11 shows a 3D view and installation process of the plunge columns. Electronic tilt-meters were installed on the plunge columns during installation to maintain the strict verticality positional tolerances.

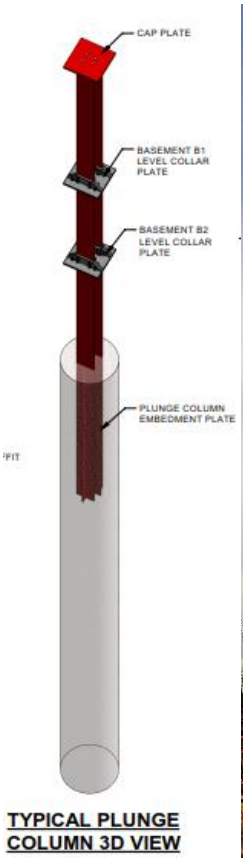

(a)

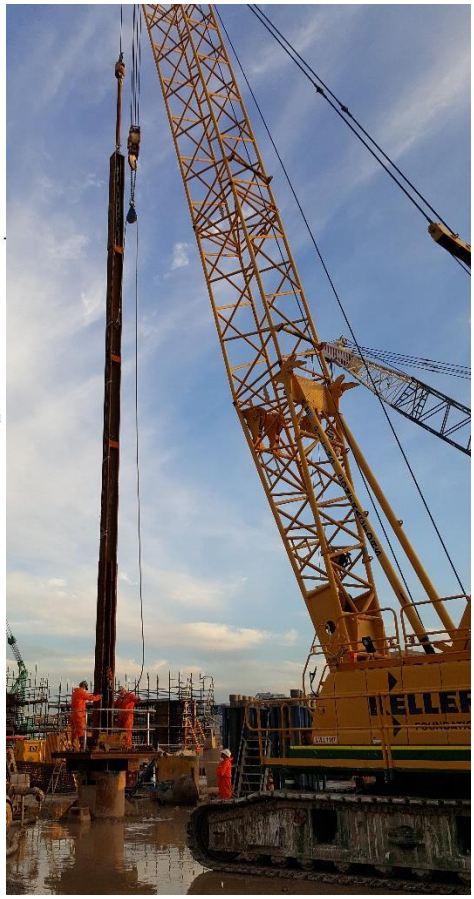

(b)

(c)

Figure 11: (a) Typical plunge column 3D view, (b) lowering plunge column into concrete, (c) Suspended I-Section

5 GEOTECHNICAL VERIFICATION

5.1 DIAPHRAGM WALLS AND BARRETTES EXCAVATION

As mentioned previously, boreholes were drilled at nearly all diaphragm wall panels and barrettes. AECOM provided a full time on-site geotechnical engineer to inspect rock sockets to ensure that they met design requirements. Rock socket requirements for D-walls and barrettes were:

(a) achieve specified socket roughness (R3 in accordance with Pells et al. 2002),

(b) clean panel bases,

(c) Socket to be founded in specified rock class.

These are discussed below.

(a) Socket roughness

Prior to commencement of construction, PCBAJV demonstrated that their construction methodology, based on using hydraulic cutters with protruding teeth was able to achieve the required socket roughness (Figure 12).

Figure 12: Hydraulic cutter with protruding teeth

(b) Base cleanliness

To achieve a clean panel base, the hydraulic cutter was kept at the excavation base level whilst pumping the debris and working bentonite out by reverse circulation techniques while fresh bentonite was pumped in at the top of the panel. The suction pump capacity was approximately 500 m^3/hr which provided adequate power to remove debris from the panel base. A bentonite slurry sample was tested for each panel after replacing the working bentonite slurry with fresh bentonite to meet the less than 2% sand content criterion.

(c) Founding Material

As discussed in section 3, boreholes were drilled at nearly all diaphragm wall panels and barrettes. At panels where boreholes were available, the borehole information was used to define the final depth of the panel. Rate of penetration of the hydraulic cutter into various sandstone rock classes was closely monitored and recorded. Daily excavation records and site observations were compared with the borehole logs.

The comparisons indicated that the clamshell grab refusal generally occurred in sandstone class V or low strength sandstone class IV (Rock classification as per Pells et al. 1998). It should be noted that the quality of rock being excavated,

the freefall weight of the clamshell grab and the clamshell grab operator are the key factors that have considerable impact on the depth of penetration that can be achieved in rock. For instance, clamshell grab refusal could be at shallower depth as a result of boulders and/or a lens of harder rock.

Comparing borehole logs with recorded site observations indicated that the hydraulic trench cutter penetration rate reduced with increase in rock strength. The penetration rate halved from approximately 2m per hour for sandstone class IV to 1m per hour for sandstone class III. The indicative average rate of penetration in the sandstone rock classes versus point load tests results is depicted in the Figure 13. Due to variations in rock characteristics (e.g. bedding planes, weak zones, and possible localized higher strength bands) the average penetration rates are indicative and can vary from site to site.

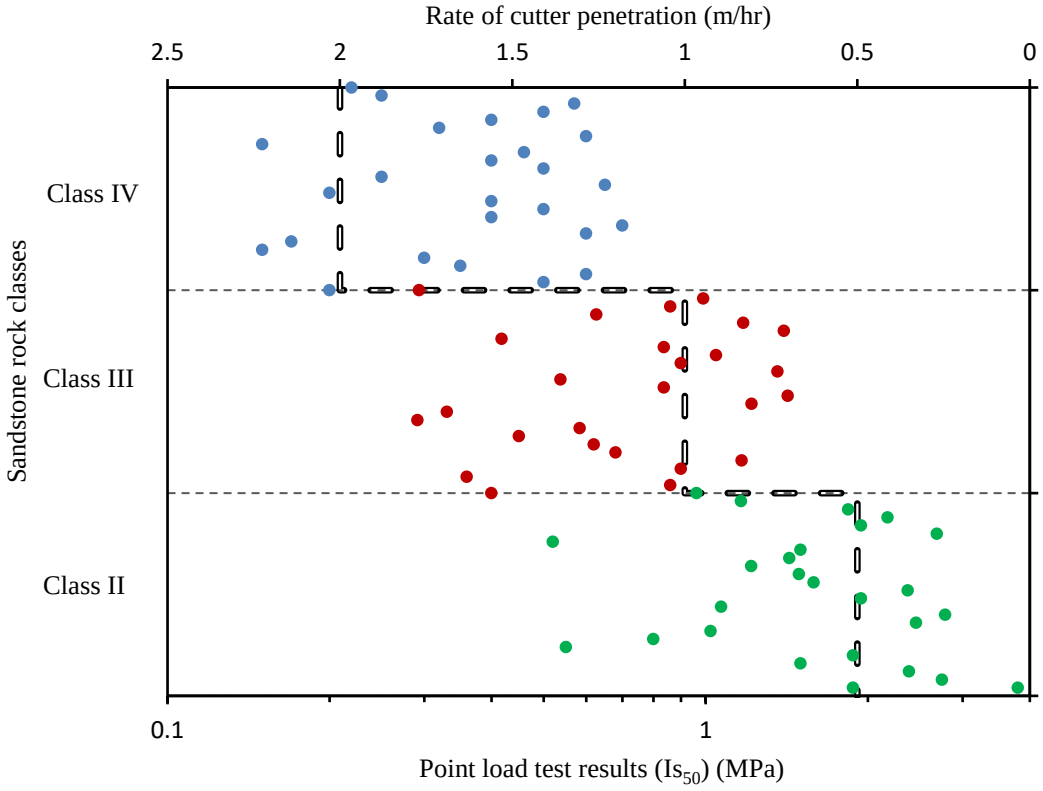

Figure 13: Hydraulic trench cutter observed penetration rate into Sydney sandstone rock classes

Dyke – Two of the diaphragm wall panels crossed the Pittman LIV Dike and one of the basement barrettes was located in the centre of the Pittman LIV Dyke. Pittman LIV Dyke rock material was Dolerite. The final design depth was required to be determined considering available geotechnical information, on site observations and daily excavation records. The socket requirement was 1.5m excavation into equivalent of class IV sandstone or better. Since the barrette was amongst the last panels to be excavated, there was a substantial record regarding the rate of penetration in various rock classes. Also, various parameters that could affect the rate of hydraulic cutter penetration into various rock classes had been observed and captured (e.g. operator). The experienced hydraulic cutter operator was requested to provide feedback regarding rock strength while excavating. Using the available geotechnical information, penetration rate, cutter input and engineering judgement, the top of rock and adequate socket length could be determined.

Clay lenses- Despite the substantial number of boreholes across the site, unidentified clay lenses were encountered at some panels during cutting. Hard clayey material cannot be easily excavated by grabs and neither by the cutters when the clay lenses occurred within the rock layers. Hence, more ground investigations could reduce the risk of encountering unexpected clay lenses. The hydraulic trench cutter was fitted with teeth for dealing with rock and not with clay and hence the clayey material sticks to cutter teeth and builds up to reduce the efficiency of the cutters significantly. (Figure 14). As a result, the cutter needed to be removed from the trench and the teeth cleaned frequently causing delays. As a solution, a different type of hybrid cutting wheel with interchangeable teeth which is more suitable for both clayey material and sandstone can be used if the clay layers are thick and expected to be highly variable across the site. However, the hybrid cutting wheel is less efficient if the clay layers are not encountered and only rock is occurring.

(a) (b)

Figure 14: (a) Cutter with clean teeth; (b) cleaning cutter teeth from clayey material

5.1 PILE EXCAVATION

AECOM provided a full time on-site geotechnical engineer to inspect rock sockets to ensure design requirements were met. Rock socket inspection requirements for piles were for confirmation of;

(a) achievement of specified socket roughness (R3 in accordance with Pells et al. 2002),

(b) cleaning of pile bases,

(c) Socket to be founded in specified rock class.

These are discussed below.

(a) Socket roughness

Prior to commencement, the contractor demonstrated that their construction methodology, based on using augers and roughening tools with protruding teeth was able to achieve the required socket roughness. Also, the performance of the drilling and roughening method to achieve the required roughness and shaft adhesion values was confirmed by reviewing and assessing the pile load test results (O-Cell tests) on the adjacent site (Site A) with the same ground conditions by the same contractor.

(b) Base cleanliness

Pile base cleanliness was assured by the construction methodology described earlier in section 4.2 (i.e. using cleaning bucket, replacing working bentonite with fresh bentonite, measuring bentonite slurry sand content and dipping piles at various points).

(c) Founding Material

A number of boreholes were specifically located at pile locations so that various parameters (e.g. rate of penetration of the piling rig into various sandstone rock classes, rock quality and rock apparent temperature) could closely monitored and calibrated against the borehole logs.

Rock quality was assessed initially by visual inspection and examining hand specimens of the excavated rock from the pile shaft and comparing with borehole logs at the piles. The lower the strength of the sandstone, the easier to mould the excavated material by hand. The excavated material tended to become friable when the strength was closer to sandstone rock class IV. Higher strength sandstone (sandstone rock class II) was excavated as sharp fragments, friable and not remouldable. Rock temperature was qualitatively recorded and compared with ambient temperature and weather as an indicator of rock strength. Higher strength rock required more torque, pressure and time for the drilling rig to excavate and consequently tended to generate much higher temperature and water vapour (steam) intermittently (Figure 15). These initial assessments and comparison with borehole logs allowed the on-site geotechnical engineer to assess founding conditions for subsequent pile sockets.

Figure 15: Excavated rock with high temperature and water vapour

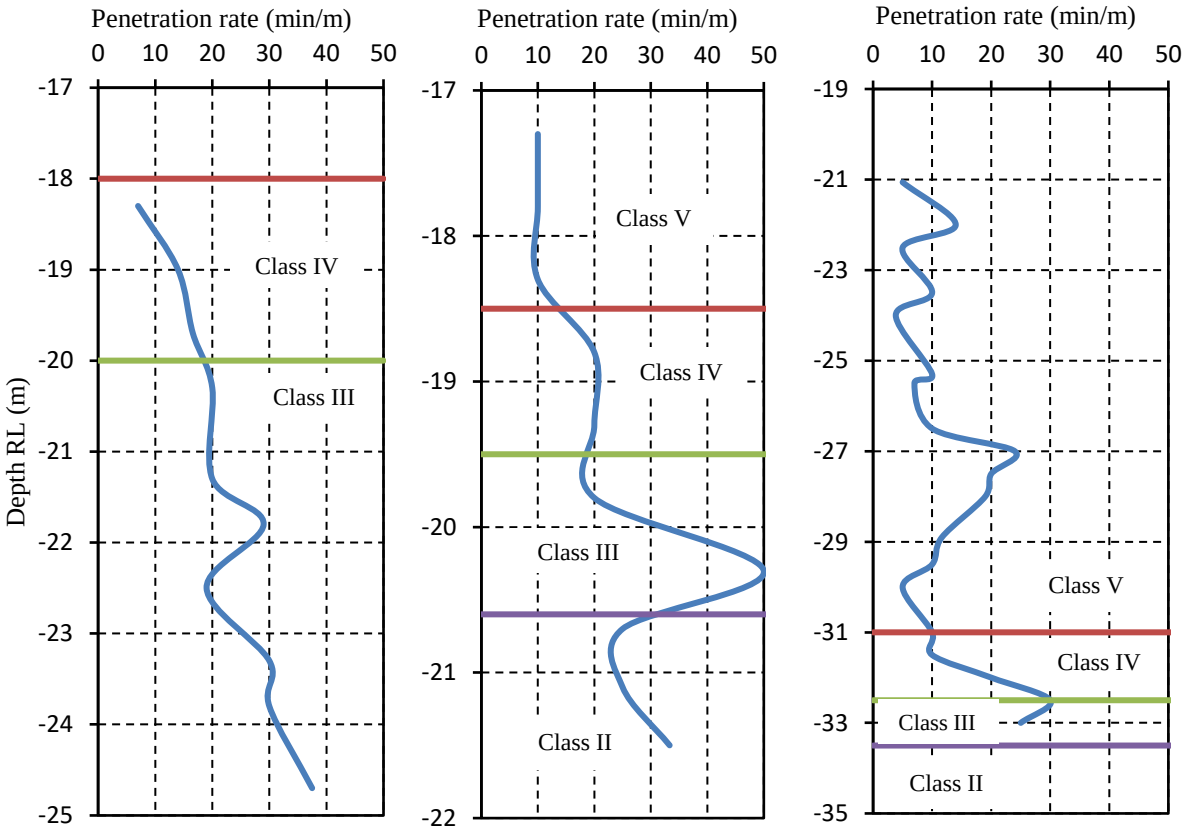

Figure 16: Example of excavation penetration rate in comparison with classified Sydney sandstone classes in nearby boreholes (piling rig) (after Azari et al. 2019)

The penetration rate for piles at borehole locations was monitored and measured to establish a baseline to assist the on-site geotechnical engineer to classify the rock on site. Figure 16 depicts three examples of excavation penetration rate compared with rock classification from nearby boreholes. Type of plant, operator experience, thin layers of high strength rock, clay lenses and tools efficiency play an important role in determining the penetration rate as can be seen in the spikes recorded in Figure 16. It is however evident that a meaningful relationship can be established between penetration

rate and rock classes in Sydney sandstone for the particular conditions at this site with the higher strength sandstone requiring more time to excavate and resulting in a lower penetration rate.

6 CONCLUSIONS

Due to the highly variable thickness of fill and alluvium layers, and as a result of variable rock levels at the site and the limited geotechnical boreholes at the pile locations, an appropriate construction methodology as well as extensive site observation were required to achieve high quality construction.

To achieve adequate roughness in the diaphragm wall and barrette sockets proper excavation tools need to be employed. Subsequently, to clean the base of the panels, the hydraulic cutter is required to be kept close to the base and pump out debris and working bentonite. To ensure a quality concreting process, the process of pumping out the working bentonite while fresh bentonite is poured to the top of the panel needs to continue until the bentonite left in the panel has less than 2% sand content.

As part of an appropriate construction methodology, apposite drilling tools are required to achieve adequate roughness in the pile sockets. In addition, a cleaning bucket is required to clean the base of piles to ensure that they are free of coarse debris. It is then essential to also completely replace working bentonite (with high sand content) with fresh bentonite. Fresh bentonite with sand content < 2% avoids sand settlement at the base of the pile in addition to ensuring a quality concreting process as it has lower density and is easily displaced during concreting.

The design and construction intents were successfully achieved by close collaboration of AECOM design team, Piling Contractors Bauer Australia Joint Venture (PCBAJV) construction team and the fulltime geotechnical representative from AECOM.

The focus of this paper is purely on the construction aspects of the project and sharing the construction geotechnical lessons learned during the site inspections. A separate paper is under preparation on the design and performance of the basement and the foundations.

7 ACKNOWLEDGEMENTS

The authors wish to thank Crown Resorts, Lendlease Building, and PCBAJV for allowing this paper to be published and providing the opportunity to work on what has been a most challenging yet rewarding project.

8 REFERENCES

Azari, B, Mirlatifi, S, Buys, H, Cullen, I (2019), Some Geotechnical Lessons Learned on Foundation Construction of Sydney's Tallest Building, Crown Sydney Hotel Resort, 13th Australia New Zealand Conference on Geomechanics, 1-3 April 2019, pp. 1157-1161.

Bertuzzi, B, Pells, P J N (2002), Geotechnical Parameters of Sydney Sandstone and Shale, Australian Geomechanics, Vol 37, No 5 December 2002.

Crown Sydney Hotel Resort (2016); Geotechnical Investigation 07 September 2016

Pells, P J N, Mostyn, G, Walker, B F (1998), Foundations on Sandstone and Shale in the Sydney Region, Australian Geomechanics, December 1998.

OPTIMISING PRECAST CANTILEVER WALLS FOUNDED IN SYDNEY SANDSTONE

[1]Antonio Ramirez and [1]Diarmuid Moriarty

[1]The Reinforced Earth Company

ABSTRACT

Linear Infrastructure projects requiring grade separations have historically used a multitude of retaining wall systems, such as gravity, piled and reinforced soil structures (RSS), depending on ground conditions. L-shaped cantilever cast in-situ walls have been used extensively in road projects in the Sydney region. These walls are costly as they use a significant amount of concrete and steel, while achieving an aesthetically pleasing finish is difficult. Such walls may not take full advantage of rock foundations prevalent in the Sydney Basin. This paper presents an updated concept for optimising retaining walls under appropriate conditions, combining precast and cast in-situ elements while increasing the effectiveness of the load transfer mechanism to the ground.

In essence, this system is a retaining solution comprising full-height precast wall facing units secured to a cast-in-situ footing forming a monolithic cantilever concrete wall. The facing units are each precast with a set of counterforts on the rear side to transfer load to the footing. This paper discusses and investigates both the design of this precast solution, focussing on counterforts and footing, and the adequacy of the solution from a geotechnical point of view, as it relates to the prevalence of rock foundations in the Sydney Basin.

1 INTRODUCTION

This paper presents an updated concept for optimising retaining walls under appropriate conditions, combining precast and cast in-situ elements while increasing the effectiveness of the load transfer mechanism to the ground given appropriate ground conditions.

This system is a retaining solution comprising full-height precast wall facing units secured to a cast-in-situ footing forming a monolithic cantilever concrete wall. The facing units are each precast with a set of counterforts on the rear side to efficiently transfer load to the footing. Continuity and load transfer between the counterforts and the cast-in-situ footing is achieved by means of construction joints between the elements and reinforcing anchor bars protruding from the counterforts which are incorporated in the in-situ footing pour.

This type of precast retaining wall is an effective solution when a standard wall stem may not be implemented due to space constraints. It is also appropriate when site conditions such as excavation on rock is required, or where backfill unavailability rules out the use of other retaining system such as Mechanically Stabilised Earth (MSE).

TechWall® combines counterfort design advantages with the efficiency of precast concrete in terms of architectural finish possibilities and reduced installation timeframes. Furthermore, it may be considered as an optimisation of retaining walls specified as cast in-situ because:

1. It is based on a standard, well understood design process. The innovative aspects of this system comprise the software used to complete the design and the marriage of precast and cast-in-situ elements. The design method is in line with generally accepted methods used in geotechnical and structural engineering
2. It eliminates significant temporary works on site
3. Temporary props can be removed once the footing is cast and cured
4. Primary structural elements (panel facing and any adjoining elements such as parapets or impact barriers) can be fabricated in a strictly controlled environment off-site
5. Significant time efficiencies are possible with rapid installation of precast elements, reducing the impact of the project works on local communities.
6. Significant efficiencies in concrete volumes in the wall facing can be realised, thus reducing the carbon footprint of the project

Key to the overall efficiency of this solution are two factors:

Firstly, the counterforts act as equivalent cantilever beams structurally connected to the footing to resist lateral earth pressure and minimise the stresses on the facing panels. This allows for relatively thin concrete facing elements.

Secondly, the footing design is key in the optimisation and sustainability of the solution, by allowing for reduced excavation and backfill in comparison with other traditional forms. The system can consider multiple footing arrangements like cast-in-situ concrete walls, including a variety of heel/toe geometries to suit the prevailing conditions on site. Further incidental efficiencies can be realised, such as the case where no footing toe is incorporated. In this scenario, the precast facing elements can also act as formwork when stitching the facing and footing elements together.

The system can incorporate reinforced concrete impact barriers (crash barriers) at top of wall by connecting barrier elements (cast-in-place or precast) to facing panels via the counterfort reinforcement. This provides a solution that can be constructed integral with the retaining walls, but primarily provides efficiency of impact load transfer to the ground. The system is known as its proprietary name "TechWall®", although it is important to note that the system does not include any proprietary elements. The system is an optimisation of existing counterfort retaining wall design and construction.

Retaining walls are typically classified into four categories, with sub-categories contained therein. The four main categories are gravity, semi-gravity, non-gravity cantilevered, and anchored. The TechWall® system falls under the semi-gravity wall category, since the system relies on structural components to mobilise the dead weight of backfill, which in turn provides lateral load resistance and load transfer to the ground. Back in the mid 1980's Tierra Armada, the Spanish branch of the Reinforced Earth Company, experienced issues with numerous contractors who could not source select backfill which was chemically and/or physically compliant with accepted MSE technical specifications. This led to the implementation of a research project to develop an alternative retaining system, which would incorporate the software development and precast expertise Tierra Armada possessed. The result of this project was the TechWall® system, and since then over 600,000m^2 of TechWall® units have been installed in Spain alone. The TechWall® system, with minor modifications, was also implemented in the United States. The system has also been used in France and most recently in Peru. Refer to **Table 1** below for TechWall® project summary over the past 30+ years.

Table 1: TechWall® Projects reference summary

Country	Total Area (m^2)	Max height (m)	Max Area (m^2) (individual project)	Timeline
Spain	600,000+	17.0	4,660	Mid 1980's - Present
United States	70,000+	11.0	800	Late 1980's - Present
France	2,000	7.0	600	2014 - Present
Peru	14,000	9.0	14,000	2017 - Present

2 TECHWALL® COMPONENTS & DESIGN PRINCIPLES

The substructure system (called TechWall®) is composed of two precast concrete structural elements: the wall elements (face panel and the counterforts), and the cast in situ footing (Figure 1). The TechWall® units are cast off-site, transported to the construction site, erected and secured in position with temporary props. The TechWall® precast wall unit is connected to the footing through the main flexural reinforcement of the counterfort, which protrudes from the underside of it, in preparation to be cast into the footing. This part of the counterfort reinforcement plays the most important role in providing a full structural interaction between the TechWall® components (precast unit and cast in-situ footing). Then the footing cage is installed, and the cast in-situ concrete footing is poured in the least possible amount of time. Once the concrete footing is set and cured, temporary propping of the precast panel units can be removed. At this point all the elements of the system are structurally joined together and backfilling can commence.

Prior to delivering the TechWall® units to site, the wall component (facing panel + counterfort) is precast in two stages. Firstly, the counterfort is cast and cured, with appropriate provision for starter reinforcement and construction joints. Counterforts are connected to the face panel through extended stirrups into the panel. This reinforcement, combined with a construction joint at the interface, provides the necessary connection such that the wall element can be considered as a single structural element. This enables a fundamental design assumption, whereby facing units are designed and analysed as T-beams; where the face panel is acting as the flange, and the counterfort as the web. Refer to Figure 2 which represents typical details for the features introduced in the TechWall® solution as an efficient alternative to the usual rectangular cross section of a traditional concrete L-shaped wall.

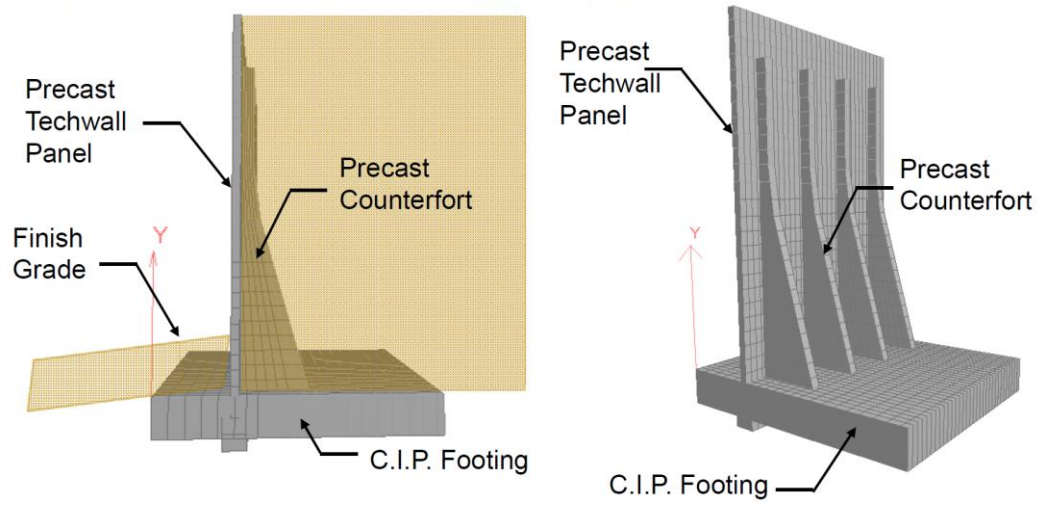

Figure 1: Typical TechWall® Components

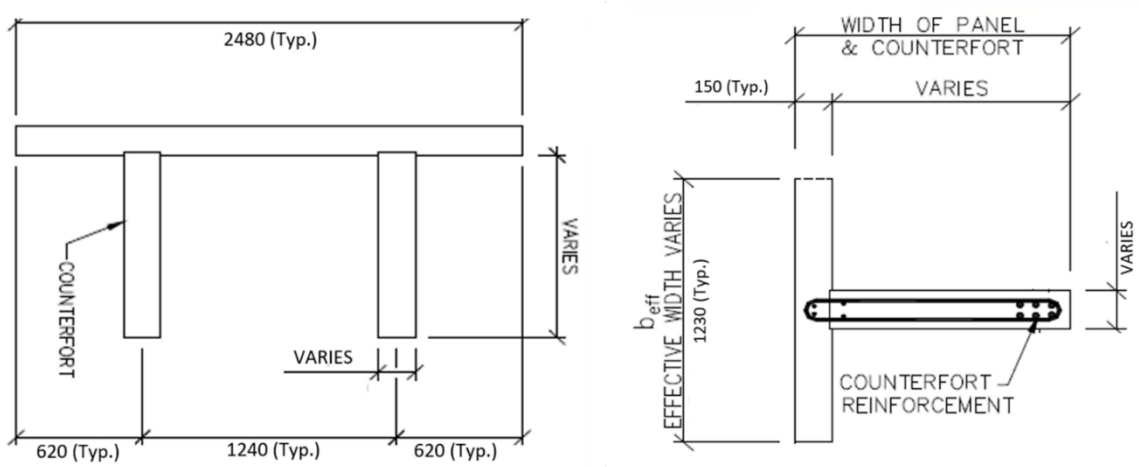

Figure 2: TechWall® T-Beam configuration

Strengthening a retaining wall with counterforts changes the structural behaviour of the retaining wall. In conventional cantilever retaining wall systems, the facing panel is the load-resisting component. However, with the introduction of counterforts, these become the main load-resisting component, where the facing panel acts as a continuous one-way slab spanning over the counterforts. This allows the cross section of the wall to be reduced significantly while satisfying the strength and serviceability requirements of the specifications.

Special attention is paid to:

- counterfort and anchorage into the footing: bottom section of the counterfort where the bending moment and shear forces are typically at a maximum.

- face panel and footing design: the midspan between the counterforts for positive moment, and over the counterforts for negative moment. Counterfort position may be considered such that positive moment is minimised, leading to rationalisation in steel reinforcement.

The load calculations are divided into vertical and lateral loads applied on the retaining wall as per the relevant codes, requirements and specific project technical specifications.

3 CONCEPTUAL DESIGN ASSUMPTIONS

The TechWall® system facing elements are assumed to deflect as a result of soil pressure action. Therefore, the soil behind the TechWall® facing units will be in the active condition as is allowed to yield sufficiently to cause its internal shearing resistance along a potential failure surface to be completely mobilised and tends to overturn or slide the wall. Thus, the coefficient of active lateral earth pressure, Ka, is used for the calculation.

Coulomb's approach is considered in calculating lateral the active lateral earth pressure as follows:

Horizontal component: $$k_a = \frac{cos(\phi+\alpha)^2}{cos^2(\alpha).\left(1+\sqrt{\frac{sin(\phi+\delta).sin(\phi-\beta)}{cos(\delta-\alpha).cos(\alpha+\beta)}}\right)^2}$$

Vertical component: $$Z_1 = \frac{k_a}{tan(\alpha+\delta)}$$

ϕ = Internal friction angle

δ = Inclination of the earth pressure

β = slope angle at top.

α = slope of counterfort face at rear.

The soil pressure distribution behind the TechWall® differs depending on where the pressure is acting.

Soil pressure on facing panels is assumed to act on a vertical plane right at rear face of facing panels. However, soil pressure on counterforts is assumed to act on a vertical plane at counterfort-footing intersection (as depicted in Figure 3).

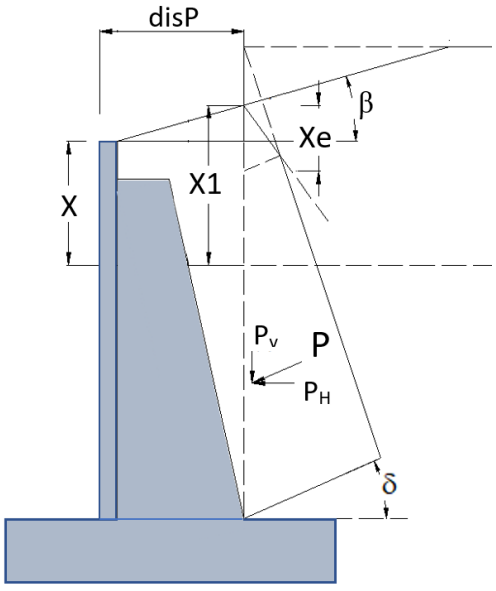

Figure 3: Soil pressure at rear face of counterfort

X: Distance from top of wall to soil pressure acting plane

Xe: Top section (height) of the soil pressure distribution.

X1: Backfill height at soil pressure acting plane.

disP: Distance from front face of wall to soil pressure acting plane

In order to capture in the design model, the restrained based of the facing panels, the pressure diagram acting on the facing panel is assumed as follows, in accordance with Huntington 1957 (**Figure 4**)

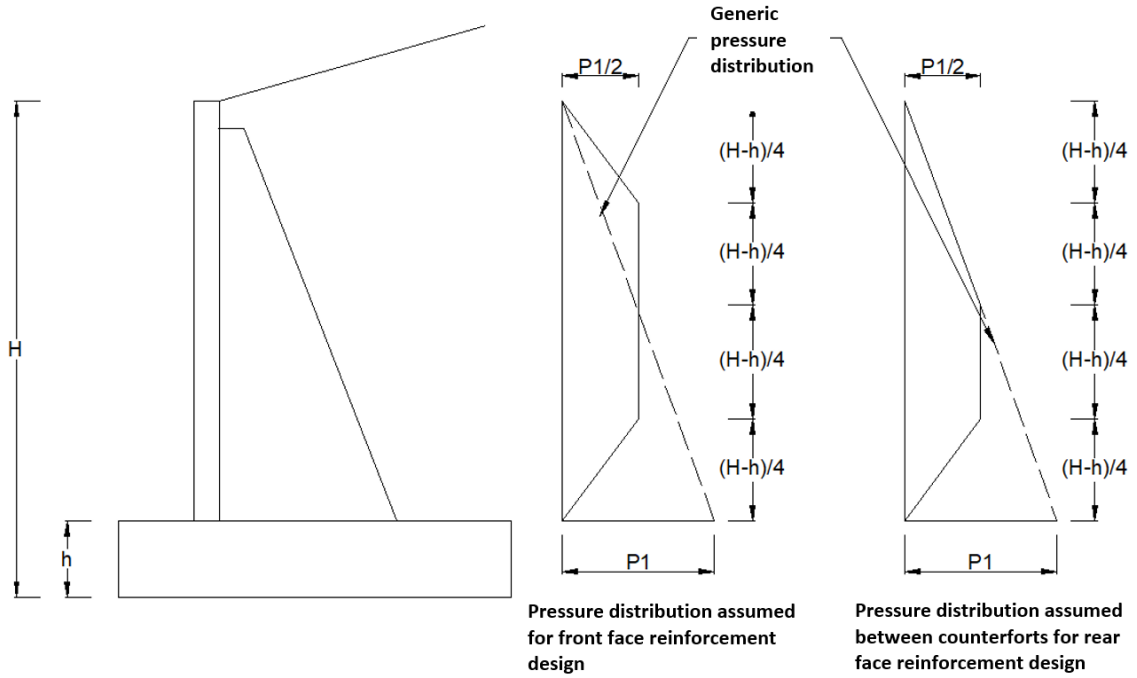

Figure 4: Soil pressure at rear face of facing panel

4 TYPICAL DESIGN PROCEDURE

The design procedure of the system is similar to that of a cast-in-place concrete counterfort retaining wall for the typical components. However, it is different for individual elements of the TechWall® system such as facing panels, counterforts and footing.

The typical design procedure is as follows:

1. **GEOMETRY:** Nominate panel width and counterfort spacing/dimensions, along with other relevant constraints (such as geometry. Two main geometric parameters contribute to the structural behaviour of TechWall® system: the counterfort spacing and the length of the counterfort at the base (Figure 5) (counterfort-footing interface). Counterfort spacing and sizing determines the load applied to each counterfort and hence the counterfort thickness and volume of steel reinforcement required

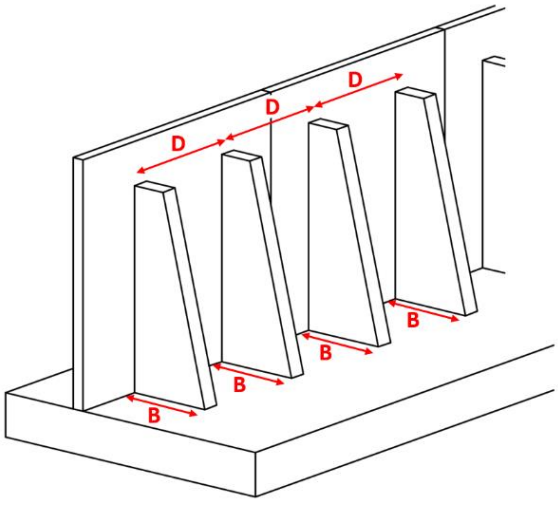

Figure 5: Counterfort wall - geometrical arrangement (dimension at base and spacing)

2. Calculate all of the applicable ultimate loads in compliance with the nominated specifications.
3. **EXTERNAL STABILITY:** Perform the necessary external stability checks to ensure that the system meets the required safety factors. The system is checked against overturning, sliding, and bearing failure modes. This stage determines the footing dimensions and arrangement.
4. **INTERNAL STABILITY:** Determine the ultimate loads acting on each TechWall® element (i.e. loads on facing and counterforts). Counterforts are assumed to be in fully connected to the footing.
    a. Design for the required ultimate moment and shear capacity required, providing steel reinforcement that meets the specifications requirements for all the TechWall® elements (wall elements and footing).
    b. Check for crack control and serviceability failure modes

In calculating the required steel reinforcement when carrying out the internal stability design, the considered forces and stresses can include but not limited to:

- Precast elements (panel + counterfort):
    - Bending Moment and shear force in the counterfort (T-Beam web)
    - Shear force at panel-counterfort interface as a result of counterfort bending.
    - Bending Moment and shear force in the panel (T-Beam flange)
    - Shear force at counterfort-footing interface
- Cast in place element (footing):
    - Bending Moment and shear force due to:
        - External forces (Dead and Live loads)
        - Axial force at counterfort-footing connection

5 OPTIMISATION

The number and spacing of counterforts affect the structural design of the facing panel and footing. When the counterfort spacing is reduced, the bending moments in the face panel are reduced and a thinner concrete face panel may be used. The choice of the counterfort spacing is based on conventional beam theory. Therefore, counterfort spacing is adjusted in order to balance positive and negative moments. (Figure 6) The resulting distribution of bending and shear stresses allows reduction of the face-panel thickness compared to a typical L-Shaped retaining wall.

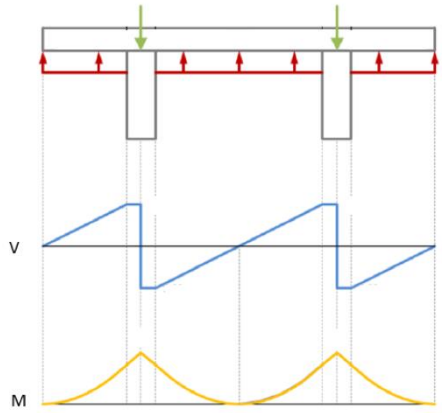

Figure 6: Typical bending moment and shear distribution along TechWall® facing panel

Finding the most efficient footing dimensions is key in order to optimise the TechWall® design. Multiple factors such as materials cost, excavation volume required, and labour associated are analysed. As a result of the combination of all these variables, hundreds of different combinations need to be computed. This intensive and time-consuming task is carried out by the in-house design software developed for this purpose. The overall efficiency of the TechWall® system relies on this footing optimisation process.

6 COMPARISON BETWEEN TECHWALL® AND L-SHAPED WALL

The TechWall® system has been optimised to provide geometric efficiency that can be reflected in the form of a reduction in the weight, sizes, and concrete volume of some of the wall components compared with traditional cast-in-situ L-shaped walls. Owing to the software used in design, the geometric efficiency does not rely on burdening designers with iterative and time-consuming work. Anecdotally, the system is considered to provide up to 40% cost reductions when materials, installation and temporary works efficiencies are realised. However, regarding materials only (being concrete and steel),

we have analysed a single retaining wall contained in a recent (2018) "For Construction" issue of drawings on an RMS road upgrade in the Sydney metropolitan area. The conforming design comprises a combination of L-shaped and cast-in-situ counterfort walls. The counterfort supports are detailed on approximately 55% of the total wall length. The counterforts are 350 mm wide at 5 m centres. Analysis shows a significant reduction in the concrete and steel volumes required is achievable if a TechWall® solution is implemented. This analysis is presented in Table 2. It is worth pointing out that the facing area has increased in the TechWall® solution proposed, owing to minor variations in geometry proposed to optimise precast panel production. A marginal increase in footing concrete is also evident, due to the variation in load transfer mechanism to the ground. However, generally in a similar approach to the panel-counterfort interaction (based on conventional beam theory) the TechWall® footing reinforcement can be optimised as a result of the reduced longitudinal Mx bending moment along the footing in opposition to the conventional L-shape footing arrangement (Figure 7).

Significant savings are realised in all other elements individually, and in aggregate, as presented in the table.

Table 2: Comparison of fully cast-in-situ vs TechWall® Solutions

Retaining Wall	Wall Area (m^2)	Footing		Facing & Counterforts		Total	
		Concrete (m^3)	Steel (T)	Concrete (m^3)	Steel (T)	Concrete (m^3)	Steel (T)
CIP	1043	554	111	616	117	1170	228
TechWall®	1304	634	69	315	42	949	111
% Difference (Techwall®/CIP)	125%	114%	62%	51%	36%	81%	49%

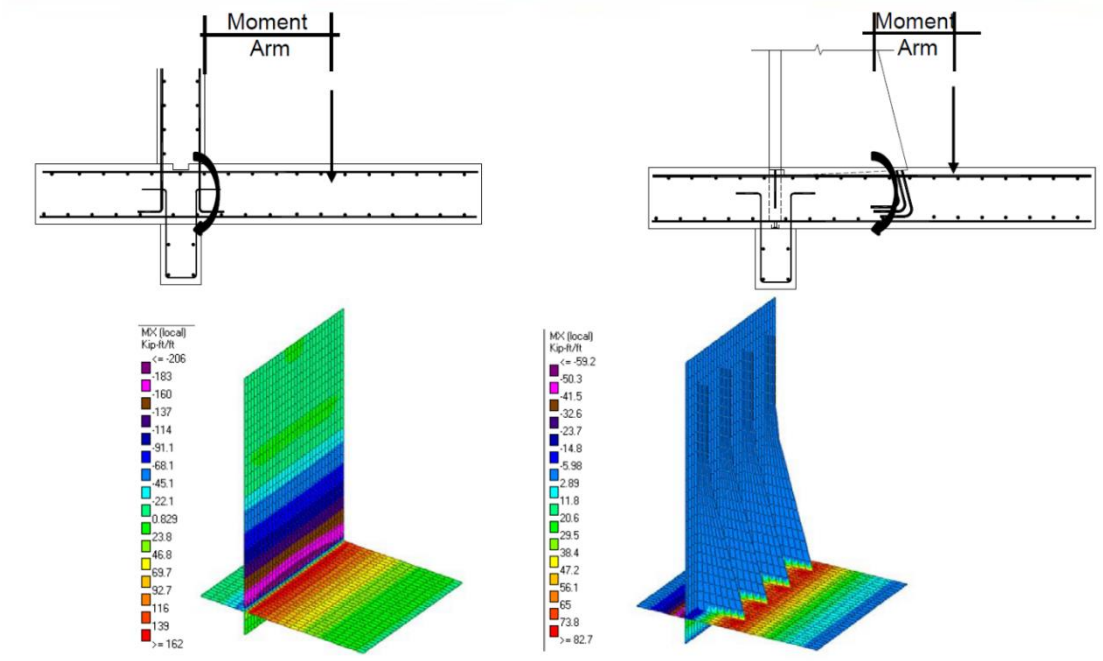

Figure 7: Footing optimisation (Mx distribution). Comparison between L-Shaped Wall & TechWall®

7 TECHWALL® FOUNDATION

The TechWall® system is not suited for all retaining wall applications. In particular, where low strength, soft ground conditions prevail, alternative retaining methods should be considered. High strength soils or preferably rock foundation is preferred for the TechWall® system. The geology of the Sydney basin consists primarily of gently-formed Triassic sandstones and shales (Branagan 1985). The geotechnical parameters of these founding materials are further described

by Pells, Mostyn and Walker (1998). While Pells et al provides guidance on strength and deformation characteristics, it should be understood that the TechWall® system relies on a strength input only, namely bearing capacity. This paper limits its discussion to a trivial assessment of bearing capacity of Sydney rock foundations only. The reader is referred to this and other literature for further discussion on Sydney Rock classifications.

In particular, where TechWall® can be founded on Class V Shale as a minimum, the ultimate bearing capacity of 3000 kPa may be used, and 700 kPa for serviceability assessment. The Table presented below (Table 3) is an abridged version of Table 5 of Pells et al,1998.

Table 3: Bearing capacities of Sydney rock foundations

Class	Ultimate End Bearing[1] (MPa)	Serviceability end bearing pressure[2] (MPa)
V Sandstone	> 3	1.0
V Shale	>3	0.7

Notes: [1]Ultimate values occur at large settlements (> 5% of minimum footing dimensions).
[2]End bearing pressure to cause settlement of < 1% of minimum footing dimension.

A brief comparative study has been carried out for the purpose of this paper. Different wall heights and foundation bearing capacities have been combined to show the adequacy of the TechWall® solution as retaining solution for firm foundation materials. The base case for material and cost comparison is the 750 kPa assumed bearing capacity case. Refer to Table 4, and Table 5 for results.

Table 4: TechWall® Footing Optimisation H =6.0m. Standard backfill conditions (ϕ=36º, ɣ=20kN/m³, C=0kPa)

Bearing Capacity (kPa)	Wall Height 'H' (m)	Optimised Cost effective solution. Dimensions (m)			Bearing Pressure (Meyerhof)		Materials		Estimated Cost. Materials Labor Excavation (%)	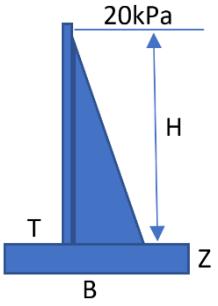
		T	B	Z	Min	Max	Conc Kg/m³ (%)	Steel m³/ml (%)		
100	6.0	2.1	4.6	0.6	86	117	350	47	215	
250	6.0	0.6	3.0	0.6	22	243	227	45	135	
500	6.0	0.5	2.6	0.3	0	370	100	103	103	
750	6.0	0.4	2.6	0.3	0	390	100	100	100	

Table 5: TechWall® Footing Optimisation H =8.0m. Standard backfill conditions (ϕ=36º, ɣ=20kN/m³, C=0kPa)

Bearing Capacity (kPa)	Wall Height 'H' (m)	Optimised Cost effective solution. Dimensions (m)			Bearing Pressure (Meyerhof)		Materials		Estimated Cost. Materials Labor Excavation (%)	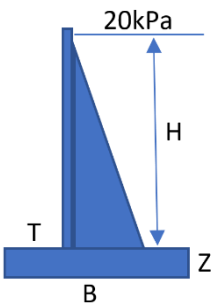
		T	B	Z	Min	Max	Conc Kg/m³ (%)	Steel m³/ml (%)		
100	8.0	Not suitable for TechWall® application								
250	8.0	1.0	4.5	0.8	72	246	170	82	155	
500	8.0	0.5	3.5	0.6	0	409	100	110	105	
750	8.0	0.4	3.5	0.6	0	430	100	100	100	

8 CONCLUSIONS

This paper presents the design principles for a partially prefabricated concrete counterfort retaining wall system TechWall®, as well as the suitability of the system from a geotechnical point of view as it relates to the prevalence of competent rock foundations in the Sydney Basin. In addition, a comparison between the proposed system and traditional cast-in-situ concrete L-shaped/counterfort retaining wall system was established demonstrating materially significant savings in concrete and steel reinforcement.

The following conclusions can be drawn:

- A partially prefabricated counterfort retaining wall system is an efficient solution for construction in congested areas on appropriate foundations.
- It provides advantages in terms of:
    - Environmental: carbon footprint reduction
    - Time: speed of construction
    - Quality: controlled fabrication process
    - Safety: reduction in temporary works
    - Community: Community impact reduction
    - Cost: reduction in materials and site works

The system is based on classic retaining wall design theory, and in the author's opinion does not contain any innovation in terms of design method. It is best suited to competent rock foundation and provides efficiencies in two primary ways. Firstly, the design software is a powerful iterative program which can automatically determine the most optimised arrangement depending on input constraints. Secondly, the precast elements provide significant advantages over cast-in-place systems in terms of quality, safety and speed of installation.

9 ACKNOWLEDGMENTS

The authors would like to thank Marcus Lindon and Angel Leon (Tierra Armada Spain) as well as David Hutchinson and Keith Brabant (Reinforced Earth US) for their support and collaboration in documenting and preparing this paper.

10 REFERENCES

Branagan, D.F. (1985). An overview of the geology of the Sydney Region *in* P.J.N. Pells, ed., Engineering Geology of the Sydney Region: A. A. Balkema, pp. 3-46.

Pells, P.J.N., Mostyn, G. & Walker, B.F. (1998) Foundations on Sandstone and Shale in the Sydney Region, Australian Geomechanics Vol 33, No.3, pp. 17-29

Huntington, W.C. (1957). Earth Pressures and Retaining Walls, New York: John Wiley and Sons. Chapter 6 "Retaining Wall Design", Article 35" Counterfort Walls" p. 470 onwards

GEOTECHNICAL INNOVATIONS IN THE TUNNELLING INDUSTRY

Robert Bertuzzi
Principal, PSM

ABSTRACT

The Australian tunnelling industry has been thriving. In Sydney alone there have been 11 major projects in the past decade: the M2 widening, Metro Northwest, NorthConnex, Sydney Opera House forecourt, Wynyard Walk, City East Cable Tunnel, WestConnex (M4 East, New M5, M4-M5 link, Rozelle Interchange) and Sydney Metro. All this work within the same geological environment has enabled much innovation in terms of geotechnical and hydrogeological understanding, analysis of primary support, waterproofing, geological mapping and recording of observations during construction. This presentation documents some of these innovations and suggests where the industry may be going in the short to medium term.

1 INTRODUCTION

"Innovate" is defined in the Macquarie Dictionary as *'to bring in something new'*. Innovation is sought and claimed by many in our engineering profession. One just has to look at any number of industry publications to see numerous headlines and advertisements featuring the word innovation (Figure 1). Interestingly, the word innovation is both loved and loathed having been included in the publisher Merriam-Webster Word of the Year list in 2014 but suggested by the news website Crikey as the worst word in 2016.

Figure 1: A recent edition of Engineers Australia's create magazine contained numerous references to innovation

This paper presents the "new somethings" that have been brought into Australian tunnelling over the author's 30 years in the industry and attempts to peer over the horizon to see where the industry might be going.

2 INNOVATIONS THAT HAVE WORKED

Many successful innovations have been brought into the Australian tunnelling industry by contractors, suppliers and designers since the 1990s. In rough chronological order these have been:

- A stacked alignment was used on the Eastern Distributor (1996-1999) to limit the impact of substratum acquisition (Figure 2). Its tunnel contains two separate traffic directions. An interesting aside to Australian tunnelling, is the stormwater management and road tunnel (SMART) in Malaysia (2007) (Figure 2). While this extraordinary tunnel is specific to Kuala Lumpur's needs, it and the Eastern Distributor provide examples of multi-function tunnels.

- Increased design life of bolts. Cement-grouted black steel bolts were used in the mid-1990s as 'permanent' support for the M2 road tunnels at Epping, Sydney. At about the same time, epoxy coated bolts were used in the Sydney Opera House Carpark and the CT-bolt was developed by Norwegian company Orsta Stal (Figure 3). Epoxy coated and sheathed rock bolts were used on the Eastern Distributor for its 50-year design life. CT-bolts and other similarly sheathed and cement grouted rock bolts, are deemed to have a 100-year design life and are the "default" bolt used.
- Remote bolting with the use of multi-boom rubber-tyred equipment removed the need to expose workers to the potentially unsupported ground as they manually installed rock bolts (Figure 4).
- Almost hand-in-hand with remote bolting, was the development of the handle-bar face plate (Figure 5). This plate provides a robust structural connection between the rock bolt and subsequently applied shotcrete layers while still fitting into the carousel of the remote rock bolter.
- Work procedures to deal with major risks associated with tunnelling, e.g. changed ground conditions or unsuitable support types.
    - The permit to tunnel (PTT) procedure is a process that allows geotechnical conditions, the performance of construction, the behaviour of the excavation and the documented design to be considered for upcoming work by the group of people most involved with tunnelling.
    - Similar to the PTT, a work procedure for installing appropriate groundwater control is enabling a targeted solution to be installed.
- Geophysical tools for recording geological structures encountered in boreholes. The acoustic televiewer (ATV) (Figure 6) enables greater clarity of structures that otherwise may be missed.
- Three-dimensional geotechnical and hydrogeological models are increasingly used to develop better understanding of ground conditions for tunnelling (Figure 6).

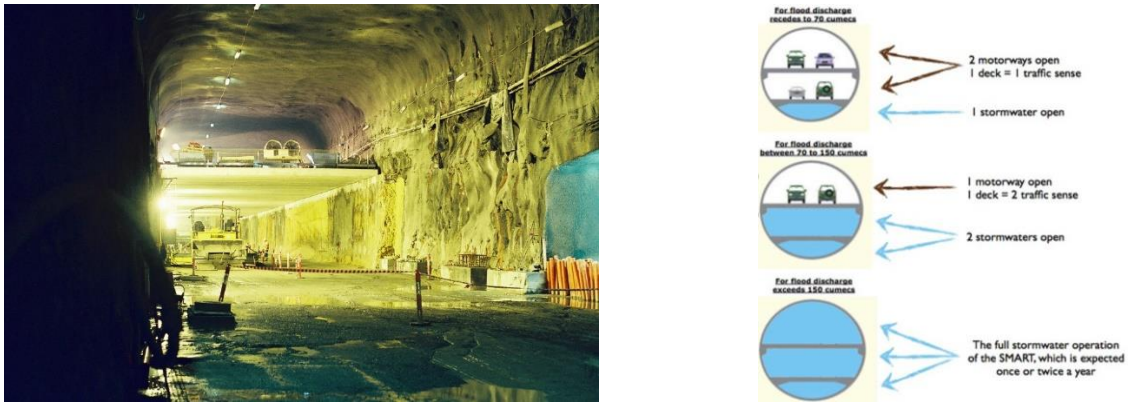

Figure 2: Double-deck Eastern Distributor (1999) – left; SMART, Kuala Lumpur, Malaysia (2007) – right

Figure 3: The CT-Bolt increased the design life to 100-years

Figure 4: Hand-installed (left) and remote bolting (right)

Figure 5: Handle-bar face plate for rock bolts.

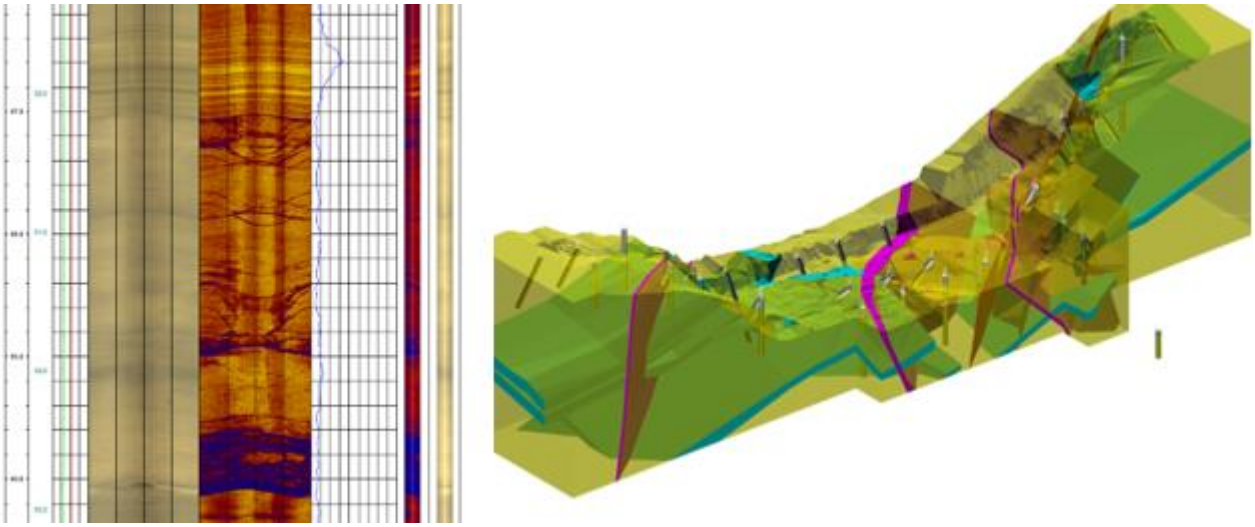

Figure 6: ATV borehole image on left. 3D geotechnical model on right

3 IDEAS THAT HAVE NOT SEEN THEIR DAY YET

This section documents a few ideas that have yet to be realised. The first two may seem frivolous but when they were mooted, it was with full intention of being the trump card to a tender win. The point of including them here is to acknowledge that innovations in our tunnelling industry are often attempted but many, maybe most, don't materialise for whatever reasons.

- Changes to road alignments are *de rigueur* during tenders for road tunnels. Realistically, most are minor tweaks to the reference design (with no offence to our road alignment colleagues), but the author is aware of a few more radical suggestions.
    - Rather than creating substratum issues and potentially affecting new third-party properties, an option of expanding capacity by tunnelling vertically beneath the existing road tunnel had been considered (Figure 7).
    - A helix / roundabout to provide connections between mainline tunnels to multiple entrances and exits without complex lane merging and under the 'one roof' (Figure 8).

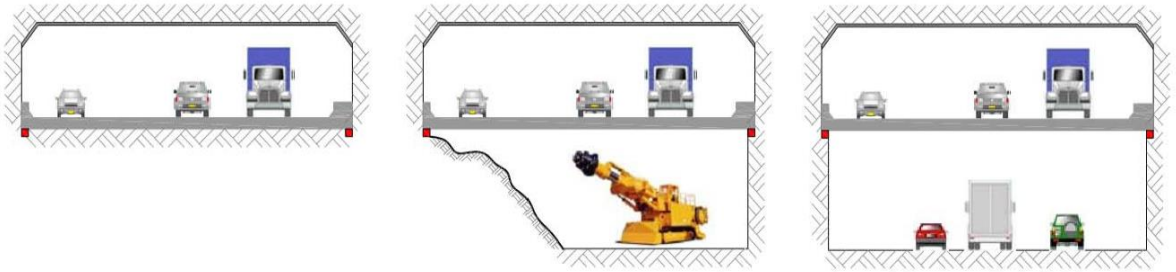

Figure 7: Expanding the capacity of existing tunnels by excavating beneath them

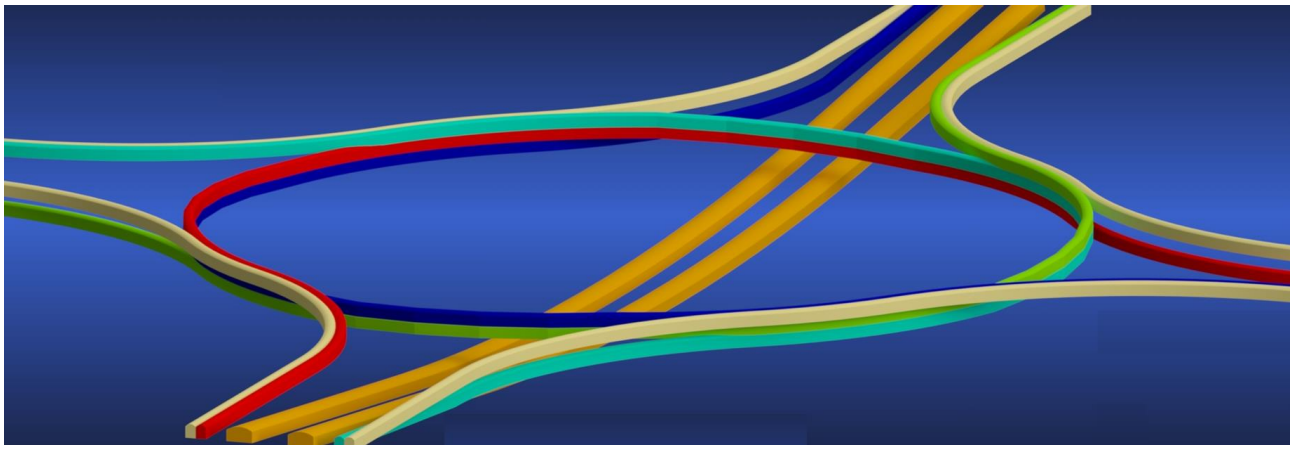

Figure 8: A helix that allows multiple entry and exit ramps without complex lane merges and underneath the one supported roof

It is unfortunate that the next two ideas have yet to find a firm footing in Australia.

- The Geotechnical Baseline Report (GBR) evolved in the USA in the mid-1990s to mid-2000s. '*The primary purpose of the GBR is to establish a single source document where contractual statements describe the geotechnical conditions anticipated to be encountered during underground and subsurface construction. The contractual statement(s) are referred to as baselines. Risks associated with conditions consistent with or less adverse than the baselines are allocated to the contractor, and those materially more adverse than the baselines are accepted by the owner.'* While the GBR concept had garnered initial interest here in the late 2000s, it has not really been embraced. In fact, recent Australian projects have taken the polar opposite view by passing the all the risk associated with the investigations which had been procured by the owner, to the contractor.
  The proponents of tunnels tend to be government agencies, who may consider a GBR offers more to the contractor by introducing uncertainty, and thereby risk, to themselves. It is noted that recent projects, notably Snowy 2.0, are trying to use it.

- Simplifying the design / review process. Bertuzzi & Rouvray (2014) addressed the design / review process and its associated cost that was in practice at the time. Disappointingly, things may have worsened rather than improved. This is further discussed in Section 6.

4 EXPECTATIONS

There is a trend for increasingly more complex geometries in underground excavations. Tunnels in the 1990s were mainly of uniform section, with no underground merges / diverges e.g. the Sydney Harbour tunnel, M2 road tunnel in Epping (Sydney), Burnley / Domain tunnels in Melbourne. Today, the Rozelle Interchange, which is part of the WestConnex project in Sydney, is a complex network of large span road tunnels. The complexity is not restricted to road interchanges as the reference design of an underground metro station shows (Figure 9).

No doubt the enviable conditions provided by the Hawkesbury Sandstone plays a major part in these designs. Such complexities can be entertained because of that rock mass. But it does raise the question are they necessary? Is the increased cost and risk justified?

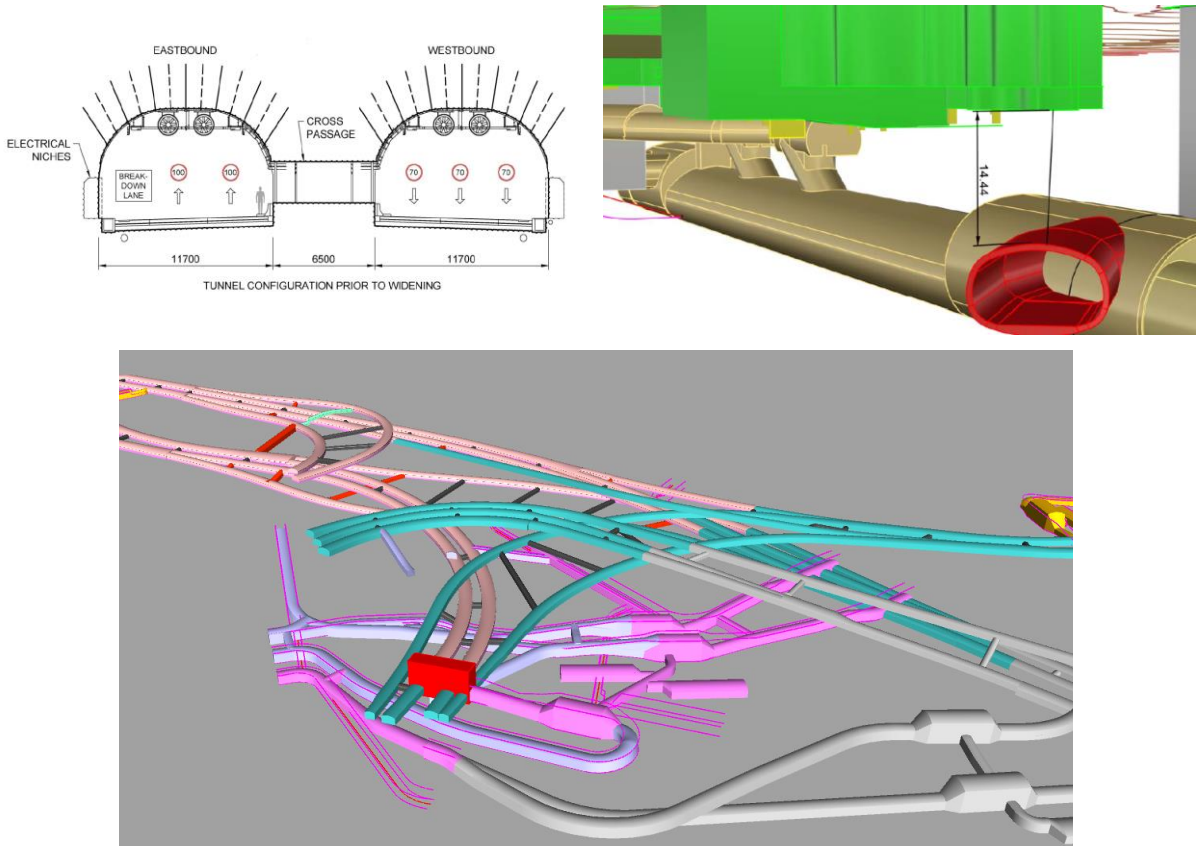

Figure 9: Increasingly complex underground geometries (top left) the M2 road tunnel in Epping (1995), (top right) metro station reference design (2017), (bottom) the Rozelle Interchange (2019)

What is acceptable in terms of the operation and maintenance (O&M) of underground infrastructure appears to be changing. For example, what was perceived acceptance of a limited but controlled groundwater inflow in the 1990s became a requirement to limit inflows a decade later, to now not allowing drips in road tunnels and for undrained rail tunnels. But along with the tighter restriction comes increased design and construction costs, not only from the additional loads and materials but also from the greater excavation volumes and construction time (Figure 10).

Counter-intuitively with more complex geometries and tighter O&M requirements, the expectation is greater productively and faster construction. Four roadheaders were used on the Eastern Distributor tunnel, 21 roadheaders were used for each of the four separate tunnelling projects that form WestConnex; 11 roadheaders were used from the one site (the Cintra site on the M4East).

Figure 10: Undrained tunnels require greater excavations and longer construction time

5 DEVELOPING IDEAS

A few innovations are currently being introduced into our tunnelling industry, largely driven by the increase in spans but also by the continuous need to improve efficiency and productivity.

- The merge and diverge of multiple lanes in road tunnels demand very wide span excavations. As too, do station platform caverns and interacting concourse caverns. Interestingly, the spans of the 90 large underground excavations listed in the seminal text book by Hoek & Brown (1980), ranged from 11.8 to 33.5 m with most between 15 and 20 m. By comparison this is now the standard width of road tunnels in Sydney. The important distinction is that the large underground excavations are at specific locations, whereas road tunnels are long linear structures and the risk of encountering unforeseen unfavourable conditions increases. Further, the merge/diverge caverns associated with the standard road tunnels are over 30 m wide and those of station platform caverns over 25 m wide.
- The support of these very wide span excavations is being achieved with a mix of cable and bar bolts (Figure 11). The mix attempts to maximise the use of the rigid bar bolts which currently can be installed much more efficiently than cables.
- The analyses of the capacities of bolts and of relatively thin layers of shotcrete is continuing to be pushed to achieve these very wide spans designs.
- Coupled with this, is the remote installation of cable bolts. Equipment design is continuing to develop a system for installing cable bolts that is as efficient as that for installing rigid bolts (Figure 12).
- Tele-remote equipment is available and proven in mining (Figure 12) but the tunnelling industry hasn't yet fully adopted it. Tele-remote equipment could provide opportunity to re-address the issue of unsupported ground.
- Laser / optical scanning for survey, material quantities (e.g. shotcrete thickness) but also for geological mapping and convergence monitoring (Figure 13).

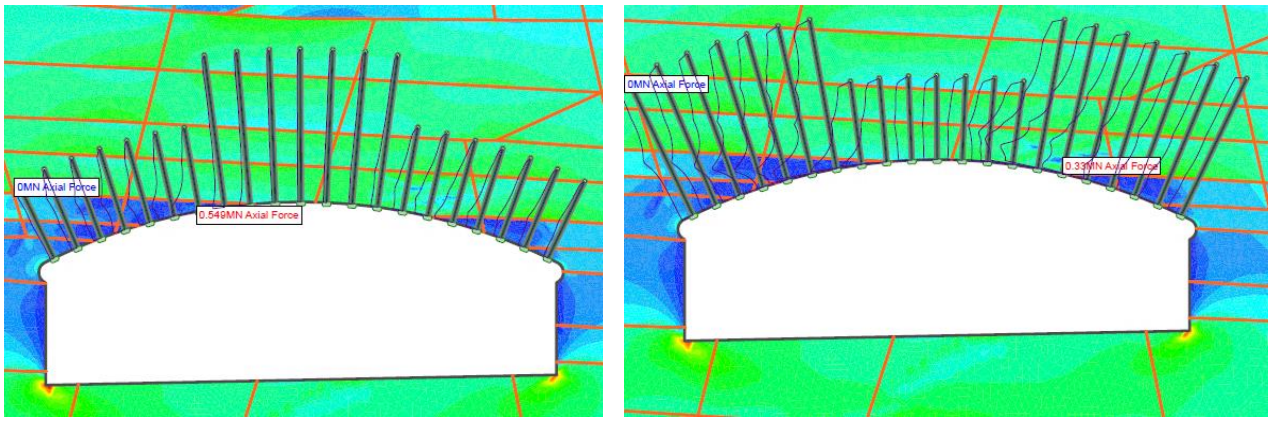

Figure 11: Alternatives to supporting very wide spans: longer bolts / cables in the centre (left) or longer bolts / cables in the shoulders

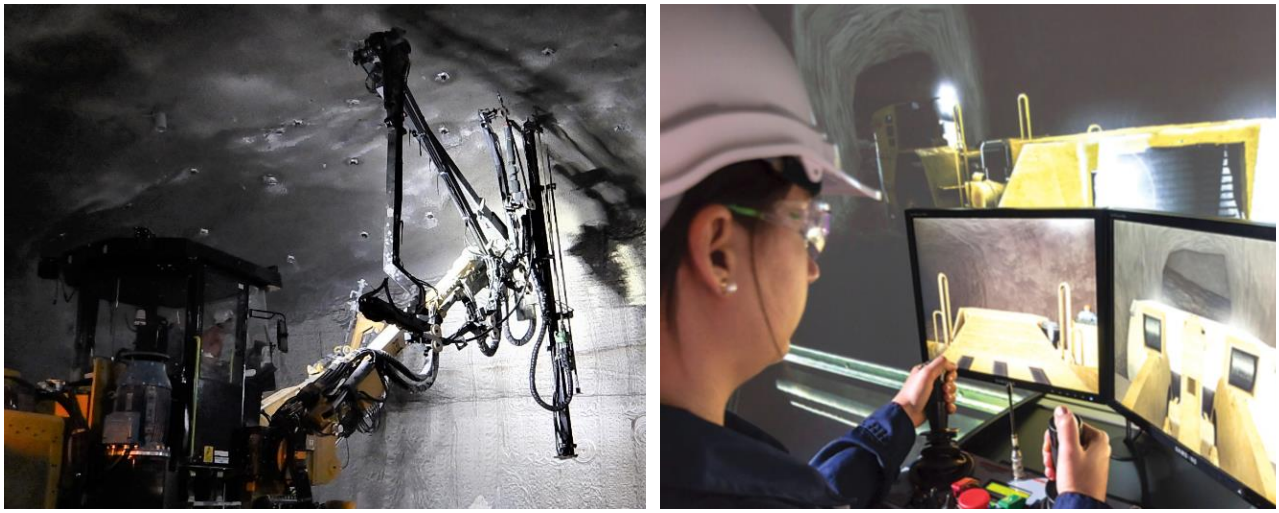

Figure 12: Left: The cable bolt rig which was used in Sydney's WestConnex M4 East road project had limited success. Right: The technology to remotely operate roadheaders, bolting rigs, shotcrete rigs, etc.

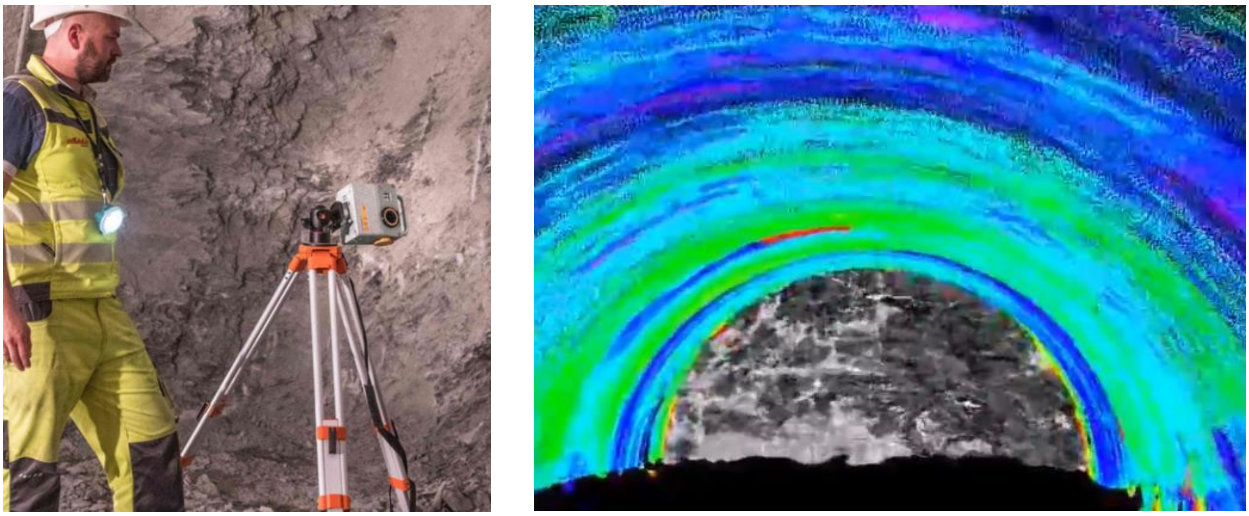

Figure 13: Scanners for surveying, geological mapping and convergence monitoring

6 WHERE INNOVATION IS NEEDED

Undoubtably this section will prove to be controversial, but in this author's opinion there are two areas that desperately need innovation: the design / review process and the timeframes for large infrastructure projects. Both of these areas require both contractor and client innovation, i.e. essentially the government agencies need to *'to bring in something new'*.

Figure 14 presents the flowchart explaining the design review process for recent tunnelling projects. That the process requires a flowchart at all, is telling. Then add the complexity of the flowchart. Then appreciate that the process passes through this flowchart four times before the design is complete and construction can start. Is it any wonder that the cost of the design / review process is now some 20 times more expensive than it was for the Eastern Distributor? Normally, it would be reasonable to expect that the item becomes cheaper the more it is made. There was approximately 1 km of road tunnels in Sydney when the Eastern Distributor was being constructed. There is now over 100 km.

As the design / review process has become unwieldly, the timeframe for projects has shortened considerably. An outsider to our industry would think that site investigations would proceed the development of a geotechnical and hydrogeological model which in turn would proceed design and construction would follow. Modern infrastructure tunnelling projects has turned this logical sequence on its head. In recent projects these naturally sequential events have overlapped so much that it is not unusual to see site investigations continuing as construction starts.

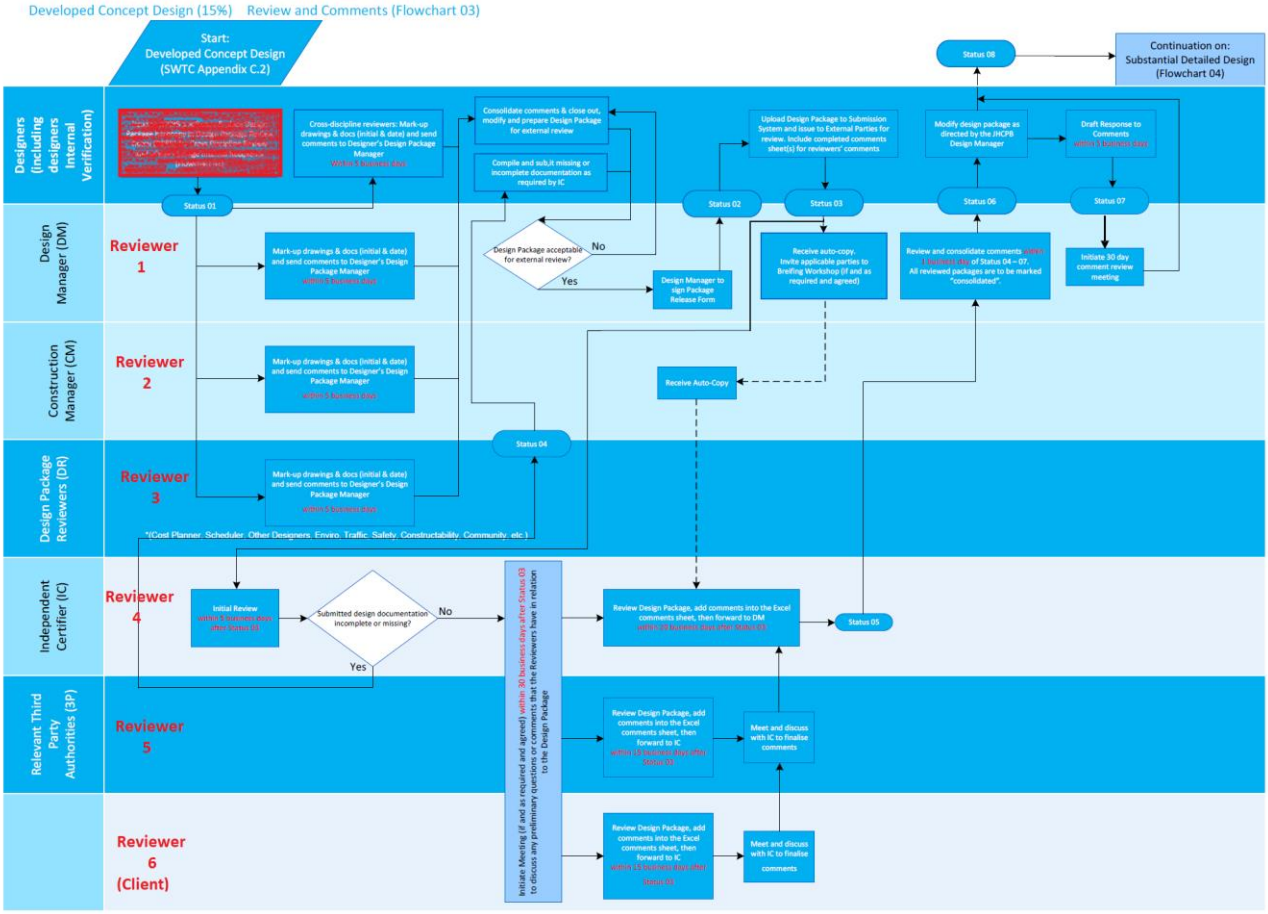

Figure 14: Flowchart of the review process for a recent project

7 CHALLENGE

One of the next tunnelling projects expected in Sydney is the F6 Extension road tunnel. It is wholly within the Hawkesbury Sandstone. So, the challenge is to the client and contractor: can we curtail the tender, how about the design / review process? Can a single cross-section be adopted for the twin tunnels? One that fits within precedence of the >100km built in Sydney. We all know what the support will comprise. How about introducing a GBR so that the risk of encountering unforeseeable conditions can be shared? Imagine the benefits of such innovation not just to our industry but to the wider community.

8 ACKNOWLEDGMENTS

I'd like to thank my colleague Daniel Strang for duping me into preparing this paper and its accompanying presentation for the 23rd AGS Symposium. Though it coincided with an extremely busy time for me, it was edifying. I hope others find it interesting. I'd also like to thank Andrew de Ambrosis who may not share my views, but always proves to be a great sounding board.

9 REFERENCES

Bertuzzi, R. & Rouvray, B. (2014). Reducing the cost of tunnel design in Australia. *Proc. 15th Australasian Tunnelling Conf*, 17–19 September, Sydney, Australia, 501-506.

Hoek, E. & Brown, E.T. (1980). *Underground excavations in rock*, London, IMM.

AN EMPERICAL MODEL TO CORRELATE ROCK MASS CLASSIFICATION AND HYDRAULIC CONDUCTIVITY, GEOTECHNICAL ENGINEERING DATA ACQUISITION AND REDUCTION PERSPECTIVE

Demeke Jembere[1*] and Yohannes Yihdego[2]

*[1]Roads and Maritime Services, Parramatta, NSW2150, Australia. *E-mail: Demeke.Jembere@rms.nsw.gov.au, djembere@yahoo.com.au*

[2]Department of Ecology, Environment and Evolution, College of Science, Health and Engineering, La Trobe University, Melbourne, Victoria, 3086, Australia

[2]Snowy Mountains Engineering Corporation (SMEC), Sydney, NSW 2060, Australia

[2]E-mail: yohannesyihdego@gmail.com

ABSTRACT

This paper presents an empirical model for estimating rock mass hydraulic conductivity of fractured Hawkesbury Sandstone in the Sydney basin. The hydraulic conductivity of a fractured crystalline rock mass can be a critical factor in tunnelling projects and dewatering designs. The Lugeon test (commonly known as the “packer test”) is a common test used to estimate the in-situ permeability of a rock mass.

The Packer test is carried out over a specific length (typically 3-6 m) within a borehole to reduce the range of variation of the affecting parameters. To construct a detailed profile of hydraulic conductivity through the rock mass a relatively large number of Packer tests are often required which can be costly and time consuming.

The new rock mass classification system called the “HC system” was proposed by Hsu et al. (2011). The HC-system assists with the hydraulic modelling of a rock mass and is based on 4 parameters which can be readily assessed from borehole logs and borehole Televiewer data, namely Rock Quality Designation (RQD), Depth Index (DI), Gouge Content Designation (GCD) and Lithology Permeability Index (LPI). A modified new rock mass classification system called the "HC-system" or HC model has been specifically developed for Hawkesbury Sandstone in the Sydney basin.

Regression analysis was conducted to assess the correlation between the calculated HC value (using the HC model) and the corresponding hydraulic conductivity from the in-situ packer tests.

To confirm the feasibility of the proposed empirical HC model, the model was subsequently used to estimate the hydraulic conductivity of similar Hawkesbury Sandstone boreholes from a range of projects that also have corresponding Packer test data for comparison.

This empirical HC model may assist with two important hydrogeological applications. The first application is to estimate hydraulic conductivity of fractured sandstone of similar geological set up based on HC-values. By using this approach, hydraulic conductivity data in a given site can be estimated from borehole data, which increases the reliability and confidence of the packer testing. Secondly, for in-situ aquifer tests the HC-system is a valuable new rock mass classification system for estimating the degree of permeability of a borehole. The results obtained confirm the validity and flexibility of the empirical approach to handle cases of onshore and offshore data sets, in relation to data acquisition and data reduction (optimisation).

Keywords: Lugeon, hydraulic conductivity, Rock Quality Designation (RQD), Depth Index (DI), Gouge Content Designation (GCD), Lithology Permeability Index (LPI), Regression analysis.

1 INTRODUCTION

Triassic Hawkesbury Sandstone occupies an area of some 12,500 square kilometres in the Sydney basin (Geological Society Australia, 1969). Sydney is currently undertaking several major transportation tunnelling projects through Hawkesbury Sandstone. In this paper, data from different projects in Hawkesbury Sandstone within the Sydney basin are considered.

Engineering tasks such as tunnel construction, slope stabilisation, dam construction, mine development and petroleum abstraction require the estimation of hydraulic conductivity of fractured rock mass. The understanding of hydraulic properties of fractured rock mass, which involves the fluid flow behaviour in fractured consolidated media, is a critical step in support of these tasks. To obtain hydraulic properties of fractured rock mass, packer testing can be adopted. Although this type of test can directly measure the hydraulic conductivity, costs of the testing can be relatively high. The precision of the packer test and reporting depends on a number of factors from the beginning to the end of the testing and interpretation. Several studies (Snow, 1970; Louis, 1974; Carlsson & Olsson, 1977; Burgess, 1977; Black, 1987; Wei et al., 1995; Yihdego 2016) have proposed the estimation of rock mass hydraulic conductivity using different empirical equations, which were based on the concept that rock mass permeability decreases with depth, however hydraulic properties of rock mass may also vary with other factors including; geostatic stress, lithology, fracture properties and filling materials.

The use of empirical methods is a common practice in the geotechnical community. This paper proposes an empirical model to estimate hydraulic conductivity (K) of fractured sandstone rock mass based on the Rock Mass Classification (RMC) concept. The new rock mass classification system called the “HC system” was proposed by Hsu et al. (2011). It is based on the following four parameters: Rock Quality Designation (RQD), Depth Index (DI), Gouge Content Designation (GCD) and Lithology Permeability Index (LPI). HC index can be calculated from borehole image data and rock core data. Hydrogeological studies are typically piggy-backed onto geotechnical investigations to reduce design and construction costs; cross correlation between data sets can provide additional insights.

Regression analysis was done to evaluate the dependence of HC-Values on measured hydraulic conductivity from Packer tests. As a result, an empirical formula was constructed to estimate the hydraulic conductivity. The details and the rating approach of each of the parameters are discussed. The feasibility of using HC-System on this study area is analysed.

In this case study a realistic and improved correlation (between RMC and K) was carried out in Sydney basin by integrating and maximising existing data and turning to useful information via data fusion, interpolation and interpretation. The results obtained confirm the validity and flexibility of the empirical approach to handle cases of onshore and offshore data sets, in relation to data acquisition and data reduction (optimisation). However, they may not provide fundamentally new insights as to the overall application of correlation indicated by the empirical model.

The purpose of this empirical model is; to reduce the cost on hydraulic testing, increase the confidence in data retrieved from packer testing and for the preliminary assessment of the degree of permeability of fractured sandstone.

2 STUDY AREA

The geology of study area is comprised of Permo-Triassic sedimentary rocks overlain by Quaternary aged sediments. Within the depth of investigation the geological sequence along the project alignment used for this assessment comprises a thick sequence of Hawkesbury Sandstone. In the more elevated areas, for example at North Sydney, Ashfield Shale of the Wianamatta Group overlies the Hawkesbury Sandstone (although it was not encountered in boreholes used for this assessment. The Hawkesbury Sandstone comprises three main facies:

- Sheet facies.
- Massive facies.
- Mudstone facies.

The sheet and massive facies make up about 95% of the total thickness of Hawkesbury Sandstone. The sheet facies comprise cross-bedded strata bounded by near horizontal bedding planes. The massive facies is composed of poorly sorted sand, and often contains clasts and flakes of mudstone (or siltstone). The mudstone facies can form strata up to about 10m thick, with interlaminated dark grey siltstone and sandstone.

3 ASSESSMENT OF AQUIFER PERMEABILITY

3.1 PREVIOUS ASSESSMENT

McKibbin and Smith (2000) quote a hydraulic conductivity range for the Hawkesbury Sandstone between 0.01 and 1 m/day (1 and 100 uL) and note that values in excess of 0.1 m/day (>10uL) are probably associated with fracture permeability.

Interpretation of the in-situ water pressure test results (packer tests) yielded a range of Lugeon rock mass permeability values from <1uL to >100uL. The permeability of the rock mass can vary rapidly with the influence of local features. The unscaled geometric mean hydraulic conductivity within Hawkesbury Sandstone may generally vary between 10^{-6} m/s to 10^{-7} m/sec (as determined by discrete borehole "packer" testing). However, individual tests in a single borehole can vary between the lower and upper bound capabilities of the test apparatus (effectively ranging from less than 10^{-8} m/sec to greater than 10^{-5} m/sec). Hewitt (2004).

3.2 CURRENT ASSESSMENT

As indicated in Table 1, assessment of 441 successful five stage Packer test results from 95 boreholes in Hawkesbury Sandstone within the Sydney area was carried out which indicates Lugeon values in the range <1uL to >100uL. Out of the total 441 packer tests 295 of the tests (67%) recorded Lugeon values < 1uL (very tight discontinuity) and were therefore excluded from this assessment. Data with the same Lugeon values were also excluded to minimise repetition. This resulted in 65 representative Packer tests used for the development of the empirical model.

Table 1: The rock mass permeability based on the packer test results (Lugeon values)

Lugeon Values	Relative Permeability	No. of Packer Tests		Percentage of Tests
		Offshore	Onshore	
<1	Low	86	209	67%
1-5	Moderate	36	23	13%
5-20	High	27	16	10%
20-50	Very High	28	4	7%
>50	Extremely High	12	0	3%
Total		189	252	100%

The field test results (Packer and slug tests) indicated that the rock mass in the study area has a hydraulic conductivity between the order of 10^{-5} m/s and 10^{-8} m/s at depth between 5m and 144m BGL.

The higher Lugeon values (>20uL or > 2 x 10^{-6} m/s) are recorded at offshore tests and close to the harbour foreshore. This is attributed to a higher incidence of open (highly permeable) rock structure induced by stress relief in the steeper topography and possibly more weathering, associated with palaeovalley. Due to these variations separate analyses were carried out for offshore and onshore investigations.

4 COMPONENTS OF NEW ROCK MASS CLASSIFICATION SYSTEM HC INDEX

The new rock mass classification system potential factors, including Rock Quality Designation (RQD), Depth Index (DI), Gouge Content Designation (GCD) and Lithology Permeability Index (LPI), that may affect the degree of permeability are considered. The rating approach for each factor that represents the magnitude of permeability is described.

Since these parameters are typically assessed during geotechnical investigations, the quality of the investigation and testing (Jembere and Yihdego 2016) can affect the correlations of the new rock mass classification system with hydraulic conductivity. Figure 1 shows the strategy used for assessing these parameters from core photos and imaging.

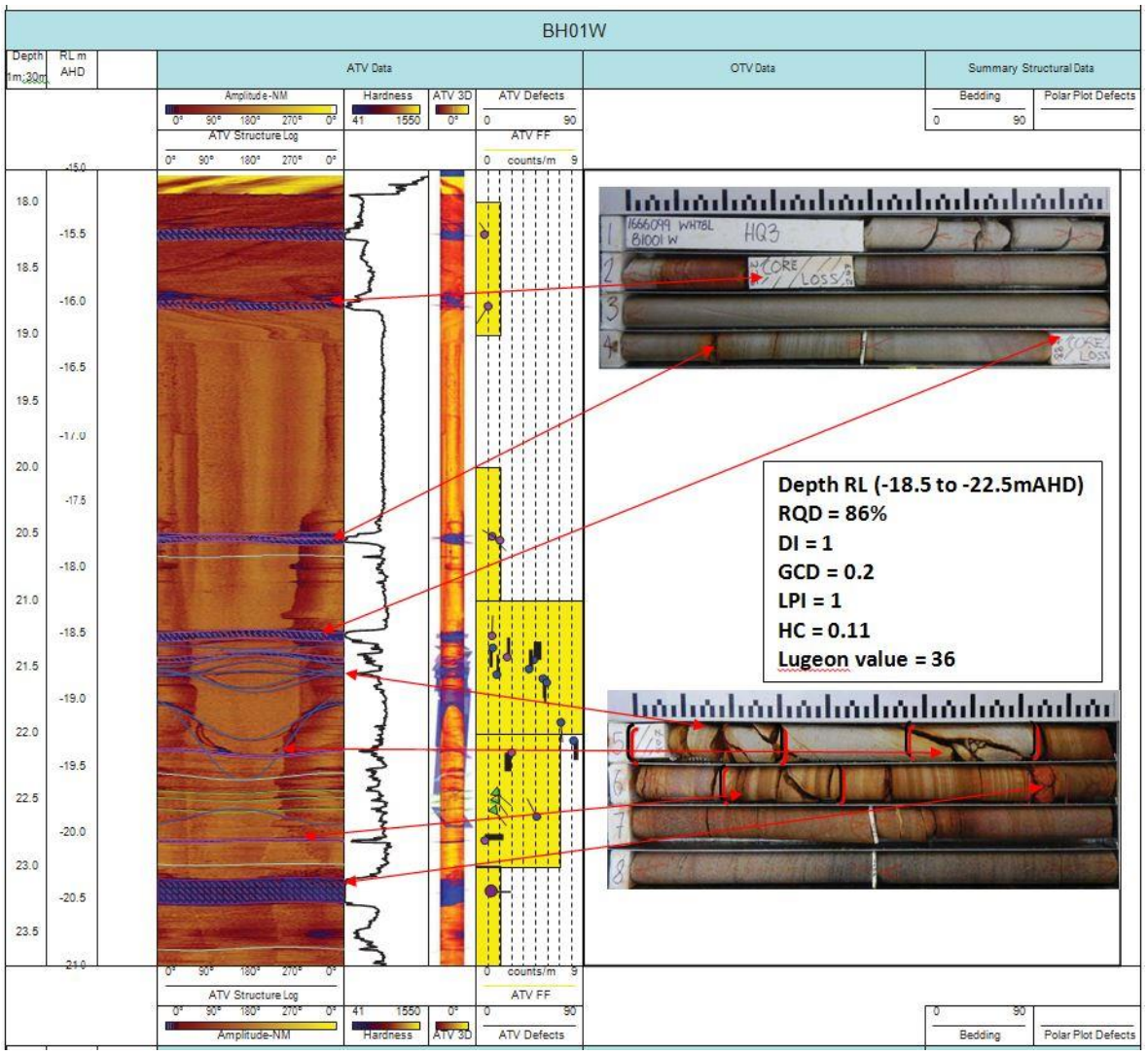

Figure 1: Identification of fractures and crushed zones from ATV image and core photo

4.1 ROCK QUALITY DESIGNATION (RQD)

The degree of fracturing may be regarded as a factor in evaluating rock mass permeability. RQD is an index to evaluate and quantify the rock mass quality developed by Deere et al. in 1967. It can be used to assess the influence of the fracture characteristic on permeability.

$$\boldsymbol{RQD} = \frac{\sum \boldsymbol{RSx100}}{\boldsymbol{RT}} \tag{1}$$

RS – Length of core pieces longer than 100mm in a run.
RT – Total length of the core run.

The HC-Value is calculated from the inverse relationship of RQD ($1-RQD/100$). The result of the equation will give a HC-Value between 0 and 1. The greater the RQD, the lower the HC-Value. If the RQD is 100%, ($1-RQD/100$) will become zero. To avoid this situation, the term ($1-RQD/100$) should be taken as 0.01 or less depending on the overall RQD values (Hsu et al., 2011).

4.2 DEPTH INDEX (DI)

Many researchers (for example Lee & Farmer, 1993; Singhal & Gupta, 1999) have indicated that rock mass permeability may decrease systematically with depth. The decrease in permeability with depth in fractured rocks is usually attributed to a reduction in fracture aperture and fracture spacing (Ku et al., 2009). The reduction is due to the effect of geostatic stresses, and therefore the permeability of fractured rocks will reduce. The depth may be considered as a factor in evaluating rock mass permeability. To assess the influence of the depth on permeability, a depth index called DI was defined as the following equation.

$$DI = 1 - \frac{LC}{LT} \quad (2)$$

LC – A depth which is located at the mid-point of hydraulic test (middle of a packer test interval in the borehole).
LT – Total length of a borehole.
The term $(1-LC/LT)$ with a number ranging from 0 to 1 is used so that a deeper depth will give a lower HC-Value.

4.2.1 Use of Depth Index in the HC value equation

The term Depth Index (DI) is calculated by equation 2, where LC is the depth at the middle of a packer test interval in the borehole and LT is the total depth of the borehole. It is the ratio of the Packer Test depth compared to the total depth of that particular borehole. It is meaningful only when all the Packer tests are done in one single borehole. For instance, if two boreholes were drilled, Borehole A is 100m deep and Borehole B is 200m deep. Two Packer tests were done at the same depth (50m) in both boreholes. Depth Index (DI) at 50m of Borehole A will be $1-50/100 = 0.5$ while at 50m of Borehole B will be $1-50/200 = 0.75$. However, the Depth Index (DI) is developed based on the presumption that the permeability of a rock mass decreases with depth due to the reduction in fracture aperture and spacing (Ku et al., 2009), they should therefore have the same value of DI for the same depth of 50m. Hence, unless the results of DI are normalized for holes with different total length, they cannot be used directly for comparison.

The study area was subjected to tectonic deformations mainly near the harbour and resulted in fractured rocks; this means that the fracture aperture and spacing of rock mass is not only controlled by depth.

To evaluate the relationship between vertical depth and hydraulic conductivity in Hawkesbury Sandstone, the mid-depth of the Packer test section and the corresponding hydraulic conductivity are plotted as shown in Figure 2 (Hewitt 2004).The plot shows that although the zones with higher permeability tend to be found in shallower depths, there is no obvious correlation between the depth and the hydraulic conductivity which does not make it a good indicator of hydraulic conductivity. It is concluded that the depth is not a significant factor on the hydraulic conductivity of this project, so the Depth Index (DI) is taken to be 1.

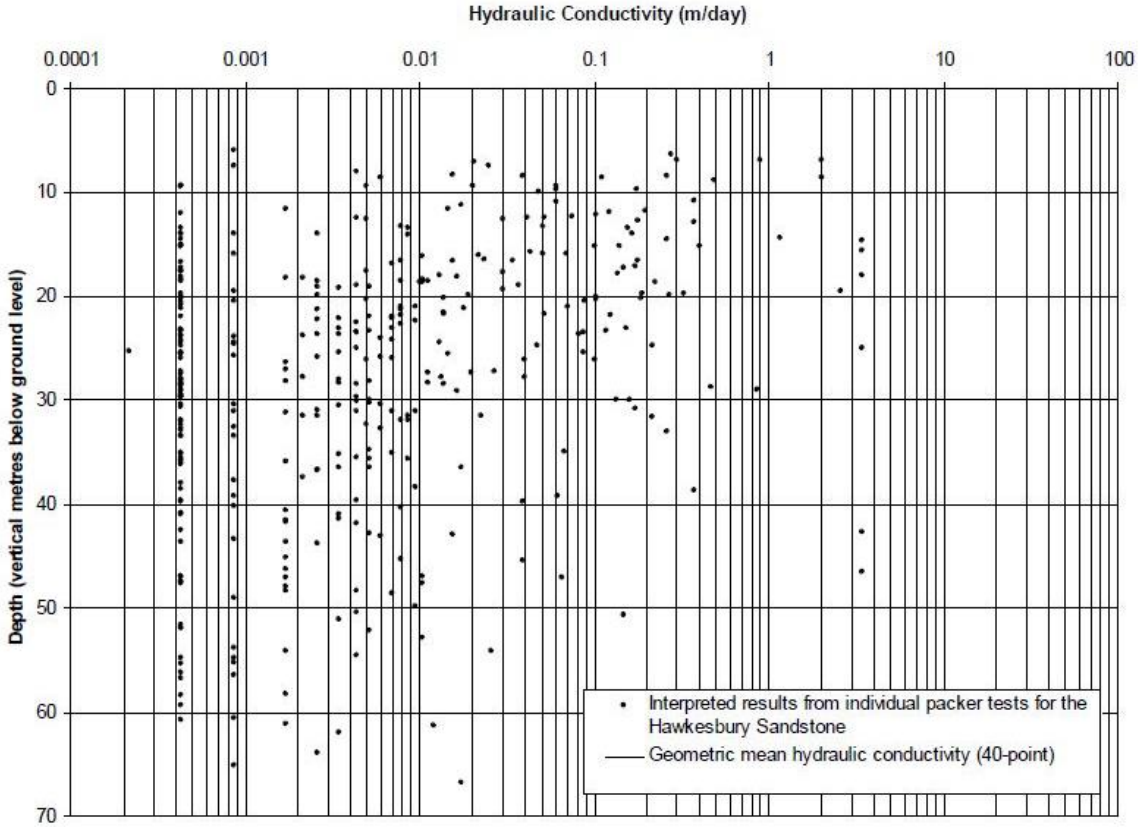

Figure 2: Hydraulic conductivity interpreted from packer tests Hewitt 2004)

4.3 GOUGE CONTENT DESIGNATION (GCD)

In general, the permeability of clay-rich gouges has extremely low values (Singhal & Gupta,1999). The RQD value may decrease by an increase of fractures in a core run. If the fractures contain infillings such as gouges, permeability of the fractures will reduce. To assess the influence of the gouge materials on permeability, a gouge content designation index called as GCD was defined as the following equation:

$$GCD = \frac{RG}{RT - Rs} \quad (3)$$

RG – Total length of gouge content from the total of core run.
RT – Total length of the core run.
RS – Length of core pieces longer than 100mm in a run.

GCD has a value between 0 and 1. With the greater length of gouge content RG, the value of GCD will be smaller and thus a lower permeability and a smaller HC value.

4.4 LITHOLOGY PERMEABILITY INDEX (LPI)

The previous three parameters, RQD, DI and GCD are factors related to fracture properties (RQD and DI: fracture aperture and spacing; GCD: infilling materials). Apart from fracture properties, the rock matrix lithology also affects the permeability. Lithology of a rock mass refers to the mineral composition, texture, grain sized and so forth (Hsu et al., 2011). The porosity of the intact rock is controlled by the size, shape and degree of sorting of the composing particles. Especially for sedimentary rocks, the particle properties greatly affect the permeability. Sandstone with larger grain size will have a higher permeability than siltstone which has smaller grain size.

To evaluate the permeability of different rock types, an index called Lithology Permeability Index (LPI) is defined (*Hsu et al., 2011*) with some suggested values for different lithology as shown in Table 2. Since all of the rocks tested in this study are sandstone, the LPI is taken as 1.

Table 2: Rating for LPI values based on lithology

Lithology	Hydraulic Conductivity (m/s)				Range of Rating	Suggested Rating
	Reference[a]	Reference[b]	Reference[c]	K average		
Sandstone	10^{-6}-10^{-9}	10^{-7}-10^{-9}	10^{-7}-10^{-9}	$10^{-7.5}$	0.8 – 1.0	1.00
Shale	10^{-10}-10^{-12}	10^{-10}-10^{-13}	-	$10^{-10.5}$	0.4 – 0.6	0.50
Siltstone	10^{-10}-10^{-12}	-	-	10^{-11}	0.2 – 0.4	0.30
Sandy Siltstone	-	-	-	-	0.3 – 0.4	0.40

[a]B.B.S. Singhal and Gupta (1999). [b] Karlbeinz Spitz and Joanna Moreno (1996) [c] Bear (1972)

5 ROCK MASS PERMEABILITY AND EMPIRICAL HC MODEL

5.1 HC INDEX

As stated in Section 4, the rock mass permeability may be dependent on the following four parameters: Rock quality Designation (RQD), Depth Index (DI), Gouge Content Designation (GCD), and Lithology Permeability Index (LPI). The permeability is possibly affected by any two factors, three factors or even all four factors. Thus, a rock mass classification scheme was applied to establish the rock mass permeability system. The new rock mass classification scheme is the product of the four parameters. It can account for the synthetic effect from the four parameters on permeability.

The new rock mass classification system called the "HC-system" is given by the following equation Hsu et al. (2011).

$$HC = (1 - \frac{RQD}{100}) \times DI \times (1 - GCD) \times LPI \quad (4)$$

Where:
HC – HC Value.
RQD – Rock Quality Designation.
DI – Depth Index.
GCD – Gouge Content Designation.
LPI – Lithology Permeability Index.

The value of each parenthesis at the right hand side of Equation (4) is always greater than zero and less than one depending on the values assigned to the four parameters. The greater the value of each parenthesis, the higher the permeability. Thus, the system performs a numerical assessment of the rock mass permeability using the four parameters. However, it should be noted that if (1−RQD) is zero, a value of 0.01 (or lower) in the term of (1−RQD) should be used to avoid the HC-value being zero. The rationality of Equation (4) must be verified by observed data through in-situ hydraulic tests.

5.2 RELATIONSHIP OF HYDRAULIC CONDUCTIVITY AND HC-SYSTEM FOR ONSHORE AND OFFSHORE TESTS

To verify rationality of Equation (4), the study collected in situ hydraulic test data (30 onshore and 35 offshore tests) to determine the relationship between hydraulic conductivity and HC-index. The HC values were plotted in a scatter plot with hydraulic conductivity from packer tests for both onshore and offshore. Borehole Id with "W" shows that tests are carried out in offshore areas and plotted separately in Figure 3.

Based on packer test results, the hydraulic conductivity (K values) in the study area was heterogeneous. The K values generally ranged from 10^{-8} to 10^{-6} m/s. The contributions of each of the four parameters are summarized in an HC index-empirical approach shown in Table 3.

To evaluate the relationship between variables and to determine how well a model fits the data, a statistical method called Regression Analysis was undertaken to estimate the dependence of HC Value on hydraulic conductivity. A total of 65 Packer tests were applied to the study. HC-values can be calculated from borehole image data and rock core data, in which the values of RQD and GCD at each test interval with Equations (1) and (3), respectively. The value of DI is not a significant factor on hydraulic conductivity for the current investigation, so the Depth Index is taken to be 1. The value of LPI for each test zone can be obtained from rock core data and Table 2.

Table 3 shows the calculated results for the HC-system based on the validated 65 Packer test data. The regression results indicate that a power law relationship exists between the hydraulic conductivity from the Packer Tests and HC values with a coefficient of determination of R^2 equals 0.95 for both onshore and offshore tests, which means 95% of test data points can be explained by the line as shown in Figure 3 . The empirical HC model is shown in Equation 5 & 6.

$$K = 1 \times 10^{-5} \times (HC)^{0.85}, \; R^2 = 0.95 \quad \textit{for onshore tests.} \tag{5}$$

$$K = 4 \times 10^{-5} \times (HC)^{1.12}, \; R^2 = 0.95 \quad \textit{for offshore tests.} \tag{6}$$

Table 3: The calculated HC values compared to the 65 Packer Tests results, ID's with "W" are offshore tests.

Hole ID	Test intervals(m)	Total Depth(m)	1-(RQD/100)	DI	1 - GCD	LPI	HC Value	K (m/s) from Packer Test
B10	45.5 - 54.4	57	0.04	1	0.50	1	0.022	3.7E-07
B10	51.5 - 54.4	57	0.10	1	0.33	1	0.034	7.2E-07
B28	05 - 11.0	19	0.08	1	0.20	1	0.017	3.8E-07
B28	15 - 19.0	19	0.10	1	0.25	1	0.025	5.5E-07
B32	65.2 - 70.5	104	0.01	1	1.00	1	0.009	2.0E-07
B38	59 - 68.0	137	0.02	1	0.75	1	0.017	2.9E-07
B40	66.4 - 75.4	113	0.01	1	1.00	1	0.010	3.4E-07
B40	101.3 - 106	113	0.05	1	1.00	1	0.049	1.01E-06
B41	33.4 - 39.4	113	0.01	1	1.00	1	0.008	1.70E-07
B77	30.5 - 38.2	79	0.05	1	0.78	1	0.039	7.4E-07
B77	33.1 - 38.2	79	0.04	1	1.00	1	0.023	6.9E-07
B77	39.9 - 42.4	79	0.15	1	1.00	1	0.15	3.4E-06
B65	20.5 - 26.5	56	0.01	1	1.00	1	0.009	2.3E-07
B6	14.09 - 25.5	86	0.005	1	1.00	1	0.005	1.9E-07
B6	47.47 - 53.27	86	0.01	1	1.00	1	0.013	3.2E-07
B34	41.5 - 48	76	0.01	1	1.00	1	0.009	2.4E-07
B210	33.2 - 39.42	53	0.06	1	1.00	1	0.065	1.5E-06
B210	39.2 - 45.4	53	0.01	1	1.00	1	0.006	2.3E-07
B211	10.4 - 15.7	57	0.04	1	0.35	1	0.013	3.0E-07
B211	14.3 - 18.3	57	0.10	1	0.57	1	0.056	9.2E-07
B211	24.9 - 28.7	57	0.07	1	0.50	1	0.034	7.7E-07
B211	33.26 – 38.8	57	0.11	1	0.79	1	0.085	1.6E-06
B211	36.1 - 41.7	57	0.05	1	0.22	1	0.011	2.3E-07
B21	10.35 - 15.59	43	0.12	1	0.44	1	0.053	1.0E-06
B221	12.3 - 15.59	43	0.19	1	0.44	1	0.082	1.5E-06
B221	15.16 - 26.02	43	0.005	1	1.00	1	0.005	1.4E-07
B233	12.5 – 20.5	53	0.01	1	1.00	1	0.005	1.7E-07
B233	35.9 - 41.8	53	0.09	1	0.17	1	0.015	4.0E-07
B238	58.5 – 69.7	144	0.01	1	1.00	1	0.005	1.4E-07
B13	51.6 - 57.6	120	0.03	1	0.25	1	0.007	2.7E-07
B02W	18 - 23	29	0.32	1	1.00	1	0.320	1.15E-05
B02W	13 - 20	29	0.15	1	1.00	1	0.150	4.3E-06
B02W	24 - 29	29	0.02	1	1.00	1	0.02	2.2E-07

Hole ID	Test intervals(m)	Total Depth(m)	1-(RQD/100)	DI	1 - GCD	LPI	HC Value	K (m/s) from Packer Test
B01W	4.85 - 8.5	23	0.14	1	0.80	1	0.112	3.6E-06
B01W	9 - 13.3	23	0.37	1	1.00	1	0.370	1.4E-05
B04W	8-15.18	26	0.097	1	0.71	1	0.069	2.3E-06
B05W	4.7 - 10.95	27	0.18	1	1.00	1	0.179	7.7E-06
B06W	18.5 - 24.5	31	0.23	1	1.00	1	0.230	1.15E-05
B08W	14.0 - 21.6	21	0.02	1	0.33	1	0.007	1.6E-07
B09W	16.5 - 22.5	79	0.01	1	1.00	1	0.005	2.7E-07
B10W	11.5 - 17.5	21	0.15	1	1.00	1	0.150	4.7E-06
B11W	28 - 32.6	70	0.11	1	0.33	1	0.043	1.1E-06
B16W	17.5 - 27	27	0.004	1	1.00	1	0.004	1.15E-07
B16W	9.5 - 12.5	27	0.03	1	0.44	1	0.013	2.3E-07
B21W	7.7 - 12.6	23	0.03	1	1.00	1	0.027	8.2E-07
B23W	6.3 - 12.2	17	0.04	1	1.00	1	0.039	1.2E-06
B24W	9.1 - 11.94	31	0.09	1	0.40	1	0.035	6.7E-07
B24W	10.8 - 17.93	31	0.05	1	0.43	1	0.021	3.9E-07
B68W	13.8 - 20	20	0.10	1	1.00	1	0.100	3.3E-06
B69W	3.7 - 9.05	15	0.08	1	1.00	1	0.079	2.4E-06
B71W	3.5 - 10.8	22	0.13	1	0.89	1	0.115	3.4E-06
B212W	32.1 - 40.53	84	0.02	1	0.50	1	0.012	3.1E-07
B212W	39.5 - 51.53	84	0.01	1	1.00	1	0.008	1.2E-07
B214W	7 - 11.5	71	0.13	1	0.66	1	0.084	2.3E-06
B214W	11 - 17.5	71	0.19	1	0.76	1	0.143	4.3E-06
B214W	47.3 - 53.5	71	0.05	1	0.50	1	0.024	3.7E-07
B215W	18 - 25	33	0.10	1	0.71	1	0.071	1.8E-06
B215W	21.3 - 25	33	0.16	1	0.75	1	0.119	4.1E-06
B215W	27 - 33	33	0.17	1	1.00	1	0.170	4.8E-06
B218W	25 - 30.3	70	0.10	1	0.27	1	0.028	6.5E-07
B108W	11.75 - 18.65	32	0.14	1	1.00	1	0.139	4.3E-06
B117W	8.8 - 15	96	0.05	1	0.50	1	0.024	7.8E-07
B117W	14.8 - 21	96	0.05	1	0.67	1	0.032	7.7E-07
B118W	21.0 - 29.8	73	0.08	1	0.43	1	0.034	7.5E-07
B118W	29.5 - 35.67	73	0.03	1	0.50	1	0.016	4.6E-07

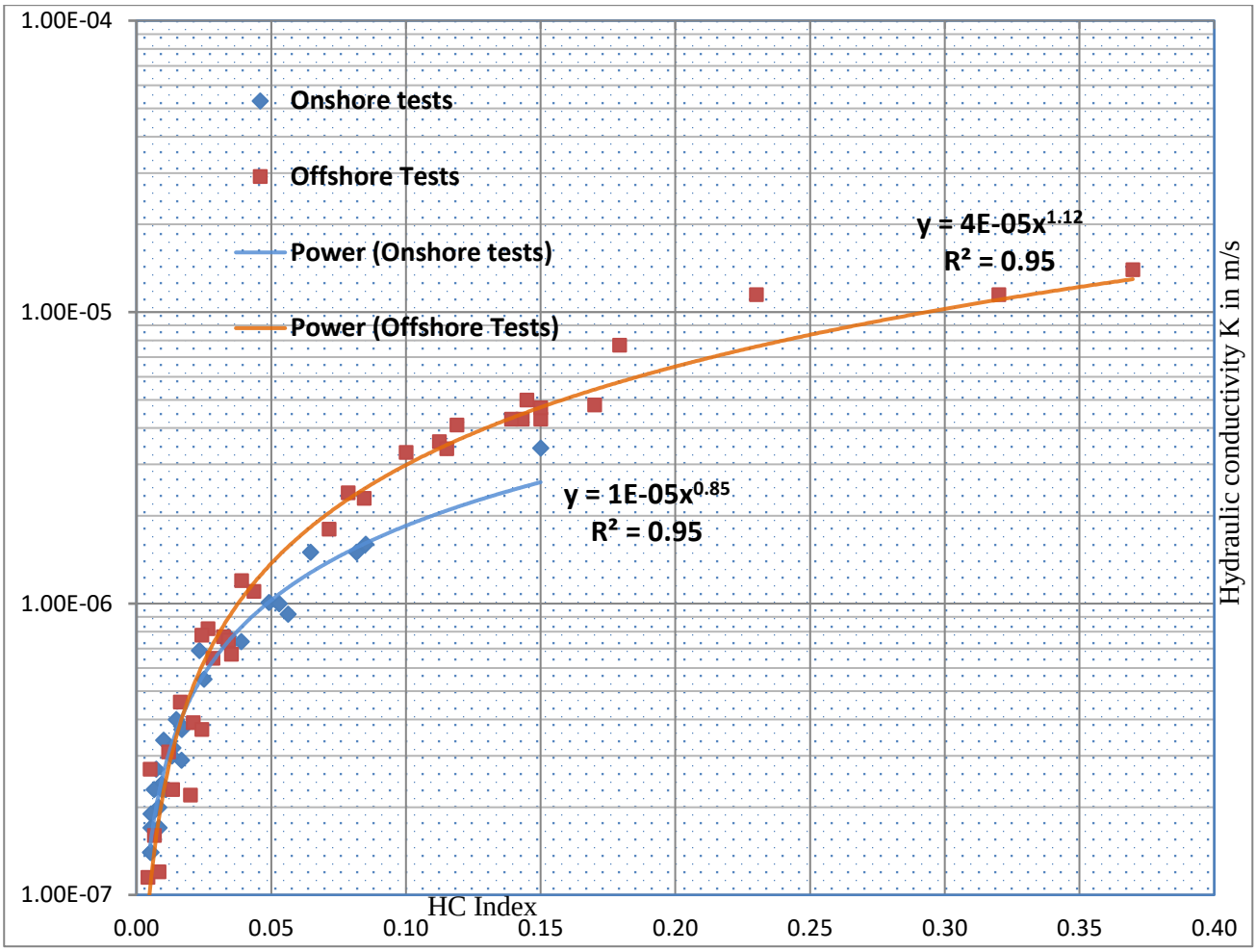

Figure 3: Correlation between HC index and Hydraulic Conductivity from Packer Test, onshore & offshore tests

5.3 THE EMPIRICAL HC MODEL VERIFICATION

To further verify the feasibility of the proposed empirical HC model, model verification has been undertaken. 14 onshore and 9 offshore hydraulic test data from different tunnel projects with similar sandstone units were used to verify the HC model. Table 4 shows 14 onshore and 9 offshore hydraulic test data for the model verification, in which $K_{HC\text{-}model}$ and $K_{in\text{-}situ}$ are represented. Borehole Id with "W" shows that tests are carried out in offshore area. The verification regression results indicated that $K_{HC\text{-}model}$ and $K_{in\text{-}situ}$ are well correlated with a coefficient of determination of R^2 equals 0.97 for both on onshore and offshore tests.

Figures 4 and 5 show the correlation between the rock mass hydraulic conductivity obtained from in situ testing and that from the estimation of the empirical HC model for onshore and offshore tests respectively. This verification example demonstrates that the empirical HC model is able to determine the rock mass hydraulic conductivity for different sites in which the lithologic conditions and geographic locations are similar.

Table 4: Result of verification borehole tests for Sandstone unit

Hole ID	Test intervals (m)	Total Depth (m)	RQD (%)	DI	1-GCD	LPI	HC	$K_{HC\text{-}Model}$ (m/s)	$K_{in\text{-}situ}$ (m/s)
SRT BH8	13.6 - 20.3	42	94.0	1	1.00	1	0.06	9.11E-07	1.20E-06
SRT BH9	21 - 27.2	35	95.2	1	1.00	1	0.05	7.62E-07	8.00E-07
SRT BH10	14.9 - 21.1	36	98.1	1	1.00	1	0.02	3.50E-07	4.00E-07
EP_BH01	7.5 - 14	40	92.0	1	0.90	1	0.07	1.07E-06	1.50E-06
EP_BH03	11.0 - 20.0	50	96.1	1	0.71	1	0.03	4.75E-07	5.00E-07
EP_BH05	16 - 21.0	50	99.2	1	1.00	1	0.01	1.65E-07	2.00E-07
EP_BH05	7.0 - 12.0	50	99.0	1	1.00	1	0.01	2.06E-07	3.00E-07
RZ_BH62	54 - 61	70	95.7	1	0.67	1	0.03	4.87E-07	5.00E-07

RZ_BH69	19 - 24	50	95.0	1	1.00	1	0.05	7.84E-07	9.00E-07
RZ_BH69	29 - 34	50	97.0	1	1.00	1	0.03	5.08E-07	5.00E-07
BHF05	38 - 42.4	65	99.1	1	1.00	1	0.01	1.85E-07	2.30E-07
BHF13	45 - 51	60	87.0	1	1.00	1	0.13	1.8E-06	2.50E-06
BHF13	50 - 56	60	91.7	1	0.70	1	0.06	8.93E-07	9.00E-07
BHF20	37.6 – 42.4	72	99.5	1	1.00	1	0.01	1.18E-07	1.20E-07
SRT BH202W	31.2 - 39	46	98.8	1	1.00	1	0.01	2.70E-07	2.00E-07
SRT BH204W	22 - 29.1	29	89.0	1	1.00	1	0.11	3.37E-06	3.40E-06
SRT BH205W	38 - 44.5	49	89.1	1	1.00	1	0.11	3.35E-06	2.70E-06
SRT BH206W	30.2 - 37.3	45	98.3	1	0.58	1	0.01	2.27E-07	2.00E-07
SRT BH211W	39.8 - 45.9	64	94.1	1	1.00	1	0.06	1.67E-06	1.60E-06
SRT BH211W	45.8 - 51.8	64	90.0	1	0.83	1	0.08	2.47E-06	2.00E-06
SRT BH213W	31.7 - 39	39	94.5	1	0.50	1	0.03	7.12E-07	5.50E-07
SRT BH214W	33.8 - 41	46	98.0	1	1.00	1	0.02	5.04E-07	5.00E-07
SRT BH215W	27.7 - 34.5	46	95.6	1	0.50	1	0.02	5.58E-07	5.50E-07

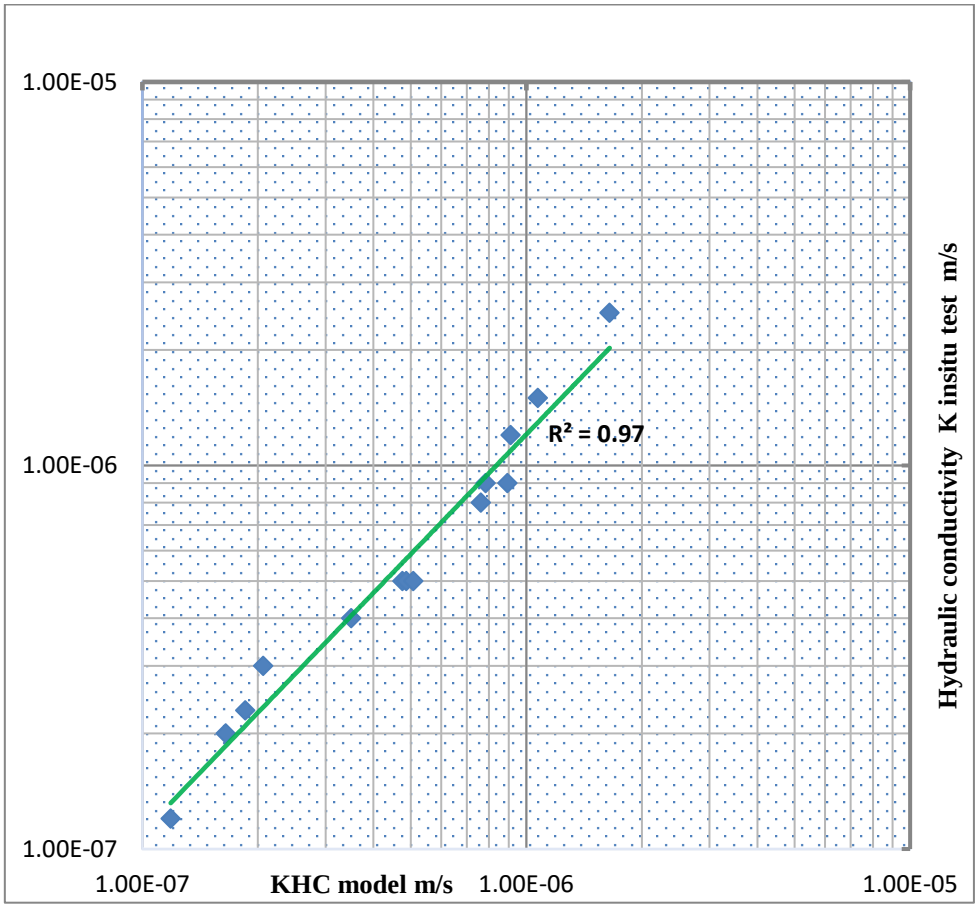

Figure 4: Correlation between $K_{HC\ model}$ and $K_{in\text{-}situ}$ onshore tests

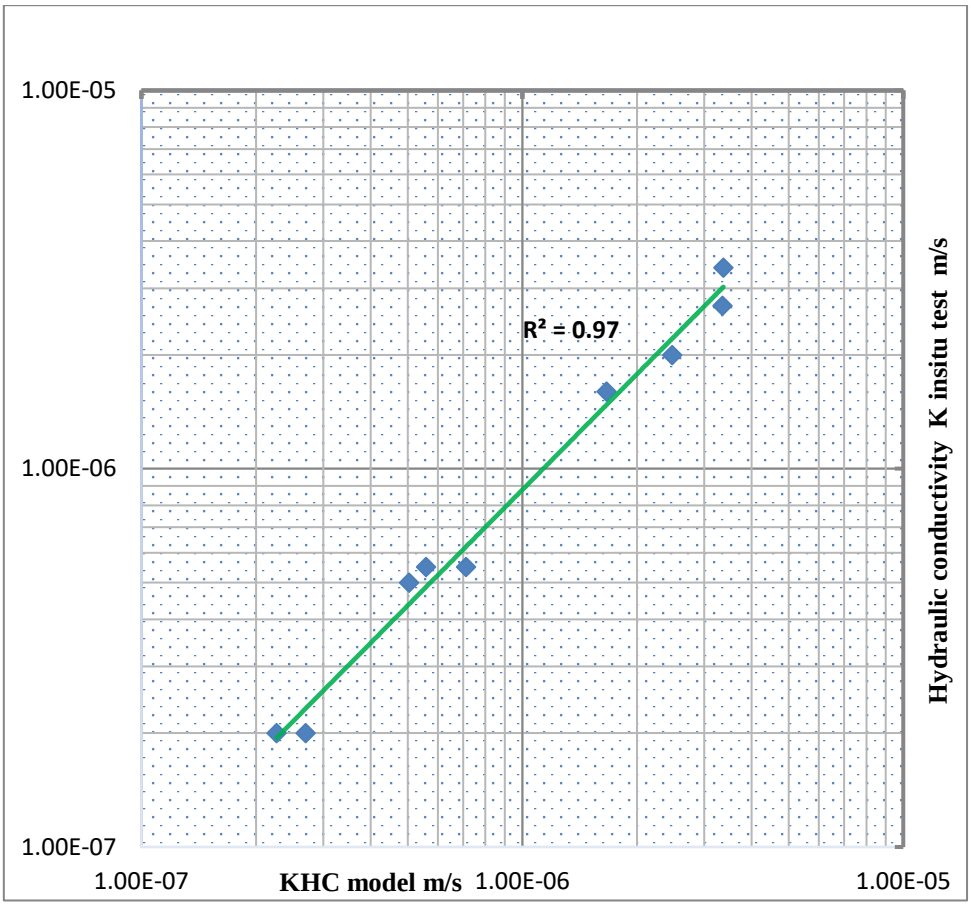

Figure 5: Correlation between $K_{HC\ model}$ and $K_{in\text{-}situ}$ offshore tests

6 CONCLUSIONS

The estimation of rock mass hydraulic conductivity using empirical equations has great advantages. As discussed in this paper, the dependence of the measured hydraulic conductivity on the section depth, RQD, gouge content and lithology was evaluated. Based on this study the following conclusions are made:

- A modified new rock mass classification system called the "HC-system" or HC model has been developed to estimate the hydraulic conductivity of Hawksbury Sandstone in Sydney basin based on the proposed Hsu et al. 2011 empirical model.
- There is no obvious correlation between depth and hydraulic conductivity in this investigation. It is concluded that the depth is not a significant factor on the hydraulic conductivity, so the Depth Index (DI) is taken to be 1.
- Hydraulic conductivity values of Hawkesbury Sandstone generally vary from 10^{-6} to 10^{-8} m/s and are predominantly controlled by fracture properties.
- The regression results indicate that a power law relationship exists between the hydraulic conductivity and HC values with a coefficient of determination of 0.95 for both offshore and onshore tests.
- The verification regression results indicate that a power law relationship exists between the $K_{HC\text{-}model}$ and $K_{in\text{-}situ}$ with a coefficient of determination of R^2 equal to 0.97 for both offshore and onshore tests.
- Regression equation (Equation (5) is capable of providing a useful tool to predict hydraulic conductivity of fractured sandstone based on measured HC-values.
- By using this empirical method hydraulic conductivity data in a given site can be estimated, which reduces the cost on hydraulic testing and increases the reliability and quality of the packer tests.
- HC-system is a valuable new rock mass classification system for preliminary assessment of the degree of permeability of a borehole.
- The correlation between RMC and K of this study is appropriate for the geological conditions in the Sydney basin. The results obtained confirm the validity and flexibility of the empirical approach to handle cases of onshore and offshore data sets, in relation to data acquisition and data reduction (optimisation).

7 ACKNOWLEDGMENTS

We would like to acknowledge Roads and Maritime Services who assisted with the data.

8 DISCLAIMER

The views, opinions, considerations and conclusions expressed in this presentation are strictly those of authors and do not necessarily reflect the views of Roads and Maritime Services.

9 REFERENCES

Black, J.H., 1987. Flow and Flow Mechanisms in Crystalline Rock, in Fluid Flow in Sedimentary Basins and Aquifers: Geol. Soc. Special Publication, vol. 34, pp. 186–200.

Bear, J. (1972). Dynamics of Fluids in Porous Media, American Elsevier Publication Co., New York. Rock Mechanics. AIME, pp. 237-302, New York.

Burgess, A., 1977.Groundwater movements around a repository—regional groundwater analysis. Kaernbraenslesaekerhet, Stockholm, Sweden, 116.

Carlsson, A., Olsson, T., 1977. Hydraulic properties of Swedish crystalline rocks-hydraulic conductivity and its relation to depth. Bulletin of the Geological Institute, University of Uppsala 7, 71–84.

Deere, D. U.; Hendron, A. J.; Patton, F. D. & Cording, E. J. (1967). Design of surface and near surface construction in rock, Proceedings of 8th U.S. Symposium. Rock Mechanics. AIME, pp. 237-302, New York.

Geology Society of Australia (1969). The geology of New South wales, Ed.G.h. Packham, Sydney, 654 pages.

Hsu S, Lo H, Chi S et al (2011) Rock mass hydraulic conductivity estimated by two empirical models. In: Dikinya O (ed) Developments in hydraulic conductivity research. InTech, New York, pp 134–158.

Jembere, D and Yihdego, Y (2016) Engineering Rock Mass Evaluation for a Multi-purpose Hydroelectric Power Plant: Case of Genale Dawa (GD-3), Ethiopia. Journal of Geotechnical and Geological Engineering 34 (5): 1593-1612. DOI:10.1007/s10706-016-0068-9. http://link.springer.com/article/10.1007/s10706-016-0068-9

Ku, C.-Y., Hsu, S.-M., Chiou, L.-B., & Lin, G.-F. (2009). An empirical model for estimating hydraulic conductivity of highly disturbed clastic sedimentary rocks in Taiwan. Engineering Geology, 109(3), 213-223.

Lee, C.H., Farmer, I., 1993. Fluid Flow in Discontinuous Rocks. Chapman and Hall, London, UK.

Louis, C., 1974. Rock hydraulics. In: Muller, L. (Ed.), Rock Mechanics. Springer Verlag, Vienna.

McKibbin and Smith (2000); Sandstone Hydrogeology of the Sydney Region. 15th Australian Geological Convention. Sandstone City University of Technology, Sydney, July 2000.

Paul Tammetta and Paul Hewitt (2004), Hydrogeological Properties of Sandstone, Australian Geomechanics Vol 39 No 3.

Singhal, B.B.S., Gupta, R.P., 1999. Applied Hydrogeology of Fractured Rocks. Kluwer Academic Publishers, The Netherlands, p. 400.

Snow, D.T., 1970. The frequency and apertures of fractures in rock. International Journal of Rock Mechanics and Mining Science & Geomechanics Abstracts 7, 23–40.

Spitz, K., Morena, J., 1996. A Practical Guide to Groundwater and Solute Transport Modelling. Wiley.

Wei, Z.Q., Egger, P., Descoeudres, F., 1995. Permeability predictions for jointed rock masses. International Journal of Rock Mechanics and Mining Science & Geomechanics Abstracts 32, 251–261.

Yihdego, Y (2016) Hydraulic In situ Testing for Mining and Engineering Design: Packer Test Procedure, Preparation, Analysis and Interpretation. Journal of Geotechnical and Geological Engineering, 35(1): 29-44. DOI: 10.1007/s10706-016-0112-9. http://link.springer.com/article/10.1007/s10706-016-0112-9

IN-SITU WASTE CHARACTERISATION FOR PRIMARY SETTLEMENT ASSESSMENT FOR HIGH EMBANKMENT BUILT OVER MUNICIPAL SOLID WASTE

F. Siahaan[1], P. K. Wong[1], A. Peiris[2] and T. Muttuvel[3]
[1]Coffey Services Australia, Australia; [2]GHD, Australia; [3]SMEC, Australia

ABSTRACT

Due to land restriction, some sections of several highway and railway projects have to be constructed over poor and uncommon foundation such as waste materials placed as part of the preceding landfill operation. Waste/Municipal Solid Waste (MSW) materials especially those comprising high amount of organic and readily degradable materials are highly compressible and have high variability in composition and void distribution. Conventional geotechnical laboratory testing and limited in-situ testing are often insufficient to characterise waste material. A design of field trial to understand the settlement characteristics will also require a reasonable understanding of the properties of waste materials.

This paper presents a basic methodology for in-situ characterisation of waste materials to enable the assessment of geotechnical properties of these materials on the basis of their composition and organic content. This includes the selection of suitable drilling method to allow for a good quality and continuous waste sample recovery. From such characterisation, a dimensionless Waste Compressibility Index (WCI) can then be derived based on procedures given in the published literature. The WCI value can then be correlated with compression ratio used to analyse primary consolidation settlement.

A case study is presented in this paper where a railway embankment was to be built over a landfill foundation consisting of existing Municipal Solid Waste (MSW) in the east coast of Australia. The foundation was treated by means of high surcharge. The abovementioned methodology has been used in the design to characterise MSW materials and assess primary settlements. The back-analysis by using settlement monitoring data indicate a reasonable agreement between the WCI related to the back-analysed compression ratio and the estimated WCI values. This agreement was obtained despite the variability in the aforementioned correlation. It shows that a basic methodology for in-situ waste characterisation on the recovered waste sample was able to provide a reasonable estimate of compressibility parameters for the purpose of analysing primary settlements.

1 INTRODUCTION

It becomes increasingly inevitable for the routes of new highway and railway infrastructures to traverse area underlain by poor or unconventional foundation materials. This area includes landfill where waste materials have been previously placed in subdivided cells. The majority of landfills were used as dumping ground for Municipal Solid Waste (MSW) with heterogeneous content and large proportion of organic materials. Consequently, the compressibility of MSW materials is relatively high and variable in comparison with the compressibility of conventional soft soil. As a result, ground improvement is usually required to limit the post construction settlements to which these infrastructures are subjected (Van Impe and Bouazza, 1997). For the design of such ground improvements, it is essential to estimate compression ratio to assess primary consolidation settlements. Magnitude and completion of the primary settlements including large void collapse are important information which will be required to assess the remaining post construction settlements.

However, the estimate of compression ratio (CR) will require the characterisation of MSW materials to allow for their treatment as geomaterials. The conventional laboratory testing is not usually practical due to large size and irregular shape of the samples, limited availability of equipment to measure large strain due to large void collapse (Landva et al., 2000), as well as health and safety issue. In-situ testing such as cone penetration testing, pressuremeter or dilatometer may not be sufficient if they are not undertaken in large quantity and in conjunction with investigations which involve sample recovery. The undertaking field trial is useful to assess the settlement characteristics but the design of such trial will require an understanding on the properties of MSW materials.

Various literatures have presented unique relationship between CR and various geotechnical properties (organic content, moisture content and density) of MSW materials. CR has been reported to decrease with the decrease in the organic content (Sower 1973; Chen et al. 2009). CR has also been observed to increase with the increase in moisture content

(Reddy et al. 2009; Wall and Zeiss 1995). An increase in MSW density has been reported to have an influence in a decrease in the compression index (C_c) of MSW materials (Landva et al. 2000; Chen et al. 2009).

It is worth noting that the primary settlement assessed by using CR is related to the physical and mechanical process involving the reorientation of particles, movement of the fine materials into larger voids and collapse of void spaces (Sharma and De 2007) under a given load. In most cases, the primary compression of MSW materials was not a result of dissipation of excess pore water pressure due to relatively high permeability and unsaturated condition of MSW materials (Wall and Zeiss 1995; Bareither et al. 2012). As organic solids are typically more compressible than other MSW constituents and consequently tend to form weaker structures around voids, the relative influence of organic solid content to the primary settlement is considered to be significantly higher in comparison to other MSW constituents.

This paper presents a basic methodology for the in-situ waste characterisation to estimate compression ratio required to assess the primary settlements. A discussion is presented on the proposed basic investigation scope to allow for a good recovery, identification and assessment of MSW constituents. Then, some equations are given to assess the equivalent geomaterial properties of MSW. The MSW materials can then be characterised by using a dimensionless index suggested by Bareither et al. (2012). This index allows an estimate of compression ratio (CR). To demonstrate the aforementioned technique, a case study is presented which involves an estimate of a compression ratio for MSW materials on which a proposed railway embankment was to be built in the east coast of Australia.

2 GEOTECHNICAL SITE INVESTIGATION

2.1 PLANNING OF INVESTIGATION

Prior to the undertaking of fieldwork investigation, it is a good practice to conduct a desktop study as part of the planning process. Depending on available information, this study may comprise the review of historical aerial photographs, waste placement records, survey record and operational records (i.e. leachate circulation, gas monitoring, etc). It is useful to obtain information regarding the type and volume of MSW constituents, landfill depth, thickness/interval of cover layers and age of landfill. Details of such planning work are given in Landva and Clark (1990).

2.2 BASIC INVESTIGATION METHODOLOGY

The majority of landfill comprise highly variable MSW materials with varying degree of placement compaction (Zekkos et al., 2006). As the MSW characterisation requires a continuous exposure of MSW sample, a suitable investigation technique should be employed. An open excavation pit may be suitable for relatively shallow landfill formation. On the other hand, an unsuitable drilling technique may result in poor sample recovery or difficulty in locally penetrating solid objects.

As most of landfill can be expected to be thicker than 5 m, and obstructions within landfills may cause difficulties to conventional drilling, it may be necessary to adopt other investigation techniques such as sonic drilling. In sonic drilling (ref. Figure 1), the core barrel is typically advanced by using a high-frequency energy transferred downwards to the drill face. This energy generated at sonic frequency liquefies the surrounding materials hence reducing frictional resistance against the barrel. The casing is then advanced around the core barrel to protect it from collapsing hole. The core barrel is then extracted along with the samples.

Figure 1: Typical sonic drilling and MSW samples recovered during sonic drilling

Physical measurements should be taken on each sample run to obtain total length, sample diameter and approximate sample weight (with or without water). Detailed inspection on the sample should then be carried out to allow for classification of materials forming the MSW materials. This includes the constituent material type, proportion (i.e. measured by thickness or area and weight), odour and colour. Where possible, notes should also be recorded on the material density, moisture condition and state of decomposition. High resolution photographs of MSW samples along with a ruler should be taken to allow for further analysis following the fieldwork completion.

Landva and Clark (1990) proposed the following classification of MSW materials based on the biodegradation potential:

- Organic Putrescible (OP) comprising readily biodegradable materials such as food waste, garden waste.
- Organic Non-putrescible (ON) comprising slowly biodegradable materials such as paper, wood, textiles, oil.
- Inorganic Degradable (ID) comprising metal with potential degradation due to corrosion
- Inorganic Non-degradable (IN) comprising typical inert materials such as construction rubbles, soil, ash, glass, ceramics.

It is imperative that the quantity and properties of OP materials are sufficiently obtained from the investigation as these and their associated changes over time will affect the compressibility and strength characteristics of MSW materials. The OP materials have high water absorption capacity and are highly compressible. As described above, the compressibility of MSW materials is typically governed by the organic solid content (OP), moisture content and density at the time of the load application.

For the purpose of primary settlement assessment, it would be necessary to obtain several geomaterial properties including bulk unit weight (γ_b) and compression ratio (CR). Once the detail of MSW constituents are obtained, the dry density (γ_d) can be obtained by the following equation (Landva and Clark, 1990):

$$\gamma_d = \frac{1}{\sum_1^n \frac{w_{si}}{w_{sc}} \times \frac{1}{\gamma_{di}}} \tag{1}$$

Where γ_d = average dry density of landfill (kN/m^3); w_{si} = solid weight of waste constituent (kg); w_{ci} = total solid weight of waste samples (kg); γ_{di} = typical dry density of waste constituent (kN/m^3). Depending on shape and condition of recovered waste materials, it could be more practical to estimate the volume of waste constituent or the volume of whole sample. This estimate can be done by physical measurement with or without the use of water as the displaced medium. Where these volumes can be reasonably estimated, the dry density can be analysed as follows:

$$\gamma_d = \frac{1}{v_t} \sum_1^n v_{si} \times \gamma_{di} \tag{2}$$

Where v_{si} = approximate volume of waste constituent (m^3 or litre); v_{si} = approximate volume of waste constituent (m^3 or litre). For practical purpose, γ_{di} for a specific material type can either be obtained from published data or representative laboratory testing. Moisture content of sample (m_d) is typically needed to estimate γ_b for a typical geomaterial. Such estimate in the field could potentially be challenging due to the use of drilling fluid and the varying absorption capacity of various waste constituents. Two possible methods are proposed. The first method involves the measurement of moisture content for representative sample for each waste constituent which is capable of absorbing water. Equation (3) below can be adopted (Landva and Clark, 1990).

$$\gamma_b = \gamma_d\,(1 + m_d) = \gamma_d \left(1 + \sum_1^n \frac{w_{si}}{w_{sc}} \times \frac{\Delta\gamma_{di}}{\gamma_{di}}\right) \tag{3}$$

Where $\Delta\gamma_{di}$ is the increase in unit weight of waste constituent (kN/m^3). The second component of the sum in the bracket in the equation (3) essentially describes the average of moisture content of various waste constituents. Alternatively, it is possible to estimate moisture content (by dry weight) on the basis of its correlation with organic content which typically has a high capacity of water absorbance. This correlation, which was developed based on field observation, was originally presented Landva and Clark, 1990 and Park et al. 2011. In this study, additional data from published literatures were added as shown in Figure 2 below. The variability in the estimate should be noted in the selection of appropriate value of moisture content. Detailed sensitivity or reliability studies may be required as part of the design. A comparison against available literature (Zekkos et al., 2006) presenting comprehensive database of landfill unit weight is also worthwhile.

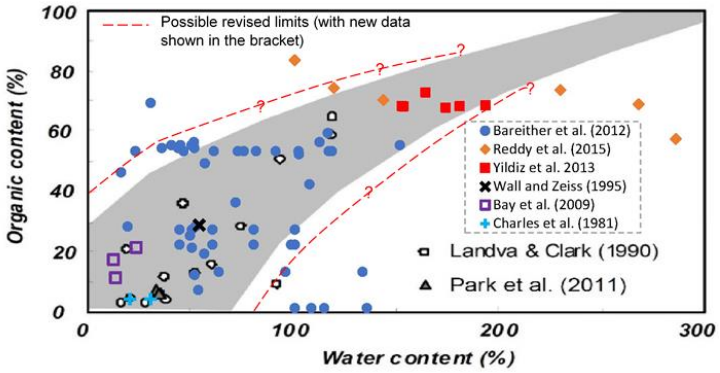

Figure 2: Extended relationship between organic content in waste materials and moisture content (Base figure from Landva and Clark, 1990)

3 ESTIMATE OF PRIMARY SETTLEMENTS

Bareither et al. (2012) proposed a dimensionless Waste Compressibility Index (WCI) based on the percentage of biodegradable materials, moisture content and MSW density.

$$WCI = m_d \left(\frac{\gamma_w}{\gamma_d}\right) \left(\frac{OP}{100 - OP}\right) \tag{4}$$

Where OP is the percentage of biodegradable materials (taken as organic putrescible materials); m_d is dry weight moisture content; γ_d is dry unit weight (kN/m^3); γ_w is unit weight of water. In soil mechanics, dry weight moisture content is equivalent to the moisture content where weight of solid excludes water.

By carrying a regression analysis on a large database of test results available in the literature and their own experiments, Bareither et al. (2012) developed a relationship to estimate compression ratio (CR) from WCI.

$$CR = 0.26 + 0.058 \log_{10} WCI \tag{5}$$

Where CR = compression ratio ($C_c/(1 + e_0)$); C_c = compression index. It should be noted that the estimate of CR can be carried out with a range of ± 0.087 for each value of WCI. Similar to the variation in the correlation between organic content and moisture content, the estimate of CR will require a judgement and, if warranted, may involve sensitivity or reliability study.

The above estimate is proposed for MSW layers where organic content is present and governs the primary compression of the MSW materials due to its higher compressibility and tendency to form weaker structures around voids. The use of WCI is also capable of capturing the variation in the organic content with time due to the decomposition of MSW materials. Where organic content becomes smaller (i.e. WCI approaches 0 %), the corresponding CR becomes relatively smaller. In the complete absence of organic content, the use of WCI is no longer applicable.

4 CASE STUDY – RAILWAY PROJECT IN EAST COAST OF AUSTRALIA

4.1 OVERVIEW

A rail embankment was to be built in the eastern coast of Australia. A section of the proposed alignment with an approximate length of 200 m had to be built over the buried landfill cells. Ground improvement in the form of surcharging was employed to reduce the post construction settlements. The ground improvements in the forms of rigid and semi-rigid inclusions as well as dynamic compaction were not adopted due to a risk of damage to the existing landfill features including the leachate circulation system and liner.

The high surcharge embankment and waiting period were designed to induce the primary settlement (reduction in void ratio) and consequently reduce the post construction settlement via the decrease of creep strain rate ($C_{\alpha\epsilon}$). It is shown that the decrease in $C_{\alpha\epsilon}$ has a distinct correlation with the reduction in void ratio (Siddiqui et al., 2013). As part of the design, the performance of ground improvement was assessed by monitoring the settlements due to the surcharge loading. Ground settlement were monitored by using Settlement Plates (SPL) and Hydrostatic Profiling Gauges (HPG) as shown in Fig. 3.

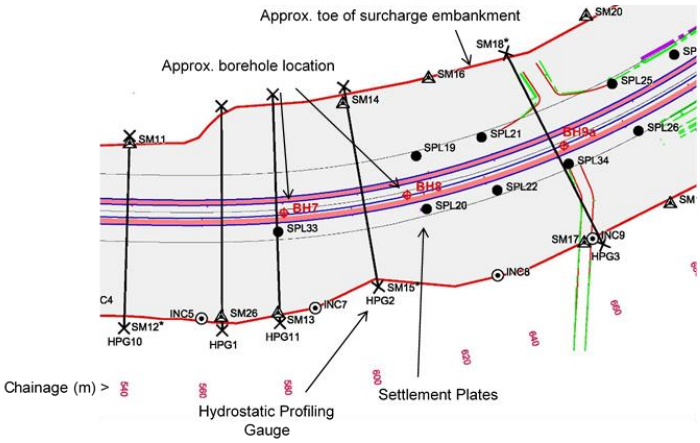

Figure 3: Plan view showing subject area (vicinity of BH7, BH8 and BH9a)

As part of pre-design investigation, several boreholes were drilled. Three boreholes BH7, BH8 and BH9a were selected for this study due to their proximity to the settlement monitoring points. Boreholes BH7 and BH8 were drilled using sonic technique with excellent sample recovery. Borehole BH9a was drilled by using conventional rotary drilling technique with Standard Penetration Test (SPT) at every 1.5 m interval. Only partial sample recovery was achieved in borehole BH9a. The majority of SPT testing resulted in refusal or blow count of over 50 per 300 mm penetration. Locations of BH7, BH8 and BH9a are shown in Figure 3.

Additionally, the settlement monitoring of a field trial conducted earlier in 1985 was also considered in the study. This field trial was conducted for other purpose in nearby area located just about 100 m to the south of area shown in Figure 3. Prior to the field trial, the investigation was undertaken by means of a test pit excavated to 5 m deep below the then ground surface. A circular trial embankment was built by using uncompacted crushed sandstone to a total height of 3 m with a top diameter of about 3 to 4 m. The settlement was monitored by means of settlement plates. Further details are available in Siahaan et al. (2014).

4.2 IN-SITU WASTE CHARACTERISATION

MSW characterisations for BH7, BH8 and BH9a have been carried out as per the method described above. The MSW composition by weight is given in Figure 4 below.

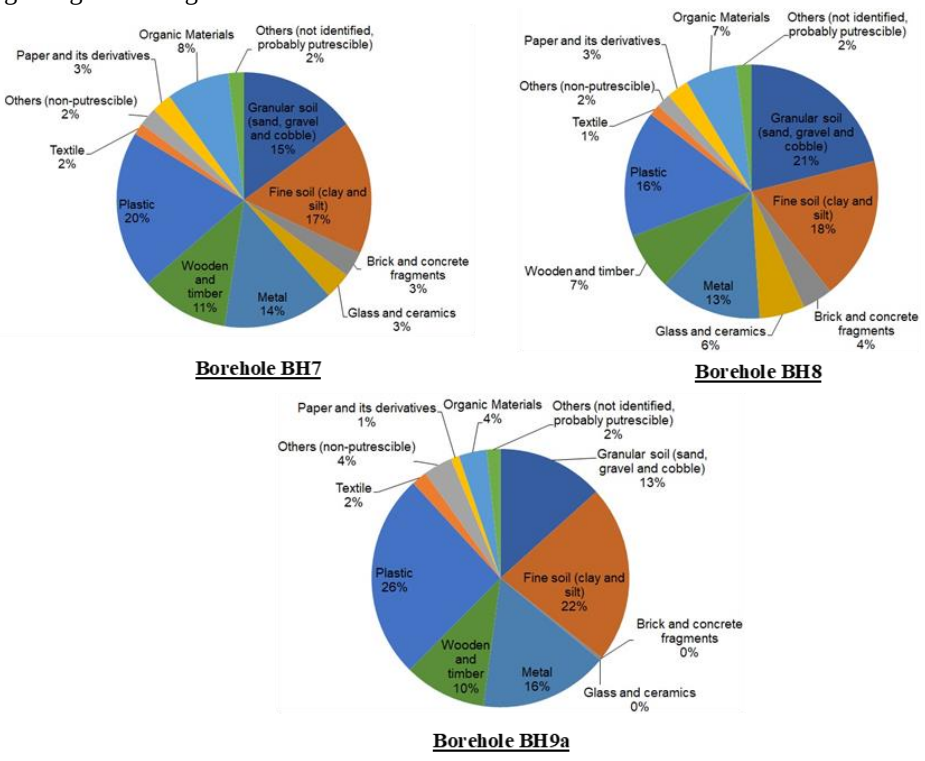

Figure 4: Assessed MSW composition by weight for BH7, BH8 and BH9a

4.3 SETTLEMENT MONITORING DATA

Results of settlement monitoring at points which were located at closest proximity to BH7, BH8, BH9a and 1985 Trial location are given in Figure 5 below. Two mechanisms of primary consolidation of MSW materials were considered to assess the end of primary consolidation. The first mechanism involves the reduction of void ratio due to particle rearrangement. The second mechanism involves the collapse of larger voids held up by weak structure. As MSW generally has high permeability, the completion of first mechanism is typically immediate. However, the completion of second mechanism may take slightly longer time than the first mechanism due to possible progressive weakening of the void structure under the given load. In general, various literatures have reported that both mechanisms were completed within 1 to 4 months (Wall and Zeiss 1995, Sharma and De 2007). Further settlements due to secondary consolidation are not shown in Figure 5 for clarity purpose.

For BH7, BH8 and BH9a, the end of primary consolidation was analysed by means of graphical assessment of settlement curve. As the primary consolidation of MSW materials under the surcharge load was not induced by the dissipation of excess pore pressure, it was not possible to reasonably undertake the back-analysis by considering the time-dependent behaviour (e.g. using pore pressure data, etc). Therefore, the end of primary consolidation was deemed to have finished by observing the following conditions:

- The secondary (creep) settlement became apparent in a semi log plot (i.e. no noticeable change in general curvature)
- Localised change in settlement curvature (i.e. sign of possible sudden void collapse) has stopped.

The assessed end of primary consolidation was generally about 3 months from the start of monitoring or about 2.5 months from the reference time which took into consideration the staged placement of fill materials.

For the 1985 Trial, the completion of primary condition could not be readily assessed particularly with respect to the end of void collapse. Due to the shallow embankment with smaller dimension and uncompacted fill, the collapse of larger and stronger voids under given load possibly have not occurred until the end of monitoring. As a result, the settlement value was extrapolated to about 3 months from the end of filling which is consistent with typical periods reported in literature and those observed in BH7, BH8 and BH9a.

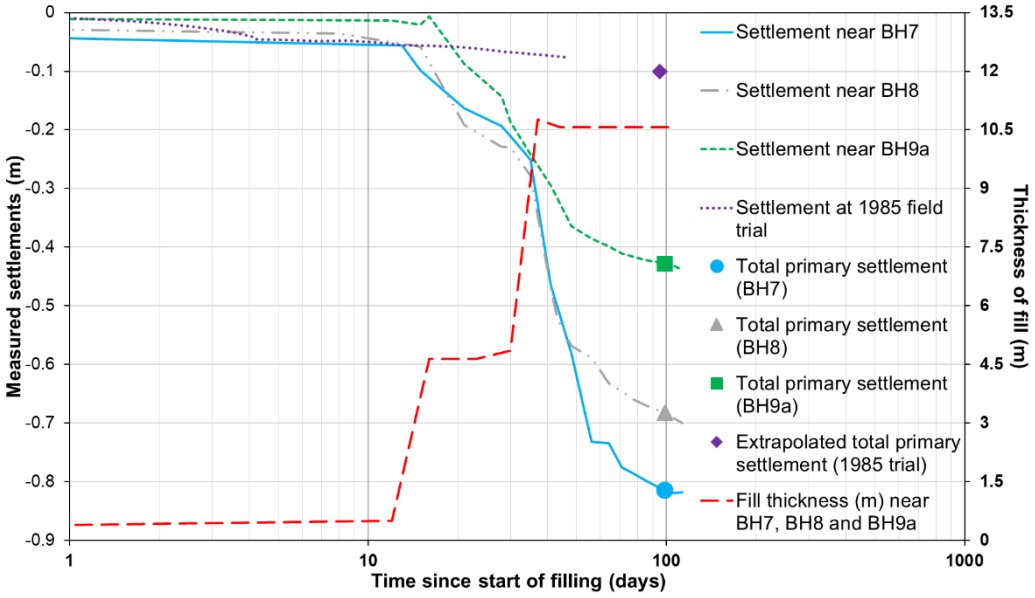

Figure 5: Settlement monitoring results and fill placement

4.4 BACK-ANALYSIS OF COMPRESSION RATIO

Subsequent to the characterisation of MSW materials, an average dry density (γ_d) was obtained for the entire MSW depth of each borehole. The γ_d value was calculated by using equation (2) and typical dry density values of individual MSW constituent (Landva and Clark, 1990). These values are consistent with those presented in Zekkos et al. (2006). Then, moisture content values of MSW were assessed based on the approximate organic content (Figure 2). As this correlation yields a range of moisture content values for a given value of organic content (OP), a range of WCI was consequently estimated for each respective borehole. The assessed WCI values are given in Table 1.

As each value of WCI is also related to a range of compression ratio CR resulting from regression analysis carried out by Bareither et al. 2012, a multi-dimensional range of WCI and CR will result in greater extent of variability. Therefore, it is necessary to initially back-analyse the compression ratio (CR) from the settlement data to limit the range of CR. The compression ratio were assessed from the measured settlements given in Fig. 5. Subsequently, each assessed CR value was plotted with a range of WCI along with the "most likely value" of the WCI. This procedure allowed a sensitivity analysis to be conducted on the variation WCI which is related directly with the variability in MSW materials.

The compression ratio (CR) was back-analysed by means of the following equation for one-dimensional settlement analysis:

$$S_{prim} = S_{prim\ (non-waste)} + S_{prim\ (waste\ WCI)} = \Delta\sigma_v \frac{H_{nw}}{D} + CR\ H_{w-WCI}\ \log_{10}\frac{\sigma'_v + \Delta\sigma_v}{\sigma'_v} \quad (6)$$

where, D = constrained modulus (kPa), $\Delta\sigma_v$ = additional pressure (kPa) due to surcharge embankment, H_{nw} = thickness (m) of non-waste layers not considered in the WCI calculation, H_{w-WCI} = thickness of waste layers considered in WCI calculation, σ'_v = initial effective stress (kPa). The non-waste layers (cover layers) which contributed to the term $S_{prim\ (non-waste)}$ for BH7, BH8 and BH9a were located above the founding levels of the SPLs and HPGs. As a result, the monitoring results registered at SPLs and HPGs were only applicable to the back-analysis of waste layers considered in the WCI calculation ($S_{prim\ (waste\ WCI)}$).

Based on settlement data shown in Figure 5, the back-analysed compression ratio for BH7, BH8, BH9a and 1985 Trial are 0.14, 0.13, 0.0875 and 0.12, respectively. Each of CR value was then plotted against the range of assessed WCI for respective location. These plots are shown in Figure 5 along with the range of relationship between CR and WCI.

As expected and shown in Figure 6, the back-analysed compression ratio are higher with higher content of organic materials (OP) with the exception of the 1985 Trial. Such observation for the 1985 Trial was possibly related to the inadequacy of data used for the assessment of WCI and other information for the 1985 Trial. As the information from 1985 Trial was obtained from a 5-m deep test pit, limitations in the investigation depth and sampling quality would have applied in the assessment of the MSW properties. This highlights the importance of a selection of appropriate investigation technique to obtain good quality MSW samples from most or entire depth coverage.

Results in Figure 6 also shows that the range of WCI for given compression ratio generally fall within the relationship given by Bareither et al (2012). It can also be seen from Figure 6 that back-analysed compression ratio for BH7 and BH8 are generally closer to and have proportional gradient to the mean line. As previously noted, the quality of recovered samples from BH7 and BH8 was generally higher than that of borehole BH9a and the test pit in 1985 Trial. This implies that a good sample recovery is beneficial to allow for a robust MSW characterisations.

Table 1: Assessed range of Waste Compressibility Index

Borehole ID	MSW thickness inferred from borehole depth (m)	Assessed organic content (%)	Dry unit weight (kN/m^3)	Assessed range of moisture content (%)	Assessed range of Waste Compressibility Index
BH7	12	12.5	11	5 – 40 (most likely value = 20)	0.0065 – 0.052
BH8	11.5	11.3	12.2	5 – 40 (most likely value = 20)	0.0052 – 0.042
BH9a	12.5	6.3	11.5	5 – 40 (most likely value = 20)	0.0029 – 0.023
1985 Trial	10*	>30	8.5	10 – 50 (most likely value = 30)	0.063 – 0.32*

Note:

* Thickness including up to 3 m of non-waste materials. Value of non-waste material was excluded in the WCI estimate.

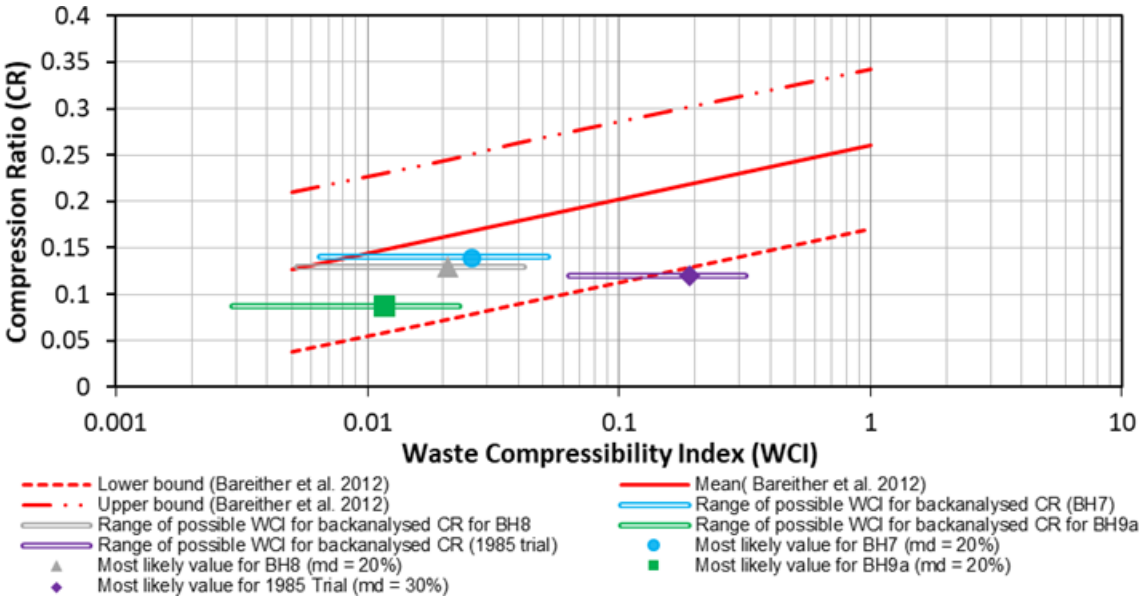

Figure 6: Plots of back-analysed compression ratio and range of WCI (Base CR-WCI relationship denoted by red lines is based on Bareither et al., 2012)

Despite its usefulness, the relationship was developed by Bareither et al. (2012) by using available database of compressibility parameters at the time of publication. Therefore, it is a good practice that this relationship is used thoughtfully especially for the range of WCI where less available data were used in regression analysis.

As indicated in Figure 5, the time taken for the completion of primary settlement is 2.5 months from the reference time which took into consideration the placement of fill materials. This period is consistent with times observed in literatures (Edil et al. 1990, Walls and Zeiss 1995, Andersen et al. 2004, Sharma and De 2007). Although the secondary settlement is not shown in Figure 5, the completion of primary consolidation requires monitoring of subsequent settlements to ensure that the curvature of settlement does not generally change in the linear-log type of semi-log graph. This practice is to ensure that larger voids, which can induce differential settlements, have collapsed under the given load. Such monitoring of void collapse can also be improved by adopting line measurement of settlements by using HPG.

5 CONCLUSIONS

This paper presents an overview of a basic investigation methodology which can be adopted for the in-situ waste (MSW) characterisation and subsequent processing of the characterised waste to obtain the compression ratio (CR) required for the estimate of primary consolidation settlement. The primary compression of MSW materials can be relatively high compared to the uncontrolled soil fill and is typically governed by the highly compressible organic solids content. The estimate of primary settlement is useful for the assessment of construction settlement as well as the design of ground improvement extent to achieve required reduction in void ratio and collapse of large critical voids.

A case study involving a railway embankment built over buried landfill cells was presented. In this case study, the ground improvement in the form of surcharging was adopted due to project requirements. The in-situ waste characterisation was carried out using sonic drilling and conventional drilling methods. A comparison against the 1985 Trial was also presented as part of this case study. The compression ratio which were back-analysed in the case study were found to be consistent with the published relationship between Waste Compressibility Index and compression ratio. In this relationship, higher organic content is typically proportional with higher compression ratio.

Given the variability in waste properties and also a range of parameters assessed from the discussed correlations, it is imperative that the basic investigation is carried out in a sufficient quantity and, where possible, should be supplemented by additional investigation. Additional assessments, such as but not limited to sensitivity, reliability and risk assessments, should also be considered in the design process. It is also a good practice to undertake an observational technique where the waste behaviour in terms of settlements was monitored during the construction or earlier operational period of a typical infrastructure. This will allow a further refinement in the settlement prediction and manage risk.

6 ACKNOWLEDGEMENT

Authors are grateful for the support provided by their colleagues at Coffey Services Australia Pty Ltd.

7 REFERENCES

Andersen, E. O., Balanko, L. A., Lem, J. M. and Davis, D. H. (2004). Field Monitoring of the Compressibility of Municipal Solid Waste and Soft Alluvium, *Proc. of Fifth Int. Conference on Case Histories in Geotechnical Engineering*.

Babu, G. L. S., Reddy, K. R., Chouskey, S. K. and Kulkarni, H. S. (2010). Prediction of Long-Term Municipal Solid Waste Landfill Settlement Using Constitutive Model, *ASCE Practice Periodical of Hazardous, Toxic and Radioactive Waste Management, 14 (2): 139 – 150*.

Bareither, C. A., Benson, C. H. and Edil, T. B. (2012). Compression Behavior of Municipal Solid Waste: Immediate Compression, *ASCE Journal of Geotechnical and Geoenvironmental Engineering, 138 (9): 1047 – 1062*.

Charles, J. A., Burford, D. and Watts K. S. 1981. Field studies of the effectiveness of dynamic consolidation. Proc. 10th *Int. Conf. on Soil Mech., Vol. 3, pp. 617 – 622*.

Chen, Y. M., Zhan, L. T., Wei, H. Y. and Ke. H. (2009). Aging and compressibility of municipal solid wastes. *Waste Management, 29 (1): 86 – 95*.

Edil, E. B, Ranguette, V. J. and Wuellner, W. W. (1990). Settlement of municipal refuse. *ASTM STP 1070, West Conshohocken, Pa. 86–103.*

Park, H. I., Borinara, P. and Hong, K. D. (2011). Geotechnical Considerations for End-Use of Old Municipal Solid Waste Landfills, *Int. Jnl. Environmental Research, 5 (3): 573 – 584*.

Landva, A. O. and Clark, J. I. 1990. Geotechnics of waste fill—Theory and practice, *ASTM STP 1070, West Conshohocken, Pa. 86–103.*

Landva, A. O., Valsangkar, A. J. and Pelkey, S. G. (2000). Lateral earth pressure at rest and compressibility of municipal solid waste, *Canadian Geotechnical Journal, 37 (6): 1157 – 1165*.

Marques, A. C. M., Filz, G. M. and Vilar, O. M. (2003). Composite compressibility model for Municipal Solid Waste, *ASCE Journal of Geotechnical and Geoenvironmental Engineering, 129 (4): 372 – 378.*

Reddy, K. R., Hettiarachchi, H., Gangathulasi, J., Bogner, J. E. and Lagier, T. 2015. Geotechnical properties of synthetic municipal solid waste, *Int. J. of Geotech. Eng. , 3 (3): 429 – 438*.

Reddy, K. R., Hettiarachchi, H. and Giri, R. K. (2015). Effects of degradation on geotechnical properties of Municipal Solid Waste from Orchard Hills, Landfill, USA. *Int. J. of Geosynth. and Ground Eng. 1:24*.

Siahaan, F., Muttuvel, T. and Peiris, A. (2017). Characterization of Municipal Solid Waste Materials for the purpose of engineering design in transport infrastructure project. *Aust. Geomech. Jnl., 52 (3): 67 – 75*.

Siddiqui, A. A., Powrie, W. and Richards, D. J. (2013). Settlement characteristics of mechanically biologically treated wastes, *ASCE Journal of Geotechnical and Geoenvironmental Engineering, 139 (10): 1676 – 1689*.

Sharma, H. D. and De, A. (2007). Municipal Solid Waste landfill settlement: Postclosure Perspectives, *ASCE Journal of Geotechnical and Geoenvironmental Engineering, 133 (6): 619 – 629*.

Sowers, G. 1973. Settlement of waste disposal fills. *Proc., 8th Int. Conf. on Soil Mechanics and Foundation Engineering, Vol. 22, Balkema, Rotterdam, Netherlands, 207 – 210*.

Van Impe, W. F. and Bouazza, A. (1996). Densification of domestic waste fills by Dynamic Compaction, *Canadian Geotechnical Journal, 33: 879 – 887*.

Wall, D. K., and Zeiss, C. (1995). Municipal landfill biodegradation and settlement, *ASCE Journal of Environmental Engineering, 121 (3): 214 – 224.*

Yildiz, S., Yaman, C., Demir, G., Ozcan, H. K., Coba, A., Okten, H. E., Sezer, K. and Goren, S. (2013). Characterization of Municipal Solid Waste in Istanbul Turkey. *Environmental Progress and Sustainable Energy, 23 (3): 734 – 639*.

Zekkos. D., Bray, J.D, Kavazanjian Jr, E., Matasovic, N., Rathje, E. M., Riemer, M. F. and Stokoe II, K. H. (2006). Unit weight of Municipal Solid Waste, *ASCE Jnl. of Geotech. and Geoenv. Engineering, 132 (10): 1250 – 1261*.

GROUND IMPROVEMENT AND VALIDATION FOR STAGE 1 IMEX EARTHWORKS

Q J Yang[1], A Succar[2], J McIlquham[3] and K Chen[4]

[1]Senior Technical Director, [2]Principal Geotechnical Engineer, [3]Principal Geotechnical Engineer and [4]Geotechnical Engineer

[1,2]Arcadis Pacific Australia Pty Ltd, Level 16, 580 George Street, Sydney, NSW 2000, Australia

[3,4]Golder Associates Pty Ltd, Level 8, 40 Mount Street, North Sydney, NSW 2060, Australia

ABSTRACT

This paper presents a case study of the use of an alternative ground improvement technique to treat contaminated uncontrolled fill other than traditional "remove and replace" for major earthworks for the proposed container Import and Export (IMEX) Terminal at Moorebank, Sydney. First, a brief discussion of the options considered for the ground improvement including removal and replacement and the Impact Roller Compaction (IRC) method will be presented. The local geological setting and the historical form of the existing Stage 1 IMEX Terminal site will be described, with the geotechnical model and associated design engineering parameters being surmised. The key points in the development of a technical specification are presented to take account of the performance requirements, including on-site IRC trial and validation testing. The primary validation measures adopted comprise plate load testing, cone penetration profiling (CPT), insitu density testing, dilatometer (DMT) testing and proof rolling after IRC treatment. Surcharging was considered for the remediated contaminated land areas where the details of the remedial treatments were not available at the Stage 1 IMEX development stage to ensure there will be no issues resulting from long-term settlement. At the time of writing this paper the Stage 1 IMEX works have been completed and are operational. The monitoring results indicate the performance of the site is satisfactory.

1 INTRODUCTION

Sydney Intermodal Terminal Alliance (SIMTA) plans to operate an Import/Export (IMEX) inland rail terminal. The Moorebank Precinct East (MPE) Stage 1 IMEX Number 1 project involves the design, construction and commissioning of all civil, rail, utilities, and other infrastructure works required to provide an IMEX Terminal and the associated rail infrastructure on the Moorebank Intermodal Precinct Terminal (MIPT) Land.

The completed terminal features:

- A terminal entry Optical Character Recognition (OCR) portal, truck processing gates, exit OCR and weigh in motion facility;
- 8 No. truck/Auto-shuttle interchange pens;
- Administration/Control facility and services structures;
- 4 No. - approximately 650 m long rail sidings;
- Automatic Stacking Crane (ASC) and Cantilever Automatic Stacking Crane (CASC) operations; and
- Eastern, central and western container stack areas.

The IMEX terminal will operate 24 hours per day, 365 days per year, other than during maintenance shutdowns. It will be initially operated manually, transitioning to fully automated operations thereafter.

The design considered the operational requirements of the Terminal Operating System (TOS) and Plant and Equipment (P&E) required for fully automated operations. SIMTA will be responsible for specifying the TOS and the major P&E.

The site is located approximately 28 km to the south west of Sydney. The site was previously occupied by the Defence National Storage and Distribution Centre (DNSDC), and comprised multistorey buildings, large storage warehouses, roads, pavement areas, outdoor sitting areas, grassed areas and a refuelling depot. The Stage 1 Proposal is located to the east of Moorebank Avenue and is an approximately rectangular parcel of land, about 400 m wide (east to west) and 850 m long (north to south). The Proposal also includes a rail link, approximately 3.5 km long, connecting the site to the Southern Sydney Freight Line (SSFL). The Stage 1 site and rail corridor footprint are presented in Figure 1.

Figure 1: Terminal Footprint (image © Google Maps)

Arcadis was originally engaged by the client as a technical reviewer. Following the commencement of this review Arcadis was approached by the client to derive an alternative solution to the traditional "remove and replace" of the existing fill option the other party was advising for the entire site as the final solution. This paper describes a case study of the ground improvement technique using the impact roller compaction (IRC) method and the validations by means of various insitu testing methods.

2 GEOLOGICAL SETTING AND LOCAL GEOLOGY

The IMEX site is relatively flat, at an elevation of approximately RL+14 m to RL+17 m AHD. Moorebank Avenue runs along the western boundary of the site, with DNSDC land bordering the north, east and southern boundaries.

The site was previously occupied by the DNSDC, which has been relocated. The site is grassed with scattered trees, occupied by low rise warehouses and administration buildings. Due to the former use of the site as a military base which was backfilled with dredged material from Georges River, unexploded ordinance (UXO) risks had to be considered during the geotechnical investigation, including completion of UXO scanning and clearance at each test location prior to testing commencing.

According to the published 1:100,000 Penrith Geological Map (NSW Department of Minerals, 1991), the IMEX site is underlain by alluvial sediments over rock. Adjacent to the Georges River the alluvial sediments are Quaternary (Holocene) age (<10,000 years) (Qha). These lie above a stratum of Tertiary (Pliocene) age fluvial deposits, consisting of clayey quartzose sand and clay (Ta). The geological map indicates that the underlying rock conditions in the area are either Triassic Hawkesbury Sandstone (Rh) or Ashfield Shale (Rwa).

The fill on the IMEX site was generally found to be about 0.5 m to 1.2 m thick, comprising mainly a mixture of sand, clayey sand, sandy clay and clay, with localised depths of up to approximately 2.3 m.

Interbedded sand and clay units were present beneath the fill to depths of up to 23 m, the depth at which CPTs refused on inferred rock. The sands are medium dense or denser and the clays stiff, very stiff or hard. Some CPTs refused at shallower depths, potentially due to the presence of ironstone layers within the alluvium.

The depth to bedrock within the site is about 17 to 23 m below existing ground level (RL -2 m to -8 m). The rock generally became deeper to the north and west, which is consistent with the published geological map.

Groundwater was at about 5 to 7 m below the existing ground level (based on observations in CPTs), equivalent to about RL 8 to 10 m AHD. The water level at a weir in Georges River to the north west of the site is about RL + 5 m AHD.

3 GROUND TREATMENT OPTIONS AND CONSIDERATIONS

3.1 GEOTECHNICAL DATA AND MODEL

The existing fill thickness profile was derived from reviewing the logs and cone penetration test results and undertaking a method of interpolation (kriging) between investigation locations (Figure 2). The derived fill thickness ranged between 0.5 m and 1.2 m, with the middle part being about 2.3m deep, based on the data provided by factual reports (Douglas, 2016 and Golder, 2017a, 2017b, Arcadis, 2017a). Some localised deeper zones of fill were identified from this assessment. These were not all confirmed during the stripping or the preliminary earthwork activities for the site.

3.2 GROUND TREATMENT CONSIDERATION AND PREFERRED OPTION

Following the review of the ground conditions, Arcadis developed an alternative solution through a workshop with the client. A cost benefit and risk assessment of three possible options were carried out during the workshop, including: 1) remove and replace of all fill materials that were not placed in accordance with either an Australian Standard, Specification or lacked appropriate compaction records; 2) dynamic compaction by dropping a very heavy weight that is dropped from significant height; and 3) the impact roller compaction (IRC) method. The option of "remove and replace" would require treatment and disposal of the potential contaminants contained within the uncontrolled fill. This would result in relatively high cost of removal of the fill material due to the presence of potential contaminants. The dynamic compaction using heavy falling weight would require a specialised plant and mitigation measures for potential noise impacts. Option 3 whereby using the impact roller compaction (IRC) method has been used for compacting both sandy and clayey soils to depths ranging between 2 m to 5 m (C. Lee et al., 2015, Choy et al., 2019). After consultation with the specialist contractors (Landpac, 2017) and the cost savings analysis it was decided to use the IRC method for the treatment of the uncontrolled and potentially contaminated fill materials for this project site.

4 IRC METHOD AND PERFORMANCE CRITERIA

4.1 IMPACT ROLLER COMPACTION METHOD

Impact roller compaction (IRC) method is a rapid controlled form of impact-oriented compaction that provides in-situ improvement to mixed fill, landfills and low strength natural soils. This allows development to proceed on high level footings rather than on more expensive deep foundations. The use of the IRC method is often guided by experience in similar soils and applications. The method works by dragging a weight along the ground. The module (weight) of varying shape is connected to the frame by a system of linkage arms that allow the module freedom of movement within its frame and linkages. Once the tow unit commences forward movement, the module is dragged forward and begins to rotate due to friction and soon reaches its operating speed. The energy delivered to the ground results in ground modification (e.g. Avalle et al., 2007). Dependent on the prevailing ground conditions and the characteristics of the impact roller, the effects are measurable by means such as surface settlement, or a relative gain in compaction or soil strength. Landpac, for example, produced the Continuous Impact Response (CIR) advanced visualisation, which will be discussed further in the following sections.

4.2 CRITERIA OF IRC PERFORMANCE REQUIREMENTS

Based on the assessment of the test pits, boreholes and laboratory testing results across the Stage 1 IMEX area it was expected that the impact roller compaction (IRC) treated ground would be improved to achieve the following:

- The treated foundation soils across the site would achieve a minimum ultimate bearing capacity of 400 kPa and a stiffness / Young's Modulus (E') of 40 MPa for all pavement, train and crane rail areas over a typical depth of 5 meters; and
- The compacted foundation soils would achieve a minimum 98% standard dry density (SDD) at the field moisture content.

It was recognised that these criteria would be reviewed and updated during the IRC ground treatment process since insufficient investigation data was available, in, around the areas where the existing building(s) and buried underground services were present.

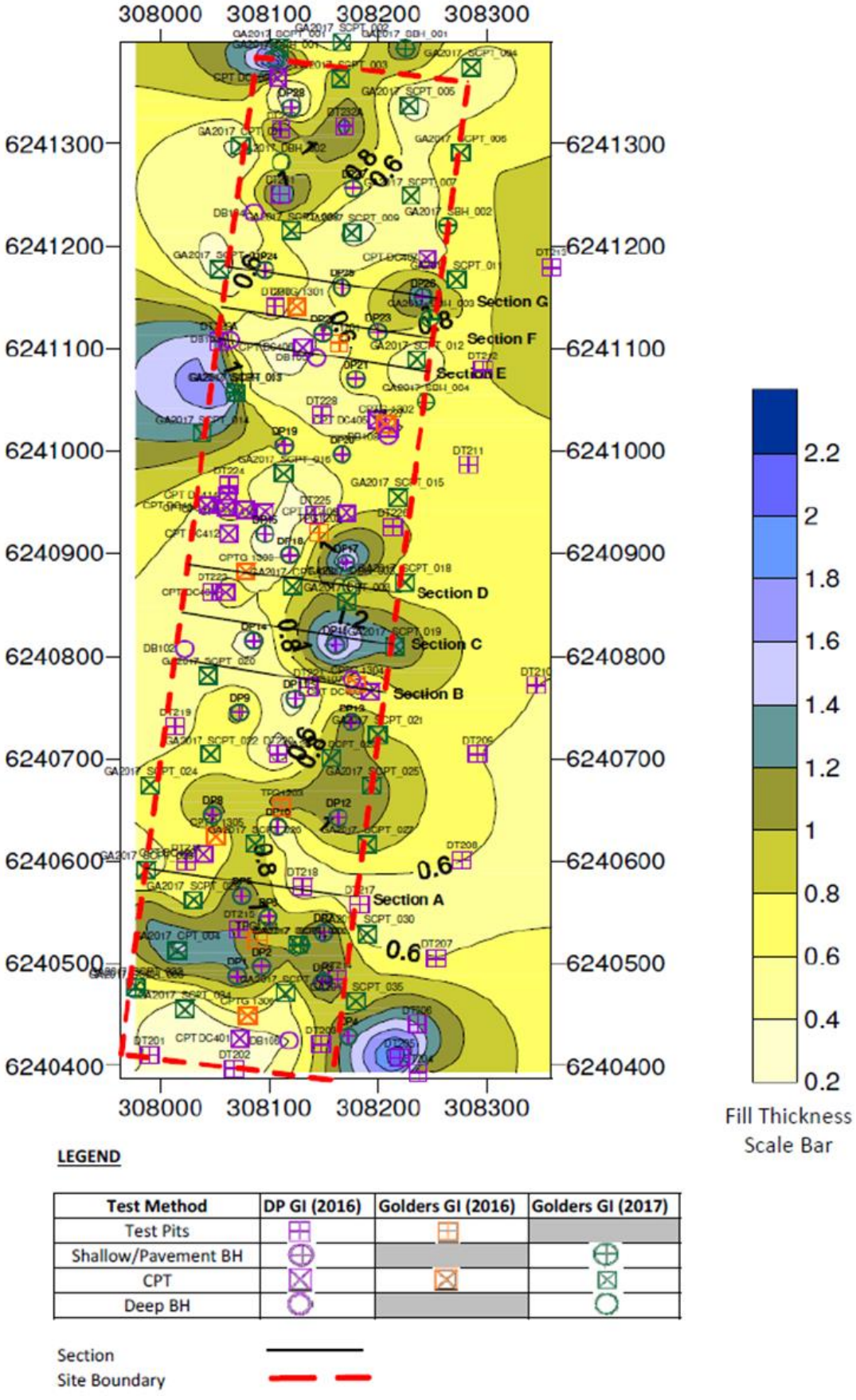

Figure 2: Interpreted fill thickness across site footprint

5 GEOTECHNICAL MODEL AND PARAMETERS

5.1 GENERAL GEOTECHNICAL PROFILE

The engineering properties of the various soil and rock units identified in the previous geotechnical investigations were assessed using test pit logs, borehole logs, cone penetration test (CPT) logs, and in-situ and laboratory test results.

The geological soil units were assessed to be pavement, existing fills, alluvium and bedrock as shown in Table 1. The bedrock has been subdivided into three sub-units, with two for siltstone/shale and one for sandstone. A generalised geological profile with detailed descriptions and associated thicknesses for each unit based on the geotechnical interpretative report (Arcadis, 2017b) is also reproduced in Table 1.

Table 1: Summary of identified geological units, descriptions and approximate thickness

Geological Unit	Material Type	Description	Approximate Thickness (m)
P	Pavements	Generally concrete, although asphaltic concrete encountered in some locations.	0.1-0.2
F	Fill (Existing)	Sand, clay and gravel mixes, generally moderately compacted to well compacted with some soft to firm clay layers identified and lack of appropriate compaction records and certification as per AS3798	< 2.3 (Average of 0.7)
AC or AG	Quaternary Alluvium: Cohesive (AC) Granular (AG)	Clay and sandy clay, generally stiff to hard, with some localised areas of soft to firm clay, as well as dense to very dense clayey and silty sand bands (Unit AG). The alluvium becomes siltier with depth.	< 18
SH-5	Class V Siltstone	Extremely low to low strength siltstone, extremely and highly weathered, extremely low and low strength.	0.4 –1.2 (average of 0.65)
SH-3	Class III and better Siltstone	Medium strength siltstone, moderately weathered, with interbedded medium to high strength sandstone	Unknown
SS-2	Class II sandstone	Medium and high strength, slightly weathered and fresh	Unknown

5.2 GEOTECHNICAL DESIGN PARAMETERS FOR VARIOUS STRUCTURES

Table 2 presents a summary of the design parameters that were derived from either testing results or published correlations.

For purposes of design a minimum design California Bearing Ratio (CBR) of 2% for the re-compaction of existing local fill up to approximately 2 m from finished surface level was adopted. The new fill placed i.e. Select Fill is assumed to have a minimum CBR of 15% and a Plasticity Index of 25.

Table 2: Geotechnical design parameters for various materials

Material Unit	Unit Weight (kN/m^3)	Undrained Conditions		Drained Conditions			
		Cu (kPa)	Eu (MPa)	v	C' (kPa)	Φ' (degs)	E' (MPa)
Ballast	20	-	-	0.3	0	42	80
Capping Layer	19	-	-	0.3	0	40	80
Concrete	24	-	-	0.15	-	-	32000
Select Fill*	20	-	-	0.3	0	35	50-80
Fill- Existing	20	65	26	0.3	0	26	20
Fill – Existing (LB)***	19	45	18	0.3	0	24	15
Fill - Treated**	20	-	-	0.3	0	35	40
Alluvium – Cohesive	19	100	41	0.3	2	28	35
Alluvium – Granular	19	-	-	0.3	0	36	80
Siltstone Class V	20	-	-	0.25	5	28	80
Siltstone Class III	24	-	-	0.2	60	30	500
Sandstone Class II	24	-	-	0.2	100	30	1000

* Select fill shall be sandstone type material from New M5 tunnel spoil or similar, which will be placed and compacted in accordance with AS3798, with a minimum density of 98% SDD

** This unit refers to the existing fill of variable materials whose shear strength presented is an equivalent value after dynamic compaction treatment.

*** This unit represents the lower bound parameters for the existing fill material (Unit F)

For reinforced concrete pavements, the upper subgrade was stipulated to have a design CBR of 33% with a lower subbase of heavily bound granular material of a minimum 4 MPa and a base comprising of a minimum 40 MPa concrete. Similar design parameters were recommended for the heavy - duty concrete block paver pavements, however, the heavily bound granular material of 9MPa (C8/C10) was adopted in lieu of 4MPa. These major elements were on the proviso that the New Fill would achieve the minimum characteristic CBR of 15% for the subgrade. For pavement structural design purposes, the combination of CBR15% fill over CBR 2% fill not thicker than 2m below Final Surface Level, was adopted.

6 SETTLEMENT AND LOADING CRITERIA

The total settlement and differential settlements for various key structural elements were developed by interaction with the operational requirements from the supplier and the published guidelines for stack container yards, crane rails, ATV area, loco area and loco shifter. The specific requirement details adopted are summarised in Table 3.

Table 3: Settlement and loading criteria for Stage 1 key structural element

Area	Loading	Settlement Criteria
5 Stack Container	40kPa based on 25T (20ft) container reduced by 20%	1.4% between any supports; 6.55m between container beam supports=92mm allowable deflection; and 2.44m width of container=34mm
	250kPa at ends of containers for a 1.8m width	
3 Stack Container	33kPa based on 25T (20ft) container reduced by 20%	1.4% between any supports; 6.55m between container beam supports=92mm allowable deflection; and 2.44m width of container=34mm
	250kPa at ends of containers for a 1.8m width	
Crane Rail A (C-ASC – outside leg)	325kN/m	40mm vertical differential between legs Maximum 1:500 longitudinal differential settlement
Crane Rail B (C-ASC – inside leg)	325kN/m	40mm vertical differential between legs Maximum 1:500 longitudinal differential settlement
Crane Rail C (ASC – west leg)	293kN/m	40mm vertical differential between legs Maximum 1:500 longitudinal differential settlement
Crane Rail D (ASC – east leg)	293kN/m	40mm vertical differential between legs Maximum 1:500 longitudinal differential settlement
ATV Areas	66kN/m	5mm between adjacent wheels
Loco Area	264kPa load on rail sleepers	70mm between rails 9mm longitudinal differential along 10m section of track, i.e. 1:1111**.
Loco Shifter	54kPa uniform load	5mm differential settlement in the longitudinal direction between the Loco Shifter and the approaching rail*

* Differential settlement in this location will be managed using an approach slab in the transition zone between the rail and the Loco Shifter

** Longitudinal differential limits taken from Australian Rail Track Corporation (ARTC) Specification ETG-05-01: Track Geometry

7 TECHNICAL SPECIFICATION REQUIREMENTS

7.1 OVERALL STRATEGY OF SPEIFICATION DEVELOPMENT

To ensure the requirements of the earthworks were met several key points were set out in the technical specifications. These include: 1) to ensure clearance of all services; 2) field trials of the IRC to check if the foundation performance can be achieved; 3) a comprehensive suite of testing to validate the earthworks; and 4) proof rolling after completion of IRC

to identify soft spots and undertake remedial actions where required. A series of hold points and witness points were incorporated into the technical performance requirements to validate the effects of the IRC process.

It was highlighted in the specification the Geotechnical Testing Authority (GTA) must submit the testing method statement and detailed procedures for approval by the Geotechnical Inspection and Testing Authority (GITA) in accordance with AS3798. The approved method statements by GITA must be submitted to the Superintendent for review and approval. GTA must submit the testing method statement and detailed procedures for approval by GITA. The approved method statements by GITA must be submitted to the Superintendent for review and approval.

Upon approval of the GITA final report a formal certification of all earthworks and testing stating full compliance with the project specifications must be issued to the Superintendent.

7.2 VALIDATION TESTING REQUIREMENTS

The testing described herein presents the minimum scope of testing for the trial area to assess if the design requirements set out on the specification have been achieved. The field testing and report was undertaken by Golder Associates.

7.2.1 Cone Penetration Testing (CPT)

A minimum of five (5) locations nominated by the GITA for cone penetration testing to assess the zone of improved ground following on from the IRC treatment. The depth of investigation with the CPT must be to a minimum depth of 5 m. An acceptable CPT profile would be determined by the Designer and approved by the Principal after the trial.

7.2.2 In-situ Density Testing

A minimum of five (5) locations were selected for in-situ density testing to assess the IRC improved subsurface profile. The testing surface may require cutting down to below the depth of surface disturbance associated with impact rolling (envisaged to be approximately 300 mm). Typically, three tests were to be undertaken at each location, namely at depths of 0.3 m, 0.6 m, and 0.9 m below ground surface. Where fill was encountered at depths greater than or equal to 2 m, additional density tests at 1.2 m, 1.5 m and 2 m must be undertaken. This was accompanied with field moisture content assessments.

7.2.3 Plate Bearing Tests (PBT)

Five (5) number plate bearing tests (PBTs) were to be undertaken at locations nominated by the GITA. The test locations were to be spread out over the area of the trial foundation area. Each test was to have three cycles, the first to the ultimate bearing pressure (400kPa), the second to 1.5 times the ultimate bearing pressure (600kPa) and third cycle to maximum load / failure – excessive deflection. The plate size was to be nominally 750 mm diameter. Location and details of the tests were to be recorded with the test results. The plate bearing tests were carried out in accordance with BS 1377-9-1990, and were accompanied with in-situ density testing and field moisture content assessments.

7.2.4 Surcharging and Monitoring

Remediation works by means of removal and replace was previously undertaken for areas where petrol tanks were buried. However, there was no compaction data available to confirm what degree of compaction level and associated testing for the areas was achieved with the exception for the material being noted as Bringelly Shale fill on the monitoring records. As such 2 metre of surcharge was placed above the finished level for a month to assess the existing compaction condition of the remediated areas. A total of 6 settlement plates was installed prior to fill placement and surcharging to gather the displacement information for further assessment.

8 FIELD TRIAL AND VALIDATION TESTING

8.1 IMPACT ROLLER COMPACTION

8.1.1 Methodology

Prior to impact roller compaction (IRC) commencing, the existing buildings and structures were demolished, and the exposed ground surface was levelled and stripped of topsoil. A “pre-IRC” proof roll of the stripped surface was carried out to identify, excavate and replace materials which were unlikely to be improved by IRC (e.g. saturated materials, organic soils or unsuitable materials).

After the trial of varying number of passes using IRC it was found that 15 passes using a 3 m wide, 15 tonne, pentagonal dynamic compaction drum towed by a 4 wheeled tractor, as shown in Figure 3, was the best IRC treatment method for the subject site. This drum operates with a drop height of 150 mm to provide 22 kJ of energy during impact rolling. Dynamic response of the ground to the roller was monitored continuously via the Continuous Impact Response (CIR) system, which generated a “coloured map” identifying the level of soil response after the different number of passes. CIR

has been adopted by others to verify IRC treatment, as discussed by Kelly and Gil (2012), and further details relating to CIR technology are presented by Landpac (2017). Following the IRC treatment, the surface was smoothed using a smooth drum roller and a "post-IRC" proof roll was also carried out to identify potential areas of concern which were initially identified using the CIR system. Deflective areas which were observed during the post-IRC proof roll generally corresponded to areas which registered low or very low responses on the CIR plots (represented by yellow and red shading in Figures 5a) and 5b) which typically were related to former service trenches or low lying areas where there was a tendency for water to pond. These areas could not be improved by IRC and were remediated using conventional methods of removal and replacement of compacted fill as shown in Figure 4.

The locations for geotechnical validation testing were nominated using both the CIR system and observations during the post-IRC proof roll. At each test location, CPT, PBT and in-situ density testing was carried out within 1 m of each other. Dilatometer testing (DMT) was also carried out during the initial IRC trial area, located towards the southern portion of the site only.

8.1.2 Interpretation of Results

Figures 5a) and 5b) compare the CIR plots after completion of the first and fifteenth pass of IRC, respectively. In general, the extent of poorly compacted areas (i.e. yellow and red areas of the CIR plot, which are unlikely to achieve the required compaction and/or subgrade stiffness), was observed to reduce with more passes of IRC. Conversely, a larger proportion of the site was observed to be well compacted (as represented in blue and green, which indicate areas which were likely to achieve the level of compaction and/or subgrade stiffness) after additional passes of IRC. The CIR monitoring system and output was demonstrated to be an efficient method of subgrade responses to the IRC actions. It should be noted that the relatively lower compaction on the south west edge in Figure 5b) was due to lack of confinement as well as corner effects where the tractor and drum had no further space to maintain the same speeds and compaction effort.

The results of in-situ field density testing indicate the subgrade generally achieved, on average, a density ratio of about 100% SDD after 15 passes of IRC.

Figure 3: Tractor and pentagonal drum used

Figure 4: Removal and replace of areas post proof rolling

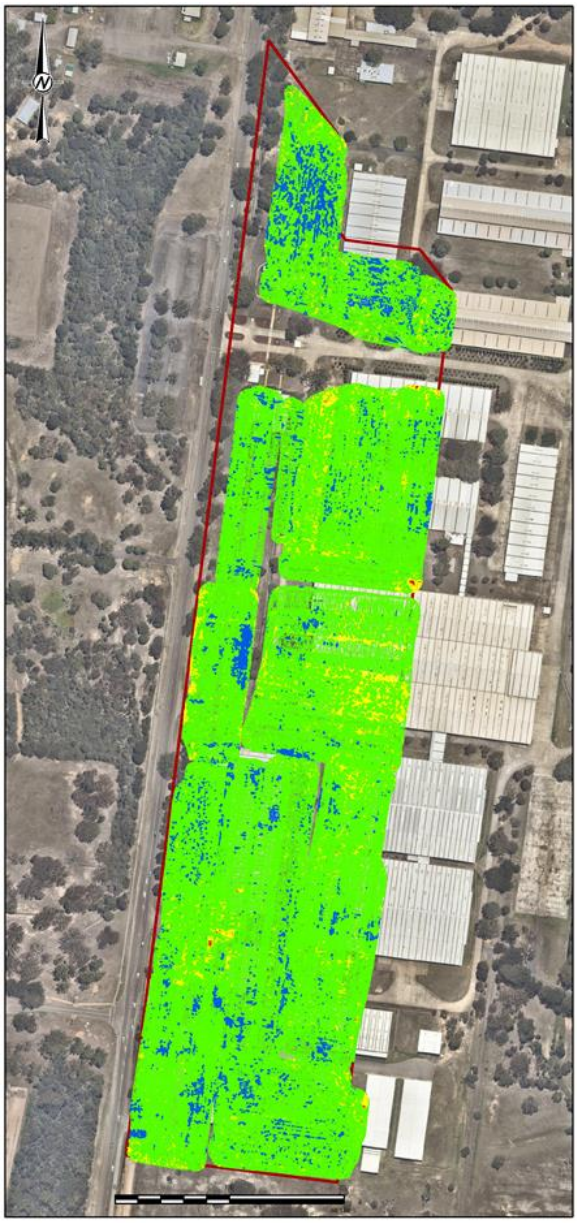

Figure 5(a): CIR plot after first IRC pass

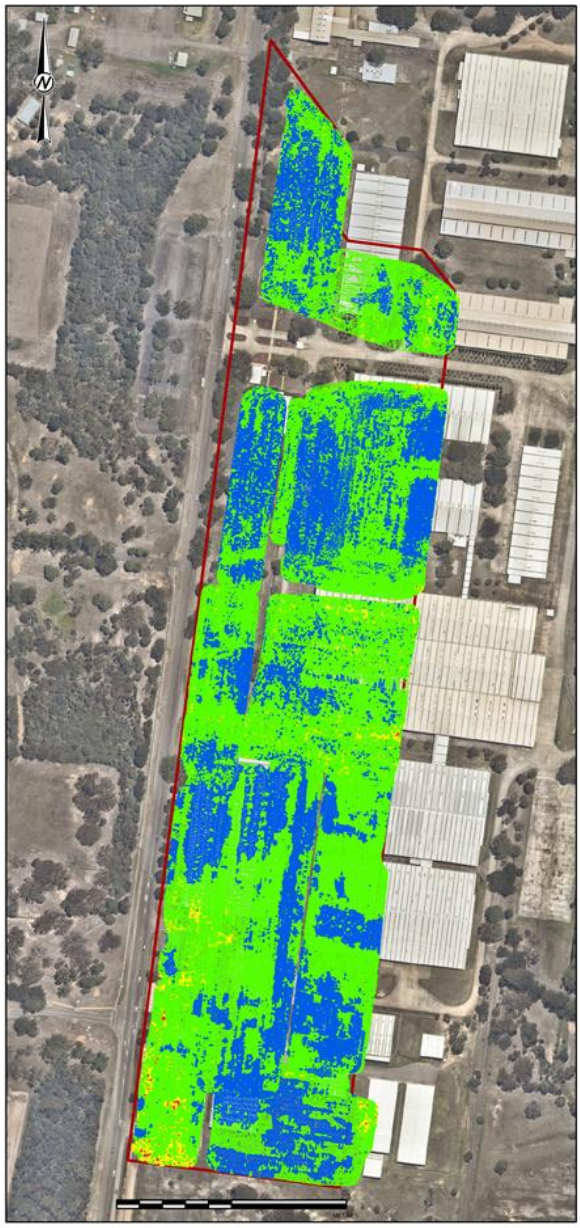

Figure 5(b): CIR Plot after 15th IRC pass

Ground stiffness is a strain dependent soil parameter which tends to be high where strains are small. Due to this strain dependency, there can be a large variation in stiffness moduli (E') obtained for the same material, depending on the method and strain level induced during testing. For this reason, the E' values interpreted from DMT testing, which induce smaller strains during testing, are typically higher than those obtained from the interpretation of CPT and PBT tests completed in the same material. The E' of the soil has been assessed using CPT data by estimating the constrained modulus of the soil (M) based on Robertson (2012) and then converting this to E' using the formula E' =0.74 x M, assuming a Poisson's ratio of 0.3.

Figure 6 compares the average E' interpreted from various field-testing methods in general, the results indicate IRC to be an effective means of preparing a uniform and suitable foundation, which has achieved the design Young's Modulus value of 40 MPa required as per specification requirement.

Figure 7 summarised the lower bound and upper bound and the average inferred Young's Modulus values with depth, indicating the lower value is about 20 MPa, occurring at depths of 0.5m to 1.5m. All the remaining values are greater than 40 MPa.

Figure 8 and Figure 9 shows the lower bound and upper bound values inferred from plate bearing tests and CPT profiles respectively, noting that the lowest value of Young's Modulus is approximately 20 MPa that only occurs at certain depths.

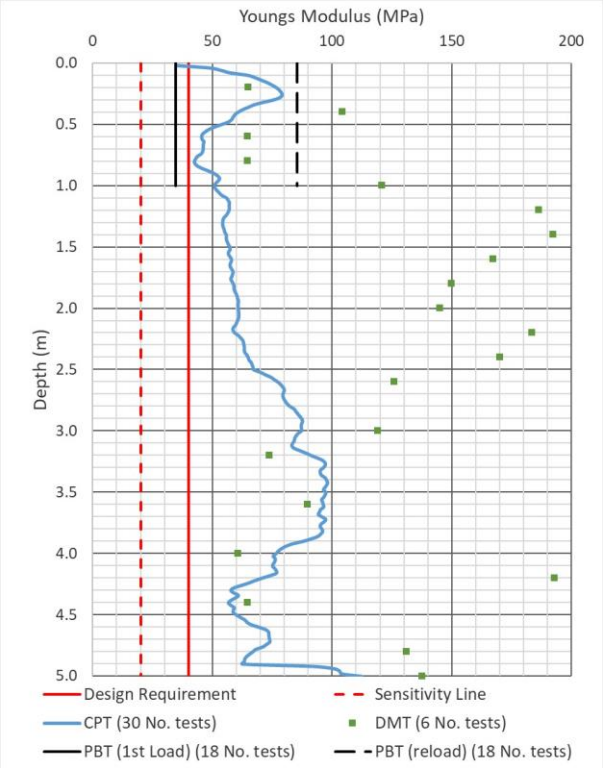

Figure 6: Average Modulus from various testing

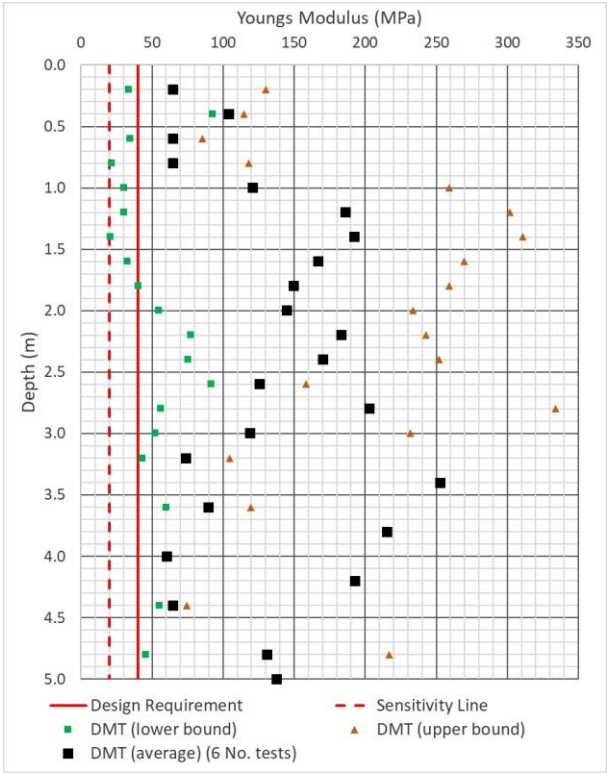

Figure 7: Lower and upper Modulus from DMT testing

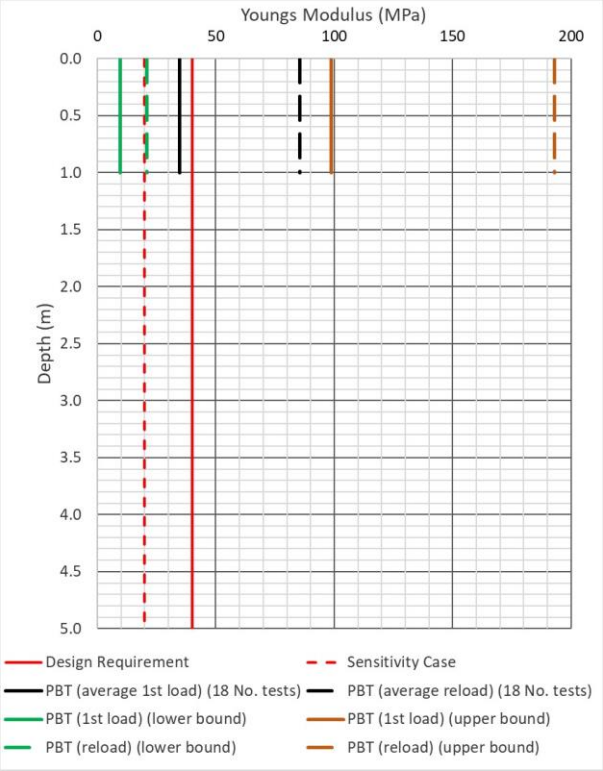

Figure 8: Modulus from various plate bearing testing

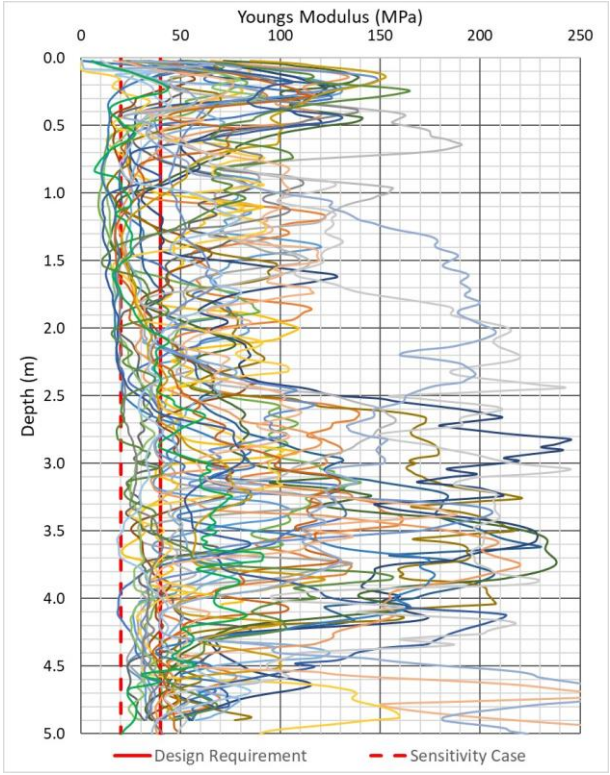

Figure 9: Modulus profiles from CPTtesting

Figure 10 presents the lowest Young's Modulus profile of CPT profile (blue line), with Figure 11 showing the stepped profile with depth in detail. It can be assessed that the Young's Modulus using a weighted average over 5m depth is 62.2 MPa, which is greater than the design values of 40 MPa.

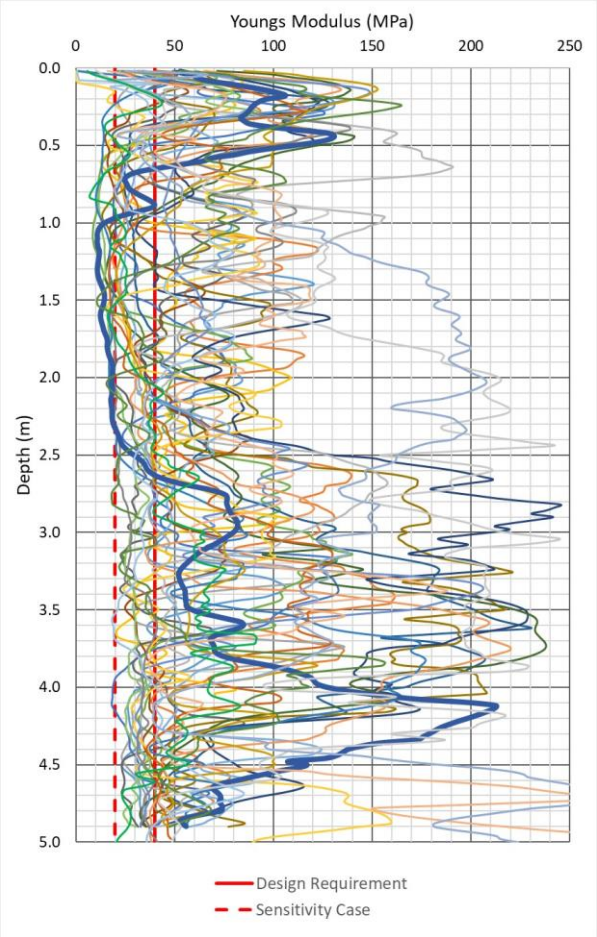

Figure 10: Modulus profiles from CPT testing

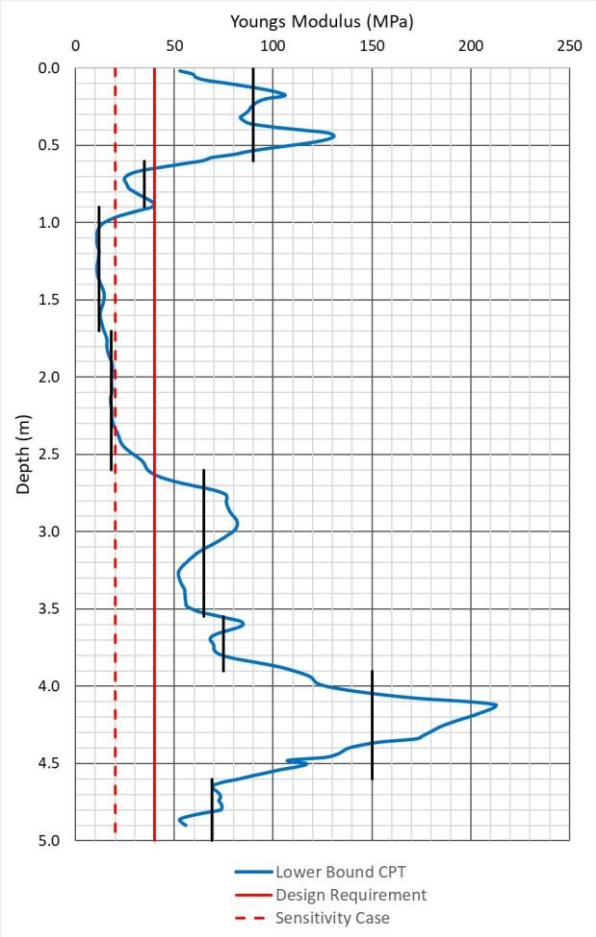

Figure 11: Modulus profile from lower bound CPT

8.1 CONVENTIONAL COMPACTION

Once the subgrade of the site had been proven and compacted using the IRC treatment method, the site levels were raised by construction of a sandstone fill platform, predominantly using sandstone fill material sourced from Sydney tunnelling projects that were running at the same time as this work. Some key issues that require consideration when re-using sandstone from tunnels are as follows:

- Variation in moisture content – depending on the source and status of the source project imported materials may be wet or dry of optimum moisture content;
- Different rock materials may be available depending on the stage of project and source of the materials;
- Excavation methods – blasting vs road header production will impact the grading of the imported fill;
- Presence of other materials mixed in the fill needs to be considered and specifications may allow a small amount of concrete and metal to account for this; and
- Average results of laboratory testing conducted on sandstone fill material used in IMEX (prepared to 98 % standard maximum dry density [SMDD] where applicable) were as follows:
    - CBR = 45%;
    - Optimum Moisture Content = 9.5%;

- 56% finer than 37.5 mm, 37% finer than 2.36 mm and 10% finer than 75 microns. Note some oversized particles were occasionally observed on site and were excluded from lab testing. i.e. visual inspection of site material required;
- Liquid limit of 24% with a Plasticity Index of 9%;
- Phi' = 37 degrees; and c' = 21 kPa.

9 SENSITIVITY ASSESSMENT USING PLAXIS 3D MODELLING

Given the variations of the inferred Young's modulus from the CPT profiling, DMT and plate bearing testing it was decided to undertake three dimensional modelling to assess the differential settlements of the container yard and the crane track formations. This sensitivity assessment was carried out using Plaxis 3D and comprised consideration of unbalanced loading along the yard and the track formations together with a variable ground profile.

The results of the sensitivity assessment, as illustrated in Figure 12, indicated that the differential settlement requirements set out in Table 3 can be satisfied with the potential profile variations at each of the crane legs, that is the lower bound at one leg and the normal condition at the leg of the crane rail track formation.

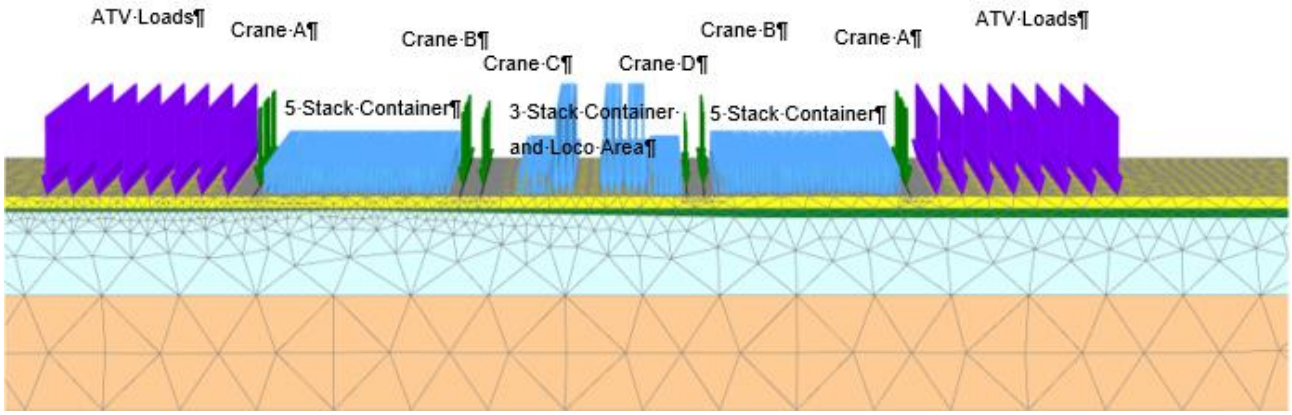

Figure 12: Plaxis 3 model for ATV loads, crane rail loads, container stack loads

10 CONCLUSIONS

The ground improvement work for the Stage 1 IMEX site has been successfully completed in early 2019. The site validation testing results show that the required bearing pressure would be satisfactory with the predicted settlements within the tolerable limits. The client is fully aware of and agreed that any potential on-going settlement post construction will be managed as part of the operation and maintenance works. Should the actual total settlement and differential settlements induced be not acceptable to the operational limits of crane, track and container stack yard pavement or crane rail formation appropriate remediation actions will be undertaken accordingly as part of the long-term maintenance works.

11 DISCLAIMERS

The authors, contributors and their respective organisations do not make any representation or warranty as to the accuracy, completeness or suitability or otherwise of the information contained in this paper and shall have no liability to any person in connection therewith.

12 ACKNOWLEDGMENTS

Many staff from Arcadis, Fulton Hogan, Golder, Qube and Tactical worked cooperatively on the Stage 1 IMEX project, both directly and indirectly, contributing to the successful completion of the project. The authors are grateful to everyone who contributed to this project. Gratitude is owed to Qube and Tactical project managers and director, who provided guidance and support and timely approvals during design and construction phases. The reviewer(s) of this paper provided valuable comments. Their contributions are greatly appreciated.

13 REFERENCES

Arcadis (2018) – Basis of Design Report, Moorebank MPE Stage 1 IMEX Number 1. (Unpublished).

Arcadis (2017a) – Basis of Design Report, Moorebank MPE Stage 1 IMEX Number 1. (Unpublished).

Arcadis (2017b) – Geotechnical Interpretative Report, Moorebank MPE Stage 1 IMEX Number 1. (Unpublished).

Australian Standard, AS3798 (2007) - Guidelines on earthworks for commercial and residential developments.

British Standard BS 1377-9:1990 (1990) - Methods of test for Soils for civil engineering purposes, Part 9: In-situ tests.

D.L. Avalle, B.T. Scott & M.B. Jaksa, (2009), Ground energy and impact of rolling dynamic compaction – results from research test site. Proceedings of the 17th International Conference on Soil Mechanics and Geotechnical Engineering, *M.* Hamza et al. (Eds.).

1:100,000 Penrith Geological Map (NSW Department of Minerals, (1991),

C. Lee, N. Narendranathan, and R. Dalugoda (2015), Dynamic Consolidation of Soft Soils – Concept and Application, International Conference of Geotechnical Engineering, Colombo, 2015.

Douglas Partners (2016), Factual Report on Geotechnical Investigation, IMEX Package 2 Moorebank Avenue, Moorebank, Ref. 85321.00.R.001.Rev0 September 2016 (unpublished)

Golder Associates (2017a). Moorebank Precinct East – IMEX, Geotechnical Data Report. Ref: 1772739-003-R-Rev1, (unpublished).

Golder Associates (2017b). Moorebank Precinct East (MPE) Stage 1 IMEX Terminal Facility – HIEDYC Trial Report. Ref: 1788977-001-R-Rev0, (unpublished).

Golder Associates (2018). Moorebank Precinct East (MPE) Stage 1 IMEX Terminal Facility – HIEDYC-007, 008, 009, 010 Compaction Reports. Ref: 1788977-009. (unpublished).

Kelly, D. and Gil, J. (2012), Monitoring HEIC using Landpac CIR and CIS Technologies, ISSMGE – TC 211 International Symposium on Ground Improvement IS-GI- Brussels 31 May & 1 June 2012.

Landpac (2017), Using the Landpac continuous impact response measurement (CIR) system as a site verification tool, Landpac, Available Online: http://landpac.com/wp-content/uploads/2017/06/CIR-Verification-of-the-Impact-Compaction-Process.pdf

Landpac (2019), http://www.landpac.com.au/

Lee Eng Choy, Qusanssori Noor bin Rusli, Muhammad Khudrie Razali and Ramu Andy, 2019, IOP Conference Series: Materials Science and Engineering, A case study of soft ground improvement by dynamic consolidation approach, Open access.

Roberson, P.K., (2009), Interpretation of Cone Penetration Tests – a unified approach., Canadian Geotechnical Journal, 46(11), pp 1337-1355

APPROACH FOR ASSESSING TIME OF PRELOAD AND SURCHARGE REMOVAL OF EMBANKMENTS ON SOFT SOILS

Kim Chan[1], Bosco Poon[2] and Ashok Peiris[2]
[1]Senior Technical Director – Geotechnics, [2]Technical Director – Geotechnics, GHD Pty Ltd

ABSTRACT

The process of preload release involves a review of the instrumentation and monitoring data. Back analysis is carried out to match field measurements with numerical predictions by adjusting relevant geotechnical model, parameters and construction sequence. Once a match is achieved, the calibrated geotechnical model is used for the prediction of long-term settlement. The removal of preload and surcharge fill is only allowed via the release of a Hold Point, when the predicted long term settlement satisfies the design criteria. This paper provides technical advice and guidance to undertake geotechnical review of preload performance as part of the Hold Point release process.

1 INTRODUCTION

Preload and surcharge with or without prefabricated vertical drains is a commonly adopted soft ground treatment method. In order to confirm that the soft ground has been suitably treated, a process of preload and surcharge release is in place during construction. The removal of preload and surcharge is only allowed via the release of a Hold Point by a nominated verified, certifying that the validated predicted total and differential post construction settlements meet the design criteria. The process of preload performance assessment involves three main steps that can be outlined in Fig. 1.

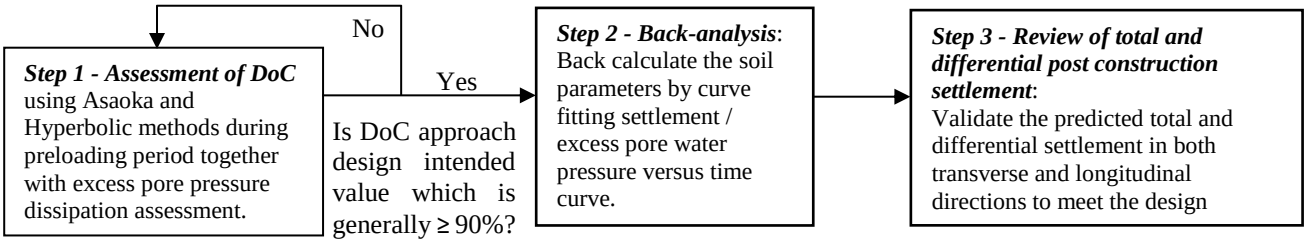

Figure 1: Three main steps involved in the preload performance assessment

By way of showing some examples cited from two soft ground projects, namely, Harwood Bridge project and Warrell Creek to Nambucca Heads (WC2NH) project, this paper provides technical advice and guidance to geotechnical practitioner on the three aspects of Hold Point release process outlined in Fig.1.

2 ASSESSMENT OF DEGREE OF CONSOLIDATION

The instrumentation data should be closely monitored during the preloading period. The objective is to assess the DoC prior to carrying out more rigorous back-analysis of the soil properties. Two observational methods, namely, Asaoka (1978) method and Hyperbolic method proposed by Tan *et al*. (1991) can be used to assess DoC, which are then compared with other DoC values assessed based on pore water pressure measured from the vibrating wire piezometers (VWP).

Asaoka (1978) method is a commonly used graphical method to estimate final total primary consolidation settlement from the settlement data obtained during a certain time period after fill placement. The measured time-settlement curve is plotted to an arithmetic scale, and the total primary consolidation settlement is given where the straight line fitted through the points during the primary consolidation stage plotted as (s_{t-1}, s_t) intersects the 45° line ($s_{t-1} = s_t$). The disadvantage with this method is that it is strongly affected by the choice of time interval Δt used in constructing the Asaoka diagram. Asaoka (1978) states that the accuracy of the graphical method depends on the magnitude of Δt, with larger Δt values giving greater accuracy. The use of a small Δt should be avoided. Fig. 2c shows an Asaoka plot constructed using Δt = 5 days, with the initial settlement data taken as the settlement at t_0 = 105 days (i.e. Point A in Fig. 2a), which was the beginning of the full load. Due to the relatively small Δt adopted, the plotted data are almost sub-parallel to the 45° line. The assessment of the total primary settlement has become very sensitivity to the subjectivity in fitting a line through these points, leading to the uncertainty of the estimated DoC value ranging from 90% to 98%. Edil *et al*. (1991) proposed a parameter j_{95} and recommended that Δt to be chosen to give a j_{95} value between 10 and 30. The j_{95} is essentially the number of samples to reach a 95% DoC and is defined as:

$$j_{95} = \frac{ln(0.05 s_p/(s_p - s_0))}{ln\beta_1} \quad (1)$$

where s_0 is the settlement at the end of the field construction period after which the added embankment load is constant. s_p is defined as $s_p = \beta_o / (1- \beta_1)$. β_o is the intercept and β_1 is the slope of the straight line in the s_t vs. s_{t-1} plot. The use of Δt = 5 days in Fig.2c gives a j_{95} value of about 60, which exceeds the recommended range suggested by Edil *et al*. (1991). By adopting Δt =20 days, the corresponding j_{95} = 20 is within the recommended range of 10 – 30, and the Asaoka plot shown in Fig. 2d exhibits a more oblique trend to the 45° line than that of using a smaller Δt value. The assessed DoC = 91% based on Δt =20 days is therefore considered to be a more reliable prediction than that using Δt =5 days.

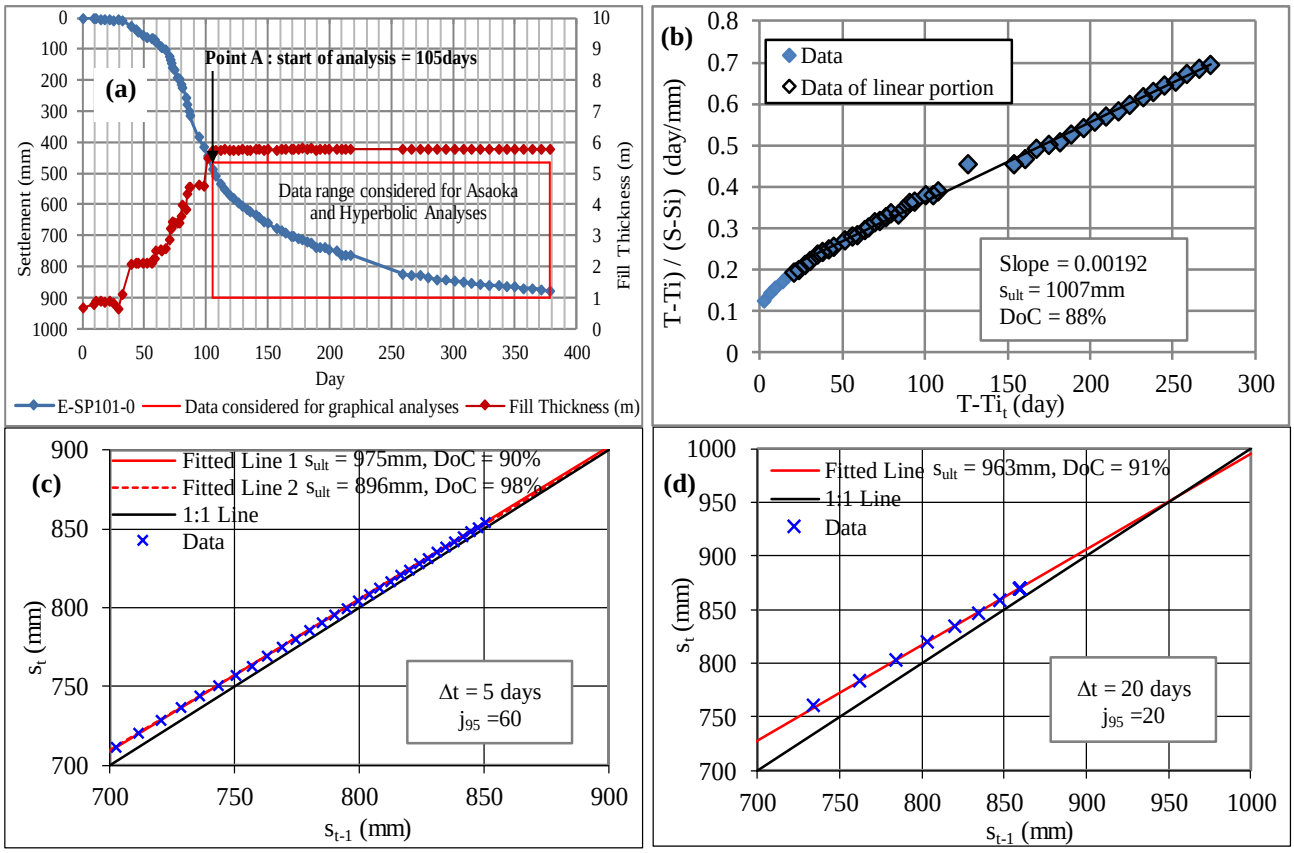

Figure 2 – (a) SP101 data, (b) Hyperbolic analysis, (c) Asaoka analysis (Δt = 5 days), (d) Asaoka analysis (Δt = 20 days)

Tan *et al*. (1991) proposed a hyperbolic relationship between monitored settlement, *s*, and consolidation time, *t*, given by $t/s = \alpha + \beta t$. Hence the ultimate settlement s_{ult} is defined as:

$$s_{ult} = \lim_{t\to\infty} s = \frac{1}{\beta} \quad (2)$$

where α and β are the intercept and slope of the initial linear line. The above equation literally means that when time tends to infinity, the inverse of the slope of the graph at linear segment will give the ultimate settlement. The main attraction of the hyperbolic method is its simplicity without the need to consider Δt value. Unlike the Asaoka's method that is based on a governing partial differential equation that considers only the primary consolidation, the hyperbolic method is based on actual data, which intrinsically includes creep settlement. As a result, the ultimate settlements obtained from the hyperbolic method are usually slightly larger than those obtained from Asaoka's method. The settlement plate SP101 data from Harwood Bridge project was assessed in Fig. 2b using hyperbolic method. The estimated ultimate settlement is compared with those assessed using Asaoka (1978) method as show in Table 1 (also include other settlement plate data in the preloading area). It can be seen that the settlements obtained from hyperbolic method are slightly larger than those obtained from the Asaoka's method, irrespective to the time interval adjustment made in the latter methods.

The assessment of DoC should also consider the excess pore water pressure measured from the vibrating wire piezometers (VWP). In the interpretation of excess pore water pressure, it is important to correct the measured total pore water pressure for the increase in pressure head due to the settlement of piezometer under load. The settlement of the piezometer with

time can be estimated from the registered settlement of the magnet in the nearby extensometer. By way of an example, Fig. 3 shows a higher excess pore water pressure inferred from a piezometer at RL-4.32 m in E-VP101 (from Harwood Bridge project) than if it was correctly interpreted with settlement correction. The corrected excess pore pressures of all piezometers fat E-VP101 are summarised in Table 2. Also refer to the nearby ACPT010 shown in Fig. 5a and the nearby boreholes, the soil thicknesses of the upper and lower clay layers, separated by a drainage layer, are 6 m and 4 m, respectively. By considering two-way drainage for each of the clay layers, the corresponding drainage distances H are 3 m and 2 m. The 'z' in Table 2 refers to the depth of the piezometer relative to the drainage boundaries. Uz (i.e. DoC at depth z) were then calculated based on the total applied fill load of 108kPa. By plotting Uz vs z/H for the upper clay layer (values calculated in Table 2) on the chart in Fig. 5b, the time factor T for the upper clay layer can be assessed to be about 0.8. The assessed average DoC from the chart given in Fig. 5c is about 88% based on T=0.8. This is consistent with graphical analysis results. In summary, the Asaoka method, the hyperbolic method and the measured excess pore pressure from the VWP indicated that the DoC at the northern abutment at the end of the preloading period was about 90 ± 2%.

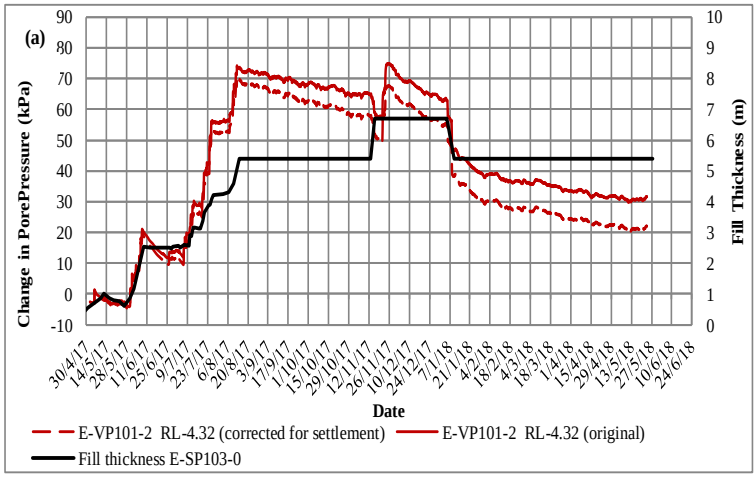

Figure 3: Excess pore pressure – time curve for piezometer at RL-4.32m in E-VP101 (Interpretation with and without correction for settlement)

Table 1: Summary of predicted DoC values

Settlement plate ID	Predicted total settlement (mm)		Assessed DoC (%)	
	Asaoka	*Hyperbolic*	*Asaoka*	*Hyperbolic*
E-SP101	963	1007	91	88
E-SP102	950	995	93	90
E-SP103	997	1060	91	89
E-EM101	1000	1065	92	89

Table 2 –Predicted Uz of piezometers at E-VP101

Layer	RL (mAHD)	z (m)	z/H	Excess pore pressure (kPa)	Uz(1)
Upper Clay: Drainage distance H = 3m					
Upper Clay	-1.02	0	0	0	100
	-4.32	3.3	1.1	20	81
Sand Layer					
Sand	-4.32	–	–	0	100
Upper Clay: Drainage distance H = 2m					
Lower Clay	-14.82	2.14	1.07	0	100

(1) Uz calculated based on a total applied load of 108kPa

3 BACK ANALYSIS PROCESS

Back analysis is usually carried out towards the end of the preload waiting period or when the assessed DoC values (based on Asaoka, Hyperbolic and VWPs) have reached the intended DoC as per design, which is in general 90% or greater. The objective of carrying out the back analysis is to verify/adjust the consolidation and compressibility parameters by curve-fitting the recorded settlement-time curves and the excess pore pressure measurements. This is followed by the review of the long term creep settlement predictions based on the actual final effective stress after the preloading and surcharging in order to validate the predicted total and differential settlement in both transverse and longitudinal directions to meet the design criteria. The discussion of post surcharge creep settlement is provided in Section 5. This section focuses on the back-analysis of engineering parameters. The analysis aspects involved in the back-analysis are provided in Section 4. In the curve fitting process as part of the back-analysis, the adjusted engineering properties shall always be reviewed by comparing with laboratory and in-situ test data, as well as published correlations. A methodological approach is outlined herein in order to provide guidance for undertaking the back-analysis.

Step 1 – Review the soil stratigraphy and total soil depth – In the back-analysis of the settlement plate and extensometer data, the soil layer thicknesses of the adopted geotechnical model shall be accurately defined based on the nearest CPTs, even though they may be different to those of the original design model. The soil model adopted in the detailed design is for an area whereby the soil depth could be the deepest or the average within the area. There is no guarantee that the soil layer thicknesses or total soil depth used in the design are representative of those at the monitoring locations. For the case of Harwood Bridge project, the soil stratigraphy has been reviewed during the back-analysis of settlement plate E-SP103 based on the nearby ACPT010. It can be seen that the upper and the lower clay thicknesses are 5.5 m and 3.6 m, respectively (see Fig. 5a), which are greater than the corresponding thicknesses of 4.5 m and 3 m adopted in the design.

Step 2 – Adjust the over consolidation ratio (OCR) and review of ground water level – Over consolidation ratio (OCR) is one of the most influential parameter affecting the predicted total settlement. During the detailed design stage of Harwood

Bridge project, the OCR values of the clay layers were assessed by using a numerical "aging" technique in conjunction with the sophisticated Soft Soil Creep Model embedded in the commercially available FEA software program PLAXIS 2D. For the case of WC2NH project, the design OCR values were derived based on SHANSEP equation (Eq. 3) and using the SHANSEP parameters of m = 0.8 and S = 0.22. In both design cases, it was found that using the design OCR values underestimate the measured total settlements. During the construction stages of both projects, the OCR values were correlated with the S_u inferred from the nearest CPT via SHANSEP while adopting m = 0.95 and S = 0.22 (see Fig. 5b and 5c). This set of SHANSEP parameters has been used in many soft soil projects along the east coast of Australia with success. It has also been used by the Authors to predict the behavior of a well-known trial embankment in Ballina (see Chan *et al.* 2018). The back-analysed OCR values via SHANSEP approach is strongly influenced by the ground water level since the vertical effective stress σ'_v is used in Eq. 3. It is therefore imperative to review the ground water table via monitoring data as part of the back-analysis process.

$$S_u/\sigma'_v = S \times OCR^m \tag{3}$$

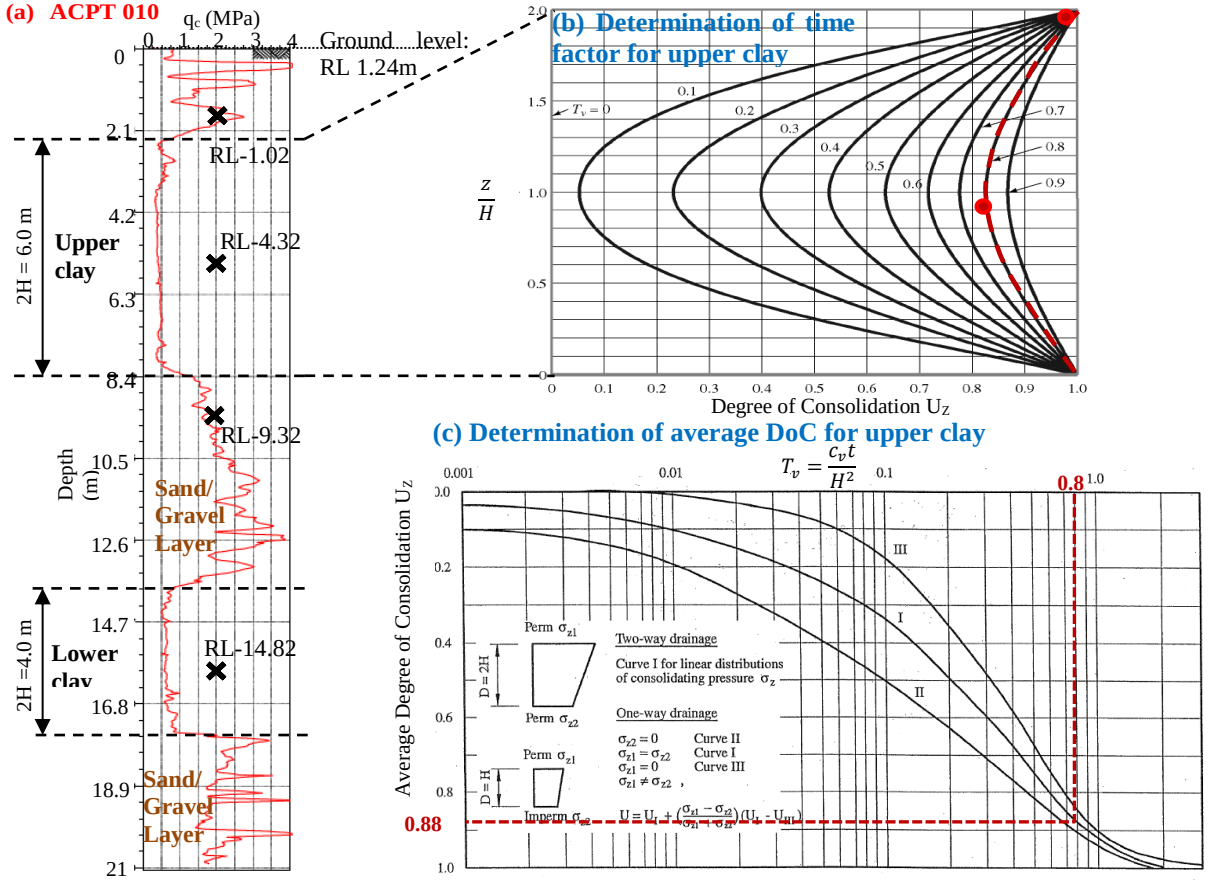

Figure 4: (a) ACPT010, (b) Time factor for upper clay layer, (c) Average DoC for upper clay

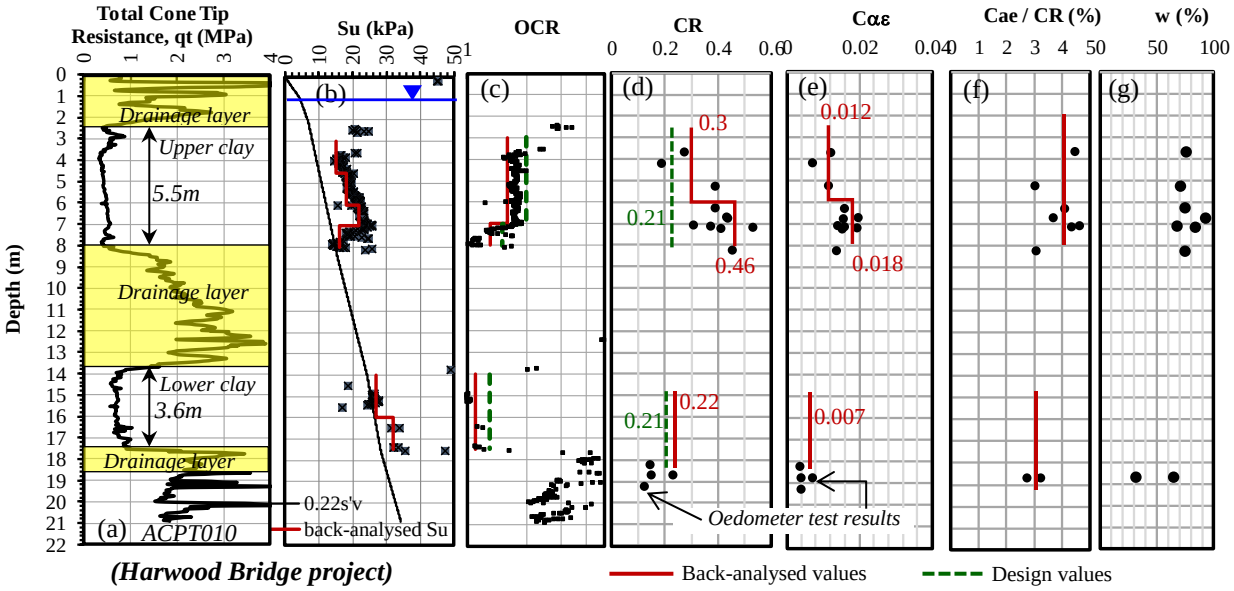

Figure 5: (a) ACPT010 q_t, (b) CPT inferred S_u, (c) CPT inferred OCR, (d) CR, (e) $c_{\alpha\varepsilon}$, (f) $c_{\alpha\varepsilon}$/CR, (g) moisture content with depth

Step 3 – Review the compression Ratio (CR) and recompression Ratio (RR) – While OCR and water level are the major parameters influencing the predicted total settlement. The adopted compression ratio (CR = $c_c/(1+e_0)$) and recompression ratio (RR = $c_r/(1+e_0)$) should also be reviewed (or adjusted if required) for their consistency with oedometer test data as part of the back-analysis process. It is not unusual to adopt a higher compressibility values than the laboratory results that are derived from disturbed soil samples. Take Harwood Bridge project for example, the adopted CR value in the design was 0.21, which lay close to the lower bound of the oedometer test results (Fig. 5d). For back-analysis, the CR value was increased to become more aligned with the upper bound of the test results. Moreover, the upper clay layer was divided into two sub-layers, with the lower layer having a higher back-analysed CR value. This was consistent with the high compressibility identified by the oedometer test data, as well as the high water content exhibited within this sub-layer (Fig. 5g). The RR value may need to be adjusted in order to better fit the proportion of settlement occurred before and after OCR =1. RR can be correlated with CR. Typical RR/CR ratio is about 0.14 and with a likely range of 0.1 to 0.2.

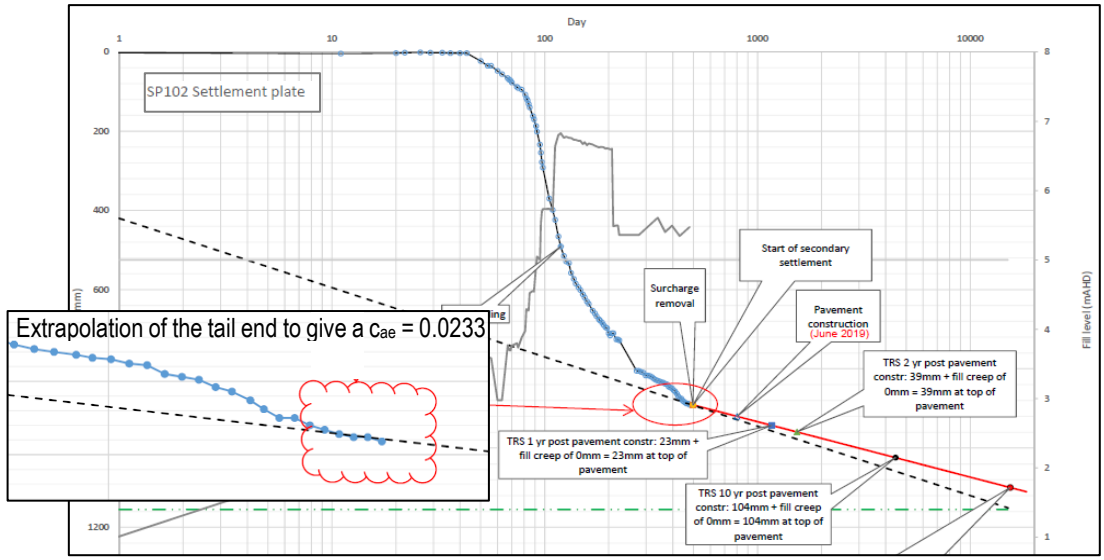

Figure 6: Extrapolation of the tail end of SP102 data (on Harwood Bridge project) to assess $c_{\alpha\varepsilon}$ (not recommended)

Step 4 – Review the normally consolidated creep strain rate $c_{\alpha\varepsilon(NC)}$ – Unless otherwise suggested by laboratory test data, the normally consolidated creep strain rate $c_{\alpha\varepsilon(NC)}$ can be taken as 4% of the back-calculated CR in accordance with the

c_α/cc law of compressibility for inorganic clay proposed by Mesri and Godlwski (1977). Figs. 5d, e and f show that the back-analysed $c_{\alpha\varepsilon(NC)}$ values based on the correlation are consistent with the oedometer test results on Harwood Bridge project. Fig. 6 shows a case where the tail end of the settlement vs. time curve was interpolate to derive a straight line. This linear line shall not be misrepresented as the pure creep settlement behavior since it may comprise a large proportion of residual primary settlement. It is the authors' opinion that using the observed settlement rate at the tail end to assess the creep rate is likely to result in excessive post construction settlement prediction. The $c_{\alpha\varepsilon(NC)}$ should more appropriately be assessed from the back-analysed CR value, and compared with the laboratory test data.

Step 5 – Refine the shape of the fitted curve – The shape of the fitted curve is largely influenced by (i) drainage boundary of the clay layers, (ii) load history and (iii) adopted coefficient of consolidation values c_v. With regard to the drainage boundary, it is imperative to review the sand-clay boundaries based on the area specific CPTs such as that outlined in Fig.5a. The applied fill load in the back-analysis should also follow closely the loading history. An example of which is shown in Fig. 10. In relation to c_v, the back analysis should consider firstly the normally consolidated $c_{v(NC)}$ by comparing the back-analysed values with piezocone measurements as well as published correlation, followed by using appropriate over-consolidated $c_{v(OC)}$ values. Fig.7c presents c_v values assessed from piezocones on WC2NH project. The c_v values were assessed based on $c_v = c_h/2$ (based on Beales and O'Kelly, 2008 and our experience in the region), where c_h is the coefficient in the horizontal direction inferred from the dissipation test results. The c_v values in Fig.7 are plotted side by side with the OCR profiles inferred from the corresponding piezocones. If the inferred c_v within the same soil unit (Unit 2a) are plotted against the corresponding OCR on a log-log plot as shown in Fig. 8b, a prominent linear trend can be seen and the intersection of the median line of this trend line with OCR = 1 gives an estimated $c_{v(NC)}$ of about 12 m^2/yr. NAVFAC (1971) developed correlations of c_v of remoulded, normally consolidated and over-consolidated clays with their liquid limits (LL) as shown in Fig.8a. The Unit 2a on WC2NH project has a LL range of 35% – 50%. By using a mean LL of 42%, the correlated $c_{v(NC)}$ is about 8 m^2/yr, which is consistent with that inferred from field measurements in Fig.8b. During the design stage, a conservative design trend line of c_v vs. OCR was adopted (on the safe side of the median line) and the adopted design $c_{v(NC)}$ and $c_{v(OC)}$ values were 7 m^2/yr and 20 m^2/yr, respectively. During construction, the back-analysed $c_{v(NC)}$ and $c_{v(OC)}$ were 15 m^2/yr and 30 m^2/yr. These back-analysed values, while greater than the design values, are more aligned with the median trend line as. The linear c_v vs. OCR trend shown in Fig. 8c is material type specific. Poon and Chan (2015) have shown that similar linear trends can be created for other soil types on the double log space. But the slope and y-intercept (i.e. $c_{v(NC)}$ at OCR = 1) would be different and are dependent on LL.

For ground treatment using prefabricated vertical drains, the smear zone characteristic of the drains such as the smear radius ratio and the permeability ratio should also be considered. For design and back-analysis purposes, the smear radius ratio of 8 -11 and permeability ratio of 2 based on the research works by Indraratna et al. (2015) may be applied.

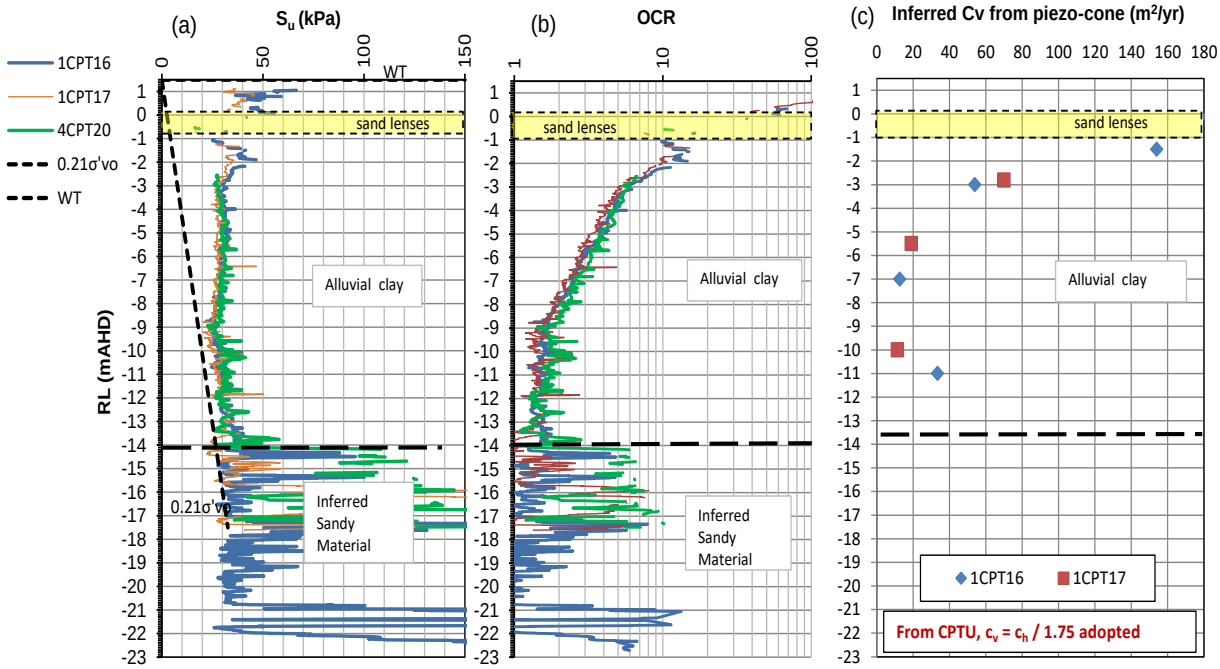

Figure 7: Typical profiles of (a) S_u, (b) OCR and (c) c_v vs. RL inferred from piezocones on WC2NH project

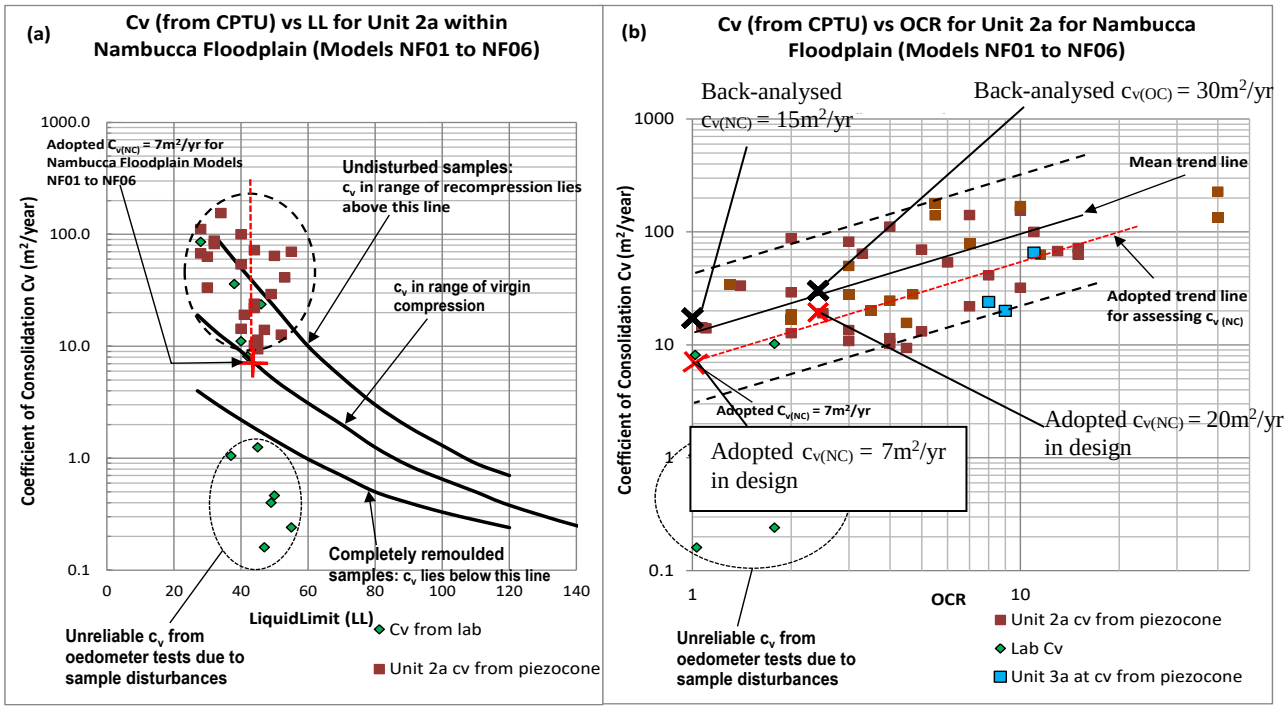

Figure 8: (a) c_v vs. LL, (b) c_v vs. OCR for Unit 2a from WC2NH project

4 ANALYTICAL TECHNIQUES FOR BACK-ANALYSIS

For back-analysis purposes, it is the Authors' preference to deploy simple 1D consolidation model in which creep settlement is assumed to commence at the end of the primary consolidation (considered to be at 90% DoC). Notwithstanding this, a more sophisticated Soft Soil Creep (SSC) model that is embedded in the commercially available software program PLAXIS 2D has gained much popularity in recent years. This model utilizes a form of time-dependent concepts of Modified Cam-Clay and visco-plasticity, thus taking into account of the simultaneous nature of primary consolidation and creep. This section provides some remarks on the use of SSC for back-analysis.

Permeability – In the FEA model, c_v is not a direct input, but is a composite parameter that depends on both the coefficient of permeability, k, and the coefficient of volume compressibility of the soil, m_v. The m_v value is calculated within the FEA program based on the input parameters of CR and RR, whereas k is related to the void ratio, e, in accordance with the permeability function: $e = e_0 + c_k \log (k/k_0)$, where e_0 is the initial void ratio, k_0 is the initial permeability value and c_k is the permeability index. k_0 and c_k are the input parameters to FEA to define the permeability function. For clays, k_0 is typically about 1e-4 m/day. k_0 can be also be converted from c_v using the following equation:

$$k_0 = k_v = 0.434 \times CR \times c_v \times \gamma_w / \sigma'_v \quad (4)$$

where γ_w is the water unit weight. The permeability index c_k is an influential parameter that affects most of the post peak excess pore pressure dissipation rate. The smaller the adopted c_k value, the slower is the rate of excess pore pressure dissipation, and the flatter is the slope of the predicted excess pore pressure vs. log time curve after fill placement as demonstrated by an example presented in Figure 9. Tavenas *et al*. (1983) proposed a correlation of $c_k = 0.5e_0$, but can be as low as $c_k = 0.25e_0$ as pointed out by Chan *et al*. 2018.

Buoyancy effect – Fig. 10 shows a fitted settlement-time curve for a settlement plate on WC2NH project using 1D consolidation analysis. Using the same set of back-analysed parameters from 1D analysis, it can be seen that the prediction given by the 2D FEA with SSC model overestimated the measured settlement. Noted that the FEA undertaken was a small strain analysis applying a constant load with time after fill placement. However, the embankment has settled a maximum of 1.1m during the preloading period. Part of the fill material that was originally above the ground water table (GWT) has settled below the GWT (GWT near ground surface). This entailed a load reduction of about 10kPa ≈ (1.1-0.1)×10kN/m^3. To investigate the buoyancy effect, a large strain 2D FEA with SSC model was conducted with updating mesh and pore water pressure. As can be seen in Fig. 10, the buoyancy effect has compensated the creep settlement accumulated during primary consolidation, leading to relatively reasonable estimate of the settlement compared to the measurements. The settlement prediction shown in Fig. 10 has demonstrated an important point that while the simple 1D analysis gives a similar predicted settlement-time curve compared to that given by the sophisticated large strain SSC FEA, its theoretical considerations were far less rigorous than the latter. Simple soil model could be used more consistently

with simple numerical method (e.g. updating mesh or buoyancy effect may not be necessary), whereas complex soil model is best to be used in conjunction with sophisticated computational approaches (e.g. large strain analysis with updating mesh and pore water pressure). Mixing complex soil models with simplified computational approaches, or vice versa, may not give desirable outcomes.

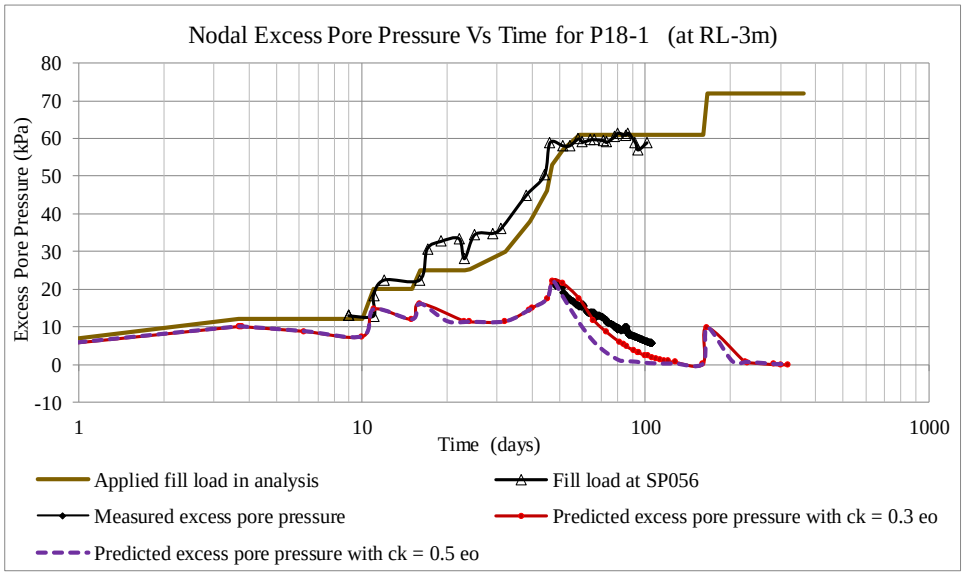

Figure 9 – Comparison of large strain SSC using c_k = 0.3 e_0 and c_k = 0.5 e_0 with measured excess pore pressure from WC2NH project

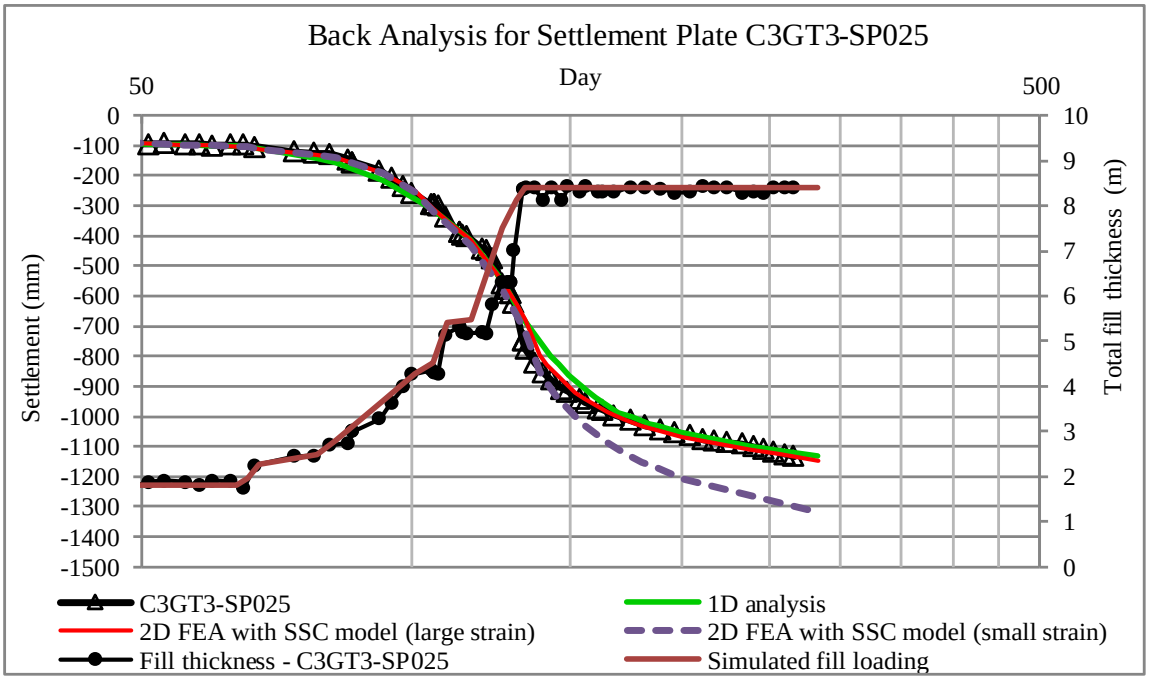

Figure 10: Numerical analysis results with measured settlement plate data (from WC2NH project)

5 POST SURCHARGE CREEP SETTLEMENT

When an over-consolidated state is induced in soil by removal of a surcharge, the creep settlement is expected to be less than if the soil remains in a normally consolidated state. The methods that are commonly used for the prediction of post surcharge creep settlement are: (i) Ladd (1989) methd, (ii) Mesri (1994) method, (iii) Yuan *et al*. (2015) method, and (iv) FEA using SSC model embedded in PLAXIS. This section provides discussion of these methods.

Based on the data presented by Ladd (1989) together with test data from recent soft ground projects in Australia including Gateway Upgrade and Ballina Bypass, Wong (2007) adopted an empirical exponential relationship for varying $c_{\alpha\varepsilon(OC)}$ to $c_{\alpha\varepsilon(NC)}$ ratio with OCR (see Fig.11) as given by:

$$\frac{C_{\alpha\varepsilon(OC)}}{C_{\alpha\varepsilon(NC)}} = \frac{(1-m)}{e^{(OCR-1)n}} + m \tag{5}$$

In Eq. 5, the constant *m* represents the minimum value of $c_{\alpha\varepsilon(OC)}$ / $c_{\alpha\varepsilon(NC)}$. The magnitude of *n* controls the rate of reduction of $c_{\alpha\varepsilon(OC)}$ / $c_{\alpha\varepsilon(NC)}$ with OCR. In the absence of site specific test data, the *n* value of 6 may be adopted for organic clays for preliminary assessment purposes. Also shown in Fig. 11 is a new $c_{\alpha\varepsilon(OC)}$ / $c_{\alpha\varepsilon(NC)}$ vs. OCR function proposed by Yuan *et al*. (2015) based on separate creep test data:

$$\frac{C_{\alpha\varepsilon(OC)}}{C_{\alpha\varepsilon(NC)}} = \frac{2}{(OCR^{7.2}+1)} \tag{6}$$

The Mesri (1994) method prescribes an over consolidated secant creep index to determine settlements after creep has recommenced. Fig.12 compares PLAXIS SSC model results and the Mesri expression for the ratio of start time of creep to rebound time. In the PLAXIS analysis rebound time (t_{pr}) is taken as 0.1 days. The start time of creep (t_l) is assessed visually where the rate of settlement is seen to increase on the settlement curve. For a given OCR, Mesri (1994) suggests that the time prior to the commencement of creep will be shorter than predicted by PLAXIS. Fig. 13 compares the secant creep index relationships at various OCR values. The rates of creep computed by PLAXIS are greater than given by Mesri (1994) for a given ratio of t/t_l. It is interesting to note that PLAXIS suggests that the secant creep strains for OCRs in the range of 1 to 1.2 will be similar, although this is very sensitive to the value of t_{pr} selected in the assessment. PLAXIS appears to broadly give results closer to Mesri (1994) in modelling post unloading creep than Ladd (1989) or Yuan *et al*. (2015) since these methods prescribes a constant creep index for all time. PLAXIS has the advantage over Mesri (1994) that it calculates creep settlements when the OCR falls below 1.2. When surcharging is used to consolidate deep soft clay layers, the lower clays may have OCR values less than 1.2 after unloading.

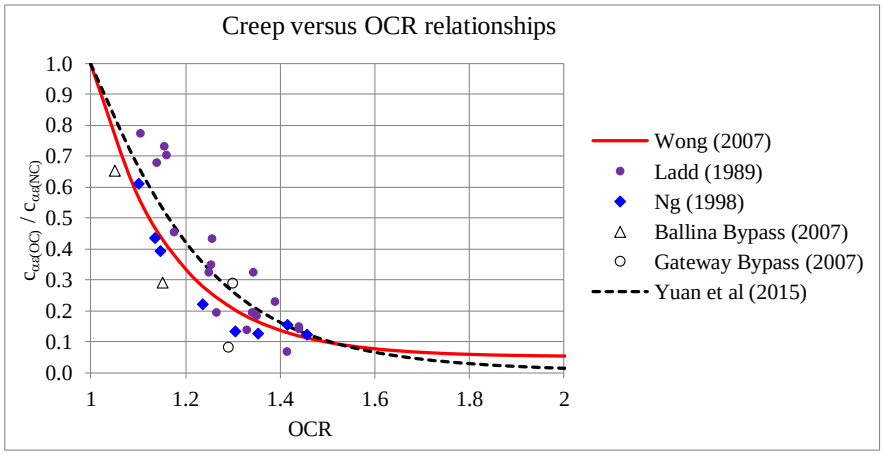

Figure 11: Creep versus OCR relationships

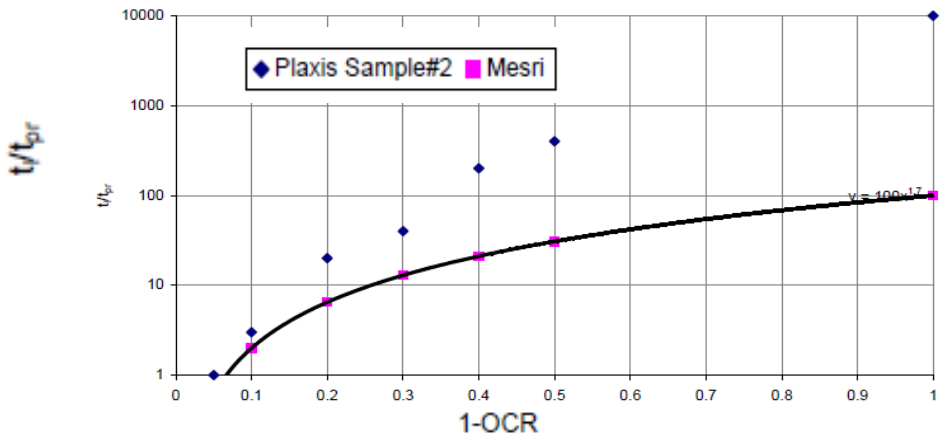

Figure 12: Start time of creep – PLAXIS SSC model compare with Mesri (1994)

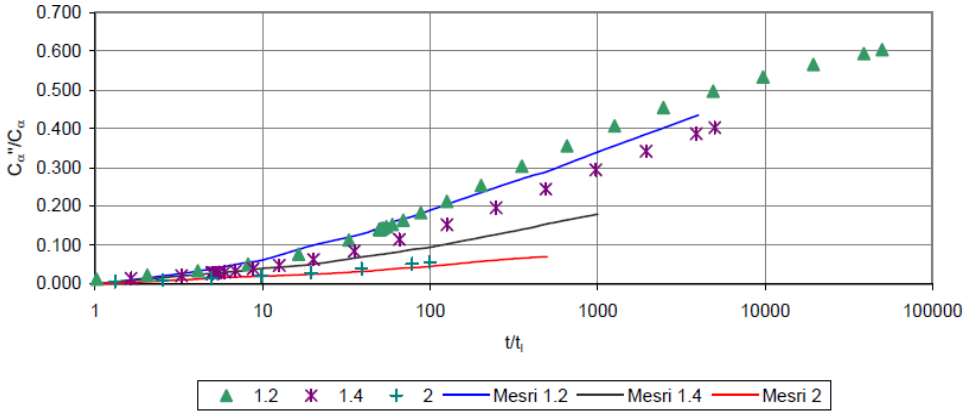

Figure 13: Secant creep index – PLAXIS SSC model compare with Mesri (1994)

6 CONCLUSIONS

The following points can be made in relation to the performance assessment undertaken as part of the preload and surcharge release process:

- The use of hyperbolic method to assess DoC is attractive due to its simplicity without the need to consider Δt. The ultimate settlements predicted by hyperbolic method are usually slightly larger than those from Asaoka's method. This is because the hyperbolic method is based on actual data, which intrinsically includes creep settlement, whereas Asaoka's method is based on a governing partial differential equation that considers the primary consolidation only.
- The assessment of DoC should also consider the excess pore water pressure measured from the VWP. In the interpretation of VWP data, it is important to correct the measured total pore water pressure for the increase in pressure head due to the settlement of piezometer under load.
- Back analysis is usually undertaken at the end of the preloading period or when the assessed DoC values have reached 90% or greater. The main factors affecting the predicted total settlement in the back-analysis are (i) soil stratigraphy and soil depth, (ii) adopted OCR values and (iii) ground water level. These elements should be reviewed based on the nearest CPTs to the monitoring location as opposed to relying on the original design model.
- For the assessment of field DoC using Asaoka's method, the use of small time interval Δt should be avoided. Edil *et al*. (1991) proposed a parameter j_{95} and recommended that Δt to be chosen to give a j_{95} value between 10 and 30.
- SHANSEP equation with parameters m = 0.95 and S = 0.22 has been used by the Authors on numerous soft ground designs and back-analyses with success.
- The $c_{\alpha\varepsilon\,(NC)}$ is best to be correlated with the back-analysed CR value c_α/cc law of Mesri. Using the observed settlement rate at the tail end to assess the creep rate is likely to result in excessive post construction settlement prediction.
- c_v is usually used as input 1D consolidation analysis. The back-analysed c_v values should be compared with the field piezocone measurements as well as published correlation, For 2D FEA, the input permeability k is linked to the void ratio e via the permeability index c_k, which has a great influence on the post peak excess pore pressure dissipation rate.
- For design and back-analysis purposes, the smear radius ratio of 8-11 and permeability ratio of 2 based on the research works by Indraratna *et al*. (2015) may be applied.
- It is the Authors' preference to carry out simple 1D consolidation analysis for back-analysis purposes. Notwithstanding this, sophisticated soil model such as PLAXIS SSC model has gained much popularity in recent years. Simple soil model could be used more consistently with simple numerical method whereas complex soil model is best to be used in conjunction with sophisticated computational approaches (e.g. large strain analysis with updating mesh and pore water pressure). Mixing complex soil models with simplified computational approaches, or vice versa, may not give desirable outcomes.
- For the prediction of post surcharge creep settlement, the PLAXIS SSC model appears to broadly give results closer to Mesri (1994) in modelling post unloading creep than Ladd (1989) or Yuan (2015) since these methods prescribes a constant creep index for all time. The PLAXIS SSC model has the advantage over Mesri (1994) that it calculates creep settlements when the OCR falls below 1.2.

7 ACKNOWLEDGEMENTS

Authors would like to thanks Roads and Maritime Services (RMS) to allow this paper to be published. Any opinions, findings and recommendations in this paper are those of the authors and do not necessarily reflect the views of RMS.

8 REFERENCES

Asaoka, A. (1978), *Observational procedure of settlement prediction*. Journal of Soils and Foundations , **18** (4), 87–101.

Buggy, F. and Peters, M. (2007) *Site investigation and characterization of soft alluvium for Limerick Southern Ring Road – Phase II*, Ireland, Soft Ground Engineering Symposium, Ireland Geotechnical Engineering, paper 1.6.

Chan, K., Poon, B. and Darshana P. (2018), *Prediction of embankment performance using numerical analyses – Practitioner's approach*. Computers and Geotechnics, **93**, 163 – 177.

Edil, T. B., Fox, P. J. and Lan, L. T. (1991), *Observational procedure for settlement of peat*. Proc., Int. Conf. on Geotechnical Engineering for Coastal Development Theory and Practice on Soft Ground, Geo Coast '91, Yokohama, Japan, 165–170.

Indraratna, B., Perera, D., Rujikiatkamjorn, C. & Kelly, R. (2015), *Soil disturbance analysis due to vertical drain installation*. Proceedings of the Institution of Civil Engineers: Geotechnical Engineering, **168** (3): 236-246.

Ladd C. C. (2007), *Unpublished Class Notes for 1.322, Soil Behaviour*, 1989, Depart. of Civil and environmental engineering, MIT, Cambridge Massachusetts. Post preload settlement charts reproduced in: Buggy, F. & Peters, M.

Mesri, G., Lo. and Feng, T. (1994), *ASCE Specialty Conf. on Geotech. Engng*, Special Pub. 1994, No. **40**, vol. 1, pp. 8-76.

Mesri, G., and Godlewski, P.M. (1977), *Time and Stress-Compressibility Interrelationship*, Journal of the Geotechnical Engineering Division, ASCE, **103**, No. GT5, pp. 417-430.

Poon B. and Chan, K. (2015), *Assessment of the Coefficient of Consolidation for Staged Preloading Operations*, 12th Australia New Zealand Conference on Geomechanics (ANZ 2015), Wellington, New Zealand.

Tan, T. S., Inoue, T., and Lee, S. L. (1991), *Hyperbolic method for consolidation analysis*. J. Geotech. Engrg., 1991. **117** (11), 1723–1737.

Tavenas, F., Leblond, P., Jean, P. & Leroueil, S. (1983), *The permeability of natural soft clays, Part 2: Permeability characteristics*. Canadian Geotech. Journal, **20**: 645-660.

Wong, P. (2007), *Preload Design to Reduce Post-construction Creep Settlement* ANZ Geomechanics Soft Soil Workshop (Brisbane, 25 October 2007).

Yuan, Y., Whittle, A.J., & Nash, D.F.T. (2015), *Model for predicting and controlling creep settlements of embankments with surcharge loading*, Proc. 6th IS-DCG, Buenos Aires.

GROUND IMPROVEMENT OF GRANVILLE HARBOUR WIND FARM FOUNDATIONS USING CMC

Babak Hamidi
Menard Oceania, Snr Geotechnical Engineer, PhD, MEng, BEng

ABSTRACT

Granville Harbour Wind Farm is located on a remote site that is approximately 35 km northwest of Zeehan on Tasmania's west coast. The project includes 31 wind turbines with the capacity to generate 112 MW of power when it is complete. Each giant turbine is 137 m from ground level to rotor hub and 200 m from ground level to blade tip. The site's ground profile consists of extremely weathered to highly weathered volcaniclastic breccia overlain with stiff clays, silts and embedded basalt cobbles. At 27 turbine locations, the ground did not meet the project's requirements and specific measures were required to improve the foundations' behaviour. Whilst piling is commonly used for improving bearing and reducing ground settlements of foundations of highly sensitive structures, in an innovative first-time approach in Australia, an alternative foundation solution using Controlled Modulus Column (CMC) rigid inclusions was considered and developed to allow the safe operation of the turbines more affordably. During this process, foundation systems were designed for eight ground models. Approximately 44,000 m of CMC were installed to support the wind turbines. The longest and shortest columns were respectively 4.5 m and 22.8 m. Quality control and assurance included the installation of trial columns, concrete testing, integrity testing and static load testing of the columns.

1. INTRODUCTION

Wind power is currently the cheapest source of large-scale renewable energy (Clean Energy Council).

Australia has some of the world's best wind resources in its south-western, southern and south-eastern regions. There is also good access to available onshore wind resources. At the same time, wind energy is the fastest growing renewable energy source for electricity generation in Australia (Australian Renewable Energy Agency) and Clean Energy Council (2019) reports that in 2018, the country's wind farms produced 33.5% of its clean energy and supplied 7.1% of the overall electricity.

Wind power is generated into useable electricity by converting the kinetic energy of the atmosphere with wind turbines. In this process the force of the wind is converted into a torque that is then used to propel an electric generator to create electricity. Wind energy power stations that are more commonly known as wind farms commonly draw on the output of multiple wind turbines through a central connection point to the electricity grid (Australian Renewable Energy Agency).

The most common type of wind turbine is the horizontal axis wind turbine (HAWT), which has an axis of rotation that is parallel to the ground. Figure 1(a) shows two wind turbines with upwind and downwind rotor configurations.

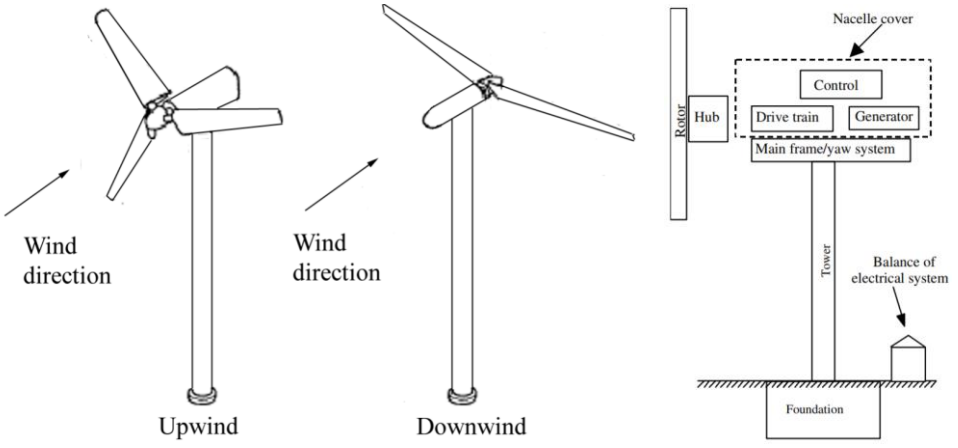

Figure 1: HAWT (a) with upwind and downwind rotor orientations, (b) major components (Manwell et al, 2002)

As shown in Figure 1(b), the main components of a typical HAWT are (Manwell et al, 2002):

- Rotor: blades and the supporting hub
- Drive train: exclusive of the rotor, the rotating parts of the wind turbine, which usually consists of shafts, gearbox, coupling, mechanical brake, and generator
- Nacelle and main frame: wind turbine housing, bedplate and yaw system
- Tower and the foundation
- Machine controls
- Balance of the electrical system: cables, switchgear, transformers and electronic power converters

Wind turbine design loads are described by the IEC (International Electrotechnical Commission, 2019) and include:

- Gravitational and inertial loads: static and dynamic loads that result from gravity, vibration, rotation and seismic activity.
- Aerodynamic loads: static and dynamic loads that are caused by the airflow and its interaction with the stationary and moving parts of wind turbines.
- Actuation loads: loads resulting from the operation and control of wind turbines, which include torque control from a generator or inverter or both, yaw and pitch actuator loads and mechanical braking loads.
- Other loads: These loads include wake loads, impact loads, ice loads and tower loads, resulting for example from vortex-induced vibrations.

International Electrotechnical Commission (IEC, 2019) specifies that load cases will be determined from the combination of operational modes or other design situations, and that all relevant load cases with a reasonable probability of occurrence will be considered, together with the behaviour of the control system. The design load cases used to verify the structural integrity of a wind turbine will be calculated by combining:

- Normal design situations and appropriate normal or extreme external conditions
- Fault design situations and appropriate external conditions
- Transportation, installation and maintenance design situations and appropriate external conditions.

There are not many publications about onshore wind turbine foundations. Manwell et al. (2002) have noted the obvious that the foundation must be enough to keep the turbine upright and stable under the most extreme design conditions. They further add that at most sites, the foundation is constructed as a reinforced concrete pad with its size chosen in such a manner to allow concrete weight to provide resistance to overturning under all conditions. Sometimes turbines are installed on rock in which case the foundation may consist of tensile elements for resisting the overturning loads.

Manwell et al. (2002) have presented a cost study analysis by Johnson (1985) for horizontal axis wind turbines constructed within the period of the 1950s to 1980s, which shows that the cost of foundations was 16.1 to 31.4% of the total cost. No information has been provided about the foundations, but with consideration of the construction period, it can be assumed that the foundations were straight-forward without application of advanced foundation construction systems.

Det Norske Veritas (DNV) and Riso National Laboratory (DNV and Riso, 2002) are more informative about the possibility of encountering unformidable ground conditions and note that depending on the ground conditions, onshore wind turbines are usually supported by either pads or by piles. However, there is no reference to the option of ground improvement. DNV and Riso further add that once a foundation concept has been selected and a foundation design is to be carried out, the geotechnical issues that need to be addressed are:

- Bearing capacity and geotechnical stability, e.g. against sliding and overturning
- Degradation of soil strength in cyclic loading
- Consolidation settlements
- Differential settlements
- Scour and erosion

As shown in Figure 2, for gravity-based pads, all forces acting on the foundation, including forces transferred from the wind turbine, are transferred to the foundation base and combined into resultant forces H and V respectively in the horizontal and vertical direction at the pad-soil interface. These forces act at load centre LC with an eccentricity e from the pad centre (DNV and Riso, 2002).

Even in its simplest form, bearing capacity analysis for wind turbine foundations is more complex than most foundations. DNV and Riso (2002) define an effective foundation area whose geometrical centre coincides with the load centre and follows as closely as possible the nearest contour of the true area of the foundation base. For a circular foundation with radius R, an elliptical effective foundation area A_{eff} can be defined as:

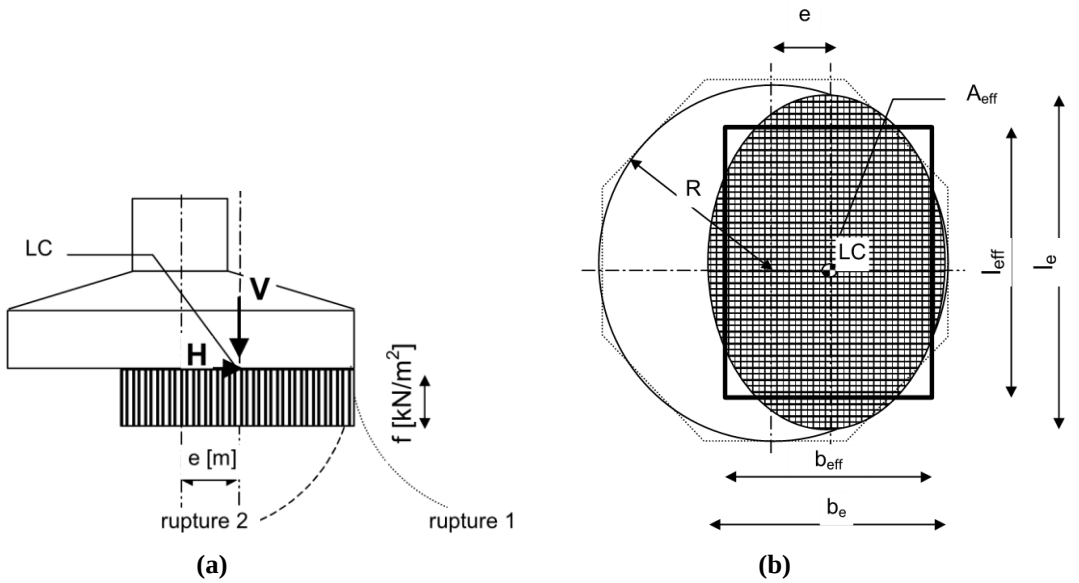

Figure 2: (a) Gravity-based pad foundations under idealised conditions (b) circular and octangular footings with effective foundation area marked out (DNV and Riso, 2002)

$$A_{eff} = 2\left[R^2 \arccos\left(\frac{e}{R}\right) - e\sqrt{R^2 - e^2}\right] \tag{1}$$

$$b_e = 2(R - e) \tag{2}$$

$$l_e = 2R\sqrt{1 - \left(1 - \frac{b}{2R}\right)^2} \tag{3}$$

A_{eff} can be represented by a rectangle with the following dimensions:

$$l_{eff} = \sqrt{A_{eff}\frac{l_e}{b_e}} \tag{4}$$

$$b_{eff} = \frac{l_{eff}}{l_e} b_e \tag{5}$$

The above formulas for the circular foundation area can be used for double symmetrical polygons (octagonal or more) if a radius equal to the radius of the inscribed circle of the polygon is used for the calculations.

2. HISTORY OF SPECIAL FOUNDATIONS AT AUSTRALIAN WIND FARMS

According to Wikipedia, there are 94 wind farms in Australia. The author is not aware of any publications regarding the foundation systems of these wind farms; however, due to his work association, is informed that ground improvement has been utilised for the wind turbine foundations of two projects.

2.1. PORTLAND II WIND FARM AT CAPE BRIDGEWATER

Cape Bridgewater Wind Farm is the second stage of Pacific Hydro's four-stage Portland Wind Energy Project in southwest Victoria. Completed in 2008, the 58 MW wind farm comprises of 29 Senvion MM82 wind turbines that are rated at 2.05 MW, have a maximum hub height of 69 m and a maximum blade tip height of 110 m (Pacific Hydro).

The geology at the site comprised dune sands derived from limestone deposits. During the geotechnical investigation works for the development, 10 of the 29 wind turbine locations were identified as having ground conditions that did not

satisfy design requirements. Dynamic compaction (Hamidi et al, 2009) was identified as the most practical solution for treating 3 to 10 m of sand to allow the use of shallow pad footings with diameters of 14 m.

2.2. WOOLNORTH III WIND FARM AT STUDLAND BAY

Studland Bay is situated on Woolnorth grazing property on the North West tip of Tasmania. The wind farm was constructed and commissioned in 2007. There are 25 Vestas V90 wind turbine generators at the site, giving a total installed capacity of 75 MW. The turbines are mounted on top of towers that are 80 m high with blades that are 44 m long. Studland Bay produces approximately 2 percent of Tasmania's electrical energy needs (Woolnorth Wind Farms).

Five of the wind turbine locations showed very poor ground conditions with SPT blow counts in the upper 10 m of silty sand frequently in the range of 0 to 7. Compaction Grouting (Chu et al, 2009) was adopted and carried out to treat these wind turbine foundations.

3. GRANVILLE HARBOUR WIND FARM

3.1. PROJECT DESCRIPTION

Granville Harbour Wind Farm (GHWF) covers an area of approximately 800 hectares and is currently under construction near Zeehan, on the west coast of Tasmania. When complete, the wind farm will host 31 Vestas V116 wind turbine generators, each rated at 3.6 MW with a maximum rated capacity of 111.6 MW, which will be enough to power approximately 46,000 homes.

The turbine foundations were designed for the heavier loads of the Vestas V126 wind turbines as shown in Table 1.

Table 1: Wind turbine foundation loads

Load type SLS/ULS*	N= Vertical (kN)	H= Horizontal (kN)	M= Moment (kNm)
ULS Fundamental	5,600	900	121,200
ULS Accidental	5,600	1,000	128,200
SLS Rare	5,600	900	121,200
SLS quasi-permanent	5,700	600	73,300

*SLS: service limit state; ULS: ultimate limit state

3.2. GROUND CONDITIONS

The geology of the site predominately consisted of outcropping Paleogene-Neogene (Tertiary) age basalts. Neoproterozic age siltstone and shales of the Oonah formation were exposed in small areas of the site due to the erosional downcutting of creeks. The geological map indicated the presence of non-marine deposits of gravel, sand, silt and clay between the Tertiary volcanic material and the Neoproterozic rock.

The geotechnical investigation of the site indicated a more complex geology with intersection of volcaniclastic sediments. The boreholes generally indicated a similar pattern of deposition to those Tertiary volcanics with tuff and breccia being deposited possibly in a submarine environment being capped with more effusive eruption products such as basalt. The erosion of previous Tertiary volcanics added complexity to the geology, which was noted to have resulted from sea level changes that left valleys within the palaeotopography. These were subsequently infilled with additional volcanic materials of potentially different composition. The topography was further modified by groundwater level changes and retrogressive spring induced creek incision during the Quaternary with further modifications that were possibly due to landslide activity.

The investigation included soil electrical resistivity testing and soil thermal resistivity testing at 33 locations, 5 test pits across the site, geophysical surveys using seismic surveys at 36 locations, 37 boreholes with at least one borehole at each proposed wind turbine generator location, Standard Penetration Tests (SPT), pocket penetrometer (PP), shear vane tests and collection of soil, rock and groundwater samples for laboratory testing. Additionally, 127 Cone Penetration Tests (CPT) were carried out with a minimum of two tests per wind turbine location. Of these, 51 tests encountered shallow refusal within cobble zones around 2m or 8m depths without reaching the full depth to rock.

It was observed that the ground profile encountered was:

- Topsoil: a thin layer of up to 0.5 m thick, which was typically sandy or gravelly silt, containing organic material

- Alluvium: generally consisting of loose to dense sands and gravels with variable silt content, fine to coarse and typically sub rounded to rounded, mostly quartz.
- Residual Soil to extremely weathered material: derived from weathering of the volcanic ash/tuff, volcaniclastic breccia and basalt, generally comprising of soft to very stiff silts with variable sand content.
- Tertiary Basalt: variable weathering from highly weathered to fresh, low to very high strength, typically highly fractured with very close to close defects. Typically considered as 'floaters' or discontinuous layers up to 5 m thick in the boreholes.
- Tertiary aged Volcaniclastic Breccia/Agglomerate: variable weathering from highly weathered to fresh, low to very high strength minerals, typically highly fractured with very close to close defects.
- Extremely weathered Metasediments: weathered to hard gravelly clay/silt, encountered in only two boreholes. Zones of highly weathered, very low strength rock within the extremely weathered matrix.
- Metasediments/Phyllite: variable weathering from highly weathered to slightly weathered, very low to very high strength typically highly fractured with very close to close defects.

Whilst the geotechnical investigation suggested highly variable ground profiles with various strength, SPT blow counts in the range of 0 to 8 were recorded at depths of 1 to 20 m in approximately two thirds of the boreholes indicated that some wind turbine foundations would not be able to safely transfer the superstructure loads to the ground.

Groundwater levels were measured to be 1.8 to 17.5 m with an average in the order of 10 m depth below natural ground level.

The geotechnical assessment of the ground conditions indicated that the location of 27 wind turbines would not be able to satisfy design requirements for construction of gravity-based footings, and specific geotechnical methods had to be employed.

3.3. FOUNDATION SOLUTION: CONTROLLED MODULUS COLUMNS

Several options including piling to competent rock and various forms of ground improvement were considered for improving foundations behaviour. The solution that was ultimately chosen was the application of Controlled Modulus Columns (CMC) with the intent to reinforce the ground in such a way to provide the required mechanical characteristics that would allow the implementation of gravity-based footings and with the foundation behaving as if it were resting on a homogenous ground.

Based on the wind turbine manufacturer's specifications, the foundation solution required a rotational stiffness in dynamic conditions, $K_{\phi\text{-}dyn}$, of not less than 54 GNm/rad to avoid the coupling phenomena with the machine's mechanical components.

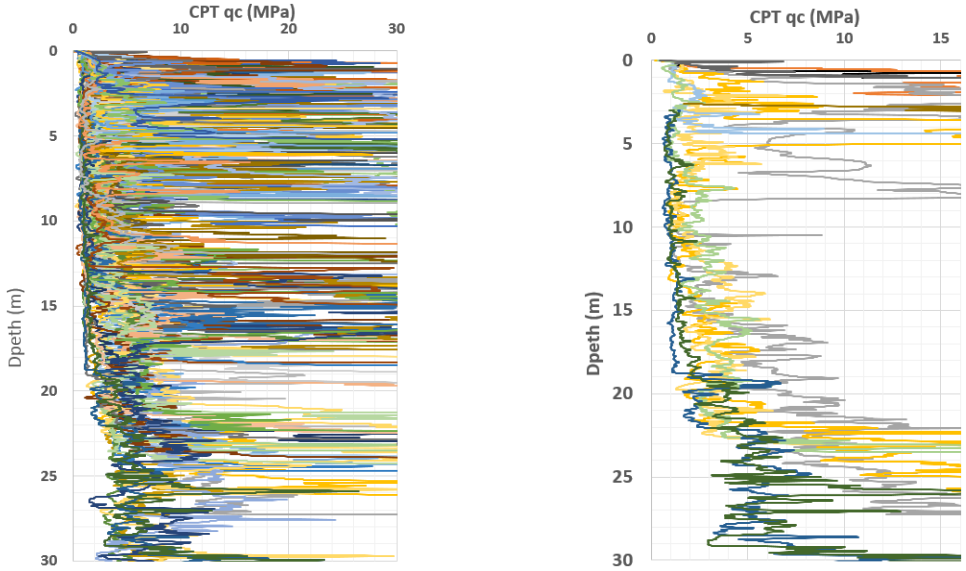

(a) **(b)**

Figure 3: (a) CPT profile throughout the site, (b) CPT profile in one of the zones

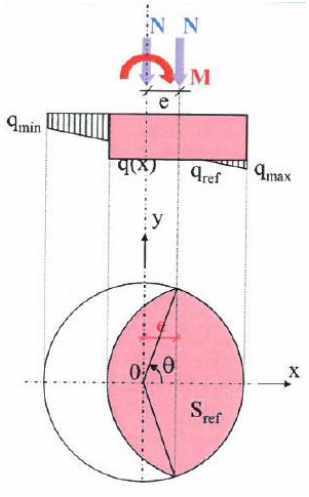

Figure 4: Reference load applied uniformly on reference area, CFMS (2002) with modifications

3.3.1. Foundation Design

As can be observed in Figure 3(a) the ground strength was highly variable throughout the site; hence, the site was divided into 8 zones with similar ground profiles and detailed design was carried out for each profile. This paper will consider only one of the profiles, for which the CPT profiles are shown in Figure 3(b), but the same procedure was used on all other profiles.

For design purpose the groundwater levels were assumed to be at the foundation base as the footing design did not consider the footings to be submerged.

For calculation purposes, in accordance with the recommendations of the French Committee of Soil Mechanics and Geotechnical Engineering (CFMS, 2011), whilst the footings were octagonal shaped, they were considered to be circular with surface areas equivalent to that of the octagons.

Similar to DNV and Riso (2002), CFMS (2011) recommendations for calculation of wind farm foundations with CMC are also based on the concept of an equivalent compression area that has been uniformly loaded. This concept is shown in Figure 4 and formulated in Equation 6 and Equation 7.

$$S_{ref} = R^2(2\theta - \sin 2\theta) \tag{6}$$

$$\theta = \cos^{-1}\left(\frac{e}{R}\right) \tag{7}$$

Where S_{ref}= reference area with equivalent uniform load q_{ref}.

Various load cases that are shown in Table 1 were considered in the design of the foundation system.

An axi-symmetrical calculation of a CMC unit cell was carried out to determine the equivalent Young's modulus of the improved ground using the quasi-permanent load case, which was the dominant load case throughout the service life of the wind turbines. Other parameters that were determined and utilised in the design included:

- Equivalent modulus of reinforced ground: 79.8 MPa
- Equivalent dynamic modulus of reinforced ground: 239.4 MPa
- Long-term rotational stiffnesses in large-strain domain: 106.8 GNm/rad
- Long-term vertical stiffness: 5 MPa/m
- Dynamic horizontal stiffness in small-strain domain: 338 MN/m
- Dynamic rotational stiffnesses in small-strain domain: 320.2 GNm/rad > 54 GNm/rad

Global bearing capacity of the foundation system was assessed for each load case. Similarly, local bearing capacity was checked for the most heavily loaded CMC cell. The results of this calculation indicated that the global bearing capacity in SLS and ULS were respectively 264 kPa and 385 kPa.

Settlement and rotation of the foundation system were calculated using the rigidities of the improved ground for SLS quasi-permanent loadings. Minimal, average and maximum settlement of the foundation were calculated to be

respectively 19 mm, 26 mm and 33 mm. Calculations showed that differential settlement would be less than the targeted value of 3 mm/m at quasi-permanent loading.

The foundation system for the wind turbines of the described ground profile consisted of octagonal shaped gravity-based footings with 20.2 m lengths and 3.7 m depths of embedment. The footings were underlain by load transfer platforms that were 0.8 m thick and resting on 133 CMCs, which were arranged in 6 concentric rings. The columns had diameters of 0.45 m and were 22.8 m long. The required compressive strength of the columns was 20 MPa.

3.3.2. Construction and Quality Control of CMCs

In all 3,333 CMCs measuring a total length of more than 41,630 m were installed at the location of 27 wind turbines. 10 of these columns, measuring a total length of 117 m, were for calibration of CMC installation rigs and lengths against the ground conditions. Depending on the ground conditions, the number of columns per wind turbine foundation varied from 107 to 133. The shortest and longest columns were respectively 4.5 m and 24.2 m long.

It was expected from the early stages of project study that the site would face construction challenges. The location of the site was relatively isolated and required pre-planning and organisation to ensure the proper and continuous supply of material, namely concrete, to the site. The wind turbines were spread throughout the site and inter-site access routes and associated travel times had to be envisaged and implemented in advance.

Furthermore, to the knowledge of the author, the world's longest CMCs in a wind farm project have been installed in up to 27 m of loess deposits at Cogealac Wind Farm in Romania (Plomteaux and Ciortan, 2010, Coghlan et al, 2016) and no other wind farm project has utilised CMCs within the range of the deepest CMCs that were designed for Granville Harbour Wind Farm. Whilst almost all CMC rigs could have reached the project's shallow and mid-range depths of installation, the deepest CMCs that had to be installed were beyond the typical range of CMC rigs. Hence, as part of the advanced planning stage, two rigs with the ability to reach the deepest required installation depths were resourced and allocated to the project. Even though the site was massive in size, due to the constrained footing sizes, scatter of wind turbine locations and distances between them, it was possible for only one rig to operate at each wind turbine location and consequently, as shown in Figure 5, it became necessary to support each CMC rig with its own ancillary equipment, namely concrete pump and excavator.

To the knowledge of the author, the 24.2 m long CMC that was installed in this project is the world's second deepest CMCs in a wind farm project.

At the beginning of the project a number of calibration CMCs were installed nearby existing geotechnical exploration holes at the various ground profiles that had been used as the basis of design. The objective of these columns was to calibrate the geotechnical data against the rig's driving forces. This information would then be used to determine the fine-tuned actually required depths of the columns.

Figure 5: Installation of CMC at Granville Harbour Wind Farm

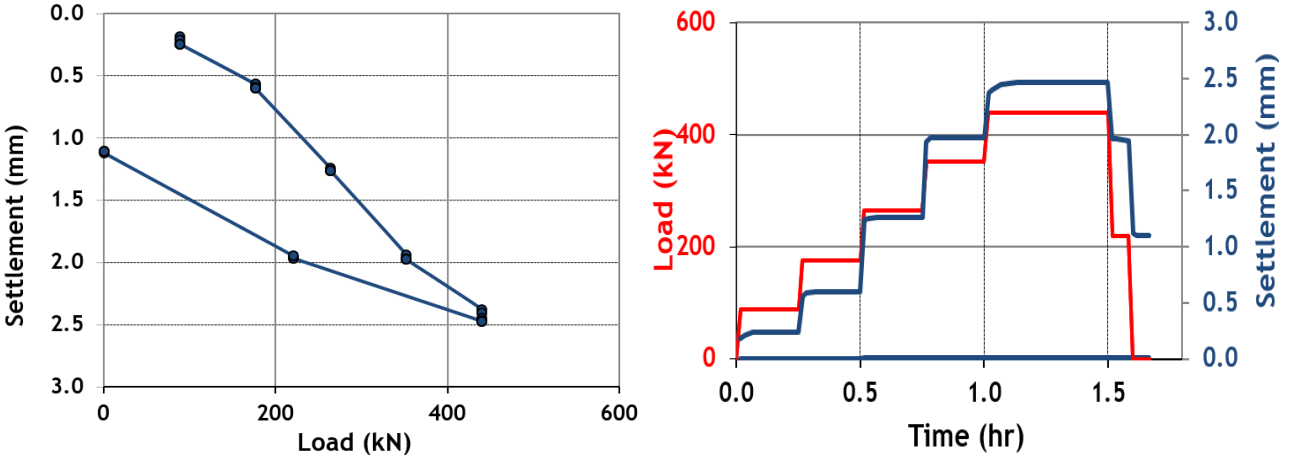

Figure 6: Static load test of an 18.9 m long CMC

As part of the quality control programme, installation records were automatically generated using special software. This information included CMC number, date and time of construction, penetration rate during drilling, rotation speed, drilling torque, column depth, uplift speed, concrete volume injected and concrete pressure.

Quality control tests included daily concrete slump tests, daily concrete unconfined compressive strength, and 15 pile impedance test (PIT) per wind turbine. It was envisaged that 2 static load tests would be carried out per wind turbine, subject to be relaxed at a later stage depending on performance of tested columns. Figure 6 shows the results of a static load test for an 18.9 m long CMC that was subjected to a loading of up to 440 kN. As the displacement per loading stage remained less than 0.02 mm/min on at least two consecutive measurements, in accordance with ASIRI (IREX, 2012) recommendation loading period in each stage was contained to 15 minutes.

.

4. CONCLUSIONS

Whilst wind energy is the fastest growing renewable energy source for electricity generation in Australia, there are no local publications on the use of special foundation measures for strengthening the ground for wind turbine structures. To the knowledge of the author prior to Granville Harbour Wind Farm only two Australian wind farm projects had utilised ground improvement, namely dynamic compaction and compaction grouting.

For the first time in Australia, CMC ground improvement technique has been used for 27 wind turbine foundations at Granville Harbour Wind Farm. Whilst specific site constraints required advanced planning of resources and material, the project was successfully completed within the intended period. This project has also set a world record by incorporating the world's second deepest CMC in a wind farm project.

5. ACKNOWLEDGEMNT

The author wishes to express his gratitude to Menard Oceania for providing the project information and Granville Harbour Wind Farm Pty Ltd for permission to publish.

6. REFERENCES

Australian Renewable Energy Agency, Wind Energy. Viewed 12 June 2019, https://arena.gov.au/about/what-is-renewable-energy/wind-energy/.

Chu, J., Varaksin, S., Klotz, U. & Mengé, P. (2009) State of the Art Report: Construction Processes. *17th International Conference on Soil Mechanics & Geotechnical Engineering: TC17 meeting ground improvement*, Alexandria, Egypt, 7 October 2009, 130.

Coghlan, K., Plomteux, C. & Racinais, J. (2016) Execution & Engineering Principles of Control Modulus Column (CMC). *First Southern African Geotechnical Conference*, Sun City, South Africa, 5-6 May, 19-24.

Comité Français de la Mécanique des Sols et De Géotechnique (2011) Recommendations for the Design, Calculation, Installation and Inspection of Wind-Turbine Foundations, Revision 1.1. 109.

Clean Energy Council (2019) Clean Energy Australia Report 2019. Clean Energy Council, 82.

Det Norske Veritas & Riso National Laboratory (2002) *Guidelines for Design of Wind Turbines, 2nd Edition*, Copenhagen, Jydsk Centraltrykkeri, 294.

Hamidi, B., Nikraz, H. & Varaksin, S. (2009) A Review on Impact Oriented Ground Improvement Techniques. *Australian Geomechanics Journal*, 44, 2, 17-24.

International Electrotechnical Commission (2019) IEC 61400-1 Wind Energy Generation Systems - Part 1: Design Requirements. Geneva, Switzerland, 173.

IREX (2012) ASIRI National Project: Recommendations for the Design, Construction and Control of Rigid Inclusion Ground Improvements, Presses des Ponts, 316.

Johnson, G. L. (1985) Wind Energy Systems, Prentice-Hall, Englewood Cliffs, N.J.

Manwell, J. F., McGowan, J. G. & Rogers, A. L. (2002) *Wind Energy Explained – Theory, Design and Application*, electronic version, John Wiley & Sons

Pacific Hydro, Cape Bridgewater Wind Farm. Viewed 23 June 2019, http://www.pacifichydro.com.au/english/projects/operations/pwep/cape-bridgewater/.

Wikipedia, Wind Power in Australia, Viewed 21 June 2019, https://en.wikipedia.org/wiki/Wind_power_in_Australia.

Woolnorth Wind Farms, Studland Bay. Viewed 23 June 2019, https://www.woolnorthwind.com.au/wind-farms/studland-bay.

Plomteux, C. & Ciortan, R. (2010) Integrated Ground Improvement Solution for the Largest Wind Farm Project in Europe. *From Research to Design in European Practice*, Bratislava, Slovak Republic, 2-4 June.

DESIGN AND CONSTRUCTION OF PLASTIC GEOCELLULAR RAIN WATER HARVESTING/STORMWATER DETENTION TANKS

Patrick Wong
Senior Principal, PKW Geosolutions Pty Ltd, NSW, Australia, pwong@pkwgeosolutions.com.au and
Senior Consultant, Coffey Services Australia Pty Ltd, NSW, Australia, patrick.wong@coffey.com

ABSTRACT

Plastic voided modular structures (known as geocellular units) were first used in the mid-1980s in Europe below pavements to store stormwater. Its use has since spread to rainwater harvesting and on-site stormwater detention for residential, commercial and industrial developments. It is an environmentally friendly and sustainable solution. However, there are engineering pitfalls associated with the design and construction of plastic geocellular structures. The main pitfalls are associated with creep rupture of plastic structures, potential construction damage and the lack of care in wrapping the cells with filter fabric and backfilling procedure. As the scale and complexity of geocellular structures have significantly increased in recent years, guidance on appropriate design and construction methods has become more essential for these structures to be adopted as safe, yet economic and sustainable solutions.

In this paper, the author will describe his design and construction experience based on research associated with a court case on the damages associated with a major geocellular on-site stormwater detention project (approx. 8.5 Mega litres), and recent conversion of his backyard swimming pool to a 40,000 litre rainwater harvesting tank. References on design and construction guidance will be described together with the author's personal opinion on the use of partial factors in the economic design of geocellular structures.

1. INTRODUCTION

The use of geocellular units for on-site stormwater detention and rainwater harvesting has gained popularity and momentum in the last decade or so. They are more economical than conventional precast concrete structures, and considered to be environmentally friendly and sustainable solutions because of their lower embedded carbon footprint. The energy required to produce plastic is only a fraction of that for precast concrete, and the installation effort is also less due to the significantly lighter weight of plastic geocellular units. The use of recycled plastic, with adequate quality control, provides further environmental and sustainability benefits.

For the above reasons, the scale of geocellular structures are getting larger. However, their design is not trivial, and involves understanding of material type and behaviour, structural and geotechnical engineering design principles, and good construction practice. The lack of good practice in any of the above can potentially lead to disastrous consequences. The following paragraph is a quote in the Summary of CIRA C737 (2016):

> *"Because of their size and below ground location many geocellular unit installations are now significant geotechnical and structural engineering designs with potentially severe consequences if failure occurs."*

In keeping with the current drive for more sustainable solutions, recycled plastic has been introduced in the production of geocellular units. This gives rise to greater variability in the properties of the plastic product to the point that they may have similar variability as geotechnical materials compared to other man-made building materials such as steel and concrete. Quality control in manufacturing including appropriate forms of testing and incorporation of material variability in the selection of design parameters is essential. Furthermore, although these units are light and easy to install manually, they are can be damaged if there is a lack of care during handling, installation and inappropriate post-installation construction activities.

Due to the lack of published data, the creep rupture properties of plastic often plays one of the most influential factor in the design of geocellular structures.

2. DESIGN AND CONSTRUCTION GUIDELINES

Schematics for stormwater geocellular structures in infiltration (Figure 1), storage and attenuation (Figure 2) modes are illustrated by Woods-Ballard et al (2007) as reproduced below.

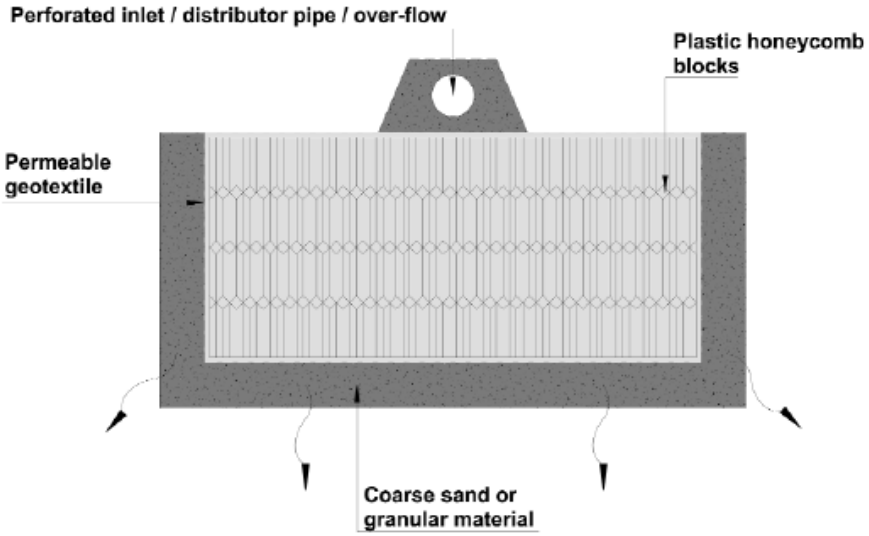

Figure 1: Infiltration system (Woods-Ballard et al, 2007)

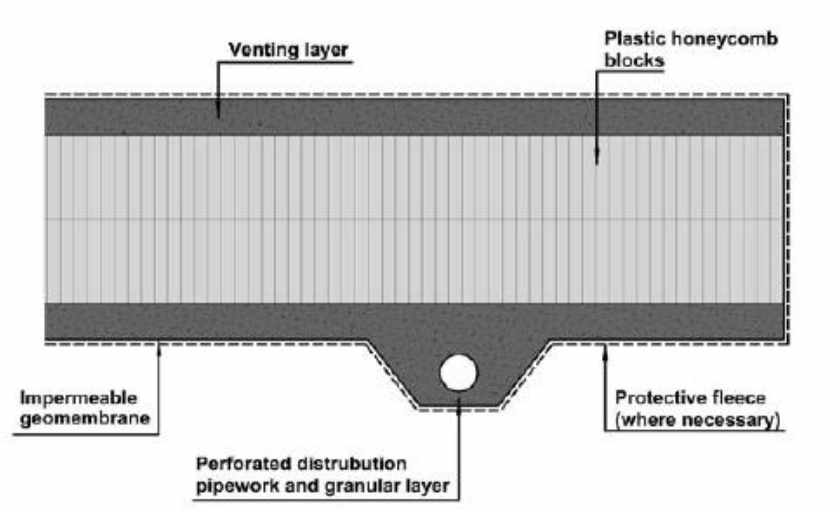

Figure 2: Attenuation or storage system (Woods-Ballard et al, 2007)

Infiltration, attenuation or storage structures are similar in that the geocellular units form a voided structure to hold the stormwater, and differ only in whether an impermeable geomembrane is used, and pipe work details.

Depending on the amount of soil cover and surface loading requirements, the geocellular units come in different construction types, geometry and strength grades. The most common types are those assembled from rectangular flat plates with increasing numbers of internal plates to provide higher load capacity as shown in Figures 3a and 3b. The plates are moulded with lugs that push together similar to Lego blocks. The assembled units are then clipped together to form a structure to the desirable size. The units are manufactured to different dimensions and can be stacked together without intermediate bottom plates to form double or triple units up to about 1.35 m to 1.5 m or more in height.

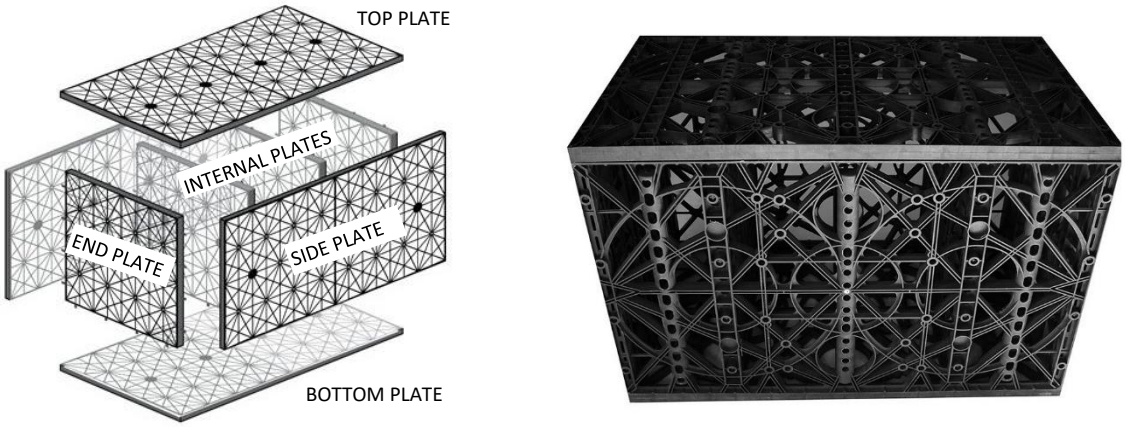

Figure 3: Geocellular unit, (left) exploded view of geocellular unit, and (right) assembled unit[1] (see Note 1 in Figure 4)

Where the application requires high load bearing, units with injection moulded internal columns are generally used as shown in Figure 4.

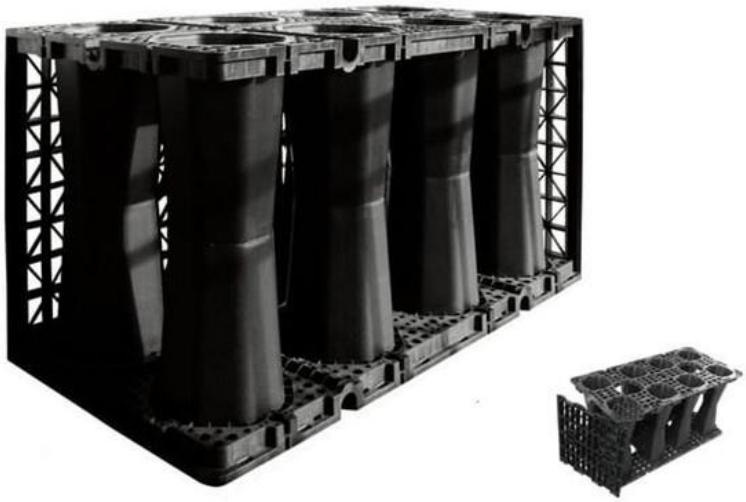

Figure 4: High load bearing geocellular unit[1]

[1]NOTE: Class B geofabric has grab strength approximately 30% less than Class C (see Table RM63A5.2 for full details of geotextile filter fabric strength classes)

The design process for geocellular structures should include the following considerations:

- Type of application (i.e. soakage, infiltration, attenuation, harvesting, storage etc).
- Geometric requirements.
- Ground conditions including groundwater and chemical environment.
- Loading requirements, including design life and creep rupture strength, construction loads.
- Selection of raw material (e.g. polypropylene, polyvinyl chloride, low density and high density polyethylene).
- Selection of impermeable membrane (if required) and filtration geotextile.

Testing of product strength is essential and allowance must be made for statistical variability of plastic products. If it is contemplated to use recycled plastic in the production of the geocellular units, greater attention should be paid to quality control and testing of different batches during the production process.

The geotechnical and structural design of geocellular structures requires knowledge of soil structure interaction, and in particular the distribution of vertical pressure from surface loading which may include soil

cover, pavement (if any) and type of building, vehicle or rail loads, and lateral earth pressure loading from backfill and adjacent surcharge. Construction loads must also be considered. Of particular importance is the careful manual placement of sufficient thickness of sand or fine gravel cover over the units prior to allowing construction vehicle loading over the units. Backfilling uniformly on all sides of the units is also critically important to avoid excessive lateral deformation and/or damage to the units.

Guidelines for the design and construction of geocellular structures are well established and include Wilson et al (2004), Woods-Ballard et al (2007), Wilson (2008) and O'Brien et al (2016). The readers are urged to consult these references before embarking on such projects.

3. CREEP RUPTURE AND LIMIT STATE DESIGN

Creep rupture in geosynthetic products (e.g. geogrids and high-tensile strength geotextile soil reinforcement fabrics), and fiberglass bolts is a well-established phenomenon, but there is very limited published data on this topic for geocellular units. This section presents some information on creep rupture testing data on units that have been exhumed from a site where a large geocellular structure (approx. 8.5 Mega litres stormwater detention project) was installed.

Creep rupture is a time dependent behaviour of a material under sustained loading, with increasing strain over time (creep) eventually leading to failure (rupture) as illustrated in Figure 5 below.

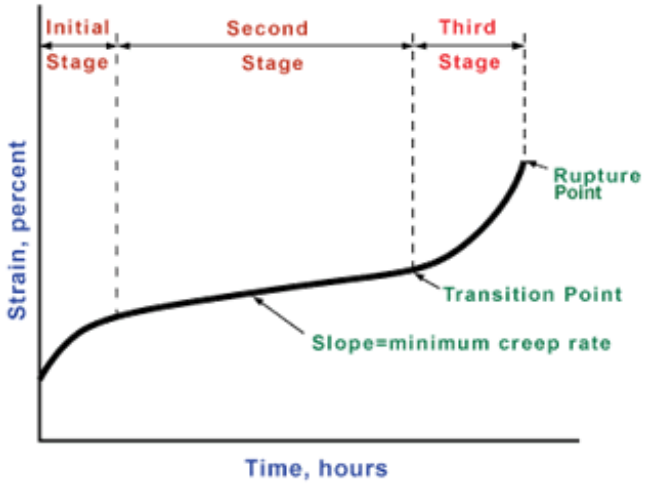

Figure 5: Typical creep rupture behaviour
(courtesy of https://www.nde-ed.org/EducationResources/CommunityCollege/Materials/Mechanical/Creep.htm)

For polymer materials under sustained tension, creep rupture may be incorrectly considered as a cross sectional area reduction (or "necking") problem due to Poisson's Ratio effect. The mechanism of creep rupture is in fact far more complex. Under a sufficiently high constant stress (but well below the short-term yield stress), the polymer chains are in fact uncoiling and begin to slip past each other. This effect is more pronounce at higher temperature. Therefore, compression members also undergo creep rupture. The author's opinion is that the creep rupture mechanism in geocellular structures can be even more complicated than a member in pure tension. This is because both the horizontal and vertical plates are under bending stresses, and the vertical plates can also undergo buckling failure. The complex loading of the plates can also lead to delayed internal fracturing of the plastic.

When combined with the greater potential for the damage of plastic materials during construction, creep rupture often becomes the governing factor in design. The Australian Standard, HB154-2002 discusses the difference between the "Available" and "Required" strength properties to allow for sufficient safety factor for the application of geosynthetics which also includes "geocontainers". Figure 1 of HB154-2002 is reproduced as Figure 6 below, which clearly shows the reduction of safety margin with time.

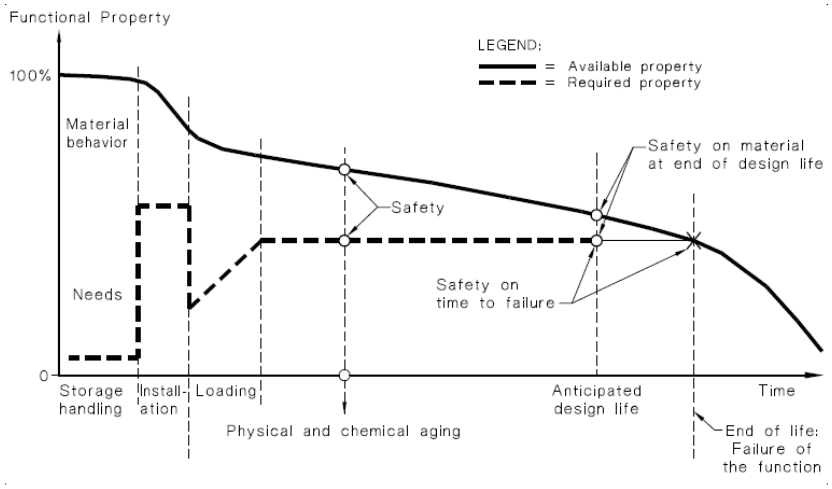

Figure 6: Available and required values as a function of time (AS BH154 – 2002)

The Limit State Design approach for geosynthetic materials such as those described in BS8006-1:1995 and AS4678 – 2002 requires the following inequality to be met:

$$\Psi_1 G + \Psi_2 Q \geq (\phi_1 \times \phi_1 \times \phi_1 \times \phi_1 \ldots\ldots) \times \phi_n \times R_{st} \qquad \text{Equation [1]}$$

where:

G = Dead Load (sustained)

Q = Live Load (transient)

Ψ_1 = Load factor on dead load

Ψ_2 = Load factor on live load

ϕ_1, ϕ_2, ϕ_3 …etc. are material strength reduction factors. Using the terminology in AS4678, they are defined as follows:

ϕ_{up} = reduction factor for manufacture variability

ϕ_{ri} = reduction factor for installation damage

ϕ_{rt} = reduction factors for environmental change in thickness (e.g. corrosion)

ϕ_{rs} = factors for environmental change in strength

ϕ_{rs} = factors for environmental change due to temperature

ϕ_{ud} = reduction factors for uncertainty in environmental degradation

ϕ_{rc} = reduction factor for creep rupture

ϕ_{uc} = reduction factor to account for uncertainty in extrapolation of test data on creep rupture, and is dependent on the length of time testing data is available.

ϕ_n = structure importance reduction factor to provide additional safety margin for structures of different importance, in particular with respect to post-disaster (e.g. earthquake) recovery functions

R_{st} = Either a "guarantee minimum" or "characteristic value" as determined from testing.

Manufacturers of geosynthetic products usually publish recommended reduction factors including creep rupture reduction depending on the extent of testing available. For geocellular units, there is very little published information on these reduction factors and designers may have to resort to published design guidelines such as those summarised in Table 1.

Table 1: Guideline strength reduction factors

Reduction Factor	AS4678:2002	HB154:2002	BS8006-1995
ϕ_{up} – manufacture	0.95 if R_{st} is characteristic value 1.0 if R_{st} is a guaranteed minimum	0.95 if R_{st} is characteristic value 1.0 if R_{st} is a guaranteed minimum	0.95 if R_{st} is characteristic value 1.0 if R_{st} is a guaranteed minimum
ϕ_{ri} – installation damage	0.6 to 0.9(1)	Could be as low as 0.5	Depending on fill type and installation procedure(4)
ϕ_{rt} – environmental change thickness	0.9 to 1	Not used	Dependent on fill type and exposure condition(4)
ϕ_{rs} – environmental change strength	0.5 to 0.9	Project specific relating to UV exposure	
ϕ_{rst} – environmental change temperature	Function of temperature	Function of temperature Generally > 0.9	
ϕ_{ud} – uncertainty in environmental degradation	0.8	Not used	
ϕ_{rc} – creep rupture reduction	0.19(2)	Could be as low as 0.17	To be based on test results(4)
ϕ_{uc} – extrapolation factor for creep rupture	1.25-0.25N(3)	Could be as low as 0.5	1.5-0.5N(3)

Notes:

(1) Dependent on particle size of soil placed against geosynthetic (0.8 to 0.9 for fine sand, to 0.6 to 0.9 for coarse gravel

(2) Extrapolated for 50 year design life from values of 0.2 for 30 years to 0.17 for 100 years

(3) N is the number of log cycles of time extrapolation of creep data to the design life

(4) BS8006:1995 provides recommendations on using reduction factors given in manufacturer's datasheets based on trials

The problem with adopting combinations of the guideline strength reduction factors shown in Table 1 is that the net resultant design value could be as low as only 5% of the short-term test strength. Creep rupture contributes to the greatest reduction, particularly if there is no such testing carried out.

On the other hand, while there may be little redundancy in the application of a single layer of geosynthetic tensile fabric in a reinforced soil layer (e.g. for strengthening of working platforms), the application of geocellular structures usually give rise to significantly greater redundancy due to the multi-unit arrangement, and therefore the combined use of installation damage factor with creep rupture reduction may be unrealistic and will likely result in an overly conservative design. In the author's opinion, the geocellular units are less prone to damage than tensile fabrics provided they are handled with care during transport and installation, and a sufficient thickness of protective layer of granular material is placed manually over the installed units prior to trafficking by machinery.

In a case study which involved the installation of a large scale stormwater detention tank in NSW using geocellular units, installed cells were exhumed and both short and long-term creep testing were carried out.

The creep rupture testing was carried out by sustained load tests at different percentage of the short-term ultimate load and measuring the time to failure. The results of this testing are presented in Figure 7.

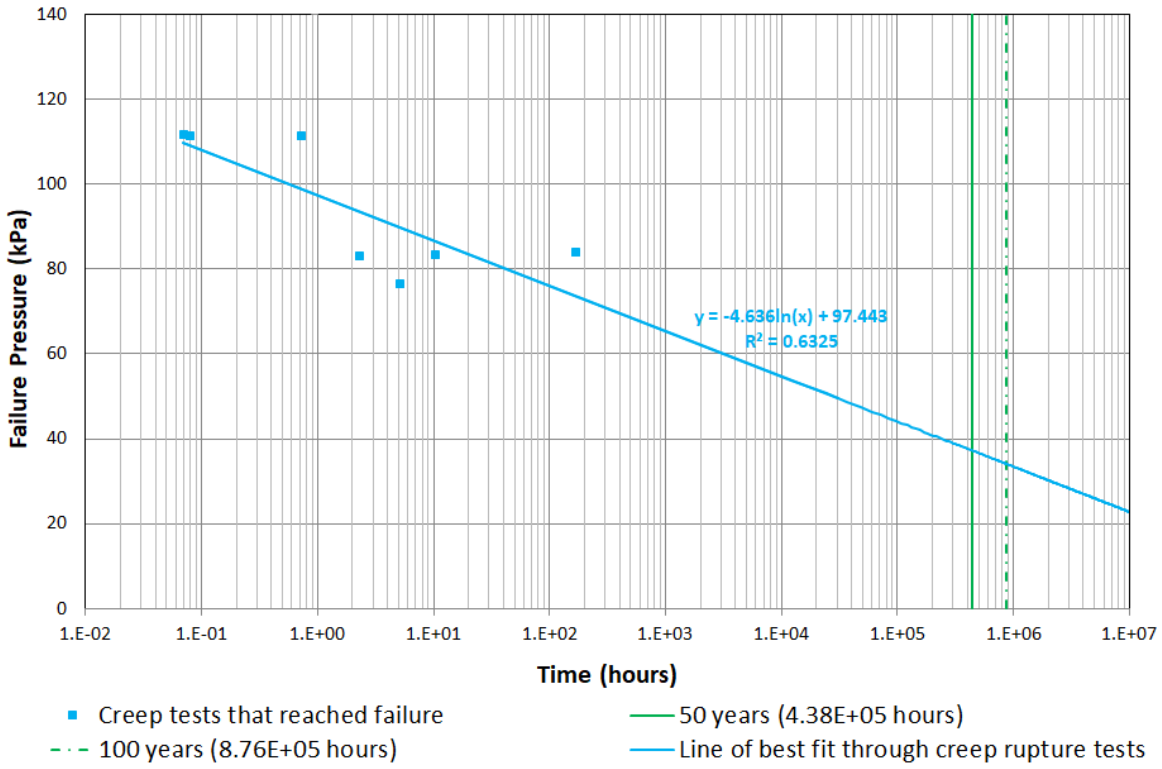

Figure 7: Creep rupture test results from a project in NSW (exhumed cells)

It can be seen from Figure 7 that the short-term compressive strength of the tested units is about 110 kPa, with an extrapolated failure strength of about 37 kPa at 50 years and 34 kPa at 100 years (i.e. about 34% and 31% of the short-term strength). There were also some test results at 50% of the short-term strength that were extended to 5,500 hours which did not reach creep rupture. For a design life say of 50 years, the creep extrapolation factor with 5,500 hours of testing based on the equation given by AS4678 would give ϕ_{uc} = 1.25-0.25N = 0.78 where N = log(4.38 × 10^5/5,500) giving a design long-term strength at 50 years of 26.5% of the short-term test strength. This is over 5 times higher than 5% of the short-term strength that would otherwise have been assessed using published guideline recommendations without testing, and clearly demonstrates the importance and benefits of having long-term test data.

It should be stressed that Figure 7 represents testing on only one particular product, with samples exhumed a few years after installation. This figure is provided as an indication only and should not be used for generic design purposes. For major projects, the author recommends long-term testing data be obtained for the specific product to be used, together with project specific testing regime including product quality control testing during construction.

4. SWIMMING POOL CONVERSION PROJECT

At the site, it was decided to convert a 60,000L swimming pool to an underground rainwater harvesting tank by installing a geocellular structure inside the existing pool. The concrete lining of the pool walls and base provided the water retention function so a geomembrane was not necessary. The design and construction comprised the following features:

Geocellular units – Polypropylene lattice plate construction with four internal vertical plates

Double units measuring 1030 mm (H) x 800 mm (L) and 490 mm (W)

Single units measuring 530 mm (H) x 800 mm (L) and 490 mm (W)

Minimum short-term compressive strength = 91 kN (or 232 kPa on top plate) and rated at 35 kPa long-term.

Geotextile filter fabric – Class C (according to RMS RM63 grading) with 300 mm overlap glued down using silicon sealant.

Backfill – Initial layer of < 1MPa LiquiFill levelling layer (refer Hanson Australia website for details https://www.hanson.com.au/products/concrete/fills/liquifill/

10 mm nominal size recycled concrete and brick aggregate around the sides and up to 360 mm above the top of the units.

Surface finishing – 40 mm thick x 10 mm nominal size river gravel confined in Copolymer Polypropylene geocells.

The individual unit (12.7 kg for each single unit and 23.5 kg for each double unit) was easy to manually assemble and the only equipment required was a rubber mallet to drive the plates (with moulded lugs) together. Prior to laying the geotextile fabric, preparation of a level surface was found to be a crucial step. Care in this step enables rapid installation of the unit together to form the final structure with no gaps between units and to minimize any stress concentrations using the backfilling operation.

The supplier of the units provided short-term load test results which are reproduced in Figure 8 below.

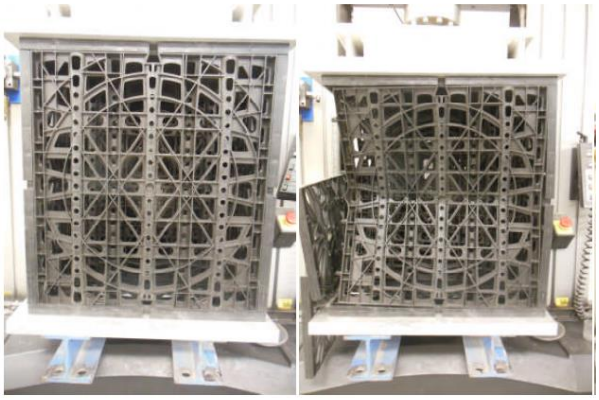

(a) Pre-test (end view)

(b) Post-test (end view)

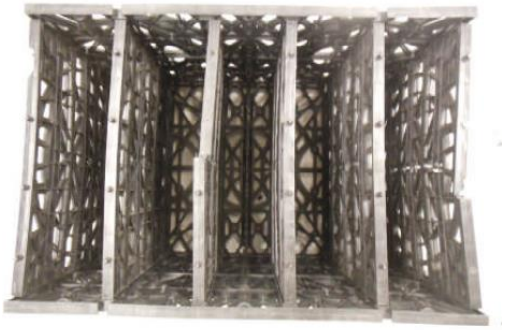

(c) Post-test (top view)

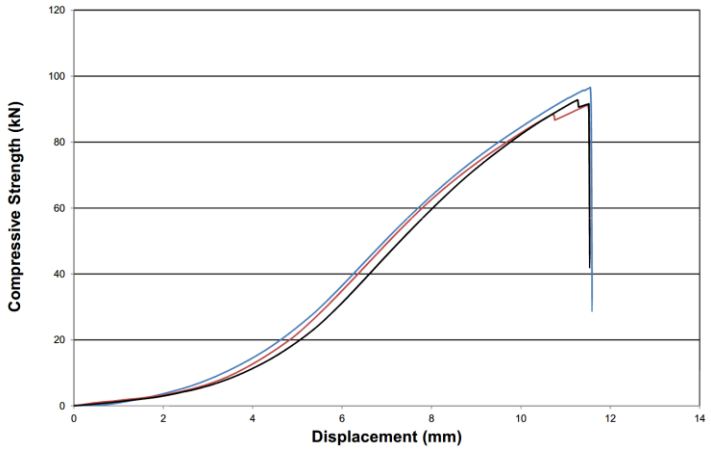

(d) Load-displacement Result

Figure 8: Test results of units provided by the supplier for the pool conversion project

According to the test report provided, the compression testing was conducted on an Instron Model 5885 Tensile/Compression Testing Machine using parallel plate loading at a rate of 2.0% of the height of the chamber per minute in accordance with ASTM F2418 (2013).

It can be seen from the load-displacement curves and post-test photographs shown in Figure 8 that the units failed in a brittle manner. Once the failure load was reach, the plastic plates exhibited cracking and buckling, leading to rapid collapse of the units. Unfortunately, the supplier did not conduct any long-term creep rupture testing. There was no sign of settlement 6 months after completion of the geocellular rain harvesting tank.

A total of 75 double cells and 35 single cells were installed. Care was taken to ensure that no damage of the units occurred during installation. The use of 4 internal vertical plates proved to give a much more robust structure against bending of the top plates during the filling process. The incremental cost of 4 internal plates versus 2 was relatively minor (< 5% of the unit cost). For the size of backfill aggregate used, a Class B[1] filter fabric would have sufficed but the incremental cost for a Class C[2] fabric was relatively small to give greater resistance to potential installation damage. Sealing of the filter fabric overlaps using silicon sealant was quick and easy, and relatively economical to provide ease of mind to improve long-term performance. Backfilling around the sides of the completed cells was carried out in a manner that limits the fill level difference to within 0.4 m on opposite sides of the structure. Some photographs of the installation process are presented in Figures 9 to 14.

Figure 9: Placement of liquifill levelling layer

Figure 10: Double units and geofabric wrap

Figure 11: Backfilling around double units

Figure 12: Single units at shallow end

[1] Class B geofabric has grab strength approximately 30% less than Class C (see Table RM63A5.2 for full details of geotextile filter fabric strength classes)

Figure 13: 40 mm thick geocell finishing layer

Figure 14: Finished installation

5. CONCLUSIONS

The use of plastic geocellular structures as a stormwater detention or rainwater harvesting solution is an environmentally friendly and sustainable engineering alternative to traditional concrete structures. This paper demonstrates the importance of conducting long-term creep rupture testing for design. Significant savings can be derived for large projects using geocellular units if long-term creep rupture testing data is available instead of having to rely on potentially overly conservative strength reduction and creep extrapolation factors.

Care in construction is important and may also be utilized to lessen the reduction in design strength to account for installation damage in combination with creep rupture. This comment also applies to the selection of the robustness of the units for installation, geotextile grade, and overlapping details, which all affect the long-term performance of geocellular structures.

REFERENCES

ASTM F2418 (2013) American Society for Testing and Materials - Standard Specification for Polypropylene (PP) Corrugated Wall Stormwater Collection Chambers.

Australian Standard (2002) Geosynthetics - guidelines on durability, HB154-2002.

Australian Standard (2002) Earth-retaining structures, AS4678-2002.

British Standard (1995) Code of practice for strengthened/reinforced soils and other fills, BS8006-1:1995

CIRIA C737 O'Brien, A.S., Hsu, Y.S., Lile, C.R., Pye, S.W. (2016) Structural and geotechnical design of modular geocellular drainage systems.

RMS RM63 Geotextiles (Separation and Filtration) published by Roads and Maritime Services of NSW.

Wilson, S., Bray, R. and Cooper, P. (2004) Sustainable drainage systems, hydraulic, structural and water quality advice, CIRIA C609.

Wilson, S. (2008) Structural design of modular geocellular drainage tanks, CIRIA C680.

Woods-Ballard, B., Kellagher, R., Martin., Jefferies, C., Bray, R. and Shaffer, P. (2007) The Sustainable Drainage Systems (SuDS) manual, CIRIA C697.

LISTENING TO THE EARTH: AN UNCONVENTIONAL SCIENTIFIC APPROACH TO UNDERSTANDING SUB-SURFACE GROUND CONDITIONS

Hugh Stallard[1], Aasha Pancha[2], Richard Sabiston[3] and Weimen Deng[4]

[1]Senior Engineering Geologist - Transport, Aurecon
23 Warabrook Boulevard, Warabrook, NSW 2304
hugh.stallard@aurecongroup.com; M +61 415197719

[2]Seismologist / Geophysical Ground Investigation Manager, Aurecon
Spark Central, Level 8, 42-52 Willis Street, Wellington, New Zealand 6011
PO Box 1591, Wellington 6140
Aasha.Pancha@aurecongroup.com; T +64 4 4718784

[3]Senior Engineering Geologist, Aurecon
Spark Central, Level 8, 42-52 Willis Street, Wellington, New Zealand 6011
PO Box 1591, Wellington 6140
Richard.Sabiston@aurecongroup.com; T +64 4 4390241

[4]Technical Director, Infrastructure, Aurecon
Level 5, 116 Military Road, Neutral Bay, NSW 2089
PO Box 538, Neutral Bay, NSW 2089
Weimin.Deng@aurecongroup.com; T +61 2 94655124

ABSTRACT

Digitally recorded background ambient noise can be used to extract details regarding subsurface soil conditions. This unique methodology has been implemented to provide comprehensive assessments of geotechnical site conditions. Ambient noise is the persistent vibration of the ground in response to anthropogenic and natural causes. In many contexts, these background vibrations are classified as noise, and efforts are made to remove these signals from recorded data. However, these background vibrations also contain valuable information regarding the materials they travel through. The refraction microtremor (ReMi) technique separates these waves from noise recordings to determine soil shear-wave velocities. Interpolation of the closely spaced one-dimensional velocity-depth profiles along linear arrays allow two or three-dimensional velocity-versus-depth representations to be produced, thereby mapping lateral variations and extending subsurface characterisations between more expensive spot borehole measurements. ReMi technique provides a non-invasive and cost-effective way of estimating vertical soil/rock shear-wave versus depth profiles. This paper examines the contribution ReMi shear-wave velocity assessments can make towards enhancing subsurface geological and geotechnical models to mitigate risk from unforeseen ground conditions.

1 INTRODUCTION

We present a unique methodology that has been implemented to provide a more comprehensive assessment of geotechnical site investigations. Digitally recorded background ambient noise is used to extract details regarding subsurface soil conditions. Ambient noise is the persistent vibration of the ground due to anthropogenic and natural environmental causes. For activities sensitive to vibrations, these background vibrations are classified as noise, and efforts are made to remove these signals from recorded data. However, these noise sources emit energy, exciting surface waves that contain information regarding the materials they travel through. The refraction microtremor (ReMi) technique separates these surface waves from ambient noise recordings to determine soil shear-wave velocities. Developed by Louie (2001), the method has widely been used to determine shear wave velocity profiles (Vs). Velocity profiles obtained using ReMi have been used extensively to characterise sites for both engineering investigations and site response evaluations (e.g. Rucker, 2003; Pullammanappallil, 2006; Coccia et al, 2010).

The technology was initially developed by Louie (2001) to rapidly and cost-effectively measure the average shear-wave velocity to 30m depth to meet U.S.A. building code requirements,but has since been further developed towards comprehensive engineering applications. The technology is owned by the State of Nevada, exclusively licensed to Optim, and only available commercially as SeisOpt ReMi (Optim 2001–2019). The methodology is being standardised by the Consortium of Organizations for Strong-Motion Observation Systems (COSMOS) "International Guidelines on Applying Non-invasive Geophysical Methods for Characterizing Seismic Site Conditions" with the United States Geological Survey.

ReMi is a non-intrusive method that involves the deployment of a linear array of instruments to record ambient noise. Recorded data are analysed to extract information from the waveforms that reveal details regarding the subsurface shear-wave velocity profile with depth. Because determination of a reliable velocity model requires a regular and dense distribution of seismic noise sources, the ReMi method thrives in noisy environments, meaning data acquisition does not require construction activities to be halted. This differs from many other geophysical seismic methods that utilise active hammer seismic sources, such as seismic refraction techniques, and multichannel analysis of surface waves (MASW), which require background noise to be at a minimum.

Geotechnical field investigation tests such as Cone Penetrometer Testing (CPT) can often be limited due to the rig encountering practical refusal in very stiff cohesive soils, dense non-cohesive soils or buried construction debris, thereby providing an incomplete vertical profile. Boreholes and downhole shear-wave methods techniques are more reliable, but are costly, and only provide point measurements at a specific location. In contrast, ReMi can detect velocity inversions, and as such, is commonly used to measure shear-wave velocity profiles for engineering applications. Traditional seismic refraction methods are unable to detect softer soils which lie underneath harder material, or material layers that are very thin, often resulting in an incorrect interpretation of shear velocities and associated depths.

Here we describe the ReMi methodology in more detail, outlining the field data acquisition, the analysis procedure, and the parameters controlling the depth of investigation and resolution. Three case studies presented in this paper demonstrate the benefits of incorporating the shear-wave velocity estimates from ReMi into the geotechnical investigations. These include identifying the location of buried stream channels, characterising palaeo-topographical features, identifying areas of low velocity which may be prone to liquefaction, and assessing the thickness and velocity variations within geological units between geotechnical point investigation tests locations. We demonstrate how use of ReMi enhances the ability to obtain a thorough geological understanding of sites, allow better characterisation of subsurface material properties, and hence minimising geotechnical risks. Use of multiple methods supports thorough understanding of subsurface conditions enabling adoption of appropriate geotechnical design parameters to support the fundamentals of "good design".

2 THE REFRACTION MICROTREMOR TECHNIQUE

The ReMi technology was initially developed by Louie (2001) as a non-invasive surface-performed geophysical survey technique, to rapidly and cost-effectively measure the average shear-wave velocity to 30m depth to meet U.S.A. building code requirements but has since been further developed towards comprehensive engineering applications. The essence of the refraction microtremor technique is that ambient vibrations contain usable signal that can be used to predict velocity structure underneath the measurement array. ReMi exploits the fact that random ambient ground vibrations generate surface Rayleigh waves that transfer significant information about the velocity structure of the subsurface materials. Rayleigh waves are a seismic surface wave that travels along the surface of the earth, causing the ground to shake in an elliptical motion. These recorded Rayleigh waves include high-frequency (short wavelengths, with frequencies >2 Hz) ground motions that have physical characteristics governed by the elastic properties of the very shallow near-surface materials through which they propagate. Meanwhile, lower frequency motion (longer wavelengths, with frequencies ≤2 Hz) are influenced by material properties at greater depth. More importantly, Rayleigh waves are dispersive, meaning that wave velocity is dependent on frequency, with low frequencies normally propagating at higher velocity. This unique property of Rayleigh waves allows information regarding the shear-wave velocities of the subsurface materials to be determined. Results from ReMi analysis have been validated through comparison to borehole profiles (Asten et al., 2005; Stephenson et al., 2005; Thelen et al., 2006), synthetic data (Heath et al, 2006), as well as MASW, and spectral analysis of surface waves (Liu et al., 2005; Stephenson et al., 2005).

2.1 DATA ACQUISITON

Testing is performed at the surface using the same conventional seismograph and vertical P-wave geophones used for refraction studies. Data acquisition is non-intrusive method involving the linear deployment of geophones, placed an even distance apart. This distance, as discussed below, is dependent on the target depth of investigation. Typically, standard vertical 4.5-Hz seismic refraction geophones are used. Where the ground is paved, the spikes will be removed and replaced by plates, as shown in Figure 1. Ambient ground motions, dominated by Rayleigh waves, are recorded by the arrays at a time-sample interval of two milliseconds for multiple records of 30 seconds each. Each seismic array placement collects

twelve to twenty 30-second recordings. Hammer hits using an 8-pound or 10-pound (3.5-4.5 kg) sledge and strike plate placed approximately 5 m and 10 m off both ends of each array augmented normal passive data collection, to increase high-frequency energy. Hammer hits may also be acquired at evenly spaced locations along the line, depending on the array length to assist with 2D analysis.

Figure 1: An example of a 4.5-Hz seismic refraction geophone used to record ambient noise.

2.2 DEPTH AND RESOLUTION OF INVESTIGATION

Although initially developed for determination of average shear-wave velocities to 30 m depth (VS30), the surface-wave theory behind ReMi technique can be applied to a multitude of applications at various scales, with the array configuration and data acquisition adjusted accordingly. The ability of any surface-wave seismic array to image velocity structure at any depth depends on the capability of the array to capture ground motion at wavelengths that sample the target depths. The wavelength content of the recorded data depends on several factors. These include the array length, geophone spacing, geophone frequency (the lower-frequency limit of motion detection), the time duration of the data records, the frequency content of the noise sources producing the recorded ground motions, and the material properties.

ReMi has been widely used for engineering applications to image very shallow subsurface material structure in the upper 10 m, using short geophone spacings between 0.5m and 3m combined with high-frequency geophones to successfully image near-surface shallow structure. For imaging of deeper structure, longer array lengths, along with larger geophone spacing and lower frequency geophones, can be utilized. The longer arrays and lower frequency geophones ensure that the longer-wavelength Rayleigh waves that sample deeper into the Earth's structure are captured by the recorded seismic data. Many studies have used the ReMi methodology with extended array lengths to successfully image subsurface velocity structure down to 200 m depth. In addition, 3km and 6km long arrays have been deployed to characterise basin geometry to 1km depth (Pancha et al., 2017). Total array length should generally be greater than twice the maximum target depth. Rayleigh waves are most sensitive to velocities and structures that are within a half-wavelength of the surface. To properly time the velocity of such a wave, the sensor array needs to be at least as long as the wavelength.

2.3 PROCEDURE TO ESTIMATE SHEAR WAVE VELOCITY FROM RECORDED NOISE

The vertical component of ambient noise, dominated by Rayleigh waves, is recorded by seismograph arrays, as illustrated in Figure 2(a). Once collected, the field data is reduced and processed by trace-equalisation and direct current offset removal. The Rayleigh waves are separated from other wave arrivals using a two-dimensional slowness–frequency (p–f) transform of the noise records. This 2D transformation creates a velocity spectrum imaging the Rayleigh-wave dispersion curve, as displayed in Figure 2(b). The spectrum is normalised as the ratio of the power spectrum at a particular frequency and slowness (inverse velocity) divided by the average value for all slowness values at that frequency. Imaging of the dispersion curve on a linear slowness scale, allows recognition of true phase velocity against apparent velocities compared to plots of the wavefield transformation on a linear scale of velocity. Use of a linear slowness scale identifies the Rayleigh-wave energy traveling parallel to the array more clearly. Energy propagating in both directions are analysed. The fundamental-mode phase-velocity Rayleigh wave dispersion curve is then picked along the minimum-velocity of the

envelope of the energy within the slowness–frequency spectral image where the gradient of the power spectral ratio is greatest (Louie, 2001; Pancha et al., 2008).

The fundamental-mode Rayleigh dispersion is then picked along the minimum-phase-velocity envelope, as shown in Figure 2(b) for which the gradient of the power spectral ratio is greatest. These points "picked" along the Rayleigh wave dispersion curve are then interactively modelled, using trial-and-error adjustments of the velocity–depth model, to obtain a shear-wave velocity that produces a calculated dispersion curve that matches the data (Figure 2(c) and 2(d)). These shear-wave velocity profiles provide both geotechnical and engineering parameters.

However, like the MASW surface wave method, ReMi suffers from non-unique interpretations, meaning that a given data set can be represented by multiple subsurface geological models. Trade-off between layer thickness and the material property generates the issue of non-unique modelling results, and as such, neither the thickness nor the material property of the layer can be independently determined. To obtain a valid model, independent physical evidence and constraints from geotechnical investigation tests are incorporated into the interpretation of the data to further constrain the possible velocity models.

ReMi is a volume-averaging surface-wave measurement, which averages the velocities where geology is laterally variable. This differs from the single-point measurements obtained by downhole logs, as concluded by Raptakis (2012). Interpolation of closely spaced one-dimensional velocity-depth profiles along linear arrays (or transects) allow two-dimensional velocity-versus-depth representations to be produced. These two-dimensional representations can thereby map lateral heterogeneity of the soil profile and geological structure and extending subsurface characterisations between more expensive spot geotechnical investigation tests. ReMi therefore provides a non-invasive and cost-effective way of characterising ground conditions across entire sites, with data acquisition able to take place in areas where drill-rig access is restricted or drill location quantities can potentially be reduced.

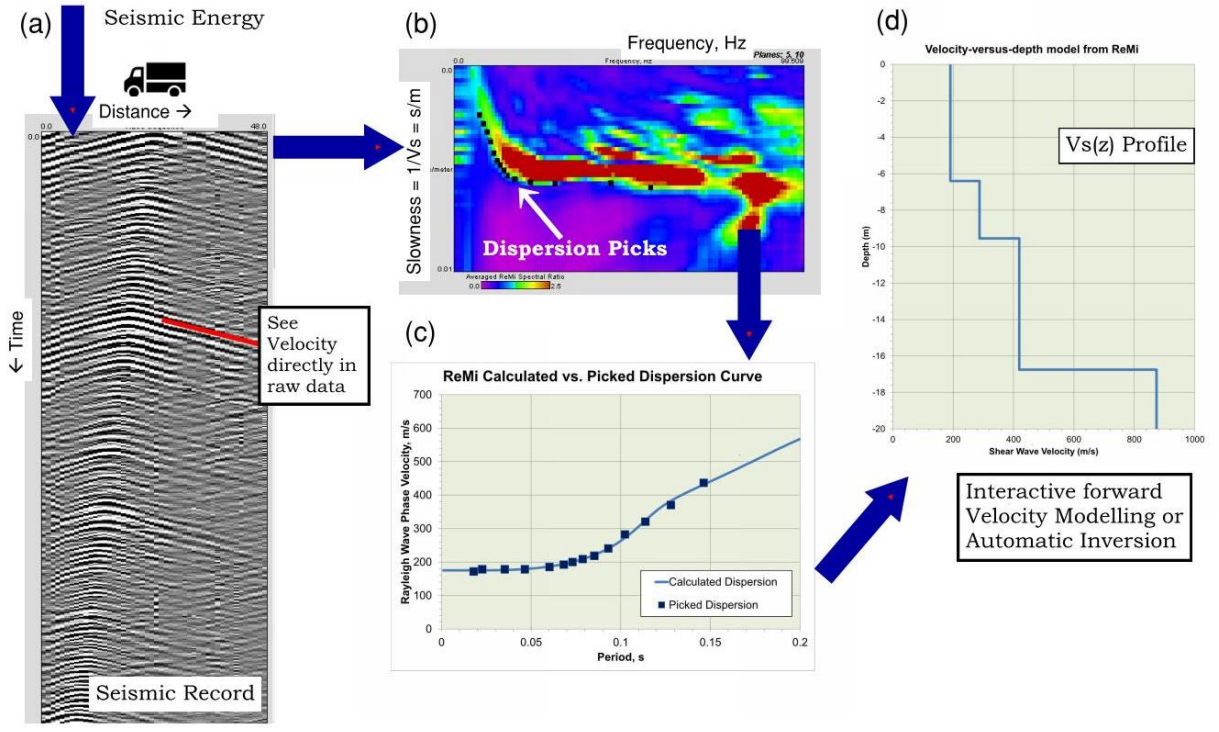

Figure 2: Schematic of the ReMi technique. (a) Refraction Microtremor involved the deployment of a linear array of vertical geophones to record Rayleigh waves generated by ambient noise. The velocity of the Rayleigh waves can often be observed directly from the raw data. (b) The recorded data are transformed into the frequency-slowness (p-f) domain (see Louie, 2001). The fundamental-mode phase-velocity of the Rayleigh wave is "picked" along the lowest-velocity envelope (black squares). (c) Dispersion curves and associated picks from p-f plots and matching fits. Modelling of the dispersion curve produces a velocity-depth model that matches the data. (d) Modelled shear-wave velocity-depth profiles.

3 KEY BENEFITS

A primary benefit of utilising ReMi measurements for geotechnical ground characterisation is the ability to increase spatial sampling density so that background and anomalous conditions can be identified early in the investigation. Because conventional seismic equipment is used to record data, and ambient noise is used as a seismic source, the ReMi method is less costly, faster and more convenient than boreholes methods and other surface seismic methods to determine shear-wave profiles. The method works best in a seismically noisy urban setting, so can be used on busy construction sites. The method thus affords itself as an effective tool for both reconnaissance for and extrapolation of more expensive geotechnical spot measurements.

ReMi surveys are not intended to replace traditional subsurface sampling and field investigation tests. However, they aid in quickly and economically extending subsurface characterisation over larger areas, correlating between the boreholes, test pits, and other investigation data points to characterise lateral changes in geology and/or material properties. More importantly, the method often allows assessment to deeper depths than the shallow geotechnical investigations. By providing details regarding different material properties of the sub-surface ground conditions, ReMi velocity models contribute towards the development of a more integrated site model.

4 APPLICATIONS OF THE REFRACTION MICROTREMOR TECHNIQUE

Refraction Microtremor has become a standard tool for assessing shear-wave velocities for many geotechnical applications and site response evaluations. ReMi is routinely used to determine velocity-vs-depth information across a range of depths from very shallow right down to a few hundred metres. It is also adept at resolving relatively thin soil layers. Shear-wave velocity data enhances the overall geotechnical investigation by providing a means of assessing soil cyclic resistance, liquefaction potential, and estimates of soil engineering properties such as low strain elastic and shear moduli.

The ReMi ambient noise data can be used to create 1D and 2D shear-wave velocity models for:

- Characterise lateral changes in the ground properties across the site.
- Estimating the strength of subsurface materials.
- Calculate engineering properties of soils and rock such as low strain elastic and shear moduli.
- Estimating Site period and site subsoil classification for NZS1170.5:2004 “Earthquake Design Actions” (Standards New Zealand, 2004).
- Mapping subsurface bedrock depth extents and topography.
- Building foundation assessment and design.
- Assessing bedrock quality.
- Assess liquefaction potential
- Mapping soil discontinuities.
- Identifying fault locations.
- Mapping basalt flows.
- Mapping subsurface voids and cavities.
- Mapping the extent of reclamation fill.
- Identifying soft spots and low shear strength layers.
- Determination of buried morphology – e.g. buried streams.
- Locating and mapping features related to historical site development.
- Finding buried cultural features, as well as landfills and piers.
- Identifying geohazards such as landslide slip planes.
- Image to deeper depths than the shallow geotechnical boreholes and test pits.
- Correlate soil profiles between the boreholes, test pits, and other investigation data points

5 CASE STUDIES

Aurecon New Zealand Ltd (Aurecon) have utilised ReMi towards supplementing data between sparsely distributed and more expensive geotechnical spot measurements (e.g. boreholes, CPT’s and test pits). We present three case studies demonstrate the benefits of incorporating the shear-wave velocity estimates from ReMi into the geotechnical investigations. Results allow the correlation and extrapolation of geotechnical knowledge between geotechnical investigation locations, and the further assessment of subsurface material properties. More importantly, the method allows assessment of soil conditions to deeper depths than the shallow geotechnical boreholes, test pits.

5.1 TERRACE TOWNHOUSES – WELLINGTON, NEW ZEALAND

Towards supplementing data between geotechnical borehole and test pit investigations, ReMi investigations were undertaken to determine the sub-surface velocity structure beneath the site of the proposed Terrace Townhouses (Figure 3). 2D velocity-versus-depth representations mapping the lateral velocity heterogeneity beneath Line A and Line C are presented in Figure 4.

Borehole data from two locations along Line A were used to constrain the velocity profile. Both boreholes terminate at the bedrock interface. These constraints were then used to produce 2D velocity-depth representations beneath each seismic array and extrapolate site condition knowledge across the entire investigation site. As seen from Figure 4(a), there were notable lateral changes that were important for the liquefaction assessment of the site, with interbedded zones of low velocity sediments defined. The non-intrusive technique was also able to define the location of a historical buried stream channel along Line A, documented to have run through the site during the mid-1800'sthat would otherwise not have been discovered.

Interpretations along Line C, shown in Figure 4(b), were controlled by stratigraphy from three test pits. Bedrock was only encountered in TP-02. An abrupt change in bedrock depth and soil thickness was revealed through the investigation. The development site was the location of a historic brick factory (circa 1895), which extracted clay material in the immediate vicinity. The increase in bedrock depth observed along Line C is interpreted to be anthropogenic in nature and was undetected and unforeseen from the geotechnical investigation.

The ReMi investigations allowed the correlation and extrapolation of geotechnical data between investigation locations, and the further assessment of material properties. More importantly, the technique permitted the assessment of material properties to deeper depths than the shallow test pits.

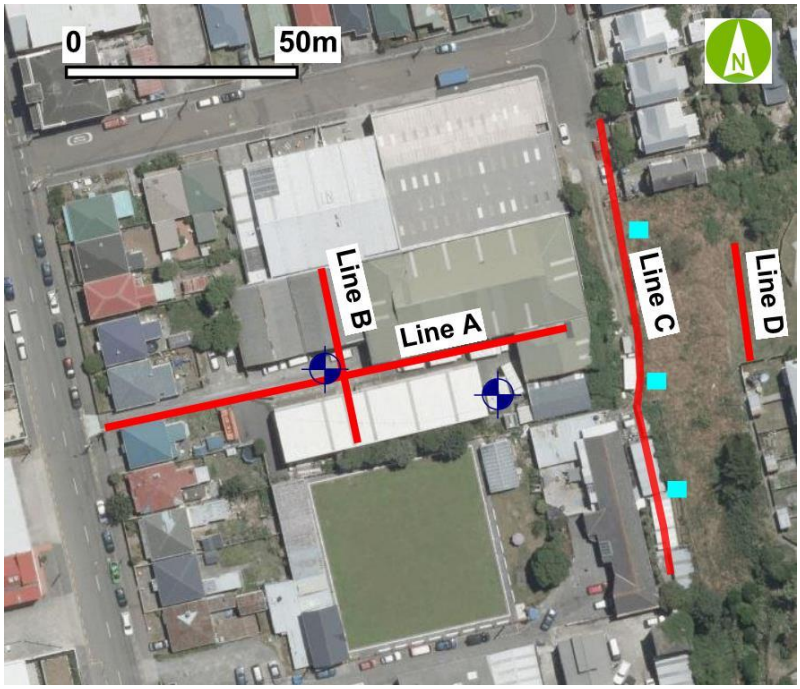

Figure 3: Locations of the ReMi seismic arrays (red lines) undertaken for the geotechnical investigation for a Terrace Townhouse development. Borehole (blue symbols) and test pit (cyan squares) locations are displayed. Aerial photograph sourced from LINZ Data Service (https://data.linz.govt.nz/data/category/aerial) and licenced under the Creative Commons Attribution 4.0 New Zealand

Use of ReMi in conjunction with boreholes and test pits for the Terrace Townhouse project enabled the ability to acquire a more comprehensive assessment of site conditions than traditional methods allowed. The geophysical ReMi data also aided in assessing the liquefaction potential of the site by identifying areas of low velocity between borehole locations, as well as assessing the thickness and velocity variability of geological units between borehole and test pit locations. Most importantly for this case study, ReMi characterised an otherwise unknown dramatic increase in bedrock depth.

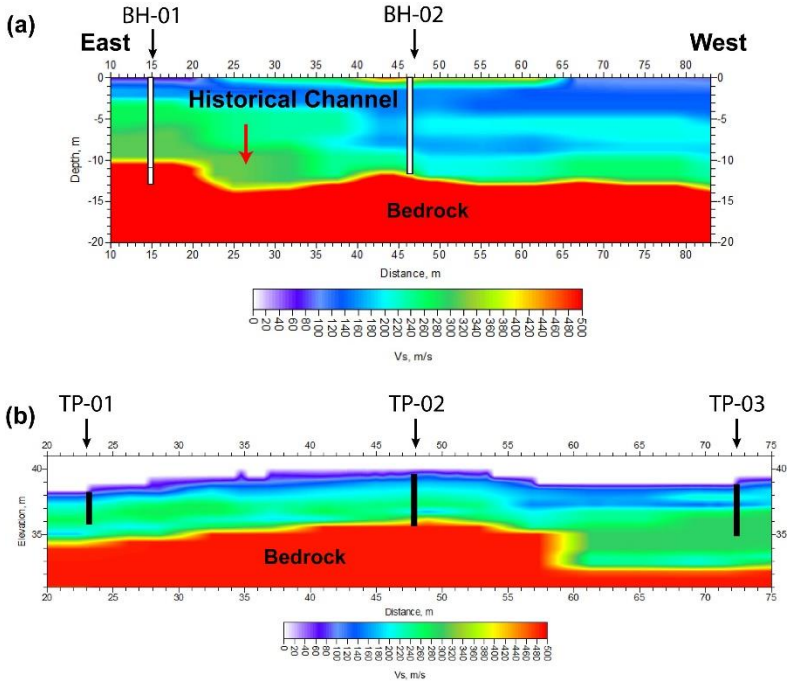

Figure 4: 2D shear-wave velocity representations beneath (a) Line A and (b) Line C. Borehole BH-01 and BH-02 terminated at the weathered bedrock interface. Relative locations of the seismic arrays are displayed in Figure 4. The shear-wave velocity scale displayed below each figure range from 0m/s to +500 m/s, with bedrock velocities > 500m/s. Warm colours indicate high velocities, while cooler colours indicate low velocities. Test pit locations and depth extent are displayed as back lines in figure (b).

5.2 WELLINGTON CHILDREN'S HOSPITAL – WELLINGTON, NEW ZEALAND

Wellington Children's Hospital Charity Limited (WCH) have begun construction of the new children's hospital on an existing carpark site, immediately to the north of the Wellington Hospital complex. The proposed building comprises a ground floor for car parking and three stories of wards built above the ground floor. WCH engaged Aurecon Ltd. to provide an initial geotechnical assessment of the site. Experience from sites within the general area, indicated variable layers of fill, (including potential infilled gully/streams and ponds), underlain by undifferentiated alluvium and greywacke rock with an extensive weathering profile were likely to make up the geological profile at the site. As part of the geotechnical investigations, a ReMi seismic investigation was carried out to determine the subsoil structure and estimate the subsoil shear wave velocity profiles to:

- Characterise the variation of soil properties across the site.
- Determine changes in the soil lithology across the site.
- Determine variations in the bedrock depths across the site.
- Calculate engineering properties of soils and rock such as low strain elastic and shear moduli.
- Determination of liquefaction potential across the site.

The site has a long and complex history of building development. Early maps indicate that site was originally a natural drainage pathway that included a swamp area and several ponds. Over the course of human occupation and subsequent building developments successive infilling has occurred up to present day. Aerial photographs dating back to 1923 through to the present day of Wellington Hospital shows numerous historical buildings have occupied the investigation area. In addition, a plan from 1939 indicate an embankment existed along western side of the investigation site. The site is known to have been underlain by 2.6m to 6m of non-engineered fill underlain by alluvial soils. The non-engineered fill was considered to be very loose and to include rubbish comprising concrete pieces, bricks, wood, nails, metal sheets, metal pieces, old pipes and isolated layers of decomposed vegetation. Figure 5 illustrates the locations of the proposed building site, the historical building, and the old drainage features.

The ReMi investigation for the site included seven seismic arrays, Line 1 to Line 7 (dashed green lines), between 47m and 92m long, the locations of which are shown in Figure 5. Results of the ReMi survey demonstrate that in general, the reclamation fill deposits consist of materials with a relatively low shear-wave velocity as compared to the underlying alluvial soils. Shear wave velocities of the non-engineered fill has shear wave velocities ranging between ~125m/s and

250m/s, while the alluvium/ colluvium overlying the bedrock range between ~175m/s and 400m/s. In comparison, the highly weathered greywacke bedrock had velocities of 300m/s to 600m/s, with >700m/s for the more competent rock.

Based on the historic evidence, both Line 1 and Line 2 traverse the historical pond, which has undergone progressive reclamation during the development of the land. The 2D velocity representations for these two investigation lines, shown in Figure 6(a) and 6(b) respectively. As seen in the cross-sections, the bedrock depth varies, delineating a depression within the bedrock terrain. Along Line 1, the greywacke bedrock beneath is deepest towards the eastern end of the array, with a maximum depth of 13.6m. Towards the western end, the bedrock is at 6m depth below the ground surface, consistent with BH-01. Where the bedrock deepens, a 300m/s layer overlies the bedrock surface. Based on correlations with the geotechnical boreholes the 300m/s layer likely represents gravels associated with the undifferentiated alluvium. In comparison, for Line 2 bedrock depths are deepest nearer the centre of the array, with a maximum depth of 12.3m becoming shallower towards both the west and the east. For both Line1 and line 2, bedrock is shallowest towards the eastern side of site, near the location of the historical embankment, shown in Figure 5.

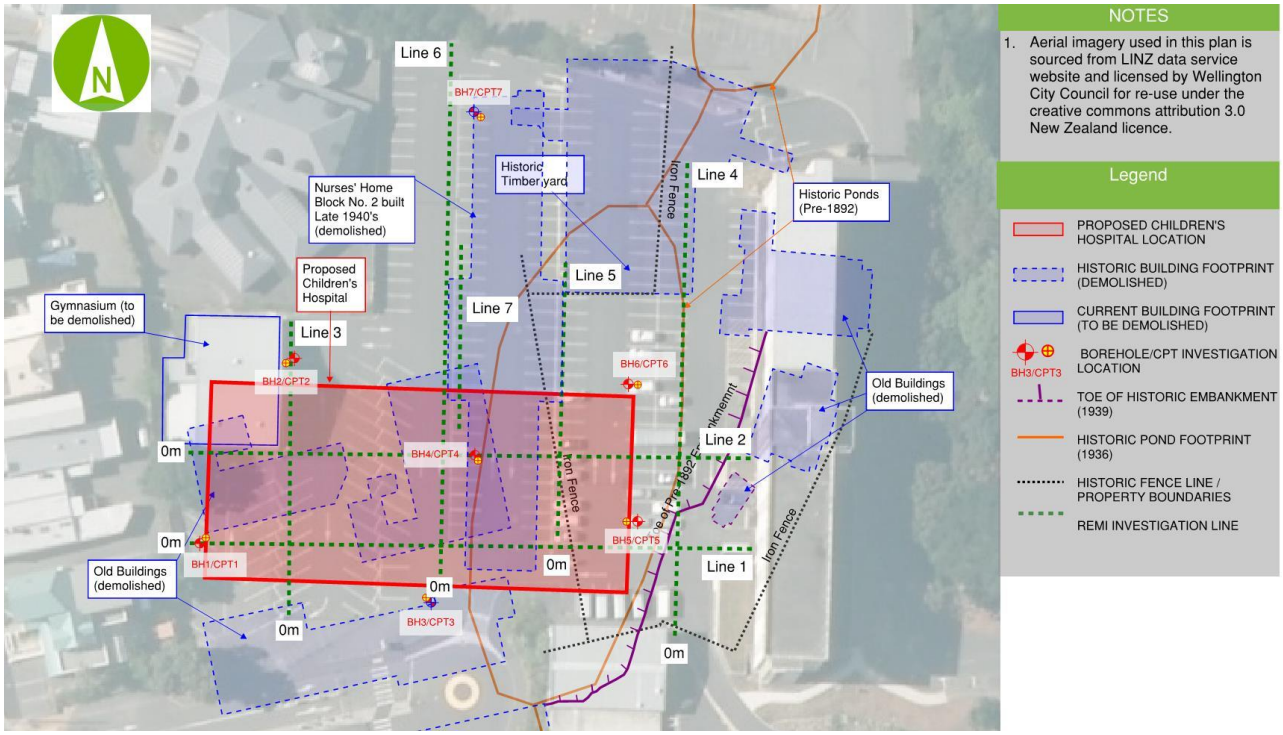

Figure 5: Map showing locations of the seven seismic array lines used to determine bedrock and soils structure beneath the site of the proposed Wellington Children's Hospital. Previous site developments and historical natural features are also displayed

Line 3 is located in a north-south orientation along the western side of the site. A notable 1.5m step down in the bedrock profile occurs at approximately 21.5m along the array. A 2D plot of the velocity-depth representation determined below this array is presented in Figure 7. Between 21m and 27m distance along the array, an area of slightly higher velocity is noted in the upper 1.3m below the surface. Historical records were used to determine the locations of old structures that previously occupied the site, as shown in Figure 5. The location of the edge of the Nurses' Home Block 2 demolished pre-1943 coincides with the approximate location of these high velocities.. It is likely that the origin of the step is associated with the foundation footprint of this demolished building.

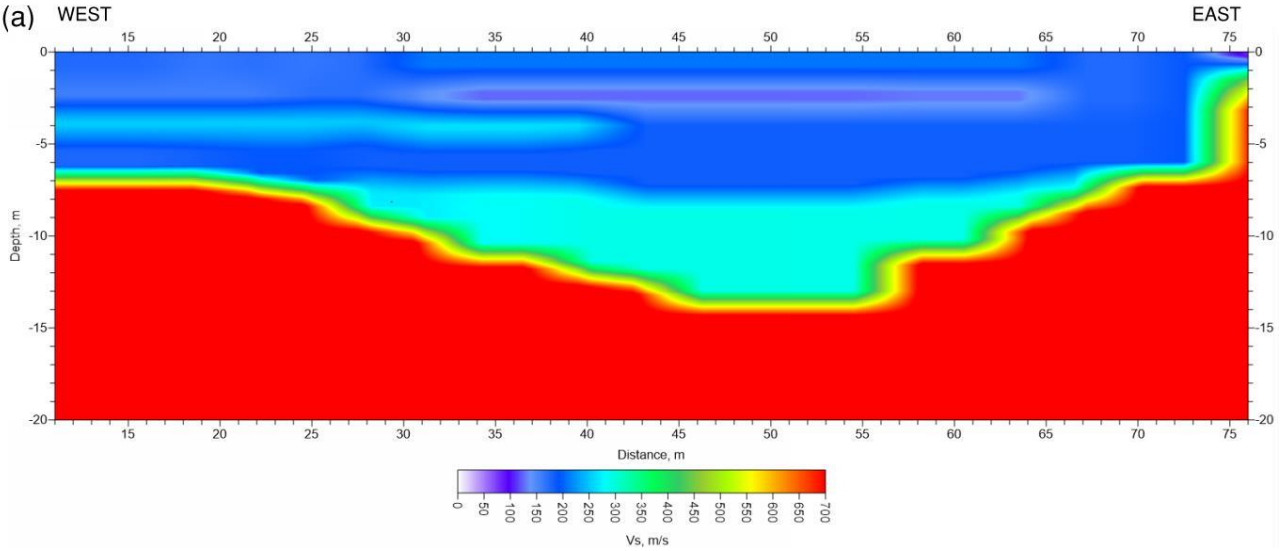

Figure 6(a): 2-D S-wave velocity (Vs) model along Line 1. Distances are from the beginning of the array as shown in Figure 5

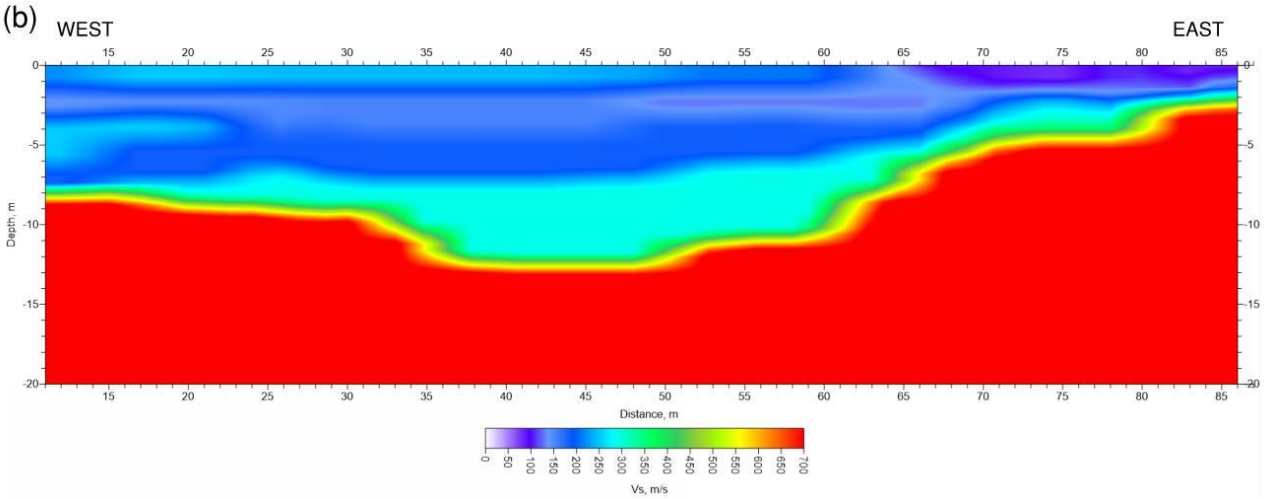

Figure 6(b): 2-D S-wave velocity (Vs) model along Line 2. Distances are from the beginning of the array as shown in Figure 5

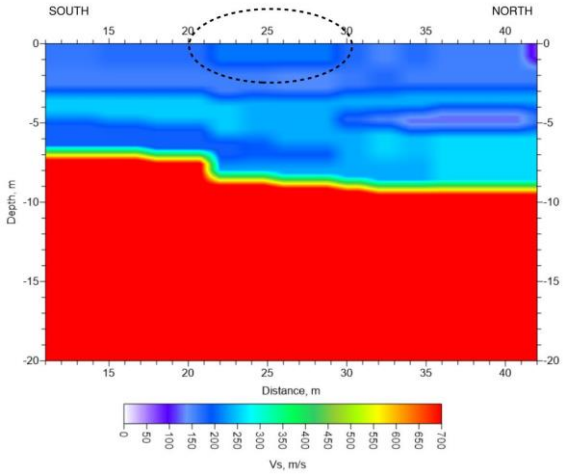

Figure 7: 2-D S-wave velocity (Vs) model along Line 3. Distances are from the beginning of the array as shown in Figure 5. The circled area highlights a zone of low velocity likely associated with the location of an historical structure

The largest historical structure that encroached onto the site was the Nurse's Home Block No.2, built in the late 1940s and demolished in 2010. Historical photos together with allowed the approximate location of the foundation, to be determined, as illustrated in Figure 5. Building plans, together with photographs taken during the 2010 demolition (Figure 8a), documented that the building foundations were still present entrenched at approximately 5.5m apart. To resolve the detailed soil structure of the fill material in the upper 5m of the surface and detect buried building foundations associated with the demolished Nurses' home (shown in Figure 5), data acquisition along Line 7 was acquired using a shorter geophone spacing of 0.5m, compared to 1m for the remaining seismic arrays. Results of the analysis are presented in Figure 8(b). The shear-wave velocity of the fill material in the upper 2m of the soil profile is found to be highly variable. In addition, areas of with a very high shear-wave velocity were detected and may be related to historic foundations of the demolished Block No. 2 Nurses' Home or buried concrete rubble.

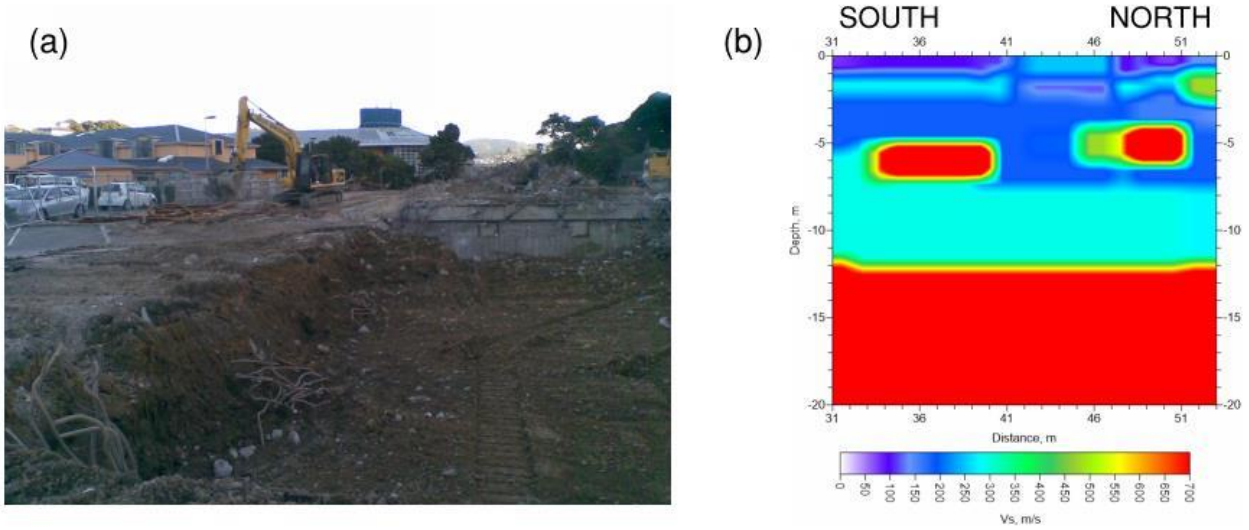

Figure 8: (a) Photo showing reinforcement rebar from the foundations of the Nurse's Home Block No.2 during demolition in 2010. (b) 2-D S-wave velocity (Vs) model beneath Line 7. Distances are relative to the beginning of Line 6 as shown in Figure 5

5.3 BOWEN CAMPUS/PARLIAMENT PRECINCT – WELLINGTON, NEW ZEALAND

Parliamentary Service were proposing to construct a four-storey extension and a new six storey block to the west of the Beehive at their Parliament Precinct, located off Bowen Street, Wellington (Figure 9). This site is located directly adjacent to Bowen Campus, which is currently undergoing seismic strengthening and redevelopment of a 15-storey and 9-storey building. For this publication, we shall consider these as a single site. Geotechnical information was required to determine foundation design parameters, liquefaction potential and site subsoil classification. Initial geotechnical investigations comprised boreholes with Standard Penetration Tests (SPT), including down-hole shear-wave velocity testing. ReMi was then used to supplement the initial geotechnical investigation, correlating between the borehole data and determining lateral changes in bedrock depth across the site.

The Wellington region is a seismically active region with potential for a high level of ground shaking. In accordance with NZS1170.5:2004 "Earthquake Design Actions" (Standards New Zealand, 2004), a seismic site classification based on geological and geotechnical properties is used in the calculation of seismic loading of buildings and structures. The site subsoil classes are defined as Class A (strong rock), Class B (rock), Class C (shallow soil site), Class D (Deep or soft soil), and Class E (very soft soils). Each class quantifies the soil's propensity to amplify, or in some cases attenuate, surface ground motion from underlying rock, where rupture occurs during earthquakes. They are based on physical soil properties, including the site period. Site period is defined as four times the shear-wave travel time from the surface to bedrock (Larkin and Van Houtte, 2014), and is a measure of the period of vibration corresponding to the fundamental frequency of the column of soil.

Amendments to NZS1170.5 in 2016 now make interpolated design shape factors between Class C and Class D based on site period an acceptable solution. Assessment of the interpolated curves demands that accurate determination of bedrock depths together with robust measurement of shear-wave velocity to bedrock are required for site period calculation. Site

subsoil classifications for these development sites were assessed in accordance with NZS1170.5:2004 using Unconfined Compressive Strength (UCS) testing of the bedrock, down-hole shear wave velocity testing and ReMi investigation data.

Using the shear-wave velocity and depth information obtained from both methods, site period measurements were mapped across the site, as shown in Figure 3. Bedrock depths varied from 16m depth below ground surface to 80m depth, with prominent deepening of the bedrock surface towards the east. The detailed mapping of bedrock depth, coupled with the 2D shear-wave velocity information allowed comprehensive assessment of both the site subsoil conditions and the variability of the fundamental period of the soil column.

Constraints from the borehole descriptions, SPT, laboratory testing and downhole velocity measurements were used to constrain the velocity profiles determined from the ReMi data. The resultant 2D seismic profiles were able to provide vital information on bedrock depths, characterising the nature of the change. Most importantly, the ReMi investigation allowed the 1D point measurements from the vertical boreholes to be extrapolated across the entire development site.

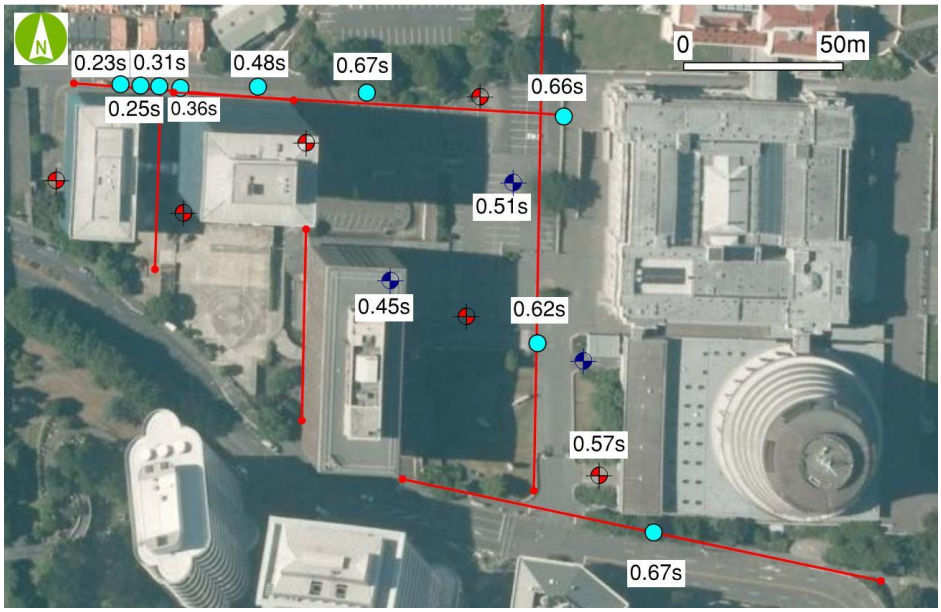

Figure 9: Locations of the ReMi seismic arrays and boreholes (red) at Bowen Campus/Parliament Precinct, Wellington, New Zealand. Site period measurement values across the site are presented, with estimates from the seismic ReMi data shown as cyan circles. Aerial photograph sourced from LINZ Data Ser-vice (https://data.linz.govt.nz/data/category/aerial) and licenced under the Creative Commons Attribution 4.0 New Zealand.

In areas of complex geology, particularly where bedrock depth is variable in seismically active regions, there is often uncertainty in whether a borehole or downhole shear wave velocity investigation has been carried out where bedrock depths is the greatest. This was true for the Parliamentary Precinct site investigation. Establishing bedrock depths together with material shear-wave velocity profiles are now crucial for the determination of site period towards site subsoil classification in accordance with NZS1170.5. However, with depth to bedrock exceeding 60m beneath many urban areas, boreholes to bedrock are very costly to drill. This poses a major issue in correctly determining site period and thus site classifications for building code implementation. ReMi allowed the lateral extension of borehole information, adding a cost-effective assessment tool, providing information regarding the variability of both shear-wave velocity and bedrock depths across large sites.

6 CONCLUSIONS

Geotechnical engineering is one of the most challenging engineering disciplines. A geotechnical engineer has the job of investigating subsurface ground conditions and material properties to determine how the ground will interact with a piece of infrastructure or buildings. All too often unexpected ground conditions are encountered. There is always an inherent uncertainty associated with characterising the subsurface. A multidisciplinary ground investigation is the most preferred option to ensure a more comprehensive assessment of engineering site conditions is undertaken. Using refraction microtremor, we can remove some of the mystery surrounding the ground conditions between spot measurements. Here

we have demonstrated how a unique unconventional approach using ambient noise recordings to determine sub-surface material properties is an effective way of obtaining a more comprehensive assessment of engineering site conditions. Refraction microtremor seismic investigations supplement the overall geotechnical investigation, enabling better characterisation of the variation of soil properties across investigation sites. The objective is not to replace traditional geotechnical investigations, but complementing them to obtain a much more comprehensive understanding of the subsurface conditions.

The three case studies presented demonstrate the considerable contribution ReMi shear-wave velocity assessments can make towards a better understanding subsurface geological and geotechnical conditions beneath large development sites. Velocity measurements from ReMi were used to provide additional information for the geotechnical investigation tests. As the data can be obtained in very noisy urban environments, obtaining shear-wave velocity information using the ReMi method is less costly and allows for faster data acquisition than many other geophysical investigation methods. The results presented here demonstrate how ReMi investigations are an effective tool allowing us to strategically plan and optimally place more expensive intrusive investigations.

7 ACKNOWLEDGEMENTS

We would like to acknowledge our gratitude to Dave Stewart from Stratum Management Ltd, for allowing us to present data from the Wellington Townhouse Development. We also thank Ryan Cater from Precinct Properties and Jim Robb from Parliamentary Service for allowing us to present results from the Bowen Campus and the Parliamentary Accommodation Development projects respectively. Wellington Children's Hospital Charity Limited are the entity proposing to construct a new children's hospital.

8 REFERENCES

Coccia, S., Del Gaudio, V., Venisti, N. and J. Wasowski, (2010). Application of Refraction Microtremor (ReMi) technique for determination of 1-D shear wave velocity in a landslide area. Journal of Applied Geophysics, 71(2-3), 71-89.

Heath, K., J. Louie, G. Biasi, A. Pancha, and S. Pullammanappallil (2006). Blind tests of refraction microtremor analysis against synthetics and borehole data, *Proceedings of the Managing Risk in Earthquake Country Conference Commemorating the 100th Anniversary of the 1906 earthquake.*

Larkin, T. and C. Van Houtte (2014). Determination of site period for NZS1170.5:2004, *Bulletin of the New Zealand Society for Earthquake Engineering*, 47(1), 28-40.

Liu, Y., B. Luke, S. Pullammanappallil, J. Louie, and J. Bay (2005). Combining active- and passive-source measurements to profile shear wave velocities for seismic microzonation, in *Earthquake Engineering and Soil Dynamics*, R. W. Boulanger, M. Dewwolkar, N. Gucunski, C. Juang, M. Kalinski, S. Kramer, M. Manzari, and J. Pauschke (Editors), *Geotechnical Special Publication 133, American Society of Civil Engineers*, Reston, Virginia, 977–990.

Louie, J.N. (2001). Faster, better: shear-wave velocity to 100 meters depth from refraction microtremor arrays. *Bulletin of the Seismological Society of America*, 91(2), 347-364.

Raptakis, D. G. (2012). Pre-loading effect on dynamic soil properties: Seismic methods and their efficiency in geotechnical aspects, Soil Dynamics and Earthquake Engineering, 34: 69–377.

Rucker, M.L. (2003). Applying the refraction microtremor (ReMi) shear wave technique to geotechnical characterization. *In Proc. In. Conf. of the third international conference on the application of geophysical methodologies and NDT to transportation and infrastructure*, Florida, 8-12.

Pancha, A., Pullammanappallil, S., Louie, J.N., Cashman, P.H. and Trexler, J.H., 2017. Determination of 3D Basin Shear-Wave Velocity Structure Using Ambient Noise in an Urban Environment: A Case Study from Reno, Nevada. *Bulletin of the Seismological Society of America*, 107(6), 3004-3022.

Pullammanappallil, S., 2006. Geotechnical and geophysical case studies involving the Refraction Microtremor (ReMi) method for shear wave profiling. *In Highway Geophysics Conference*, December, 5-7.

Standards New Zealand (2004). *NZS 1170.5:2004 Structural design actions—Earthquake actions, Section 3—Site Hazard Spectra, Standards New Zealand*, 81 pp.

Stephenson, W. J., J. N. Louie, S. Pullammanappallil, R. A. Williams, and J. K. Odum (2005). Blind shear-wave velocity com-parison of ReMi and MASW results with boreholes to 200 m in Santa Clara Valley: Implications for earthquake ground motion assessment. *Bulletin of the Seismological Society of America*, 95(6), 2506–2516.

Thelen, W. A., M. Clark, C. T. Lopez, C. Loughner, H. Park, J. B. Scott, S. B. Smith, B. Greschke, and J. N. Louie (2006). A transect of 200 shallow shear-velocity profiles across the Los Angeles basin, *Bulletin of the Seismological Society of America*, 96(3), 1055–1067.

GREEN SQUARE – ENABLING URBAN RENEWAL THROUGH SMART RETAINING WALL DESIGN AND TRENCHLESS CONSTRUCTION

[1]Henry Zhang, [1]Paul Hewitt, [1]Nick Taylor, [1]Robert Kingsland, [1]Gareth Evans
[1] WSP Australia; email: Henry.Zhang@wsp.com

ABSTRACT

Green Square is one of the City of Sydney's key urban renewal precincts, which is being transformed from old industrial land into a major new residential, retail and cultural hub. The Green Square Stormwater Drain (GSSD) is the culmination of a strategic alignment between City of Sydney and Sydney Water to provide flood protection in the Green Square area. Through a process of optioneering and hydraulic analysis, a new 2.5 km long underground drain consisting of multiple 1800 mm diameter pipes was installed by microtunnelling, and an open trench box culvert was replaced with channel widening via an anchored retaining wall in the final 300 m from Maddox St to Alexandra Canal. The new drain augments the existing trunk drain system and reduces flood hazard, allowing Australia's largest urban renewal project to proceed.

The channel widening section of the GSSD was originally intended to be constructed into the bank of the existing open channel. A constructability assessment for installation of the box culvert within the narrow corridor between the existing open channel and adjacent buildings indicated that open trench box culvert construction would not be cost effective. This paper describes an innovative solution, where the existing channel was widened using an anchored retaining wall, replacing the proposed box culverts.

The trenchless (microtunnel) solution offered an alternative, value for money approach with significantly reduced environmental impact and achieved comparatively minimal community disruptions.

This paper also describes the ground engineering challenges and solutions employed on the site which included difficult ground conditions, landfill and addressing impacts of wall construction on adjacent infrastructure such as roads, bridges and buildings. Ground engineering risks were successfully managed through detailed scoping of investigations, numerical modelling of designs and adoption of observational methods during construction. The specification requirements, design, installation, monitoring and performance of the successful microtunnel drain and anchored wall system are discussed.

1. PROJECT OVERVIEW

Located about 3.5 km south of the Sydney CBD, the Green Square urban renewal area is Australia's largest urban renewal project, delivering significant economic benefits, including 31,500 residential dwellings housing 60,000 new residents and catering for a permanent workforce of 22,000 by 2030. The population density in Green Square will be 50% higher than Pyrmont/Ultimo in inner Sydney, which has the highest current population density in Australia. Total urban renewal development costs are forecast to exceed $13 billion.

The Green Square Town Centre (GSTC) is located at the heart of this urban renewal area. Prior to development, this area was part of a series of ponds, swamps and creeks that drained through to Botany Bay via the Botany Aquifer and the Cooks River. Urbanisation changed the hydraulic character of the area, from a natural water reservoir and waterway corridor to an area of hazardous, flash flooding. As old industrial land gives way to modern high-density development, these existing flood hazards needed to be resolved to protect a growing community.

Sydney Water and City of Sydney share stormwater management responsibilities in the Green Square area under a complex ownership arrangement. Sydney Water is the owner and manager of the "trunk" drainage system, while City of Sydney owns and manages the "local" drainage system. Effective flood risk management required close collaboration and strategic alignment to arrive at a trunk drainage solution that meets the key project objectives of ensuring community safety during floods and enabling urban renewal. The preferred solution involved the installation of 2.5 km of new conduits with the specific aim of reducing high hazard flooding to low hazard in the 1% annual exceedance probability (AEP) flood.

With flow capacity of almost 30 cumecs and a capital value of $100 million, the GSSD is the largest brown-field urban drainage project in Sydney for 30 years. The City of Sydney, Sydney Water and NSW and Australian Governments are jointly funding the project.

The project presented many technical, logistical and community related challenges from solving complex hydraulic and geotechnical issues to installing large conduits in heavily built-up areas with extensive existing utility clashes and potential major traffic disruption. To meet the construction challenge, minimise the social impact and minimise cost the Drying Green Alliance (consisting of City of Sydney, Sydney Water, WSP, Seymour Whyte, UGL and RPS Manidis Roberts) adopted a design and construction method that uses tunnel boring machines to install 1800mm diameter pipes using microtunnelling.

Design and construction of the GSSD was awarded to the Drying Green Alliance following a competitive alliance process. Two alliance consortia were short-listed, on their respective concept designs and total out-turn costs based on the provided reference design and hydraulic models prepared. The Drying Green team developed an alternative design that used microtunnelling of twin and triple reinforced concrete jacking class pipes in parallel instead of open trenched box culverts.

Figure 1: GSSD plan showing retaining wall (left end) and microtunnel sections

2. PROJECT CHALLENGES

The area immediately south of Sydney CBD was originally low-lying swamps and sand hills and following development, has become naturally flood prone. The ground consists of sands interspersed with peat and clay with high groundwater and bedrock about 10 m below the surface. This required extensive dewatering and groundwater management in the microtunnelling up to 10 m deep for the GSSD and construction of local drain inlet structures. The ground is typically contaminated with unregulated fills, affecting microtunnelling progress. The microtunnel GSSD passed under a number of arterial roads with major utility crossings. The trenchless construction methodology ensured minimal impact on these critical roads and utilities including crossing under a 120-year old trunk sewer constructed of bricks.

The retaining wall between Maddox St and Huntley St is four to six metres away from existing warehouses and was constructed in sands interspersed with peat and contaminated fills with high groundwater, requiring a special design to provide a robust and

durable solution. Due to the proximity of the buildings, tight design criteria were placed on horizontal deflection and inclinometer and survey monitoring of the wall and adjacent buildings was undertaken during excavation to ensure no damage to the buildings.

2.1 DESIGN CRITERIA ON THE RETAINING SYSTEM

The design criteria on overall stability and ground movements for the retaining wall included:

1) The Factor of Safety (FOS) against slope failure:
    - In the short term (during construction): 1.2.
    - In the long term (permanent state): 1.5.
2) Maximum horizontal wall deflection: 30 mm.

The horizontal deflection limit of 30mm was set to limit vertical ground settlement under the warehouse buildings to an acceptable level so that the integrity of the building structure was protected.

The design of the proposed retaining wall system is in accordance with following design references/standards:

- CIRIA C760 Embedded retaining walls – guidance for economic design.
- AS5100.3 Bridge design—Foundations and soil supporting structures.
- Roads and Maritime Services (RMS) QA Specification R56 Ground Anchors.
- The Standards in the Structural Design Criteria Report 100-2262014B-WAT-REP008.

2.2 THE GROUND CONDITIONS

Subsurface conditions were interpreted based on the available geotechnical information from previous investigation work and additional geotechnical investigation carried out, which involved cone penetrometer testing (CPTu) and Marchetti Dilatometer Testing (DMT) comprising CPT/DMT-01 to CPT/DMT-08. CPT and DMT test locations were located side-by-side at each CPT/DMT location. No additional geotechnical testing was undertaken south of Huntley St (the last 100m of the GSSD) due to access restrictions.

Based on the available geotechnical information, a geotechnical model was developed as shown in the geotechnical long section in Figure 2. Between chainages of approximately CH100 to CH380 (from just south of Huntley Street to Maddox Street) the subsurface conditions were broadly described as comprising fill (very loose to loose sand) overlying a layer of alluvial soil comprising peat and clay. This layer is then underlain by a layer of medium dense to dense sand followed by a second alluvial clay layer. Between chainages 40 and 100 no geotechnical information was available and the profile just south of Huntley Street was assumed to extend to CH 40. The assumptions were later verified through exposure of the ground during construction.

The ground profile for each section analysed considered the nearest borehole or CPT/DMT test location as appropriate. The adopted geotechnical design parameters are summarised in Table 1 below.

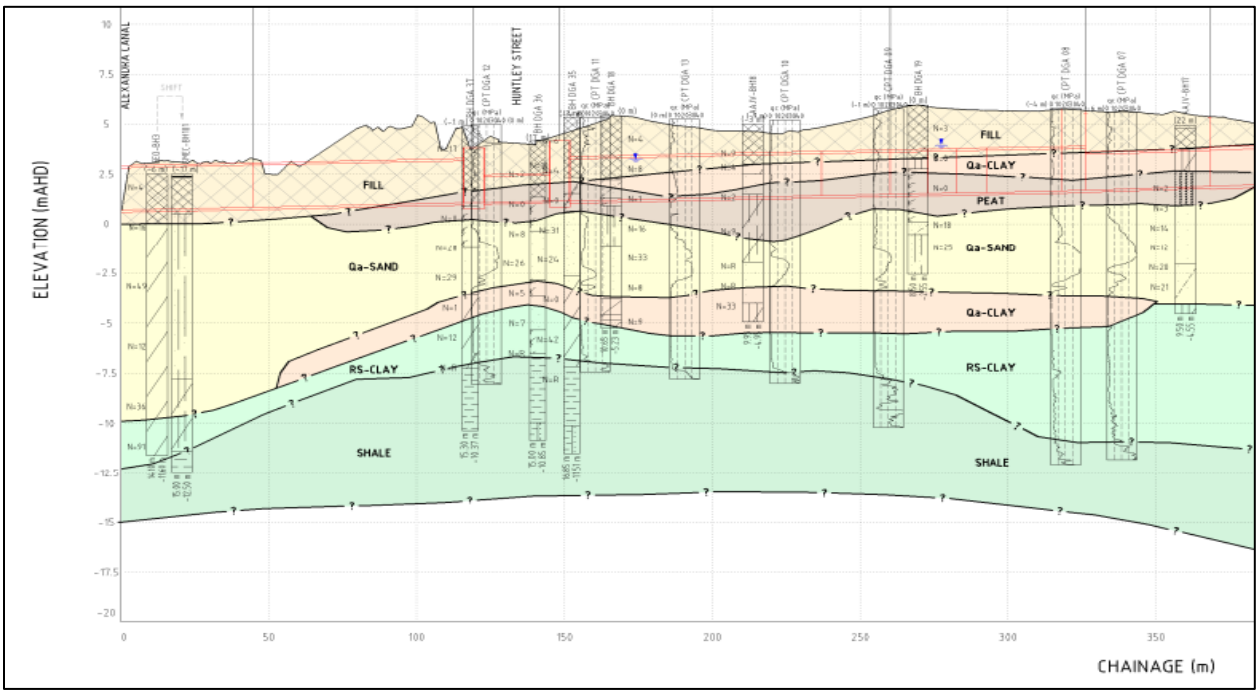

Figure 2: Interpreted geological profile at channel widening area

Table 1: Geotechnical design parameters

Material type	Unit weight (kN/m3)	Undrained shear strength (kPa)	Effective cohesion, c' (kPa)	Effective friction angle, ϕ' (°)	Young's modulus, E (kPa)
Top fill	17.0	-	0	30	7,500
Very loose to loose sand	16-18	-	0	30	7,500-30,000
Peat	16	15-20	0	25	3,000-6,000
Medium dense to dense	19	-	0	35	35,000-60,000
Alluvial clay	19	30 to 60	5	27	40,000-60,000
Residual Clay	20	100-200	10	27	50,000

3. CHANNEL WIDENING

3.1 OPTIONS ASSESSMENT

During the early design stage, the following options for the retaining wall were considered:

1) 600 mm diameter contiguous bored pile (CBP) wall at building side and 300mm CBP wall at existing channel side and temporary struts for construction of the box culvert.

2) 1000 to 1200 mm diameter cantilever CBP wall at the building side only for construction of the box culvert.
3) 2 to 3 rows of 400 mm slope stabilizing piles supporting a widened channel.
4) channel widening involving 600 mm diameter CBP wall with or without one layer anchor at wall top or reaction piles where an inclined anchor could not be installed due to proximity of the neighbouring property boundary.

Option 1 was ruled out due to constructability and time concerns. Option 2 was also ruled out because the site constraints and poor ground condition prevented using a larger piling rig for diameter of 1.0m and greater. Option 3 was not preferred due to the requirement to construct a shared path in the space between the cannel and buildings.

Option 4 was finally adopted with three scenarios on the retaining system:

- A Contiguous Bored Pile (CBP) Wall with one layer of permanent ground anchors. Where there was no room for anchorage, reaction piles (outside the active wedge) are proposed to provide the passive resistance to the CBP wall. At CH0-20 a cantilever wall was adopted due to the shallower excavation and relatively good ground conditions.
- A temporary sheet pile wall with ground anchors adjacent the existing buildings was required to enable the construction of capping beam for the CBP wall as the difference in levels did not allow a stable temporary slope.
- A cantilever temporary sheet pile wall in front of CBP wall at south of Huntley Street to form a temporary piling platform for installation of CBP wall.

Due to space restrictions between CH200 and CH310 inclined ground anchors could not be installed within the property boundary. A row of widely spaced reaction piles was adopted. The reaction piles were connected to the CBP pile wall by the longitudinal capping beam and transverse tie beams at 4m spacing. In selection of the retaining wall system, the consideration was given to site constraints, e.g. steep batter and proximity to the existing buildings. The objective of the design analyses was to determine the required size, spacing, embedment depths and anchor angle, length of the various elements of the system to meet the performance criteria outlined in Section 2.

3.2 THE FINAL DESIGN

The analysis of the excavation and lateral support system was based on the recommendations in CIRIA C760. The design comprised the following items:

- Serviceability Limit State (SLS) analysis to estimate deflection, forces and bending moments on the retaining wall using PLAXIS/WALLAP.
- Overall stability check using PLAXIS/WALLAP.
- Structural design on the structural elements of proposed retaining wall system based on the SLS analysis results from the PLAXIS/WALLAP analysis to determine the sizes of elements for retaining wall system, such as CBP piles, capping beam, sheet pile wall and ground anchors.

Above design procedure was iterated to confirm the stability of retaining system and that it could control the horizontal deflection at the existing structures within the design limits using the construction sequence below. PLAXIS program was frequently used to analyse deep excavations and embedded retaining walls, e.g. Zhang & Donohue (2014). PLAXIS 2-D was used on this project to assess the deep excavation effects on the adjacent buildings and structures and to calculate the wall forces for structural design.

The predicted deflections were the result of analysing the key construction stages at critical sections and determining the cumulative horizontal ground deflection adjacent the building at the completion of construction. A typical predicted deflection of the CBP wall from a 2-D FEM is shown in Figure 3 below.

3.3 PLAXIS MODEL/OUTPUT

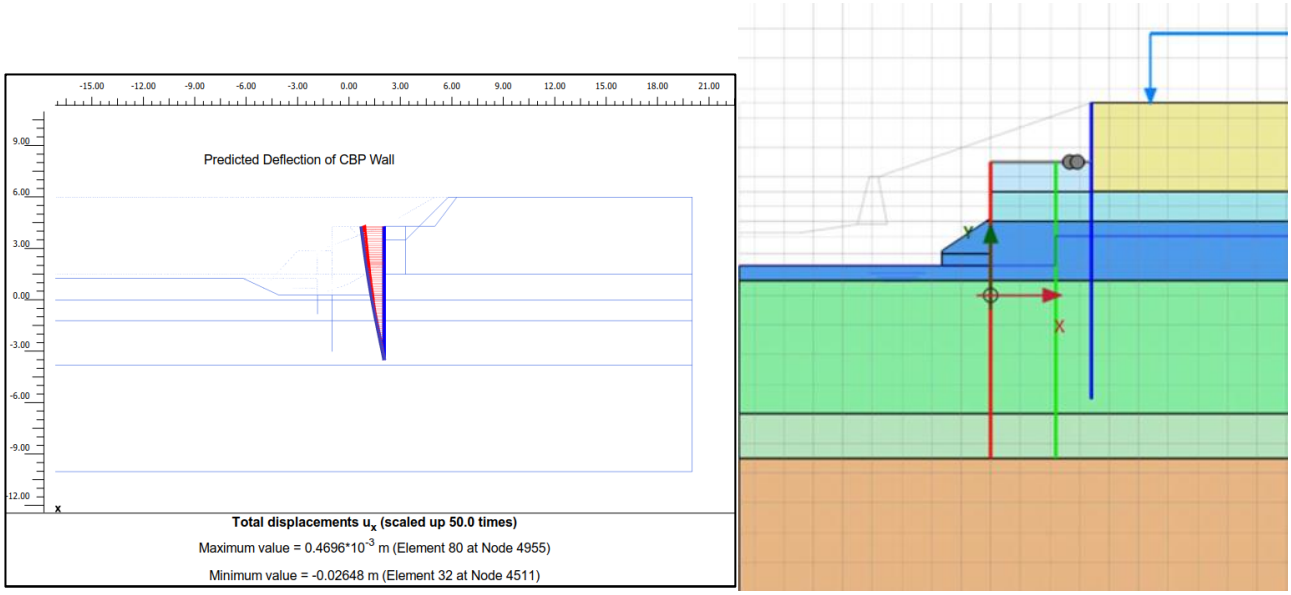

Figure 3: Left: Predicted CBP wall deflection at final excavation level; right: a typical Plaxis 2D model

3.4 ANCHOR TESTING

Anchor pull-out testing was conducted in accordance with RMS Specification R56 Ground Anchors to verify the pull-out resistance of the anchors before final design. Ultimate bond strength of 85 to 155 kPa was estimated from 6 anchor pull-out tests in soil. A lower bound resistance 85kPa was adopted for final design of the anchors.

3.5 INSTRUMENTATION AND MONITORING

An instrumentation and monitoring program was implemented during construction of the channel widening to manage construction risk during excavation in this high risk environment. Instruments included inclinometers, piezometers, building settlement survey markers and 3D survey prisms. The Alert Level of 18 mm and Work Suspension Level of 25 mm were adopted to the inclinometers behind the CBP wall; The sheet pile wall deflection Alert and Work Suspension Levels respectively were 11 mm and 15 mm respectively. All these instruments were installed with a base line reading taken prior to excavation works. The instruments were protected from damage from construction activities and monitored at a frequency of minimum twice per week during construction (from excavation to backfilling to final surface level). The frequency was adjusted during construction with review of the monitoring results. The monitoring frequency was reduced to weekly/fortnightly after backfilling to final surface level was completed.

The monitoring program showed wall deflections (max recorded ~ 15 mm) well within the predicted values and validated the design as robust and durable. Figure 4 shows a typical inclinometer deflection profile taken during construction and movements of prisms on the temporary sheet piles. The finished section of the retaining wall and a photo during construction are shown in Figure 5.

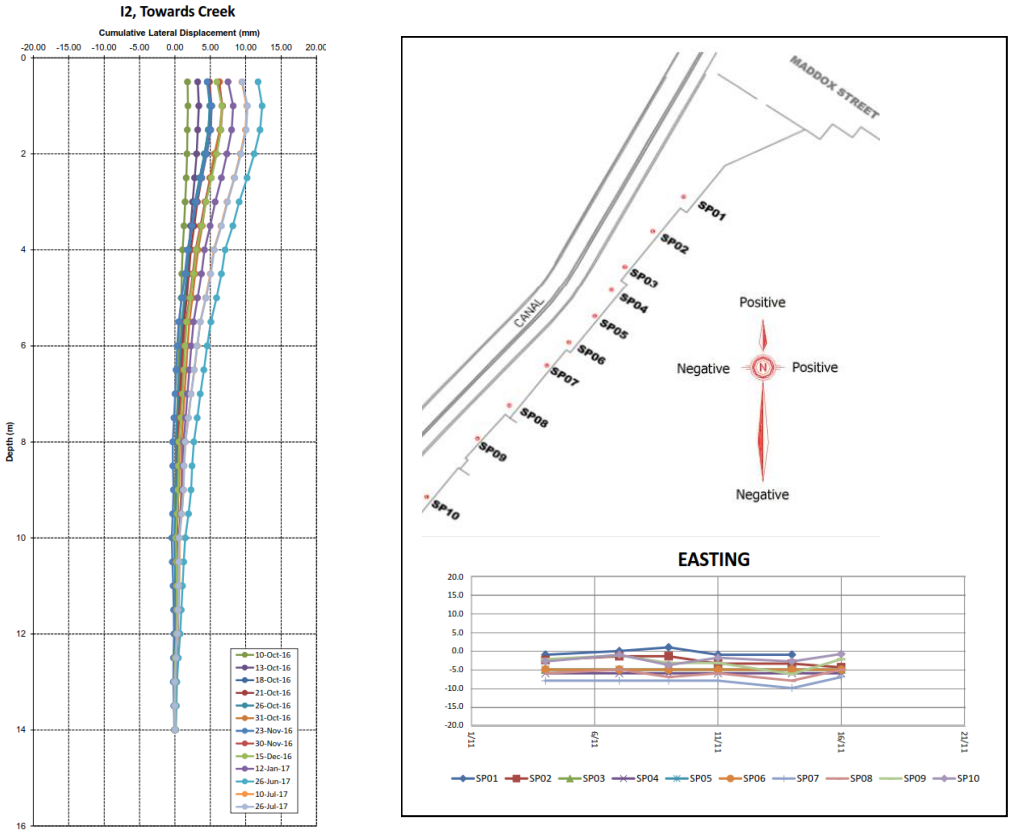

Figure 4: Left: a typical inclinometer plot; right – survey point showing lateral movements at wall top

Figure 5: Left: channel widening near Alexandra Canal outfall (artist's impression); right: photo during construction

4. MICROTUNNELLING

4.1 GROUND CONDITIONS

Ground conditions along the microtunnel drives for the GSSD comprised uncontrolled fill materials, overlying Quaternary deposits, residual soils and rock, as shown in Figure 6. The depositional nature of marine materials, and the uncontrolled nature of fill materials meant the variable ground profile presented significant geotechnical engineering challenges. These risks were managed by adequately scoping investigations, numerically modelling designs and adopting observational methods during construction.

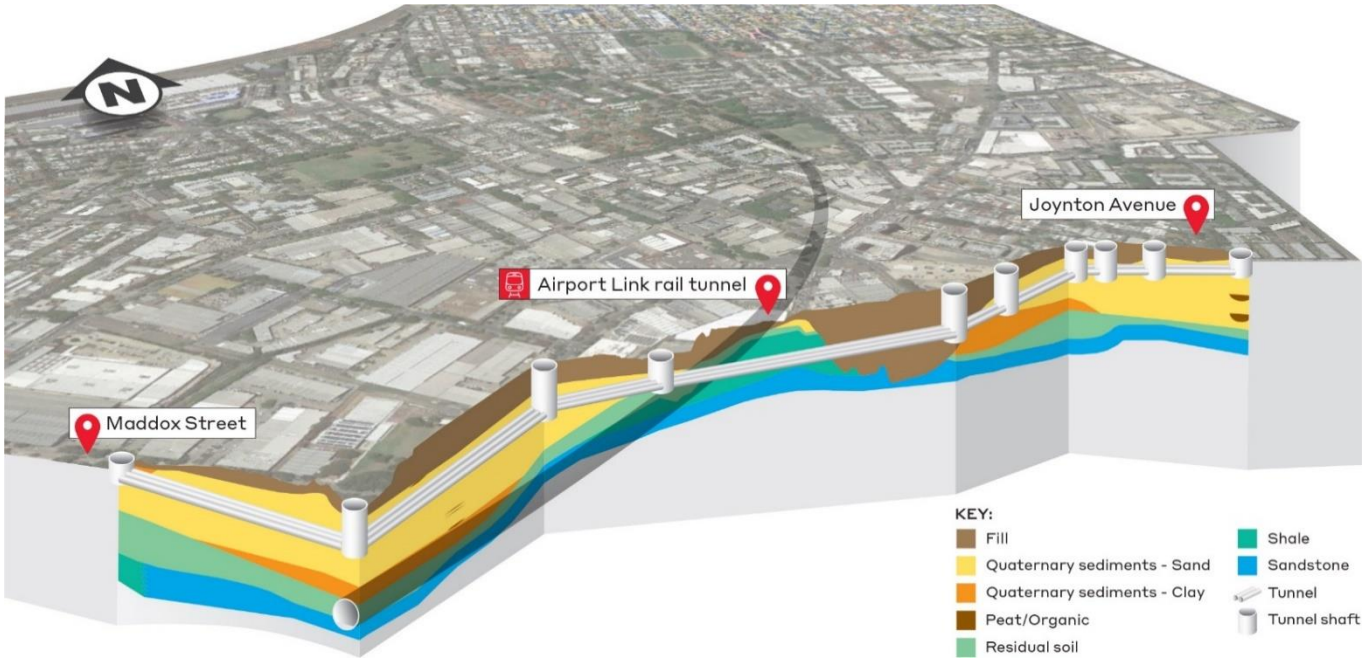

Figure 6: Schematic view of microtunnel drives showing route alignment and stratigraphy

4.2 TRENCHLESS SOLUTION

Conventional "dig and replace" solutions using box culverts were evaluated, however the pipeline geometry and poor ground conditions, difficult construction, impact on utilities and structures, spoil and dewatering disposal, as well as impact on the community and traffic made it undesirable. Subsequently, the Alliance developed its bid-winning proposition to change the stormwater drain's reference construction methodology from open trenching to a trenchless solution.

For the microtunnelling a boring machine (MTBM) was pushed through the ground by advancing multiple 1800mm diameter pipes from jacking shafts (caissons). Ground behaviour at the face of excavation depended on the composition of the ground. The project adopted a slurry MTBM which provides constant face pressure to counterbalance earth and groundwater pressures by pumping engineered drilling fluid into the MTBM face. The fluid pressure should be kept greater than the earth and groundwater pressures to avoid over excavation, settlement and sinkholes (Figure 7).

Iseki Microtunnel Boring Machine (MTBM) used the 'closed-face slurry shield' with no tail void grouting and bentonite to help the drilling process. The slurry spoil transport system provides earth pressure balance, which is controlled by adjusting the flow rate from the control room. Consequently, the rate of spoil removal from the drilling head's cutting face, directly relates to the

pace the drilling head advances. Varying the slurry cycle according to specific ground conditions, allows microtunnelling to continue in soils without reducing performance.

Figure 7: Microtunnel installation in caisson

4.3 CAISSON CONSTRUCTION

Using cast in-situ techniques, construction started on five caissons at ground level, and worked downwards, which was faster, quieter, and safer than traditional construction methods such as secant pile walls. Concrete segments were cast on-site to form rings (one on top of the other), which were then pushed below ground level to form the wall of the shafts 10–12-metres deep (Figure 6). The circular shape allowed the caisson was self-supporting by mobilising hoop stress without struts or ground anchors. To ensure this worked, the overall excavation sequence was given detailed attention to avoid asymmetry/unbalanced forces.

Given how close many of the construction sites were to buildings, roads, and trees, it was important to create as little disruption as possible for those living, working and commuting nearby. In-situ caisson construction proved well-suited for the project and required a significantly smaller site footprint than many traditional methods.

4.4 SETTLEMENT AND GROUND MOVEMENT ASSESSMENT

Microtunnel works had the potential to impact multiple third-party assets comprising over-ground structures, buildings, underground structures and utilities within tight space constraints. Each asset had to be assessed for the impact from predicted ground movement to manage impacts within acceptable limits. Where needed, mitigation measures were developed and implemented to ensure all third-party assets were not impacted throughout construction. As an additional complication, tunnelling was carried out close to the Airport Line rail tunnel, which extends from Sydney CBD to Sydney Airport (Figure 8). Predicting ground movement and assessing impacts followed the well-tested and understood Gaussian curve empirical methods for bored tunnels, which was 1 to 5 mm with a similar volume loss. Finite-element analysis was used next to critical locations to create a combined ground displacement model, which could be used to assess the level of impact on adjacent assets.

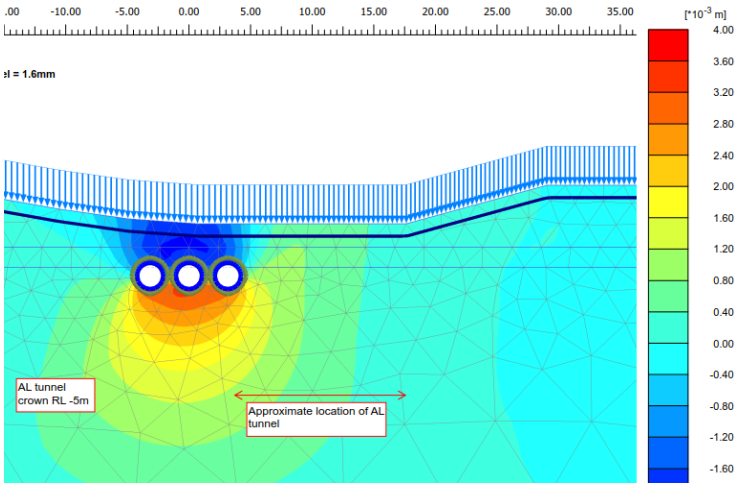

Figure 8: Typical microtunnel section showing estimated displacement (U_Y)on Airport Line rail tunnel using Plaxis 2D

4.5 MICROTUNNELLING BENEFITS

Pipe jacking and microtunnelling systems reduce the social and environmental disturbance when installing services in urban areas. Benefits are summarised in Table 2 and included:

- Minimum impact on more than 120 underground utilities crossing the GSSD alignment.
- Minimum impact on existing roads and developments (no open cut).
- Minimum environmental impact (spoil and dewatering).
- Minimum community impact (no open cut).
- Cost-effective hydraulic solution.

Table 2: Comparison with conventional trenching at depth, between Maddox Street and Joynton Avenue

Item	Microtunnelling	Typical Trench
Spoil volume	10,000 m^3	80,000 m^3
Groundwater volume removed	40kL/day	1,000 kL/day
Footprint disturbed	~8,000 m^2	~25,000 m^2
Services (diverted or supported)	5	86
Greenhouse gas	Saved 28% CO_2 emissions	

4.5 LESSONS LEARNED

The microtunnelling section of this project was particularly difficult in the poor ground conditions, with tight logistical constraints, contamination and numerous obstructions. In review of the chain of events, the authors offer the following reflections:

- Address risk of obstructions in landfill prior to route selection.
- Confirm every known utility, existing foundation, or abandoned structure is clear of the alignment, prior to tunnelling.
- Install instrumentation points at appropriate depths along the alignment for feedback regarding MTBM performance. When alarm values are reached, take appropriate action.
- Slurry composition and slurry management are critical to reducing ground loss in mixed face conditions.

5. CONCLUSIONS AND RECOMMENDATIONS

The GSSD is a complex project that was essential to eliminate the high-hazard flooding from the area to deliver a livable urban renewal of this inner-city area. It was delivered through the cooperation of local and state government, construction contractors and designers in an alliance framework.

This paper discusses the major challenges and innovative engineering solutions of the design and construction of the 300 m long earth retaining system to meet the tight design criteria in order to protect existing warehouse buildings, underground services and to accommodate the tight site constraints, e.g. steep batters, weak ground conditions, a very narrow corridor between existing buildings and the proposed retaining wall which limits the use of ground anchors.

The Alliance developed a robust design which involved the following:

- Suitable in-situ testing (CPT and DMT) to better understand the ground profile and to estimate realistic design parameters.
- Innovative retention solutions including cantilever, CBP wall with anchor and CBP wall with reaction pile.
- Advanced numerical modelling to assess ground and structural deformations in staged construction, construction testing and verification.
- Comprehensive instrumentation and monitoring system for construction control.

The monitoring data indicated that the retaining wall deflection, building lateral displacement and settlement were well within the allowable limits, which proved that the design was robust and durable.

Changing the construction methodology of the stormwater drain from open trenching to a trenchless solution achieved close to $A100 million in project cost savings when compared with the original design solution, and significantly reduced environmental impacts and community disruption. The adopted microtunnelling methods successfully addressed the site ground engineering challenges including difficult ground conditions and landfill, while also addressing construction impacts on adjacent infrastructure.

6. ACKNOWLEDGEMENTS

The authors acknowledge the contributions of the all parties involved in this technical paper. Any opinions, findings, conclusions and recommendations in this paper are those of the authors only, and do not necessarily reflect the views of Sydney Water and the Council of Sydney.

7. REFERENCES

Gaba A.R., et al. (2017). Guidance on Embedded Retaining Wall Design. CIRIA Report C760

Taylor N., Kent D. Woodbury K., Lewis M. & Muralitharan S. (2017). Green Square: Protecting communities and enabling urban renewal through effective flood risk management.

RMS QA Specification R56 (2012) Ground Anchors (Schedule of Rates)

Zhang H & Donohue J (2014), Case Study: Design of a diaphragm wall based on 3D FEM for TBM launching in soft clay on Brisbane Airport Link project, *Earth Structures and Retention Conference 2014*, 27-28 May 2014, Sydney, Australia.

A NOVEL MULTIPLE-LINER DESIGN FOR PREVENTING DESICCATION OF GEOSYNTHETIC CLAY LINERS

Bowei Yu[1] and Abbas El-Zein[2]
[1] *PhD Candidate, School of Civil Engineering, USYD, bowei.yu@sydney.edu.au*
[2] *Professor, School of Civil Engineering, USYD, abbas.el-zein@sydney.edu.au*

ABSTRACT

Geosynthetic clay liners (GCLs) covered by geomembranes (GMB) often constitute a major component in barrier systems. They are used in waste containments systems such as landfills, brine ponds and solar ponds. In many of these cases, high temperatures can develop as a result of exothermic biodegradation or direct solar radiation and can cause significant desiccation of the bentonite in the GCLs. In addition, the self-healing ability of bentonite may be compromised by exposure to chemically aggressive permeants that are commonly found in such applications.

A new multiple-liner design is proposed in this paper, with two GMB-GCL composite liners sandwiching one layer of geocomposite (GC). The new design is able to actively hydrate top and bottom GCLs through the middle GC layer with clean water. A set of column model experiments simulating a typical bottom profile under a brine pond were conducted to investigate GCL hydration before and after continuous heating at 78±1°C for 14 days. The results were compared to the more conventional GCL-GMB designs. The findings revealed that the new multiple-liner system speeds up hydration of bentonite in the GCL by a factor of more than 3, increase its water content at the end of the hydration stage by up to 50%, and prevent its desiccation when exposed to high temperatures.

Key words: GCLs, desiccation, hydration, multiple-liner, active hydration

1 INTRODUCTION

Geosynthetic clay liner (GCL) is generally composed of a thin layer of powder or granular bentonite clay that is either glued to a geotextile or sandwiched by two geotextiles. Although the thickness of GCLs is typically than 1 cm, they exhibit extremely low hydraulic conductivities (~10^{-10} to 10^{-11} m/s) when sufficiently and properly hydrated (Bouazza, 2002; Rowe, 2005). GCLs have been widely adopted together with geomembrane (GMB), as the GCL-GMB composite liner system, to serve as barriers in waste containing facilities such as landfills and other industrial reservoirs like brine ponds and solar ponds.

Traditionally, before coming into service, GCLs are first covered with GMB and a thin protective layer of soil, then allowed hydrate from the subsoil on site, before any waste or contaminants are placed in the system. A gravimetric water content of around 100% or more is usually required for acceptable performance. Studies have revealed that reaching such a hydration require consideration of subsoil characteristics, including grain distribution (Rayhani et al., 2011; Anderson et al., 2012; Chevrier et al., 2012), initial water contents (Southen and Rowe, 2005; Anderson et al., 2012), pore water chemistry (Rowe, 2005; Bouazza and Gates, 2014), as well environmental and operational factors such as temperature and stress conditions (Chevrier et al., 2012; Barclay and Rayhani, 2013; Sarabadani and Rayhani, 2014) during the liner placement and operation.

On the other hand, in many cases, GCLs are exposed to elevated temperatures during their service life. For example, biodegradation in landfills can lead to temperatures higher than 50°C in the containment chamber (Rowe, 2005; Southen and Rowe, 2005), and direct exposure to sunshine increase liquid temperatures up to 90°C in industrial waste ponds (El-Zein et al., 2013). Exposure to high temperature can lead to dehydration of the GCLs and eventually desiccation cracks can develop throughout the bentonite layers (Southen and Rowe, 2005; Azad et al., 2011; Ghavam-Nasiri, 2017; Ghavam-Nasiri et al., 2017; Yu and El-Zein, 2019). Yu and El-Zein (2019) reported that the desiccation risks were especially high when highly permeable sands are selected as the subsoil, as temperatures as low as around 40°C can lead to significant desiccation of a GCLs, even those with high bentonite mass per unit area (M_a).

In this paper, a new multiple-liner design consisting of two sets of GCL-GMB and a layer of geocomposite (GC) is proposed as a way of preventing desiccation under thermal gradients, and consequent loss of performance. The new design was tested using a set of instrumented soil column experiments that replicate the operation of a barrier system in brine ponds. In the tests, the new liner design was subjected to the high temperatures observed in such systems during daytime (78°C) for 14 days. The performance of the new design was compared to that of a more conventional GCL-GMB composite liner system, which had been found in the past to develop severe desiccation during the same tests.

2 DESCRIPTION OF NEW DESIGN

Conventional composite liner system design has been revealed to be prone to desiccate when exposed to high temperature applications and Figure 1 shows samples of these designs. The simplest design with GCL-GMB liners shown in Figure 1a can show severe desiccation in GCL when subjected to high temperatures (Southen and Rowe, 2005; Ghavam-Nasiri, 2017; Yu and El-Zein, 2019). Bouazza et al. (2017) suggested an extra layer of geocomposite liner (GC) may decrease the top temperature applied on the top of GCL and thus might decrease the risk of GCL desiccation (see Figure 1b). Further investigations show that in certain conditions (i.e., high temperature, low overburden stress and highly permeable subsoils) the extra GC can decrease the top temperatures but not able to avoid the desiccation (Yu and El-Zein, 2019). More complex design like double composite liner system (Figure 1c) has also been tested and desiccation was also observed in the top GCL layer (Azad et al., 2011).

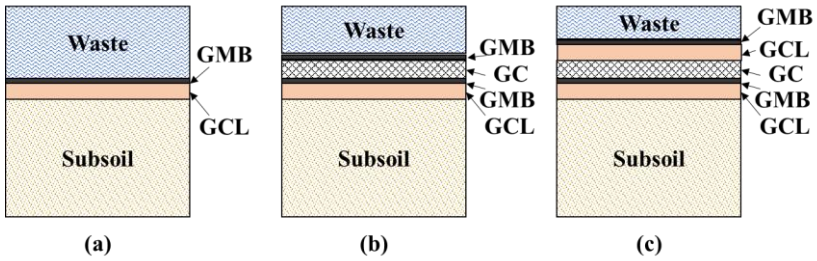

Figure 1: Conventional composite liner system designs

The new multiple-liner design presented in this study (see Figure 2), is modified from the double composite liner system in Figure 1c by introducing two changes. First, the secondary GMB is placed below rather than above the secondary GCL. Second, artificial hydration is conducted through the geonet, now that both GCLs are in direct contact with the geonet. Hence, in the new design, the top and bottom GCLs are sandwiched by two GMBs, making possible artificial hydration (by liquid water or water vapor) through the centre GC layer. In addition, the top GMB layer prevents the contaminant liquids from entering the liner, while the bottom GMB adds extra protection against any leakage and/or diffusion of contaminants through the liner. In conventional designs, no GMB is placed between the GCL and the subsoil because it would prevent hydration of the former by the latter, a requirement that is obsolete in the proposed design. Artificial hydration has the following advantages: (1) avoiding of cation exchanges due to any salinity in the subsoil's pore water; (2) ensuring sufficient and quicker hydration before the liner system is put in use; and (3) keeping GCLs in hydrated condition during the service life by supplying water or vapor where necessary.

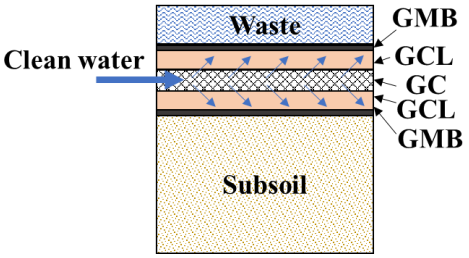

Figure 2: A schematic diagram of the novel multiple-liner design

3 MATERIALS AND METHODS

3.1 GCL AND SUBSOILS

The GCL used in this study was a needle-punched and thermally reinforced type, with granular Na-bentonite, provided by Terrafix Geosynthetic Inc. Canada. The basic properties and configurations of the GCL are shown in Table 1. Its soil-water characteristic curve (SWCC) and thermal conductivity (λ_k) variations under different water contents can be found in Figure 3.

Table 1: Basic properties and configuration information of GCL used in this study

	Values or Descriptions
Top Geotextile	Nonwoven
Dry mass per unit area (g/m^2)	200 (MARV) 255 (Tested)
Carrier Geotextile	Scrim Reinforced Nonwoven
Dry mass per unit area (g/m^2)	200 (MARV) 249 (Tested)
Bentonite type	Granular Na-bentonite
Swelling indexes (mL/2g)	>24
Dry mass of bentonite per unit area (g/m^2)	3660 (MARV) 4341 (Tested)

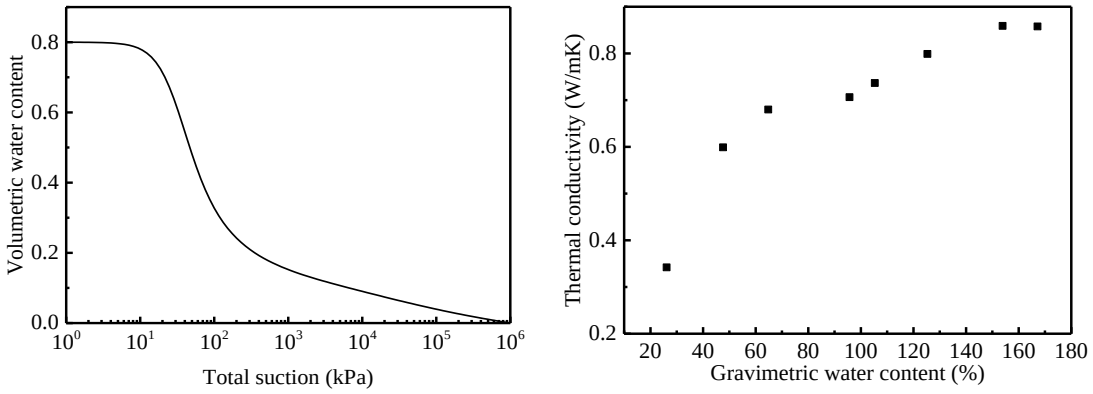

(a) SWCC (b) Thermal conductivity

Figure 3: Hydraulic and thermal properties of GCL used in this study

The subsoil selected in this study was a well-graded river sand (SW) collected from Sydney, Australia. Previous studies have shown that this specific type of sand can sufficiently hydrate GCL specimens in 7-8 weeks thanks to its low water retention and high hydraulic conductivities (k_s=3×10^{-4} m/s). The subsoil was compacted into the columns with a predetermined dry density (ρ_d=1.78 g/cm^3) and water contents (w=11%) as illustrated in detail in Ghavam-Nasiri et al. (2017) and Yu and El-Zein (2019).

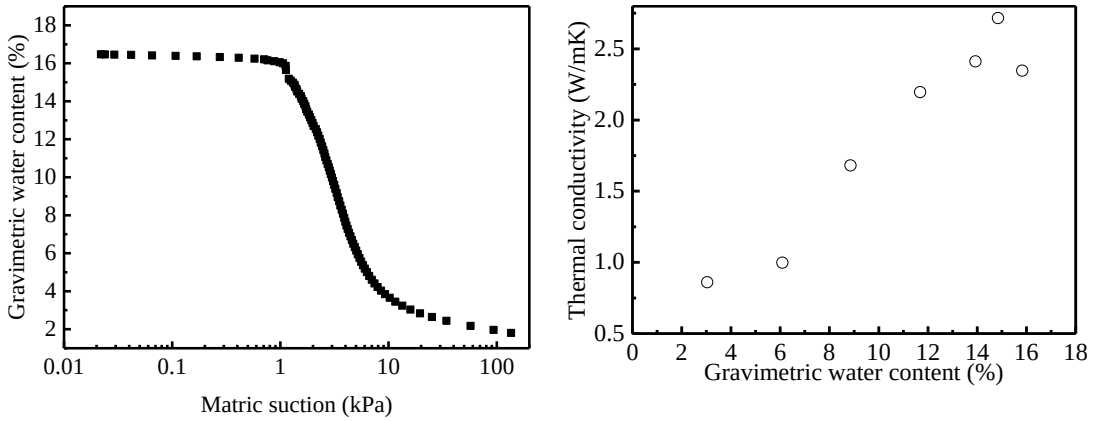

(a) SWCC (b) Thermal conductivity

Figure 4: Hydraulic and thermal properties of subsoil used in this study

3.2 COLUMN MODEL EXPERIMENTS

The column model apparatus (Figure 5a) adopted in this paper was similar to the one described in Ghavam-Nasiri (2017) and Yu and El-Zein (2019) but modified to allow the testing of the new design as described in the next paragraph. For details on this apparatus, readers are referred to these two sources. For tests on conventional GCL-GMB composite liners, GCL specimens were installed in the column with as-arrived water contents (w≈6-9%) and hydrated from subsoils under

a 20 kPa overburden stress for 7 weeks. After that, the heating stage started and the temperature on top of GCL was kept at 78±1°C for 14 days, then the specimen was removed, and x-rayed to assess the extent of desiccation. At the end of each stage (hydration+ heating), the specimens were carefully taken out and their weight and height were measured.

To investigate the performance of the new multiple-liner design, several modifications were made to enable the active hydration of GCLs, as shown in the close-up in Figure 5b. A pipe is run through a slot on the side to connect the top chamber to the water supply, in order to use external water supply to irrigate/hydrate the GCLs. The slot connection was designed so as to allow the pipe to move freely in the vertical direction as specimens' height changed during the tests. The hydration stage elapsed for 14 days, when the LVDT suggested no further hydration swellings were observed from the specimens (see Figure 6); hence, reducing hydration time to less than one third of its value under passive hydration from the subsoil. The heating stage was made to last for 14 days, which was the same as tests for GCL-GMB composite liners.

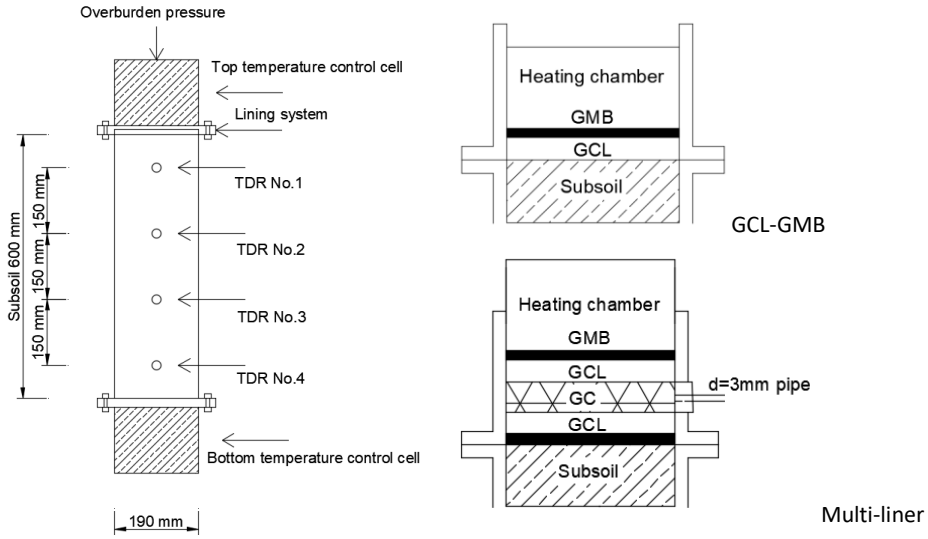

(a) Column test appratus (b) Close-up of liner installation

Figure 5: Design diagram of the column tests with close-up on composite liner installations

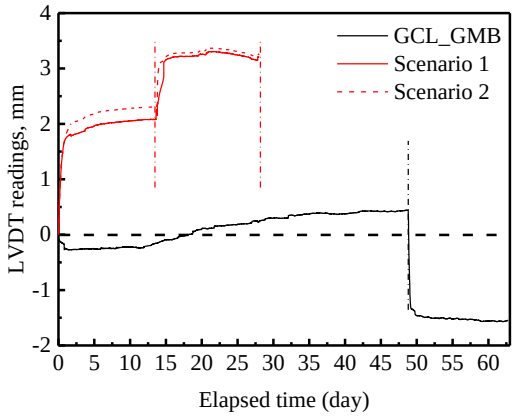

Figure 6: Comparison of stable temperature profile during heating stages in column test

Two scenarios (namely scenario 1 and scenario 2) were tested in the column model tests for the multiple-liner design. The differences between the two scenarios occurred at the heating stages whereby, under scenario 1, active irrigation continued while, in scenario 2, water supply was cut off prior to the heating stage.

3.3 X-RAY IMAGING TESTS

X-ray imaging technology was used to detect the desiccation crack patterns in GCL specimens in the DynamiX laboratory of the University of Sydney, Australia. Specimens were carefully put on a detection board located 1.2 m away from the X-ray source with a small filament. The X-ray power was kept at 60 kV and 2 mA, which was consistent with Yu and El-Zein (2019). For specimens that show clear crack patterns, the Particles (Pores) and Cracks Analysis System (PCAS

v2.319) was adopted to conduct image analysis on the crack properties, e.g., the crack areas, crack width, etc. (Liu et al., 2011 and 2013; Yu and El-Zein, 2019).

4 RESULTS AND DISCUSSION

4.1 MOISTURE AND TEMPERATURE PROFILE VARIATIONS DURING COLUMN TESTS

The variations of water contents in subsoils recorded by the four TDR sensors are shown in Figure 7. Results for the conventional GCL-GMB liner, including a repetition test, can be seen in Figure 6a. The consistent patterns of the two tests confirm the reliability and repeatability of the column model tests. In GCL-GMB liner test, heating starts from the 49th day when temperature on top of the composite liner system is increased to 78±1^{o}C. Within several hours significant changes can be observed in the top three sensors, especially for TDR sensor No.1 (changes from 0.12 to 0.15 and then gradually falls back to around 0.13) and No.3 (increases from 0.22 and 0.23, then gradually up to 0.26). The results are similar to those reported in Yu et al. (2018) and Yu and El-Zein (2019), for a powdered-bentonite GCL. Specifically, the sharp increase in TDR No.1 indicates downward moisture movements from GCL and upper subsoil caused by the high temperature.

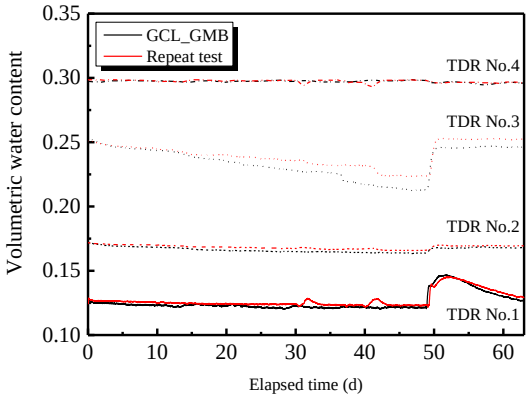

(a) GCL_GMB group

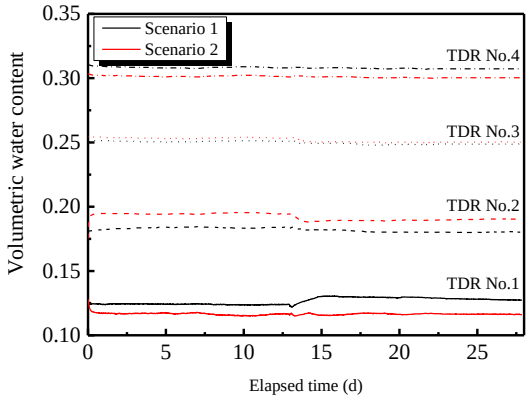

(b) Multiple-liner design group

Figure 7: Comparison of subsoil moisture redistribution during column test

Very different patterns are revealed by the tests on the proposed multiple liner under both working scenarios. Once the heating stage starts around the 13th day, much slower and gentler increases are recorded by TDR sensor No.1, suggesting only liquid water and vapour at top of the subsoil sand, not the liner, are driven down by the high temperature, because water in the liner system is contained by the top and bottom GMBs.

The temperature profiles at the heating stage are plotted in Figure 8. Averages of the last 7 days sensor reading values are shown here, because temperatures along the column depth remained stable during the last week of heating in all tests. Figure 8 shows a non-linear temperature profile in all tests. In the subsoils (depth<0), slightly lower temperatures occur for the multiple liner, compared to the GCL-GMB liner, due to the larger thickness of multiple-liner system. The large decreases in temperatures (lower from 78±1^{o}C to around 25-28^{o}C) at the top of columns suggest very high temperature gradients can be found between the top and bottom of liner system, which can lead to significant desiccations of GCLs in GCL-GMB composite liner system under similar conditions, reported by Yu et al. (2018) and Yu and El-Zein (2019).

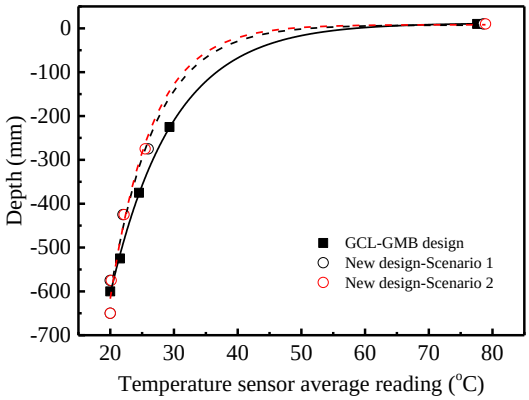

Figure 8: Comparison of stable temperature profile during heating stages in column test (average of last 7 days)

4.2 LINER PROPERTY VARIATIONS

The LVDT sensor data collected from the column tests are shown in Figure 8. The LVDT sensor data cannot be regarded as the actual liner thickness variations because other factors such as subsoil consolidation and column diameter variation due to temperature also contribute to their change (Yu et al., 2018). However, LVDT readings are still expected to be a good indicator of the swelling or shrinkage of the clay layers in the liner system. At the hydration stage, in the conventional GCL-GMB system, where GCLs hydrate from subsoils, after the initial consolidation caused by the 20 kPa overburden pressure, very little swelling occurs in the first 14 days. Once the heating stage starts at 49th day, instant drop in LVDT reading indicates fast shrinkage and desiccation.

LVDT data patterns for the new multiple liner design are completely different. GCLs start swelling almost as soon as external water supply is introduced into the GC layer. The fast hydration of the two multiple-liner groups end around day 2 and they both reach to around 1.8 to 2 mm, which are significantly higher than the 0.5 mm reached by GCL-GMB group after 49 days hydration, confirming the efficiency of irrigation/hydration in the new design. The GCLs in these two groups keep swelling at a slower rate for another 11 days until they stabilize around 2 mm. What's more, significant increase in LVDT data upon the heating stage indicate the new designs do prevent the dehydration of GCLs with the help of the bottom GMB. Although from Table 2 it can be seen that under both scenarios GCLs showed increasing water contents after 14 days heating, the significant differences in final stage water contents found in GCLs from the two scenarios weren't accompanied by differences in the LVDT readings. Therefore, the observed sudden increase in LVDT readings was more likely resulted from the heat expansion of GCLs.

The hydraulic and swelling states of the GCLs at the end of the irrigation/hydration and heating stages can be seen in Table 2. For the GCL in the GCL-GMB group, it takes 49 days to hydrate to w=94.5% (S_r=74.1%). On the other hand, after 13 days of hydration, all GCLs in the multiple-liner groups exceed the water content of 100%. After 14 days of heating, significant water content drop can be seen in GCL from GCL-GMB group, down to a residual w of 5.9%. On the other hand, GCLs in both testing scenarios of multiple-liner design show increases of w after 14 days heating, which confirm the LVDT sensor data.

Table 2: GCL index variations during column tests

Designs and Scenarios	Properties	Initial conditions	End of hydration stage	End of 14 days heating stage
GMB-GCL	Water content, w (%)	7.9	94.5	5.9
	Height (mm)	7.4	9.0	7.5
Multiple liner design Scenario 1	Water content, w (%) Top Bottom	10.4 9.8	117.0 110.3	183.7 191.1
	Height (mm) Top Bottom	6.9 6.7	8.5 8.8	12.7 13.1
Multiple liner design Scenario 2	Water content, w (%) Top Bottom	11.8 10.2	109.9 116.3	115.5 133.5
	Height (mm) Top Bottom	6.3 6.8	9.2 9.1	10.1 10.0

GCLs in scenario 1 show the largest increases of w, as moisture in the top GCL increases from 117.0% to 183.7% and bottom GCL increase from 110.3% to 191.1%, thanks to the continuous external water supply during the heating stage. In scenario 2, as water supply is cut out during heating, the GCLs can only obtain moisture from the water left in

the GC layer. Therefore, the increase in *w* is more moderate in this case with moisture in the top GCL rising slightly from 109.9% to 115.5% and from 116.3% to 133.5% in the bottom GCL. More importantly, the results confirm that the new design, which places the GCLs between two GMB has succeeded in preventing water escape out of the liner system.

4.3 DESICCATION AND HEALING OF GCLS

Photos of the vertical sides of the GCLs after heating are shown in Figure 9. While cracks can be directly observed in the bentonite of the GCL-GMB design, all GCLs in the multiple-liner design remain sufficiently hydrated and their bentonites in gel form where with no cracks apparent. An X-ray photo of the desiccation cracks of GCL at the end of the heating stage of GCL-GMB is shown in Figure 10, which shows cracks develop throughout the bentonites as water is driven out by the temperature gradient. Details on the crack properties are shown in Table 3. For GCLs, remaining sufficiently and properly hydrated is critical to remain their hydraulic barrier performances when they are exposed to chemical aggressive conditions, as many previous studies have revealed (Petrov and Rowe, 1997; Lin and Benson, 2000; Bouazza et al., 2007).

a. GCL-GMB b. Multi-liner-Scenario 1 c. Multi-liner-Scenario 2

Figure 9: GCL side shots after 14 days heating stage

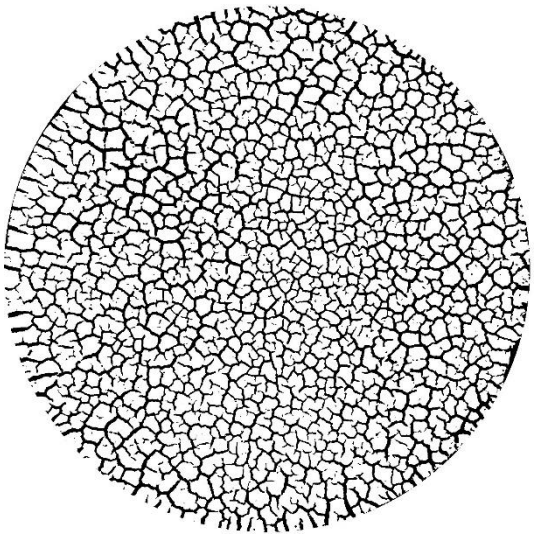

Figure 10: Desiccation cracks of GCL in GCL-GMB group

Table 3: Desiccation information of GCLs after column tests

	Water content, *w* (%)	Desiccation crack	Crack area proportion (%)	Average crack width (mm)
GCL-GMB	5.9	Y	28.44	0.728
Multiple-liner				
Scenario 1: Top GCL	173.2	N	/	/
Bottom GCL	181.0	N	/	/
Scenario 2: Top GCL	106.5	N	/	/
Bottom GCL	125.6	N	/	/

5 CONCLUSIONS

A new type of multiple-liner design with two different operation modes are proposed to prevent desiccation when liners are exposed to thermal gradients. The proposed design is characterised by two key modifications compared to conventional double composite liners: a) geomembranes (GMBs) are placed at the top and bottom of the liner to minimise dehydration under thermal gradients and b) a geocomposite (GC) layer allows faster artificial hydration of the geosynthetic clay liners (GCL) with clean water. Experimental testing was conducted to compare the performance of the proposed design to that of a more conventional GMB-GCL liner. The results confirmed the advantages of the proposed design, namely faster moisture uptake, higher water content at the hydration stage and no loss of moisture at the heating stage, even when no irrigation is provided after heating starts. Future research needs to confirm our findings which can be relevant to other types of GCLs (e.g., powder-bentonite). In addition, conducting field testing for new designs would be necessary to confirm their practicality.

6 REFERENCES

Anderson, R., Rayhani, M.T. and Rowe, R.K. (2012). Laboratory investigation of GCL hydration from clayey sand subsoil. *Geotextiles and Geomembranes*, *31*, pp.31-38.

Azad, F.M., Rowe, R.K., El-Zein, A. and Airey, D.W. (2011). Laboratory investigation of thermally induced desiccation of GCLs in double composite liner systems. *Geotextiles and Geomembranes*, *29*(6), pp.534-543.

Gaudin, C., Simkin, M., White, D.J. and O'Loughlin, C.D. (2010). Experimental investigation into the influence of a keying flap on the keying behaviour of plate anchors. *Proc. 20th Int. Offshore and Polar Engineering Conf.*, Beijing, China, 533-540.

Barclay, A. and Rayhani, M.T. (2013). Effect of temperature on hydration of geosynthetic clay liners in landfills. *Waste Management & Research*, *31*(3), pp.265-272.

Bouazza, A. (2002). Geosynthetic clay liners. *Geotextiles and Geomembranes*, *20*(1), pp.3-17.

Bouazza, A., Jefferis, S. and Vangpaisal, T. (2007). Investigation of the effects and degree of calcium exchange on the Atterberg limits and swelling of geosynthetic clay liners when subjected to wet–dry cycles. *Geotextiles and Geomembranes*, *25*(3), pp.170-185.

Bouazza, A., Ali, M.A., Rowe, R.K., Gates, W.P. and El-Zein, A. (2017). Heat mitigation in geosynthetic composite liners exposed to elevated temperatures. *Geotextiles and Geomembranes*, *45*(5), pp.406-417.

Bouazza, A. and Gates, W.P., 2014. Overview of performance compatibility issues of GCLs with respect to leachates of extreme chemistry. *Geosynthetics International*, *21*(2), pp.151-167.

Chevrier, B., Cazaux, D., Didier, G., Gamet, M. and Guyonnet, D. (2012). Influence of subgrade, temperature and confining pressure on GCL hydration. *Geotextiles and Geomembranes*, *33*, pp.1-6.

El-Zein, A., Ghavam-Nasiri, A., Bouazza, A. and Rowe, R.K. (2014). Performance of GCLs in brine ponds for coal-seam gas extraction sites: An investigation. In *7th International Congress on Environmental Geotechnics: iceg2014* (p. 1209). Engineers Australia.

Ghavam-Nasiri, A. (2017). Thermo-Hydro-Mechanical Behaviour of Composite Geosynthetic Lining Systems under High Temperature and Low Pressure.

Ghavam-Nasiri, A., El-Zein, A., Airey, D. and Rowe, R.K. (2017). Hydration and desiccation of geosynthetic clay liners in composite lining systems under brine pond conditions: A laboratory investigation. In *Proceedings of the 2nd Symposium on Coupled Phenomena in Environmental Geotechnics (CPEG2), Leeds, UK*.

Lin, L.C. and Benson, C.H. (2000). Effect of wet-dry cycling on swelling and hydraulic conductivity of GCLs. *Journal of Geotechnical and Geoenvironmental Engineering*, *126*(1), pp.40-49.

Liu, C., Shi, B., Zhou, J. and Tang, C. (2011). Quantification and characterization of microporosity by image processing, geometric measurement and statistical methods: Application on SEM images of clay materials. *Applied Clay Science*, *54*(1), pp.97-106.

Liu, C., Tang, C.S., Shi, B. and Suo, W.B. (2013). Automatic quantification of crack patterns by image processing. *Computers & Geosciences*, *57*, pp.77-80.

Petrov, R.J. and Rowe, R.K. (1997). Geosynthetic clay liner (GCL)-chemical compatibility by hydraulic conductivity testing and factors impacting its performance. *Canadian Geotechnical Journal*, *34*(6), pp.863-885.

Rayhani, M.T., Rowe, R.K., Brachman, R.W.I., Take, W.A. and Siemens, G. (2011). Factors affecting GCL hydration under isothermal conditions. *Geotextiles and Geomembranes*, *29*(6), pp.525-533.

Rowe, R.K. (2005). Long-term performance of contaminant barrier systems. *Geotechnique*, *55*(9), pp.631-678.

Sarabadani, H. and Rayhani, M.T. (2014). Influence of Normal Stress on Hydration of GCLS from Subsoil. *The Journal of Solid Waste Technology and Management*, *39*(4), pp.292-303.

Southen, J.M. and Rowe, R.K. (2005). Laboratory investigation of geosynthetic clay liner desiccation in a composite liner subjected to thermal gradients. *Journal of Geotechnical and Geoenvironmental Engineering*, *131*(7), pp.925-935.

Yu, B., El-Zein, A., and Rowe, R. K. (2018). Effect of bentonite mass per unit area on the desiccation of geosynthetic clay liners under high temperature and low overburden pressure. In *Proceedings of 11th International Conference on Geosynthetics (11ICG)*, Seoul, Korea.

Yu, B. and El-Zein, A. (2019). Experimental investigation of the effect of airgaps in preventing desiccation of bentonite in geosynthetic clay liners exposed to high temperatures. *Geotextiles and Geomembranes*, *47*(2), pp.142-153.

A FEW NOTES ON EMBEDMENT DESIGN WITH THE 'WHAT YOU DESIGN IS WHAT YOU GET' WYDIWYG METHOD FOR PROPPED CANTILEVER WALLS

Chi-Kuen Stanley Yuen
Transport for New South Wales

ABSTRACT

The WYDIWYG method for stability design of propped cantilever walls was recently published in the 2019 ANZ Geotechnical Conference. The new method has been shown to be consistent between total and effective stress designs, numerically friendly, stable, and also produces economical designs. The paper focussed the consideration on overturning stability, which is a critical design for this type of structures. In geotechnical engineering designers often treat passive earth pressures as soil resistances and active earth pressures as soil loads. Are active pressures really loads and passive pressures really resistances? It raises an interesting question and the proposition forms an important assumption in the formulation of the new method. Given the interests from the geotechnical design community a more general discussion on the model development will be given together with application of the method to design. Worked examples are also included to demonstrate simplicity of the design process.

1 BACKGROUND

In the 2019 ANZ Geotechnical Conference, the new 'What You Design Is What You Get' WYDIWYG method was introduced for embedment design of propped cantilever walls (Yuen, 2019). To establish the new model, the paper stated a few assumptions:

- the disturbing load on the active side of the wall extends below the excavation level but only to the depth at which the wall is at critical equilibrium
- the earth pressure on the passive side remains passive above the critical depth
- the embedded wall beyond the critical depth provides a 'reserve' capacity to stability and such capacity is derived from the 'net' limiting earth pressures on either side of the wall

The WYDIWYG model is shown below:

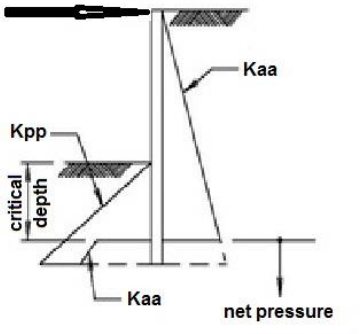

Figure 1: The WYDIWYG model

Where: K_{aa} is the active earth pressure on the retained side of the wall

K_{pp} is the passive earth pressure on the excavated side of the wall

On the basis of the model shown in Figure 1, the Factor of Safety on overturning, $FoS_{overturning}$, may be expressed as follows:

$$FoS_{overturning} = 1 + M_r/M_{pcr} \quad (1)$$

Where Mr is the reserve moment capacity and

$Mpcr$ is the restoring moment capacity at critical equilibrium

The new design method raised a few questions with the design community and this paper attempts to provide clarification to the queries which are needed for establishment of the new design method. A couple of worked examples are also included to demonstrate simplicity of the calculation process.

2 IS THERE A NEED FOR A NEW METHOD

Many methods exist for evaluation of a margin on overturning stability and most designers are used to these methods. For obvious reasons one may argue that the existing methodologies are adequate for design purpose. Yuen (2019) pointed out the key issues with the existing methods. A principal concern is the design community until now have not had a consistent platform for communication of the margin of stability for embedment design of cantilever walls. It is not easy to understand the value calculated by the factor of safety associated with each individual method. Table 1 compares the calculated factor of safety for a given problem using four different methods, and they include the Codes of Practice (CP2), British Steel (BS), Burland et al (BP) and Strength Factor (SF). For demonstration purpose no water was considered in the effective case, which if present will need to be considered in the usual way. One will notice the calculated values vary between 1.26 and 2.66, a wide range for a problem with the same margin of stability. Although a similar ratio of resistance to disturbing load is used in the calculation, it is clear that without attributing the values to a particular method of calculation it is not possible to understand the kind of stability included in a design nor is it possible to compare between design cases to gauge adequacy of a design. It is recognised that some of these factor of safety values may not necessarily convey the intended state of stability but could instead provide a misleading sense of security. This is particularly so for permanent structures which need a higher level of certainty on stability throughout their service life.

Table 1: Comparison of existing design methods

Model	Case 1: Effective Stress		Case 2: Total Stress	
	FoS[4]		FoS[4]	
	Calc	Acceptable	Calc	Acceptable
CP2	1.63	1.5-2.0[1]	1.36	2.0
BS	2.66	2.0	2.01	2.0
BP	1.72	1.5-2.0[1]	1.19	2.0
SF[3]	1.26	1.2-1.5[2]	1.15	1.4-2.0[2]

[1] the acceptable factor varies with strength of the materials and nature of the works

[2] these values vary with design standards

[3] the acceptable factor varies with method of analysis

[4] FoS computed using commercial package WALLAP

There seems still a need to clarify between the design communities and stakeholders on what margin of stability is being adopted in designs, both objectively and consistently. This would also help evaluate and ascertain an optimal stability margin for modern day developments.

In the sections below we will explore the justifications to the few assumptions forming the basis for the new model.

3 WHAT IS THE CRITICAL DESIGN SOIL LOAD

In the calculation of factor of safety a simple engineering ratio is often used between resistance and load. The conventional design approach generally does not differentiate between active earth pressure and load, and hence earth pressures on the retained side, often referred to as the active side, are treated as loads and those on the excavation side as resistances. The CP2 approach is one typical example where the earth pressure on the retained side is taken to be a load extending to the design toe level of the wall. Questions are asked should the design loads be applied over the full depth of the wall, would they have been over estimated, what if they are not, where should they be?

To elucidate the point, let us take a step back to consider a propped cantilever wall at critical equilibrium. The active load on the retained side is balanced by the passive resistance on the excavation side, and the disturbing moment is balanced by the restoring moment provided by the passive resistance about a support at the top of the wall.

This critical condition is not acceptable for construction and additional wall embedment is needed to provide for safety, and also for functional performance on strength and deformation of the wall. Would the additional embedment affect the design load? As embedment is increased the earth pressures on the retained side change in response to the increased toe fixity. This will have an effect on the earth pressure distribution and hence change the structure loads. In modern day computation of wall bending moments and shear forces lateral earth pressure distributions that take into account of soil structure interaction are used.

For stability design using the WYDIWYG method limiting earth pressure conditions are considered instead. The lateral earth pressures above the critical equilibrium level stay at their limit states and hence the loads remain unchanged. The consideration leading to this ultimate condition on the embedded wall is discussed in the next section. Another situation that could affect the design load is the change of water flow condition below the wall toe due to increase of wall embedment. Where there is no water balance considered at the toe, the design load will remain the same. Where toe water balance is considered, change in the design load could be expected. For the purpose of stability design the change in this load is not expected to be significant if a similar approach is adopted between the calculations. For the above reasons and because there is no change in the excavation geometry or external loading conditions, the total design load for stability design can be taken to be similar to that at critical equilibrium. Byrne et al (1995) suggested wall design bending moments and shear forces to be determined based on the wall at critical equilibrium. Although the author does not necessarily agree with this recommendation it does suggest that the disturbing load at critical equilibrium is appropriate for design.

The schematic WYDIWYG model shown in Figure 1 shows the design load to extend to the critical depth. This load is balanced by the passive resistance, which forms the second assumption above. As the wall embedment is increased to provide the needed stability, we will explore how these earth pressures on the extra length of wall are considered for the proposed WYDIWYG model.

4 IS EARTH PRESSURE A LOAD

As said above for acceptable stability the wall embedment needs to be increased beyond the critical depth and the earth pressures will act instantaneously on either side of this extra embedment. Traditionally designers seldom differentiate between load and active earth pressure. These terms are used interchangeably for L-shape retaining wall or embedded walls at limit equilibrium. The active pressure is taken to be a load. For embedded walls engineers have long been aware of a fix-earth support situation for walls penetrating beyond the critical equilibrium level. There have been practical difficulties to locate the theoretical pivot point on the embedment where the role of earth pressures as load and resistance changes. The differentiation has been made difficult by the fact that neither instrumentation nor numerical calculation is able to identify the earth pressures as loads or resistances, which may be engineering terms to define conditions creating disturbance and restoration for stability consideration respectively. The free earth support became a favourable simpler model to use where all earth pressures on the retained side are treated as loads. However, if the earth pressures on the retained side of this extra embedment are considered as a load then the total load will be larger than that considered for the design excavation, and one could be analysing a different problem. In the CP2 model, the earth pressures on the active side are considered as loads, extending to the toe level of the wall. Higher load requires higher resistance with deeper wall embedment, and the conservatism of the CP2 model was readily recognised (Burland et al, 1981; Yuen, 2019). Variations to this model occurred to improve the stability safety margin. Figure 2 shows a schematic pressure distribution of the common methods.

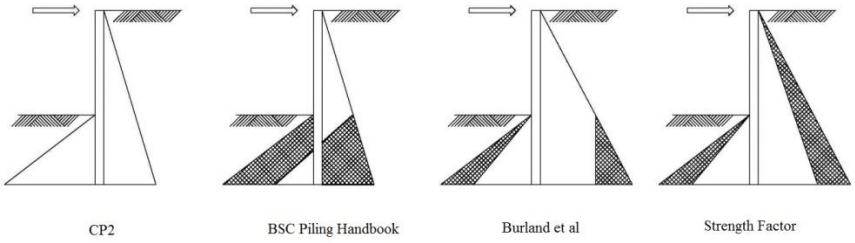

Figure 2: Schematic pressure distribution used by the common methods

Most of these models consider earth pressure modification from below the excavation level and the modified loads still extend to the toe of the wall. From this conjecture, one may interpret that the CP2 design load was considered excessive and the earth pressure modifications by the other methods were introduced to allow a better estimate of the design load. These model developments were based on logic but the questions on magnitude and extent of the active design load have never been adequately addressed. In the following paragraphs we will explore via a different perspective to show the role of the earth pressures on this extra embedment below the critical equilibrium depth.

In L-shape retaining walls, the definition of load in terms of earth pressure on the structure is fairly straight forward. The structure is moving away from the retained soil, and the active earth pressure developed is a load. Equilibrium is achieved by mobilising the frictional resistance on the wall base. Additional sliding and overturning stability are often obtained by extending the wall base. For propped cantilever walls at critical equilibrium the active earth pressure condition is similar to that of the L-shape wall and the active pressure is a load. The passive earth pressure over the critical embedded length is comparable to the frictional resistance from the base of an L-shape wall at critical equilibrium. The earth pressures on the extra embedment though may not be interpreted as straight forward. The earth pressure condition changes as the wall embedment is increased beyond the critical depth to derive stability. Figure 3 shows the earth pressure changes for a wall at critical equilibrium to one of a stable condition following an increase of wall embedment.

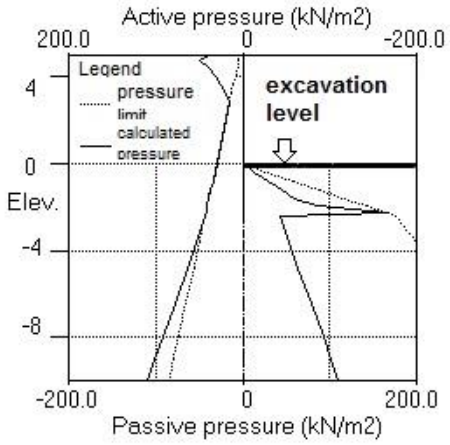

Figure 3: Pressure diagram for a stable wall (by WALLAP)

Earth pressure redistribution occurs once the wall embedment is beyond the critical depth. It is apparent from Figure 3 that the earth pressures are no longer at limiting conditions. The earth pressure on the retained side increases whilst that on the excavation side decreases. The wall is stable and the stability must have been derived from the extra embedment beyond the critical depth. The argument follows that the earth pressure on the retained side of the extra embedment is not a load. It serves as a component to provide extra capacity for stability such that the wall can sustain additional load. As the passive pressure also acts coherently with the active pressure, it is logical to consider that the net of these pressures are responsible for the additional capacity. This is referred to as the reserve capacity in the WYDIWYG

method (Yuen, 2019) and in Equation 1 above. The maximum reserve capacity that the ground can provide for stability occurs when these net earth pressures are returned to their respective pressure limits. The consideration is similar to the BSC approach only it commences from below the critical depth. It should be pointed out that the pressure limits adopted here are for the sole purpose of calculating the reserve capacity for stability. This should not be confused with the earth pressures from soil-structure interaction used for wall deformation, bending moment or shear force calculations. The calculation of the wall functional performance is beyond the scope of the current discussion but it suffices to say that such pressure distributions should be considered for more realistic calculation of wall structure loads.

5 SUMMARY OF CHARACTERSITICS OF THE NEW MODEL

The above discussion provides justification for the three assumptions made for the model and that they enable the factor of safety to be expressed neatly in terms of the moment of restoring capacity at critical equilibrium and what you designed is what you get. For example if the design factor of safety is 2 then the design stability is 2 times what is available at critical equilibrium. The unique formulation is able to provide a measure of stability that is tangible and comprehensible. The favourable characteristic could allow consistent margins of stability to be calculated and meaningful comparison made between design cases. The method is consistently applicable to all soil conditions, i.e. total and effective stresses. This is in contrast to some of the existing methods that exhibit numerical problems when performing total stress analysis under some soil conditions. The brief analysis in the paper (Yuen, 2019) also indicates an economic margin when compared with the other methods.

Below are worked examples to demonstrate the calculation process to determine the embedment depths for two different soil conditions.

6 WORKED EXAMPLES

To illustrate application of the WYDIWYG method to embedment design, the two simple examples in the ANZ paper (Yuen, 2019) are used. Instead of calculating the factor of safety (FoS) from a given wall embedment, the FoS is chosen to suit a given design requirement. The first example is a 5 m deep supported excavation in a uniform soil with an internal friction angle of 35 degrees propped at the top of the wall. A 10 kPa surcharge is considered at the crest level of the wall and no groundwater is considered. The target FoS is 1.84. The second example is similar to the first one with 5 m deep excavation, but in uniform clay with an undrained cohesion of 40 kPa. Given the temporary condition for this case the target FoS is 1.55.

The embedment design using the WYDIWYG method is a two-step process, firstly to calculate the critical wall depth and then from there to determine the critical effective restoring moment. The second step is to proportion the wall embedment to provide the required reserve restoring moment to satisfy the design FoS requirement.

The critical wall depth may be calculated by hand for simple problems and for more complex problems it may be worthwhile to consider technical software instead. In the above examples the critical wall depths for both cases are calculated by using a commercial software called WALLAP. For the total stress case, a minimum fluid pressure of 5 kPa has been considered in the calculation.

6.1 EXAMPLE 1 – EFFECTIVE STRESS CASE

Step 1

The first step in the process is to determine the wall embedment at critical stability, i.e. FoS = 1. The critical embedment depth below the excavation level is calculated at 1.61 m. The earth pressure distribution is shown in Figure 4 for ease of reference.

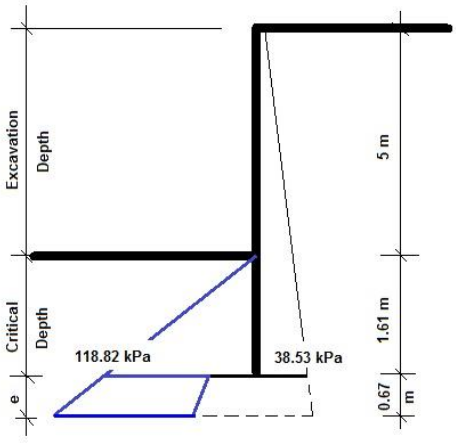

(Not to scale)

Figure 4: Earth pressure distribution for effective stress case

Depth to toe of wall, H, retained side

$$H = 5 + 1.61$$

$$= 6.61\ m$$

The earth pressures at the critical depth are calculated using the following equations:

Earth pressure at critical wall toe, retained side, K_{aacr}

$$K_{aacr} = (\gamma * H + \sigma_s) * k_a \quad (2)$$

$$= (20*6.61+10)*0.27$$

$$= 38.53\ kPa$$

Where γ is the unit weight of soil, kN/m^3

H is the overall length of the wall, m

σ_s is the traffic surcharge, kPa

k_a is the coefficient of active earth pressure

Earth pressure at critical wall toe, excavation side, K_{ppcr}

$$K_{ppcr} = \gamma * h * k_p \quad (3)$$

$$= 20*1.61*3.69$$

$$= 118.82\ kPa$$

Where h is the wall embedment length below the excavation level, m

k_p is the coefficient of passive earth pressure

The restoring moment capacity at critical equilibrium, M_{pcr}

$$M_{pcr} = K_{ppcr}/2*h*(5 + 2/3*h)$$

$$= 118.82/2*1.61*(5+2/3*1.61)$$

$$= 580.91\ kNm$$

Step 2

The next step is to determine the additional wall embedment to satisfy the required stability. For a given FoS the required reserve moment capacity can be calculated using Eqn 1:

$$M_r = (FoS_{overturning} - 1) * M_{pcr}$$

Since the required FoS is 1.84 the above equation becomes

$$M_r = (1.84 - 1) * 580.91$$

$$= 0.84 * 580.91$$

$$= 487.97 \text{ kNm}$$

The extra wall embedment is then proportioned to obtain the reserve moment capacity. Take the extra embedment beyond the critical depth to be e, the earth pressures at the new toe level are expressed as follows:

Using equation (2)

$$K_{aa} = [20 * (6.61 + e) + 10] * 0.27$$

$$= 38.53 + 5.42e$$

Using equation (3)

$$K_{pp} = 20 * (1.61 + e) * 3.69$$

$$= 118.82 + 73.8e$$

The reserve moment, M_r, may be expressed as follows:

$$M_r = (K_{ppcr} - K_{aacr}) * e * (H + e/2) + [(K_{pp} - K_{aa})/2] * e * (H + 2*e/3)$$

$$= (118.82 - 38.53)e(6.61 + e/2) + [(73.8e - 5.42e)/2]e(6.61 + 2e/3)$$

$$= 22.80e^3 + 266.15e^2 + 530.72e$$

From above $= 487.97 \text{ kNm}$

Solving the cubic equation, e = *0.67 m*

The design wall embedment, D, is hence

$$= 1.61 + 0.67$$

$$= 2.28 \text{ m}$$

And the design wall length is 5 + 2.28 = 7.28 m.

6.2 EXAMPLE 2 – TOTAL STRESS CASE

Step 1

The calculation for the total stress case is similar to that of the effective one, and the critical embedment depth is calculated using WALLAP to be 0.8 m. The schematic pressure distribution is shown in Figure 5 for ease of reference.

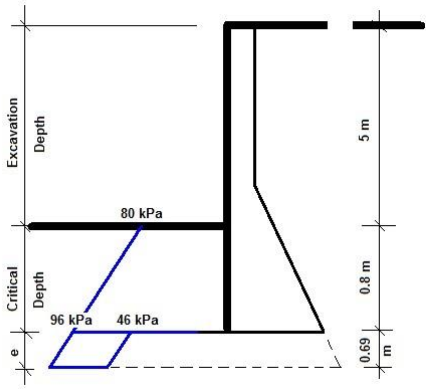

(not to scale)

Figure 5: Pressure distribution for total stress case

Depth to toe of wall, H, retained side

$$H = 5 + 0.8$$
$$= 5.8\ m$$

Earth pressure at excavation level, retained side, K_{aa}

$$K_{aa} = (5*\gamma + \sigma_s)*k_a - k_{ac}*C_u$$
$$= (5*20 + 10)*1 - 2*40$$
$$= 30\ kPa$$

Earth pressure at critical depth, retained side, K_{aacr}

$$K_{aacr} = (\gamma*H + \sigma_s)*k_a - k_{ac*}C_u$$
$$= (20*5.8 + 10)*1 - 2*40$$
$$= 46\ kPa$$

Where k_{ac} is equal to 2

C_u is the undrained cohesion, kPa

Earth pressure at excavation level, excavation side, K_{pp}

$$K_{pp} = k_{pc}*C_u$$
$$= 2*40$$
$$= 80\ kPa$$

where, k_{pc} is equal to 2

Earth pressure at critical wall toe, excavation side, K_{ppcr}

$$K_{ppcr} = \gamma*h*k_p + k_{pc}*C_u$$
$$= 20*0.8*1 + 2*40$$
$$= 96\ kPa$$

The restoring moment capacity at critical equilibrium, M_{pcr}:

$$M_{pcr} = K_{pp}*h*(5 + h/2) + [(\gamma*h*k_p + k_{pc}*C_u) – (k_{pc}*C_u]/2*h*(5 + 2h/3)$$

$$= 80*0.8*(5 + 0.8/2) + (96 – 80)/2*0.8*(5 + 2*0.8/3)$$

$$= 345.6 + 35.4$$

$$= 381\ kNm$$

Step 2

Again using Eqn 1

$$M_r = (FoS_{overturning} – 1) *M_{pcr}$$

The required $FoS_{overturning}$ for this case is 1.55

Therefore $M_r = (1.55 – 1)*381$

$$= 209.55\ kNm$$

For total stress cases, the calculation of the extra embedment is slightly simpler since the rate of lateral earth pressure increase on either side of the wall is constant, the net pressure on this part of the wall is uniformly distributed. Hence taking e as the extra embedment,

$$M_r = (Kpp – Kaa)*e*(5.8 + e/2)$$

$$= (80 – 30)*e*(5.8 + e/2)$$

$$= 25e^2 + 290e$$

$$= 209.55\ kNm$$

Solving the quadratic equation:

$$e = 0.69\ m$$

The design wall embedment, D, is hence

$$D = 0.8 + 0.69$$

$$= 1.49\ m$$

And the design wall length is 5 + 1.49 = 6.49 m.

7 DISCUSSION AND SUMMARY

Stability design for embedded walls is a critical consideration in geotechnical engineering design and the stability is commonly measured by a factor of safety. The concept of factor of safety as a ratio of resistance and disturbing load is sound only the definition of the resistance and disturbing load are not so well defined. The simplistic CP2 approach taking the disturbing load to the toe of the wall was considered conservative and variations emerged over the years to provide improved estimation of the ratio. The different approaches to approximate the load and resistance have resulted in a wide range of factor of safety stability values for the same problem. Because of the different formulation it is not possible to objectively comprehend the stability margin offered in a design, and some methods are more conservative than the others. To the owners and asset operators the uncertainty in such designs should be a concern, and there is a need for improved level of certainty to balance between economics of construction and margin of stability in design.

The WYDIWYG method introduces a new set of assumptions to assist the development of the model. The discussion on active earth pressures refreshes the view on disturbing load, how far it should extend. It follows that load on the structure should have been adequately considered by extending it to the critical depth below the excavation level, at which the wall remains at critical equilibrium. This view is also shared by some engineers (Byrne et al, 1995) where they recommended wall loads to be determined from walls at critical equilibrium.

The role of the extra wall embedment beyond the critical depth has not been previously analysed the same way. The fact that it is solely responsible for stability suggests that the earth pressures over this part of the wall are neither a load nor a resistance. This is crucial in the development of the model. The change in the pressures from their limiting states indicates that the increased embedment brings about a reserve in restoring stability. The wall reaches the restoring capacity when these pressures are idealised at their limiting states. Since the limiting pressures are acting coherently it

is reasonable to consider that their net pressure on this part of the wall is responsible for the reserve restoring capacity. It is worthwhile to clarify that the aforementioned pressure distribution is only used for stability calculation. For wall load calculations, e.g. bending moments and shear forces, the conventional soil structure interaction earth pressure distribution should be used for more realistic results. For the WYDIWYG method, this process is undertaken after the final wall embedment is determined.

In summary, the critical parts for development of the WYDIWYG model are being analysed and rationalised. The process enables a new definition on load and resistance, and hence a new formulation of the factor of safety. It has been shown that the formulation can be consistently applicable to all soil conditions. As the FoS is made a function of the restoring capacity at limit equilibrium, its design value takes on a tangible meaning, which is unambiguous and straight forward. For example using the WYDIWYG method for design, a FoS of 2 ensures the restoring capacity is 2 times its capacity at limiting equilibrium. This could be a favourable characteristic for assessing stability of this type of walls. It may also allow meaningful comparison of stability performance between design cases and amongst the design community.

Two step-by-step examples are included to demonstrate simplicity of the calculation process. For more complex situations, the calculation may be accomplished by using a spreadsheet, or ideally using a codified program incorporating soil structure interaction for comprehensive and simultaneous consideration of stability and functional performance of the structure.

8 ACKNOWLEDGEMENT

The author would like to thank Transport for New South Wales for the permission to publish this paper and Filomena Manalo on word processing. The opinions expressed in this paper are those of the author and do not necessarily represent those of Transport for New South Wales.

9 REFERENCES

BS8002:1994. Code of practice for earth retaining structures. *British Standards Institution*, *amended 2001*, London.

BSC Piling Handbook (1988), 6th Edition. *British Steel Corporation*.

Burland, J.B., Potts, D.M. and Walsh, N.M. (1981). The overall stability of free and propped embedded cantilever retaining walls. *Ground Engineering*, July 1981.

Byrne, G, Everett, J.P., Schwartz, K. (1995). A guide to practical geotechnical engineering in Southern Africa, 3rd edition, *Franki*.

Civil Engineering Code of Practice No.2 (1951). Earth Retaining Structures. *Institution of Structural Engineers.*

WALLAP, Geotechnical design software – Earth retaining structures by *Geosolve*.

Yuen, C. K. S. (2019). What you design is what you get – An economical way to the stability design of propped cantilever walls. *13th Australia New Zealand Conference on Geomechanics*, Perth, (eds H.E. Acosta-Martinez & B.M. Lehane) 483-488. Australian Geomechanics Society.

STRENGTH VARIABILITY OF DEEP CEMENT MIXED COLUMNS ON THE OVERALL PERFORMANCE OF COLUMN-SUPPORTED EMBANKMENTS

Manasi Wijerathna[1] and Samanthika Liyanapathirana[2]

[1]GHD Pty Ltd, 29 Christie Street, St. Leonards, NSW, Australia, 2065, manasi.wijerathna@ghd.com

[2]School of Computing, Engineering and Mathematics, Western Sydney University, Penrith, NSW, Australia, 2751, s.liyanapathirana@westernsydney.edu.au

ABSTRACT

Deep Cement Mixed (DCM) column improved ground is known to have large strength variability across the material domain. However, the effect of strength variability on the performance of embankments supported by DCM columns is not well studied due to scarcity of numerical modelling facilities to incorporate spatial variability of material properties directly into a finite element analysis and lack of comprehensive field monitoring data. This paper investigates the effect of spatial variability on the performance of an embankment with attached DCM column walls beneath the side slopes. The analysis was carried out using numerical models developed using ABAQUS finite element program incorporating the spatial variability of DCM columns. The strength field in the material domain was randomly generated, from a lognormal distribution, using a computer program written in MATLAB. The sensitivity of embankment deformations to spatial correlation length, coefficient of variation (COV) and partial factor of safety (PFOS) was investigated by analysing a series of models. The reliability of the embankment in each analysis case was assessed using 1500 Monte Carlo realizations. Results demonstrate that the spatial correlation length of strength properties has a great influence on the reliability-based performance of the embankment. Larger spatial correlation lengths resulted higher upper bound in the lateral deformation data of the embankment. COV also affected the upper and lower bounds of the lateral deformation data. The PFOS significantly affected the skewness of the deformation distribution, however PFOS does not affect the upper and lower bounds of the distribution.

Key words: Spatial variability, Reliability based performance, Deep cement mixing, Finite element modelling, Monte Carlo method

1. INTRODUCTION

Deep cement mixing is a well-developed ground improvement technology that is in practice in many regions around the world. However, achieving uniform material properties in Deep Cement Mixed (DCM) soils is highly unrealistic due to several influence factors such as; non uniform mixing, natural variability in the ground and non uniform curing conditions. As a result, DCM soils show a large variability of properties over the material space. The coefficient of variation (COV) is a measure of the degree of strength variability in a material, which is derived as the standard deviation normalized by the mean strength. According to the literature, COV of DCM soil strength normally varies from 0.3 to 0.8 (Filz and Navin 2010; Kasama et al. 2012; Larsson et al. 2005b). While the strength properties of DCM soil are spatially variable, the strength field is also spatially correlated (Honjo 1982). The reported horizontal and vertical correlation lengths vary from 0 to 12 m (Al-Naqshabandy et al. (2012a), Kasama et al. (2012), Liu et al. (2015)). In comparison to the dimensions of a typical embankment, these correlation lengths are small. These correlation lengths suggest that the strength properties of DCM soil can gradually vary within a single project resulting localized zones of low and high strengths. Therefore, design of DCM column-supported embankments assuming uniform DCM soil strength properties is not a realistic representation of the actual situation.

Many reliability studies considering spatial variability in natural soils are available in the literature (e.g. Jiang and Huang (2016), Kasama and Zen (2011), Liu et al. (2017a)). However, the studies specific to spatial variability in DCM soils are limited (Kasama et al. 2012; Liu et al. 2015; Namikawa 2016; Namikawa and Koseki 2013; Zhang et al. 2017). In some cases, the reliability based performance was investigated considering natural and cement mixed soils as a composite system (Al-Naqshabandy and Larsson 2013; Al-Naqshabandy et al. 2012b; Huang et al. 2015; Navin 2005; Navin and Filz 2006). All these studies highlighted the importance of spatial correlation length in establishing the strength profile of DCM soil in reliability studies.

In this study, the performance of an embankment with side slopes supported on DCM wall panels was evaluated considering the spatial variability of strength properties, using a reliability based approach. The analysis was carried out using two-dimensional plane-strain finite element models developed using the ABAQUS/Standard

(2014) finite element program. Material properties for different cases were randomly generated from a lognormal distribution with a specific mean strength and a COV using a computer program written in MATLAB. The ABAQUS/Standard (2014) finite element analysis was executed for each case within this MATLAB program. The finite element analyses were based on a coupled analysis where pore water pressure generation and dissipation were included. Reliability was evaluated using the Monte Carlo method. A series of reliability analyses were conducted assuming finite spatial correlation distances. The embankment performance was investigated for different mean strengths, coefficients of variation and spatial correlation lengths to identify the sensitivity of spatial variability on the reliability of the embankment performance.

2. NUMERICAL MODEL

The analysis was carried out using two-dimensional plane-strain numerical models developed using the ABAQUS/Standard (2014) finite element program. In this study, DCM panels beneath the embankment slopes were converted to a plane-strain model based on the equivalent properties approach. Accordingly, the width and height of the DCM panel were not changed and the equivalent properties for DCM panels (E_{eq}, c'_{eq} and φ'_{eq}) were calculated using Equations 1 to 3 (Ariyarathne et al. 2013; Chan and Poon 2012; Huang et al. 2009; Yapage et al. 2014).

$$E_{eq} = E_c a_r + E_s(1 - a_r) \tag{1}$$

$$c'_{eq} = c'_c a_r + c'_s (1 - a_r) \tag{2}$$

$$\phi'_{eq} = \tan^{-1}\left(\frac{(1 - a_r)\tan\phi'_s + n a_r \tan\phi'_c}{(1 - a_r) + n a_r} \right) \tag{3}$$

where E_{eq}, E_c and E_s are the elastic modulus of the equivalent panel, DCM panels and the surrounding soil, respectively; a_r is the area replacement ratio of DCM panel; c'_{eq}, c'_c and c'_s are the effective cohesion of the equivalent panel, DCM panels and the surrounding soil, respectively; and φ'_{eq}, φ'_c and φ'_s are the effective friction angle of the equivalent panel, DCM panels and the surrounding soil, respectively and n is the ratio of stress over DCM wall to stress over surrounding soil, known as the stress concentration ratio. The value of n was considered as 3.5 in this study, which is based on the average stress concentration ratio calculated using a three-dimensional numerical model of the embankment.

2.1. EMBANKMENT GEOMETRY AND BOUNDARY CONDITIONS

Figure **1** shows the geometry of the embankment selected for this study. The embankment has a height of 5.5 m and a width of 30 m at the crest level. The gradient of the embankment side slopes is 2:1 and the width of the embankment at the base level is 52 m. There is a 10 m thick soft clay layer immediately below the embankment fill, underlain by a 5 m thick silty sand layer and a 5 m thick stiff to hard clay layer, respectively. The soft clay layer beneath the slope of the embankment was improved with DCM panels with a width of 11 m and a height of 10 m. Normally wall panels are used underneath sloping sides to minimise the lateral deformations and to improve the stability of the embankment (Yapage et al. 2014). Each DCM wall panel consists of eighteen 0.8 m diameter attached DCM columns with 0.2 m overlap. The panels were spaced at 2 m in the longitudinal direction of the embankment. Hence, the area replacement ratio (ARR) beneath the side slopes was 35.5%. The ground-water table was at the ground surface. A geosynthetic layer was placed at 0.25 m above the ground surface.

The embankment was constructed in 5 stages. The first four fill layers have a thickness of 1 m and each layer was constructed over a period of 10 days at a uniform rate of 0.1 m/day. A 1.5 m thick fill layer was added during the fifth stage over 15 days.

The variability incorporated analysis was carried out using half of the embankment geometry assuming symmetry of the embankment, which will assist to save analysis time and computer memory during the Monte Carlo simulations. Since the DCM panel is located 15 m away from the centreline of the embankment, the influence of the strength variability of the DCM wall on the deformations at the centreline is very small. Therefore, a symmetrical boundary condition at the centreline was considered as a reasonable assumption for this problem, although it is not symmetrical with respect to material space. The vertical boundary at the far end of the embankment was set at 60 m away from the toe of the embankment and the deformations were restrained in the horizontal direction. At the bottom of the subsoil deposit (stiff to hard clay layer), movements were restricted in both vertical and horizontal directions. A zero pore water pressure boundary was set along the level

of the water table. Coupled effective stress – pore water pressure analysis was carried out, below the ground-water level. The bottom boundary and the two vertical boundaries were considered as impermeable.

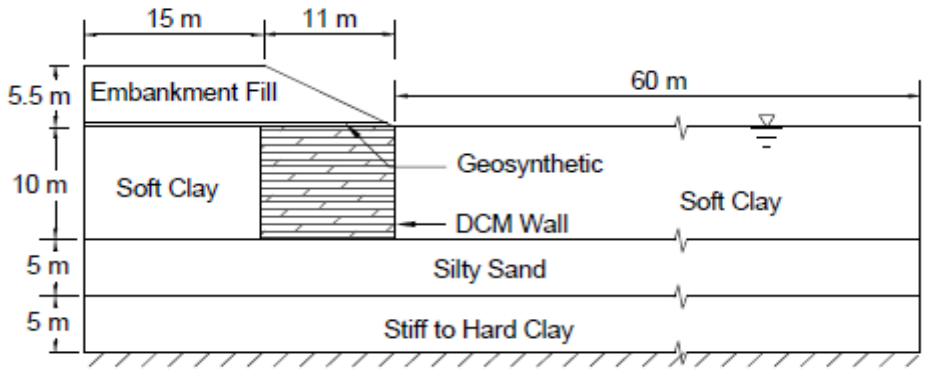

Figure 1: Geometry of the embankment and layout of DCM walls and geosynthetic reinforcement layer

2.2. FINITE ELEMENT MESH AND MATERIAL MODELS

The soil layers and DCM walls were modelled using eight-node quadrilateral elements with reduced integration and pore pressure degrees of freedom at the corner nodes (CPE8RP). Eight-node quadrilateral elements with reduced integration and without pore pressure degrees of freedom (CPE8R) were used to model the embankment fill. The three soil layers, DCM panel and the embankment fill were modelled using the Mohr-Coulomb material model. Although an extended version of Mohr-Coulomb model incorporating strain-softening behaviour has been proposed by the authors for DCM columns, in this paper Mohr-Coulomb model with elastic, perfectly plastic behaviour has been adopted to reduce the complexity of Monte-Carlo simulations. The geosynthetic layer was modelled using three-node quadratic truss elements (T2D3), which do not resist bending and compressive stresses but resists tensile stresses.

2.3. SELECTION OF MATERIAL PARAMETERS

The material properties used for DCM walls, soft clay layer, silty sand layer and stiff to hard clay layer and embankment fill are shown in Table **1**. The elastic modulus, E_c, and the effective cohesion, c'_c, of the DCM soil are considered as proportional to the unconfined compressive strength, q_u, of the DCM soil. The relationship between the elastic modulus and the unconfined compressive strength of DCM soil was assumed as $E_c = 100q_u$ (Bruce and Bruce 2003; Huang et al. 2009; Yapage and Liyanapathirana 2014). According to the literature, the cohesion of DCM soil varies within the range of $0.2q_u$ – $0.5q_u$ (Andromalos et al. 2000; Broms 1999; Euro Soil Stab 2002; Yapage et al. 2014). Therefore, the effective cohesion of DCM soil was assumed as $c'_c = 0.4q_u$. Same relationships were used to vary E_c and c'_c in proportionate to the strength of DCM soil in the probabilistic analysis. The recommended values for the drained friction angle, ϕ'_c, of DCM soil ranges from 30^0-35^0 (Broms 1999; Euro Soil Stab 2002). Since ϕ'_c varies over a small range for DCM panels, it was considered as a deterministic parameter with a value of 30^0.

Table 1: Material properties used for DCM wall, soft clay, silty sand and stiff to hard clay

Parameter	DCM Wall	Soft clay	Silty sand	Stiff to hard clay	Embankment fill
Saturated unit weight, γ_{sat} (kN/m^3)	18	18	18	16.5	19
Permeability , κ (m/s)	5×10^{-8}	5×10^{-8}	8.3×10^{-7}	5.3×10^{-7}	-
Poisson's ratio, ν	0.3	0.3	0.3	0.3	0.3
Effective cohesion , c' (kPa)	250	1	1	1	10
Elastic modulus , E (MPa)	62.5	5	15	17	20
Drained friction angle , φ'	30^0	25^0	30^0	25^0	30^0

The geosynthetic reinforcement was assumed to have an elastic modulus of 100 MPa, yield strength of 75 MPa and a Poisson's ratio of 0.3. The thickness was assumed as 1 mm. The interaction between the geosynthetic layer and the embankment fill material was modelled as a surface to surface contact with an interface friction coefficient of 0.8.

3. RELIABILITY-BASED PERFORMANCE OF THE EMBANKMENT

In this section, a probabilistic analysis was carried out considering the variability of strength properties of DCM panels to evaluate the reliability based performance of the embankment. The strength variability was introduced to the model considering spatially varying strength properties with spatial correlation, within a DCM panel. The main function of DCM panels is to resist the lateral deformations in the subsoil closer to the toe of the embankment. Therefore, the maximum lateral deformation beneath the toe of the embankment was used to monitor the performance of the embankment in the probabilistic analysis. For the current analysis, the target deformation was set as 34 mm, which is the lateral displacement beneath the toe of the embankment corresponding to a deterministic analysis with DCM panel strength of 625 kPa. A tolerance of 10% was allowed for the lateral deformation in the probabilistic analysis. Therefore, an embankment exceeding 37.5 mm lateral displacement beneath the toe of the embankment was considered as an unsatisfactory performance. The probability of unsatisfactory performance, P_u, was obtained as the ratio of frequency of unsatisfactory performance to the number of Monte Carlo realisations. 1500 Monte Carlo realisations were used in this study.

Table 2: Parameters used in the probabilistic study

DCM column properties	Range of values
Mean strength, μ_q (kPa)	625, 750, 1000, 1250
PFOS	1, 1.2, 1.5, 2
Effective cohesion, c'_c	$0.4q_u$
Friction angle, φ'	30^0
Elastic modulus, E_c	$100q_u$
COV	0.3, 0.5, 0.7
Monte Carlo iterations	1500
Spatial correlation length, θ	0, 0.5, 1, 2, 4

The compressive strength, elastic modulus and effective cohesion of DCM soil were considered as stochastic parameters in the probabilistic analysis. The c'_c and E_c were varied in proportionate to q_u as discussed in the "Selection of material parameters" section. The strength variability within the surrounding natural soil was not incorporated into this study. Many studies have shown that both lognormal and normal distributions are suitable to characterise the strength distribution within DCM soil (Honjo 1982; Kasama et al. 2012; Namikawa and Koseki 2013; Navin 2005). In this study, the compressive strength of DCM soil was assumed to have a lognormal distribution with a specific mean strength and variance instead of a normal distribution to avoid generating negative stiffness and strength properties within the material space.

According to the literature, spatial correlation lengths in DCM improved ground are different in the horizontal and vertical directions (Al-Naqshabandy et al. 2012a; Larsson et al. 2005b; Tang et al. 2001). However, data for cross correlation between horizontal and vertical spatial correlation lengths are not available. Therefore, in this analysis correlation length was assumed as equal in all directions within the plane of the panel. Table 2 shows the parameters used in the analysis.

3.1. RELIABILITY ANALYSIS

DCM panel strength values were randomly generated from a lognormal distribution with a specific mean strength and a COV using a computer program written in MATLAB. The ABAQUS finite element analysis was executed for each case within the MATLAB program.

The autocorrelation function shown in Equation 4 was used to determine the correlation coefficient of compressive strength between two nodes in the DCM panel (Honjo 1982; Namikawa and Koseki 2013).

$$\rho(d) = \exp\left(-\frac{d}{\theta}\right) \tag{4}$$

where ρ(d) is the correlation coefficient, d is the distance between two nodes and θ is the spatial correlation length.

The compressive strength at ith node, q_i, is a lognormally distributed random field with mean, μ_q, coefficient of variation, COV_q, and spatial correlation distance θ and was calculated as:

$$q_i = \exp\left(\mu_{\ln q} + \sigma_{\ln q} \cdot G_i\right) \tag{5}$$

where $\mu_{\ln q}$ and $\sigma_{\ln q}$ are calculated using Equations 6 and 7, and G_i is a random variable with a spatial correlation distance of θ, calculated using equation 8. The range of G_i was bounded between +4 and -4 to avoid extremely large or small q_i values.

$$\sigma_{\ln q} = \sqrt{\ln\left(1 + COV_q^2\right)} \tag{6}$$

$$\mu_{\ln q} = \ln \mu_q - \frac{1}{2}\sigma_{\ln q}^2 \tag{7}$$

$$G_i = CR_n \tag{8}$$

where, C is the Cholesky decomposition of the correlation coefficients matrix and R_n is a normally distributed random variable with zero mean and unit variance.

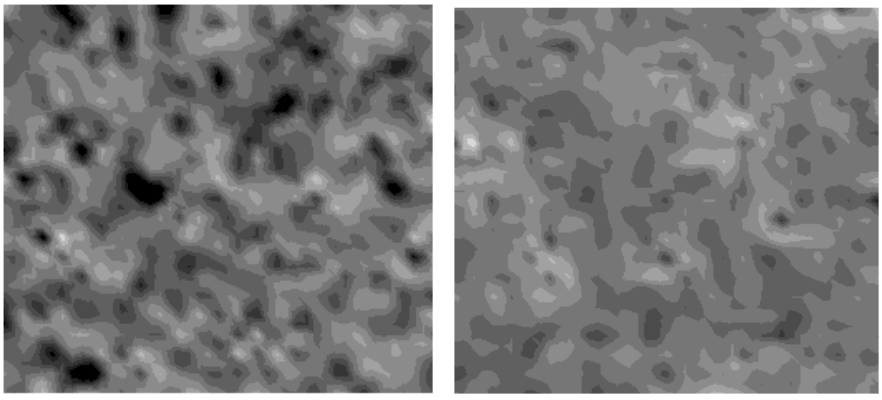

(a) (b)

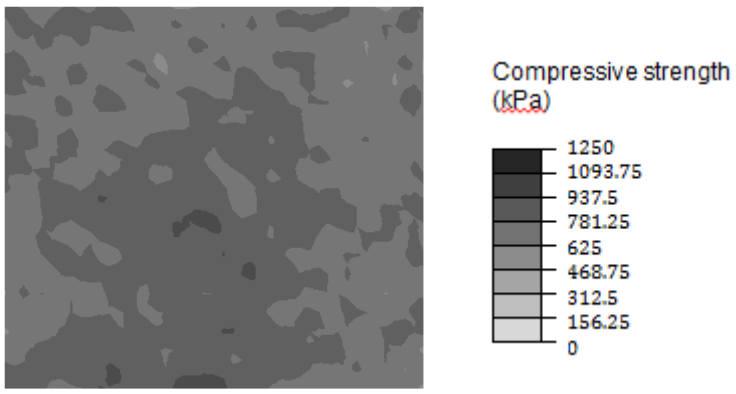

(c)

Figure 2: Typical samples of compressive strength profiles within DCM panel when spatial correlation length is (a) 0 m, (b) 1 m, (c) 4 m

This procedure was repeated for each Monte Carlo realisation to generate different strength profiles in the DCM panel. The elastic modulus and cohesion were changed across the DCM panel in proportionate to q_i as discussed in the "Selection of material parameters" section. The compressive strength profiles in the DCM panel generated in typical Monte Carlo realisations for cases with different correlation distances are shown in 2. In Figure , darker regions indicate higher strengths and lighter regions indicate lower strengths.

Figure 2 shows the performance levels of the embankment with different spatial correlation lengths for the case with mean strength of 625 kPa. P_u was less than 1/1500 for all the considered spatial correlation distances when the COV was 0.3. For the cases with COV 0.5 and 0.7, P_u was maximum when spatial correlation length was 2 m. The ratio of the spatial correlation length corresponding to the peak P_u to the width of DCM wall is 0.18. P_u reduced when correlation length is greater than 2 m. A strength profile with a small spatial correlation length indicates a highly variable strength distribution over the material space. Therefore any possible failure surface may encounter both strong elements and weak elements in equal proportions. As a result, P_u decreases towards zero, when spatial correlation length reduces below 2 m.

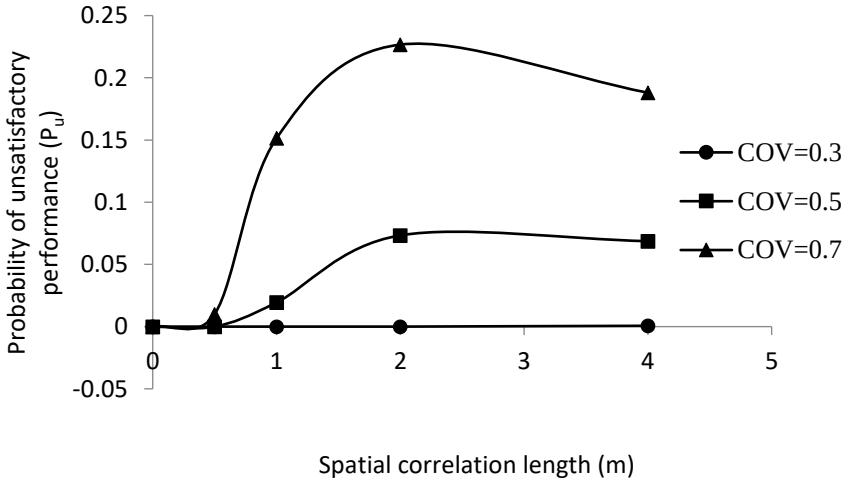

Figure 2: Reliability based performance of the embankment

3.2. OBSERVED TRENDS IN THE MONTE CARLO SIMULATION RESULTS

The maximum lateral displacement beneath the toe of the embankment is expected to vary linearly with the strength of the DCM wall panel when the panel strength is uniform over the section. Therefore, the Monte Carlo simulation that assumes uniform strength of DCM wall and lognormal distribution of strength values among the

realisations produces a set of maximum lateral deformations that fit into a lognormal distribution. However, when the DCM panel strength varies spatially, the type of distribution of the resulting lateral deformations cannot be pre-determined. An attempt was taken in this study to identify the type of distribution of the lateral deformation data generated from Monte Carlo simulations. Figure 3 shows results from three cases along with their normal and lognormal probability density functions. The deformation data generated from Monte Carlo realisations show a poor fit with normal and lognormal probability distributions. Hence, the P_u predicted using the best fit normal and lognormal distributions largely differed from the P_u values obtained from the Monte Carlo simulations (Figure 4).

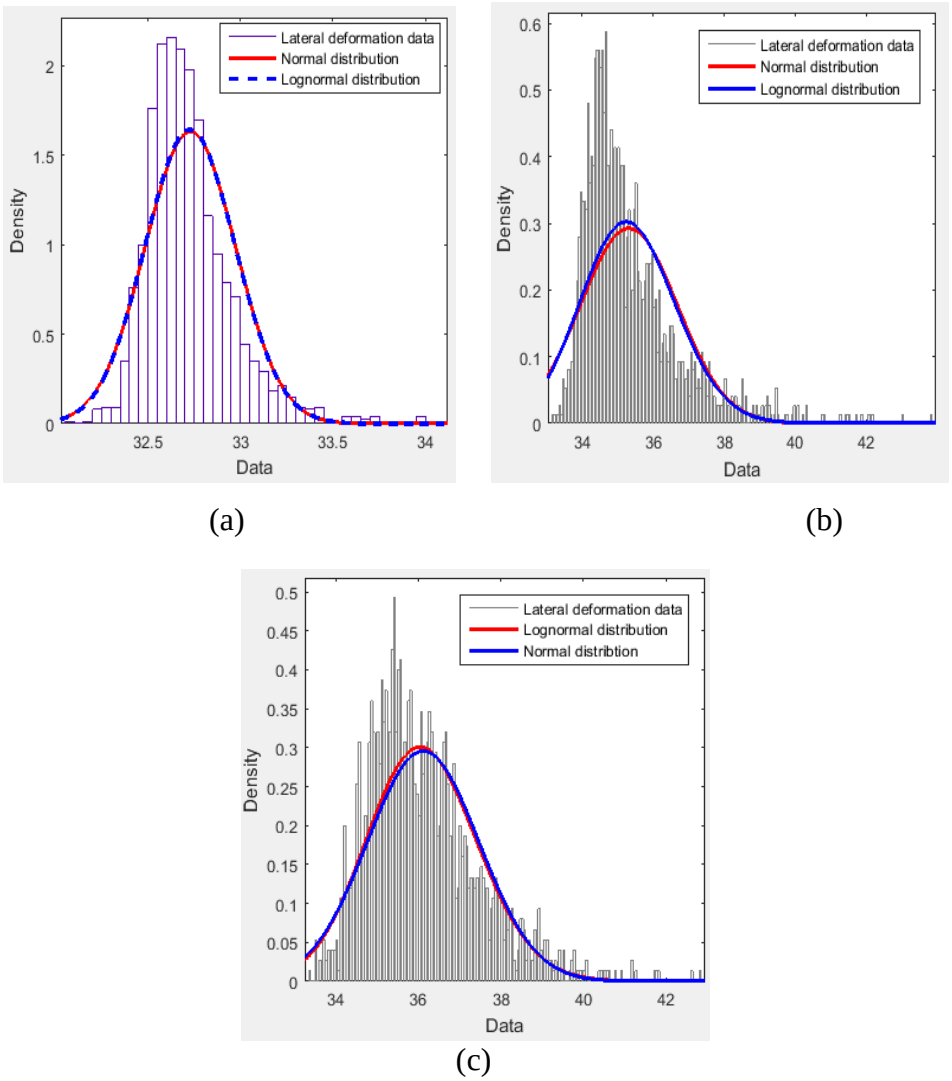

Figure 3: Best fit normal and lognormal distributions for the lateral deformation data obtained from Monte Carlo simulations (a) PFOS=2, COV= 0.3 and θ = 2 m; (b) PFOS=1, COV= 0.5 and θ = 2 m and (c) PFOS=1, COV= 0.7 and θ = 1 m

Although the Monte Carlo simulation results do not fit into a probability distribution, the deformation data showed some trend with changing characteristics of the strength field. Table 3 shows the change in lateral deformation data with increasing spatial correlation length, when PFOS=1 and COV=0.7. The lower bound of the lateral deformation data do not change more than 1 mm when spatial correlation length varied between 0 to 4 m. The upper bound of the deformation data increased gradually from 34.7 mm to 47.3 mm with increasing spatial correlation length from 0 to 4 m. As a result, the span of the deformation data distribution also increased with increasing spatial correlation length. The lateral deformation data tend to deviate more from a normal or lognormal distribution with increasing correlation length.

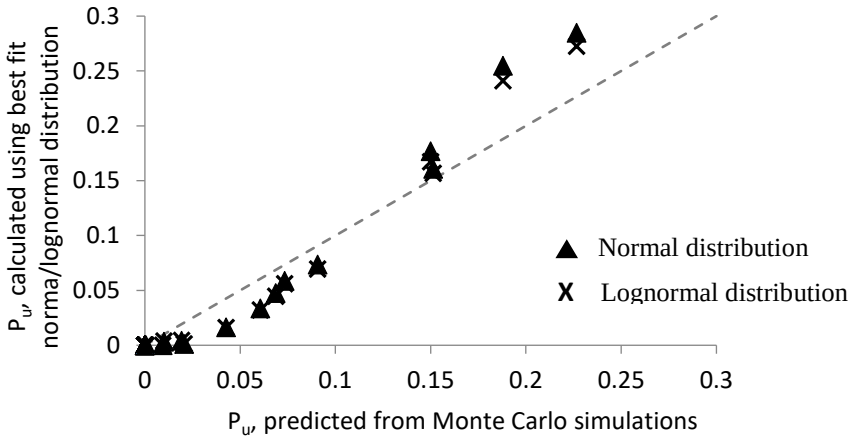

Figure 4: P_u predicted from Monte Carlo simulations Vs P_u calculated using best fit probability distributions

Table 3: Changes in the distribution of lateral deformation data when increasing spatial correlation length (PFOS=1 and COV=0.7)

Spatial correlation length, θ	0	0.5 m	1 m	2 m	4 m
Lower bound (mm)	33.696	34.039	33.388	33.172	33.294
Upper bound (mm)	34.668	39.949	42.817	46.505	47.307
Span of the distribution (mm)	0.972	5.91	9.429	13.303	14.013

As shown in Table 4, both upper and lower bounds of the lateral deformation data changed slightly with increasing PFOS. The difference in the span of data is also less than 1 mm between the four cases shown in Table 4. This indicates that PFOS does not change the upper and lower bounds of the data set. However, the skewness of the data distributions increased in the positive direction with increasing PFOS.

Table 4: Changes in the distribution of lateral deformation data when increasing PFOS (COV=0.7 and θ=2 m)

PFOS	1	1.2	1.5	2
Lower bound (mm)	33.172	32.402	31.733	31.437
Upper bound (mm)	46.505	46.408	46.028	45.644
Span of the distribution (mm)	13.303	14.001	14.295	14.207
Skewness	1.3872	1.5082	1.7105	1.9041

Changes in the lateral deformation data with increasing COV are shown in

Table **5**. The lower bound did not vary significantly with changing COV. The upper bound and the span of lateral deformation data increased with increasing COV.

Table 5: Changes in the distribution of lateral deformation data when increasing COV (PFOS=1 and θ= 2 m)

COV	0.3	0.5	0.7
Lower bound (mm)	33.491	33.166	33.172
Upper bound (mm)	37.285	43.808	46.505
Span of the distribution (mm)	3.794	10.642	13.303

4. CONCLUSIONS

This study investigates the performance of a DCM panel supported embankment beneath the slopes, using reliability based approach. The spatial variation of strength properties of DCM panels were incorporated in this analysis along with the spatial correlation characteristics. The strength field within DCM panel was varied among the different realisations of Monte Carlo simulations. The analysis was carried out for 21 analysis cases considering different combinations of spatial correlation length, coefficient of variation (COV) and partial factor of safety (PFOS). 1500 Monte Carlo realisations were carried out for each analysis case and the probability of unsatisfactory performance, P_u , was predicted. Results of this study show that a peak for P_u was observed when spatial correlation distance was 0.18 times the width of the DCM wall. P_u reaches zero with decreasing correlation length below 2 m as well as decreasing COV. The deformation data obtained from Monte Carlo simulations incorporating spatial variability of strength properties did not fit well into a normal or lognormal probability distribution. However, the lateral deformation data showed some clear response to changing spatial correlation length and COV of the input strength field. The upper bound and the span of the deformation data increased with increasing spatial correlation length and COV. The skewness of the deformation distribution shifted to left with increasing PFOS. The upper and lower boundaries of the lateral deformation data were not affected by the PFOS. Although these results cannot be directly applied to field problems, they clearly show how the variability if material properties influence the overall performance of embankments. Unsatisfactory performance changes with both COV and correlation length. If a 10% tolerance is allowed, it can be achieved with COV of 0.3, irrespective of the spatial correlation length of the DCM strength within wall panels.

5. REFERENCES

ABAQUS/Standard. (2014). *ABAQUS version 6.14 - Computer software*, Dassault Systèmes Simulia Corp., Providence, Rhode Island, USA.

Al-Naqshabandy, M.S., Bergman, N.S., and Larsson, S. (2012a). "Strength variability in lime-cement columns based on CPT data." *Ground improvement*, 165(1), 15-30.

Al-Naqshabandy, M.S., and Larsson, S. (2013). "Effect of uncertainties of improved soil shear strength on the reliability of embankments." *Journal of Geotechnical and Geoenvironmental Engineering*, 139(4), 619-632.

Al-Naqshabandy, S., Bergman, N., and Larsson, S. (2012b). "Effect of Spatial Variability of the Strength Properties in Lime-Cement Columns on Embankment Stability." *Proceedings of the Fourth International Conference on Grouting and Deep Mixing*, New Orleans, Louisiana, United States, 231-242,February 15-18, 2012.

Andromalos, K.B., Hegazy, Y.A., and Jasperse, B.H. (2000). "Stabilization of soft soils by soil mixing." *Proceedings of the Soft Ground Technology Conference, United Engineering Foundation and ASCE Geo-Institute, Noordwijkerout, Netherlands*,May 28 – June 2.

Ariyarathne, P., Liyanapathirana, D.S., and Leo, C.J. (2013). "Comparison of different two-dimensional idealizations for a geosynthetic-reinforced pile-supported embankment." *International Journal of Geomechanics*, 13(6), 754-768.

Broms, B.B. (1999). "Keynote lecture: Design of lime, lime/cement and cement columns." *International Conference on Dry Mix Methods: Dry Mix Methods for Deep Soil Stabilization*, Balkema, Rotterdam, 125-153.

Bruce, D.A., and Bruce, M.E.C. (2003). "The practitioner's guide to deep mixing. ." *Grouting and Ground Treatment, Geotechnical Special Publication No. 120*, 474-488.

Chan, K., and Poon, B.O.S.C.O. (2012). "Designing stone columns using 2D FEA with equivalent strips." *Proc., Int. Conf. on Ground Improvement and Ground Control*, 2, 609-620.

Cho, S.E. (2007). "Effects of spatial variability of soil properties on slope stability." *Engineering Geology*, 92(3), 97-109.

Euro Soil Stab. (2002). "Development of design and construction methods to stabilize soft organic soils: design guide soft soil stabilization"*CT97-0351, Project No. BE 96-3177*. Industrial and materials technologies programme (Brite-EuRam III), European Commission.

Fenton, G.A., and Griffiths, D.V. (2008). *Risk assessment in geotechnical engineering*, John Wiley and Sons.

Filz, G.M., and Navin, M.P. (2010). "A practical method to account for strength variability of deep-mixed ground." *GeoFlorida 2010: Advances in Analysis, Modeling & Design, Geotechnical special publication No. 199*, 2426-2433.

Honjo, Y. (1982). "A probabilistic approach to evaluate shear strength of heterogeneous stabilized ground by deep mixing method." *Soils and Foundation*, 22(1), 23-38.

Huang, J., Griffiths, D.V., and Fenton, G.A. (2010). "System reliability of slopes by RFEM." *Soils and Foundations*, 50(3), 343-353.

Huang, J., Han, J., and Oztoprak, S. (2009). "Coupled mechanical and hydraulic modeling of geosynthetic-reinforced column-supported embankments." *Journal of Geotechnical and Geoenvironmental Engineering*, 135(8), 1011-1021.

Huang, J., Kelly, R., and Sloan, S.W. (2015). "Stochastic assessment for the behaviour of systems of dry soil mix columns." *Computers and Geotechnics*, 66, 75-84.

Jiang, S.-H., and Huang, J.-S. (2016). "Efficient slope reliability analysis at low-probability levels in spatially variable soils." *Computers and Geotechnics*, 75, 18-27.

Kasama, K., Whittle, A.J., and Zen, K. (2012). "Effect of spatial variability on the bearing capacity of cement-treated ground." *Soils and Foundations*, 52(4), 600-619.

Kasama, K., and Zen, K. (2011). "Effects of spatial variability of soil property on slope stability." *Vulnerability, Uncertainty, and Risk Analysis, Modeling and Management, 2011 conference*, Reston, VA, USA, 691–698.

Larsson, S., Stille, H., and Olsson, L. (2005). "On horizontal variability in lime-cement columns in deep mixing." *Géotechnique*, 55(1), 33-44.

Liu, L.-L., Cheng, Y.-M., and Zhang, S.-H. (2017). "Conditional random field reliability analysis of a cohesion-frictional slope." *Computers and Geotechnics*, 82, 173-186.

Liu, Y., Lee, F.-H., Quek, S.-T., Chen, E.J., and Yi, J.-T. (2015). "Effect of spatial variation of strength and modulus on the lateral compression response of cement-admixed clay slab." *Géotechnique*, 65(10), 851-865.

Namikawa, T. (2016). "Conditional probabilistic analysis of cement-treated soil column strength." *International Journal of Geomechanics*, 16(1), 04015021.

Namikawa, T., and Koseki, J. (2013). "Effects of spatial correlation on the compression behavior of a cement-treated column." *Journal of Geotechnical and Geoenvironmental Engineering, ASCE*, 139(8), 1346-1359.

Navin, M.P. (2005). *Stability of embankments founded on soft soil improved with deep-mixing-method columns*, Doctoral Thesis, Virginia Polytechnic Institute and State University,Blacksburg, VA, USA.

Navin, M.P., and Filz, G.M. (2006). "Reliability of deep mixing method columns for embankment support." *GeoCongress: Geotechnical Engineering in the Technology Age*.

Tang, Y.X., Miyazaki, Y., and Tsuchida, T. (2001). "Practices of reused dredgings by cement treatment." *Soils and Foundations*, 41(5), 129-143.

U. S. Army Corps of Engineers. (1995). *Introduction to probability and reliability methods for use in geotechnical engineering. Eng. Tech. Letter No 1110-2-547*. U.S. Army Corps of Engineers, CECW-ED.

Yapage, N.N.S., and Liyanapathirana, D.S. (2014). "A parametric study of geosynthetic-reinforced column-supported embankments." *Geosynthetics International*, 21(3), 213-232.

Yapage, N.N.S., Liyanapathirana, D.S., Kelly, R.B., Poulos, H.G., and Leo, C.J. (2014). "Numerical modeling of an embankment over soft ground improved with deep cement mixed columns: Case history." *Journal of Geotechnical and Geoenvironmental Engineering*, 140(11), 04014062.

Zhang, R.-J., Hasan, M.S.M.S., Zheng, J.-J., and Cheng, Y.-S. (2017). "Effect of spatial variability of engineering properties on stability of a CSMC embankment." *Marine Georesources & Geotechnology*.

WOOLGOOLGA TO BALLINA PACIFIC HIGHWAY UPGRADE – RELIABILITY ASSESSMENT OF SOFT GROUND TREATMENT DESIGN

Viet D. Nguyen[1], Patrick K. Wong[2], Henry Zhang[3]
[1]Associate Geotechnical Engineer, Coffey Services Australia Pty Ltd
[2]Senior Consultant, Coffey Services Australia Pty Ltd & Senior Principal, PKW Geosolutions Pty Ltd
[3]Principal Geotechnical Engineer, WSP Australia Pty Ltd

ABSTRACT

Eleven road sections with an approximately 20 km total length out of the 155 km Pacific Highway Upgrade project between Woolgoolga and Ballina (W2B), NSW traverse areas having significant depths of soft soils. At Maclean Interchange or Clarence River Interchange, soft soil thickness was up to 20 – 25 m under the road alignment. Soft ground treatment design for the identified soft soil areas was undertaken in 2014. The main objectives of the soft ground treatment were to provide certainty of delivery of the highway upgrade within a given time during the main contract with a satisfactory long-term pavement performance.

The highway section between Whytes Lane and Pimlico Road of approximately 3.85 km is one of the longest road sections underlain by up to 8 m thick soft soil that required ground treatment. Due to the significantly length of the soft ground treatment for this road section, one of the main objectives was to reduce or optimise the cost of soft ground treatment.

During the detailed design stage, soft ground treatments using preloading with or without Prefabricated Vertical Drains (PVD) were considered. Due to issues such as sample disturbance during soil sampling and transporting, limitations of the adopted soil testing methods and equipment, limitations of the available geotechnical investigation information, there was a possibility that the actual ground behaviour could be different from the predicted behaviour using the design soil parameters. Reliability analyses were carried out to assess the potential variability of material parameters on embankment settlement and ground treatment requirements.

The reliability assessment provided quantitative confident levels of the ground treatment designs and suitable contingency measures. The reliability assessment provided indication of the cost and risk balancing. The target confidence level was minimum 70% for the soft ground treatment design with the proposed observation method and contingency measures such as placement of additional surcharge or additional preloading time to respond to changes during the preloading period. The reliability assessment also effectively assisted the client's decision on the preferred soft ground treatments.

The adopted reliability assessment method as described in Duncan (2000) and the assessment results for the soft ground treatment design were presented. The embankment settlement was monitored during the preloading stage and was back analysed. The reliability assessment results, which were analysed in the design stage, and the ground treatment design were reviewed against the actual embankment settlement performance.

1 INTRODUCTION

Over the approximately 155 km project length from Woolgooga to Ballina, there are a total of eleven highway sections underlain by soft alluvium, with lengths ranging from about 0.5 km to 4 km. The soft soil sections are numbered as Soft Soil Sections 1 to 11. At these areas, soft soil thickness ranges from 5 m up to approximately 26 m depth and extends over kilometres of distance. These soft soil sections are part of Clarence River Floodplain or Richmond River Floodplain.

The highway section between Whytes Lane and Pimlico Road of approximately 3.85 km is one of the longest road sections underlain by up to 6 - 8 m thick soft soil that required soft ground treatment. This soft soil section is called Section 11 in this project. Due to the significantly length of the soft ground treatment for this road section, one of the main objectives of the soft ground treatment design was to reduce or optimise the cost of soft ground treatment.

During the detailed design stage, soft ground treatments using preloading with or without PVD were considered. Reliability analyses were carried out to assess the potential variability of material parameters on embankment settlement and ground treatment requirements. The reliability assessment provided indication of the cost and risk balancing. The reliability assessment also provided quantitative confident levels of the ground treatment designs and suitable contingency measures. The reliability assessment also effectively assisted the client's decision on the preferred soft ground treatments.

This paper first presents a brief site location and geology descriptions of this soft soil Section 11 and the highway upgrade requirements followed by the reliability assessment, and the embankment settlement back analysis results. The adopted reliability assessment method by Duncan (2000) was summarised together with soil parameters. Typical reliability assessment results and associated discussions were presented. Based on the assessment, suitable soft ground treatment using surcharge with PVD was used for Section 11. The embankment settlement was monitored during the preloading stage and was back analysed. The reliability assessment results, which were analysed in the design stage, and the ground treatment design were reviewed against the actual embankment settlement performance.

2 PROJECT INFORMATION

The 3.85 km of Section 11 along the Pacific Highway started from Whites Lane (CH159900) to Pimlico Road (CH163750) is shown in Figure 1. The highway upgrade included embankment widening along the western side of the existing highway to form a two-lane dual carriageway. The new embankment height generally ranged from 1.8 m to 3 m. The detailed civil and geotechnical design of the soft ground treatment was completed in 2014 for a target completion of the highway upgrade at the end of 2019. It was anticipated that 3 years (2015 to 2017) would be available for the early works (EW) soft ground treatment and 2 years (2018 to 2019) would be available for the main construction of the highway.

Figure 1: Location of the highway upgrade soft soil Section 11 (Whytes Lane to Pimlico Road)

3 GEOLOGICAL SETTING

The extent of Section 11 crosses the floodplain of the Richmond River, underlain by thick sandy and clayey alluvium and estuarine sediments of Quaternary (Holocene and Pleistocene) age. The Quaternary sediments were deposited in alluvial, estuarine, and marine environments largely reflecting changes in sea level, which occurred over about the last 250,000 years. The Holocene clay (very soft to firm) thickness ranges from approximately 6 m to 8 m along the highway alignment. The Pleistocene deposits, which is underlies the Holocene, comprises of stiff to very stiff clayey soils followed by loose to dense sandy soils to approximately 20 m to 30 m depth. These Quaternary sediments are underlain by residual soils and sedimentary rocks of the Bundamba Group and Neranleigh Fernavle Beds.

Figure 2 shows a typical geotechnical long section along approximately 200 m length of the upgrade highway alignment from CH160950 to CH161250. Soil Units 2c and 2e represent the Holocene soft soils, which is of highly compressible and low permeability. Due to the extensive 3.85 km length of this section, only the representative geotechnical long section of 200 m length has been shown. Other area has relatively similar soft soil unit thickness.

Geotechnical investigation included boreholes and CPTs at approximately 200 m spacing. We considered that the available geotechnical information for the EW design was relatively light over 3.85 km embankment length. However, given the total thickness of the soft soil layers was not excessive and the design embankment height is relatively low the level of geotechnical information for this section was considered acceptable for detailed design of the EW soft ground treatment. During the installation of PVD and monitoring instrument, the geotechnical information was reviewed and confirmed since the construction started in early 2016.

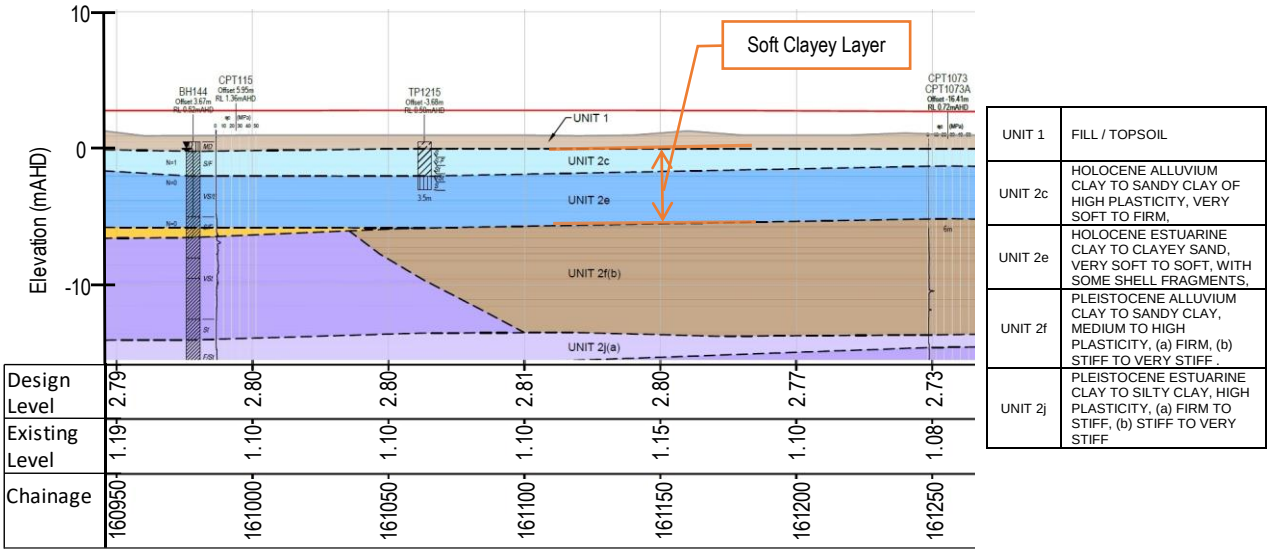

Figure 2: Typical Geotechnical Long Section

4 SOFT GROUND TREATMENT DESIGN

In the EW ground treatment design in 2014, Post Construction Settlement (PCS) criteria over 40 years was 200 mm for general embankment with flexible pavement and 120 mm for culverts respectively. Preloading and surcharge without vertical drains was designed for general embankment section from CH159900 to CH163000. Preloading and surcharge with PVD at 2.5 m centre to centre spacing was designed for embankment sections from CH163000 to CH163750, where there are five proposed new culverts. The available EW preloading time was from 2.5 years up to 3.5 years, inclusive of PVD installation and embankment construction time. Nominal surcharge of 0.4 m to 0.5 m thick fill was allowed in the EW design.

Figure 3 shows a typical cross section of the EW embankment over the proposed widening area adjacent to the existing highway. Soft ground treatment design was carried out using analytical and finite difference methods using the software CAOS (Consolidation Analysis of Soils) developed by Professor Harry Poulos with modification to include post surcharge creep reduction using the method described in Wong (2010). The design considers the following embankment preloading aspects:

- 2-dimensional stress distribution with depth under a fill embankment,
- ground consolidation with PVD including smear effect,
- large embankment deformation and settlement,
- time dependent settlement (creep settlement) and creep reduction due to surcharge removal and over consolidation effect, and
- embankment construction staging.

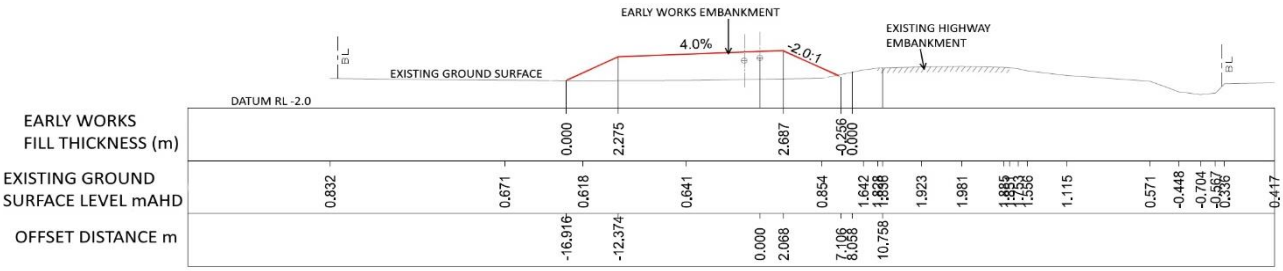

Figure 3: Typical Highway Upgrade Section at CH160,120

5 RELIABILITY ANALYSIS

Due to issues such as limitations of the available geotechnical investigation information, sample disturbance during soil sampling and transporting, limitations of the adopted soil testing methods and equipment, there was a possibility that the

actual ground behaviour could be different from the predicted behaviour using the design soil parameters. The available number of laboratory testing for soft soil layer over this road section were limited, i.e. there were only 6 oedometer test results for 3.85 km embankment length. The geotechnical test locations were at relative wide spacing of up to 200m.

In the EW detailed design, reliability analyses were carried out to assess the potential variability of material parameters on embankment settlement and ground treatment requirements. This section presents the reliability assessment, which was carried out and reported as part of the EW design in 2014. Two representative embankment sections with or without PVD were analysed. Two scenarios of preloading time of 2.5 years and 3.5 years (inclusive of construction time) were considered.

2.1 RELIABILITY ANALYSIS METHOD

Reliability analysis using First Order Reliability Method (FORM), specifically Taylor series method, was adopted to evaluate the effect of uncertainties in the estimated settlements and surcharge. Details of this method and its applications in geotechnical engineering design have been presented by Duncan (2000). In the reliability analysis, the critical soil parameters OCR, CR, CRR, $C_{\alpha e}$, c_h and c_v, thickness of soft soil (Units 2c and 2e), and thickness of the high c_v zone were varied. The steps involved in the reliability assessment are as follows:

1. Assess the Most Likely Values (MLV) of the critical soil parameters involved in the calculation and compute the required settlement and surcharge.
2. Assess the Highest Conceivable Values (HCV) and Lowest Conceivable Values (LCV) of the parameters involved in the calculation.
3. Estimate the Standard Deviations (SD) of the parameters using the "Three-Sigma Rule" approximation. The SD is estimated as SD = (HCV – LCV) / 6.
4. Compute the settlement and surcharge with each independent variable increased by one SD and then decreased by one SD from its MLV, while holding other parameters at their MLV. The compressibility parameters CR, CRR, $C_{\alpha e}$ are considered to be dependent variables (i.e. they relate to each other) and therefore the parameters are varied by ±SD together in this calculation step.
5. Use the computed MLV settlement and surcharge thickness values from Step 1 and the series of values from Step 3, the Coefficient of Variability (CV) of the result is assessed using the Taylor's series method. The probability that the actual settlement and surcharge may be greater than the computed most likely settlement and surcharge thickness is then assessed based on the Lognormal Distribution reliability index method.

2.2 RELIABILITY ASSESSMENT PARAMETERS

The profiles of MLV, HCV, LCV, SD, and CV values for the critical parameters of soft soil Units 2c and 2e have been identified and shown in Figure 4. At the time of the soft ground treatment design, there were a total of 6 oedometer testing results available for the soft soil units over the entire 3.85 km of Section 11. Due to the low available number of oedometer tests for Section 11, a correlation of compression index with moisture content using the oedometer testing results of soft soil units from other road upgrade sections of this project have been carried out. Figure 5 shows the compression index (CR) against moisture contents from for soft soil units over Sections 4, 5, 8, and 11 of the W2B project. Based on this plot, a site-specific variation of CR with moisture content was established to derive the reliability parameters of compression indices. The OCR profile based on CPT and interpreted undrained shear strength (using corrected vane shear test results and CPT) has been used in the design, and the scatter of results have also been used to assess the MLV(OCR), HCV(OCR) and LCV(OCR) values.

For the extent depth of the high c_v zone derived by the back analysis of the BBA observed embankment settlements, we have adopted the deepest extent depth (HCV) of this zone is 5 m which is corresponding with the back-analysis result. It was reported from BBA design team that the extent depth of the high c_v zone could be up to 7 m. The shallowest extent depth (LCV) of this zone is 1 m, which is the nominal depth of a crust layer near the surface, where high OCR and c_v values are often measured. For each of the soil parameters, the SD values have been estimated so that the corresponding CV are not less than the recommended minimum values of CV by Duncan (2000). The minimum CV values for each of the soil parameters are listed in Table 1.

Table 1: Adopted Values of *CV* for Reliability Analyses.

Soil Parameters	OCR	CR, CRR, $C_{\alpha e}$	c_v and c_h	Thickness Soft Soil	Depth of high cv zone
Adopted CV	20%	15%	40%	12% (0.5m - 1.5m)	22%
Duncan (2000)	10-35%	10-37%	33-68%	-	-

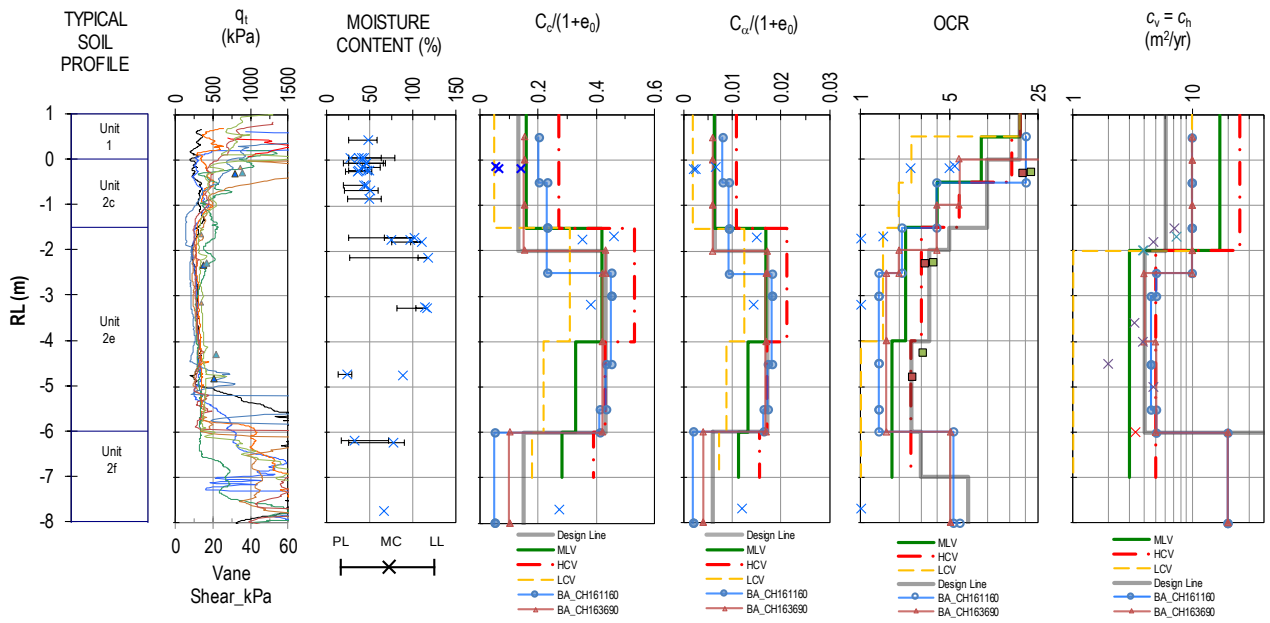

Figure 4: Typical Geotechnical Profile and Parameters

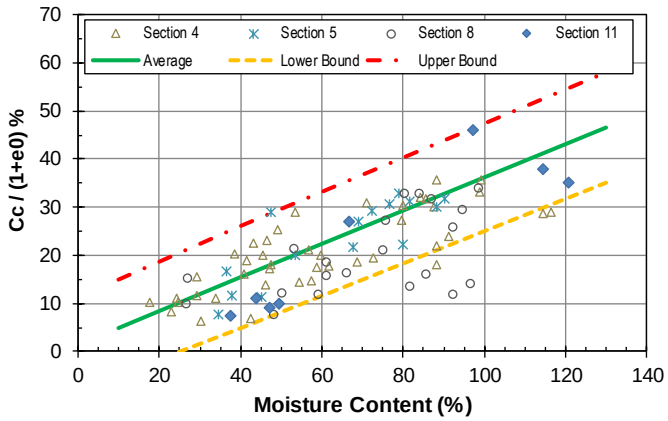

Figure 5: Project Specific Compression Index CR against Moisture Content

2.3 RELIABILITY ASSESSMENT RESULTS

The reliability assessments have been carried out for critical sections with or without PVD using analytical and finite difference methods using the software CAOS. The details and results of reliability assessments for the identified critical sections are shown in Figure 6.

As can be seen from Figure 6(a), the reliability assessment results for embankment settlement at critical sections are generally in the order of 55% confidence over areas without PVD and more than 90% confidence over areas with PVD at 2.5 m centre to centre. The reliability assessment results for preloading settlement indicate that an additional fill thickness of up to 0.3 m above the EW design height may be required to achieve a reliability level of 90% for area without PVD.

Figure 6(b) presents reliability assessment results of the predicted PCS in two scenarios of the assumed preloading periods (2.5 years or 3.5 years). With a preloading period of 2.5 years, the reliability to achieve the PCS criteria for flexible pavement (200 mm / 40 years) would be 74% over areas without PVD and to more than 90% over areas with PVD. The reliability to satisfy the PCS criteria for rigid pavement are relatively lower than that for flexible pavement, i.e. 30% and 50% over areas without and with PVD respectively. An additional 1-year preloading time (increase from 2.5 years to 3.5 years) would increase the reliability to 70% - 87% to achieve the PCS criteria for rigid pavement. In addition, the reliability could be improved by placement of additional surcharge fill thickness and preloading in the main contract (after EW).

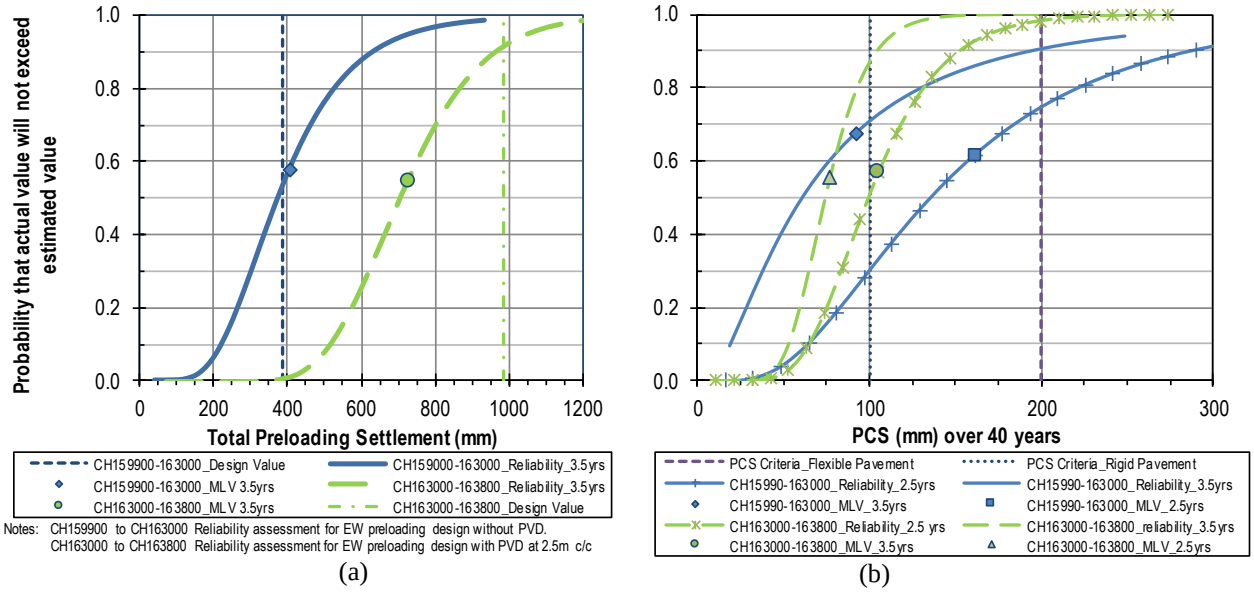

(a) (b)

Figure 6: Reliability Assessment Results of Early Works Ground Treatment Design

6 PREFERRED SOFT GROUND TREATMENT

The detailed EW soft ground treatment design for Section 11 was submitted in November 2014. Embankment construction of Section 11 started in early 2016. Because the actual construction for the upgrade over the existing highway and the road widening areas be undertaken in different stages, preloading time of up to 2.5 year or 3.5 years as assumed in the 2014 ground treatment design was not available for the widening. Hence, in early 2016, PC requested Coffey to revisit the design considering PVD for the whole soft soil length of Section 11 with a total construction and preloading time up to 1.5 years.

In the 2016 design, PVD at 1.5 m centre to centre spacing and 0.4 – 0.5 m thick surcharge were specified as the soft ground treatment for Section 11. Based on the reliability assessment results in the 2014 design, it was anticipated that the use of PVD at 1.5 m spacing and preloading with 0.4 – 0.5 m surcharge up to 1.5 years would likely satisfy the PCS criteria for rigid pavement. The expected reliability confidence level of the design would be in excess of 90% for both the preloading settlement magnitude and the predicted PCS over 40 years of operation. The updated ground treatment design was re-issued in March 2016 as the same time as the PVD installation, monitoring instrument installation, and embankment construction. Review of the installation records showed relative consistence of the soft soil thickness with that was assumed in geotechnical design.

7 SETTLEMENT MONITORING AND BACK ANALYSES

Figure 7 shows the monitored embankment thicknesses and settlements with time and with the project alignment chainage from CH159900 to CH163750. The final settlement reading was at 14 December 2019, which was assessed to reach 90% to 95% consolidation completion of the ground. The predicted preloading settlement in the design was also plotted against the chainage. The predicted preloading settlement generally close to the monitored settlement, except approximately 700 m embankment length between approximately CH161000 and CH161700, where the monitored settlement was about 200 mm higher than the prediction. This observation indicated that there was a variation in the soft soil stiffness along the alignment. Under relatively similar fill and soft soil thickness between section CH161000 - CH161700 and section CH161700 – CH162500, the former settled approximately 100 mm to 150 mm more than the later.

Back analysed settlement results of the settlement plates and nearby extensometers at approximately CH161100 and CH163700 are shown in Figures 8 and 9. The back analysed soil parameters are shown in Figure 4. PVD disturbed (smear) zone has been considered in the back analyses. The radius of the smear zone was assumed as twice as that of the band drain PVD. The ratio of the undisturbed soil permeability to the smear zone permeability was assumed as 4.5.

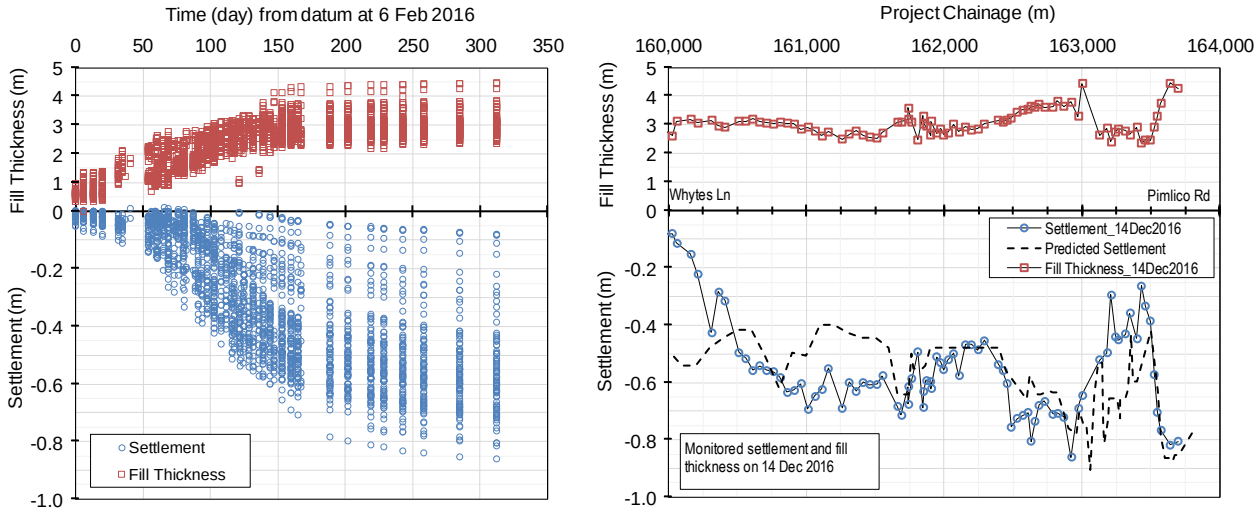

Figure 7: Monitored Ground Settlements

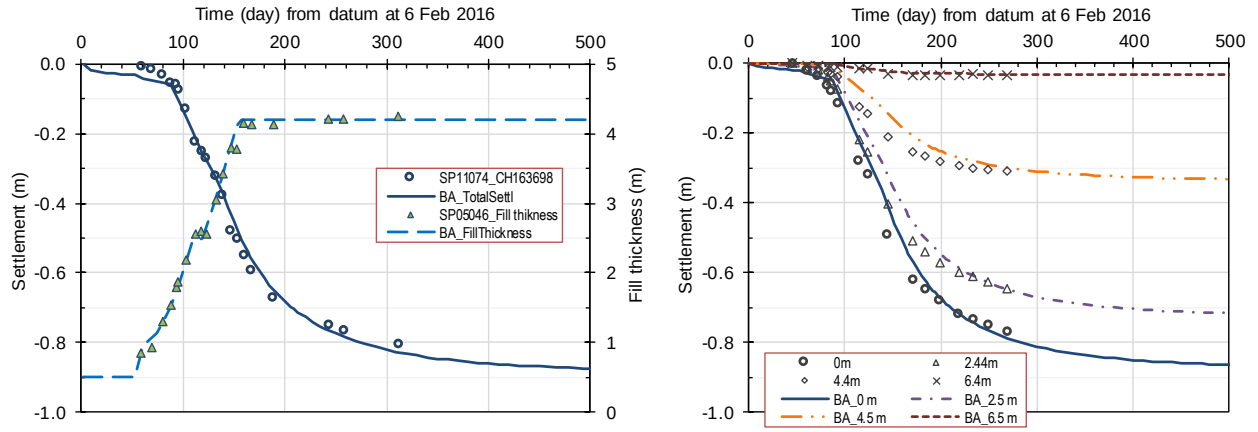

Figure 8: Settlement Back Analysis at CH 163700 (Settlement Plate & Extensometer)

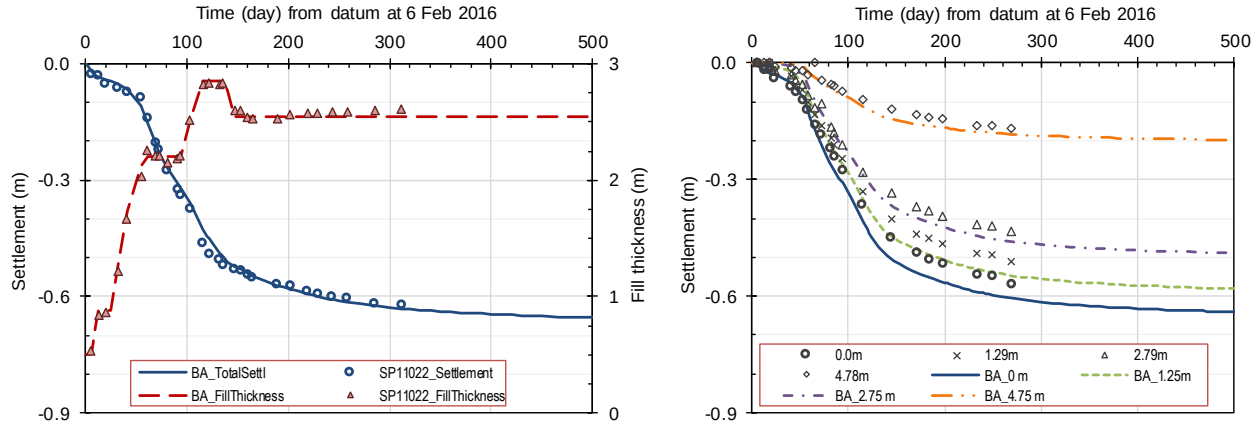

Figure 9: Settlement Back Analysis at CH161,100 (Settlement Plate & Extensometer)

8 BACK ANALYSIS VERSUS DESIGN

What would the PCS have been if the EW design using preloading for 2.5 to 3.5 years with 0.4 – 0.5 m surcharge but without PVD for embankment area from CH159900 to CH163000 was constructed? Would the minimum confident level of 70% for a soft ground treatment design successfully meet the design criteria? To answer these questions, a hypothetical

settlement analysis (without PVD) was carried out for the back analysed embankment section at CH161100 using the back analysed soil parameters.

Figure 10 shows the hypothetical analysis results of the preloading settlement and the forward PCS prediction. The predicted preloading settlement could have been approximately 500 mm or 600 mm at 2.5 years or 3.5 years preloading. The forward prediction of PCS could have been 185 mm/40 years for the former and 125 mm/40 years for the later. According to the reliability assessment in Figure 6 for preloading without PVD, a design settlement with reliability confidence of 80% to 90% would likely be the required minimum level to meet the monitored preloading settlement. For the predicted PCS, a confidence level of 70% - 80% would be sufficient to meet the PCS design criteria.

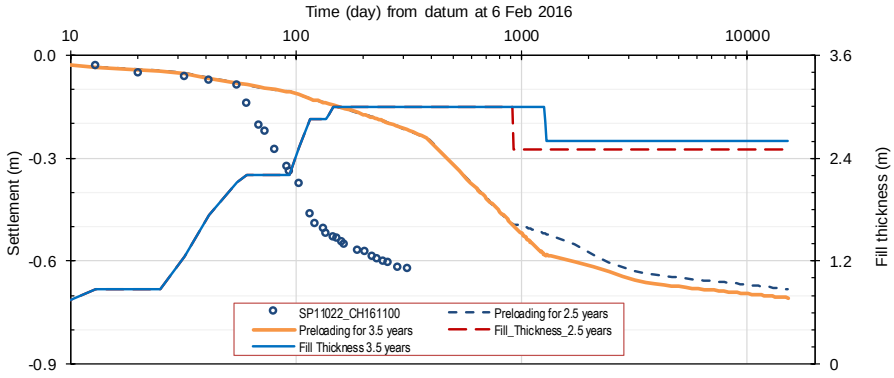

Figure 10: Hypothetical Settlement Analysis at CH 161100 with Back Analyses Soil Parameters without PVD

9 CONCLUSIONS

During the soft ground treatment design stage, reliability assessment was adopted to evaluate the effect of uncertainties in the estimated settlements and surcharge. It is important that reasonable soil parameters be derived for the design and reliability assessment. Site specific soil stiffness parameters have been correlated using the available geotechnical testing results from the project. The adopted variability ranges of soil parameters in the reliability analyses were within the recommended variability ranges by Duncan (2000).

The reliability assessment provided an indication of the design confidence level and the potential contingency measures such as applying additional fill or extending preloading time that may be required depending on the monitoring results. The reliability assessment effectively assisted the client's decision on the preferred soft ground treatments.

Back analyses of the monitored embankment settlement during construction and preloading was carried out and compared very well with the design. The monitoring indicated that the soft ground treatment for the widening embankment was successfully designed and constructed. The predicted forward PCS predictions are within the design criteria for flexible pavement.

10 ACKNOWLEDGEMENTS

The authors are grateful to the NSW Roads and Maritime Services and Pacific Complete for the use of the monitoring data and results and their approval for publishing this paper. Any opinions, findings, conclusions and recommendations in this paper are those of the authors only, and do not necessarily reflect the views of NSW Roads and Maritime Services.

11 REFERENCES

Duncan, J. M. (2000) Factors of Safety and Reliability in Geotechnical Engineering. *Journal of Geotechnical and Geoenvironmental Engineering*, 126(4): 307-316

Kelly, R. and Huang, J. (2015) Bayesian Updating for One-dimensional Consolidation Measurements, *Canadian Geotechnical Journal*, 52: 1318-1330.

Poulos, H. G. (2008) CAOS User Manual, Consolidation Analysis of Soils.

Wong, P. K., (2010). Comparison of experimental methods for assessing secondary consolidation settlement of soft soil after surcharging. *Australian Geomechanics Society Perth Chapter Symposium Ground Improvement Seminar*, June 2012.